

# Characterization of Biofilm Formation in

## *Mycobacterium abscessus*

By

**Anja Đokić**

A thesis submitted to the University of Birmingham

for the degree of

**DOCTOR OF PHILOSOPHY**

Institute of Microbiology and Infection

School of Biosciences

College of Life and Environmental Sciences

University of Birmingham

July 2021

**UNIVERSITY OF  
BIRMINGHAM**

**University of Birmingham Research Archive**

**e-theses repository**

This unpublished thesis/dissertation is copyright of the author and/or third parties. The intellectual property rights of the author or third parties in respect of this work are as defined by The Copyright Designs and Patents Act 1988 or as modified by any successor legislation.

Any use made of information contained in this thesis/dissertation must be in accordance with that legislation and must be properly acknowledged. Further distribution or reproduction in any format is prohibited without the permission of the copyright holder.

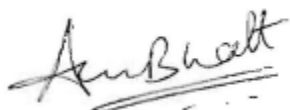
## ABSTRACT

*Mycobacterium abscessus* is a non-tuberculous mycobacterium (NTM) and an emerging opportunistic human pathogen associated with difficult to treat pulmonary infections, particularly in patients suffering from cystic fibrosis. Resembling other NTMs, *M. abscessus* is capable of forming biofilms in the environment, on medical devices and, alarmingly, in patient lungs, however not much is known about the composition and formation of this biofilm. Therefore, this work describes pellicular biofilm formation in the *M. abscessus* type strain (ATCC 19977) and six pulmonary clinical isolates. Using scanning electron micrographs and fluorescence microscopy it was shown that *M. abscessus* biofilms produce an extracellular matrix composed of lipids, proteins, carbohydrates, and extracellular DNA. Transcriptomic analysis of biofilms revealed an upregulation of pathways involved in the glyoxylate shunt, redox metabolism, and mycolic acid biosynthesis. Genes involved in elongation and desaturation of mycolic acids were highly upregulated in biofilms and biochemical analysis of mycolates revealed corresponding molecular changes. Additionally, six pulmonary clinical isolates of *M. abscessus* from a strain collection were biologically characterized and compared based on genetic sequences. Main differences amongst the isolates were related to variation in colony morphology, with half of the isolates presenting as smooth (presence of surface glycopeptidolipids) and half as rough (absence of glycopeptidolipids) colonies on agar. All clinical strains formed biofilms, and exhibited a lipid profile similar to the type strain. Whole genome sequencing identified that two of the strains belong to the *M. abscessus* subspecies *M. massiliense* and *M. bolletii*, and that the *M. abscessus* complex has a high degree of genetic uniformity. Together these results give us a novel understanding of biofilm formation in *M. abscessus* and a deeper insight into the *M. abscessus* complex, the understanding of which may be adapted for clinical use in treatment of biofilm infections.

## **DECLARATION**

The work presented in this thesis has been carried out under the supervision of Dr Apoorva Bhatt and Dr Tim Overton in the School of Biosciences at the University of Birmingham, UK, B15 2TT during the period January 2017 to June 2021. The work in this thesis is original except where acknowledged by reference. This work has resulted in one first-author publication. The publication may have similarities to Chapters 2, 3 and 4. These similar sections included in my thesis are my original work with no significant contribution to the text by Dr Apoorva Bhatt. No part of the work is being, or has been submitted for a degree, diploma or any other qualification at any other University.

**Dr Apoorva Bhatt**

A handwritten signature in black ink, appearing to read "Apoorva Bhatt".

## **PUBLISHED WORK ASSOCIATED WITH THIS THESIS**

Dokic, A., Peterson, E., Arrieta-Ortiz, M.L., Pan, M., Di Maio, A., Baliga, N., Bhatt, A., 2021. *Mycobacterium abscessus* biofilms produce an extracellular matrix and have a distinct mycolic acid profile. *Cell Surf.* 7, 100051. <https://doi.org/10.1016/j.tcs.2021.100051>

*This thesis is dedicated to my parents.*

## **ACKNOWLEDGEMENTS**

I would like to take this opportunity to thank the people who made this thesis and the work behind it possible. Firstly, my supervisor Dr Apoorva Bhatt for the opportunity to conduct this research project and his support and guidance through the development of this thesis. I would also like to thank the Darwin Trust of Edinburgh for funding this PhD.

I want to acknowledge the many people who contributed to this work: Eliza Peterson, Min Pan, Mario Arrieta-Ortiz and Nitin Baliga who hosted me in the Institute for Systems Biology in Seattle and provided expertise on transcriptomic analysis; Dr Laurent Kremer (Institut de Recherche en Infectiologie de Montpellier) who provided the pMV306-eGFP plasmid; Dr Vartul Sangal (University of Northumbria) for his help with genome sequencing analysis; Dr Natacha Verapeen for her help with any and all chemistry-related questions, and Dr Alessandro Di Maio for his guidance in confocal microscopy.

To everyone in the Bhatt, Besra, Alderwick and Moynihan labs - thank you for your support and advice over the past four years! Special thanks to my friends and fellow PhD students with whom I've shared the ups and downs of this journey, especially: Stephen, the ultimate DM, for his support; Christopher, for always being there and for sharing snacks; Bala, for being an inspiration for hard work; the Alices and their margaritas, for being a source of comfort and love when it was most needed.

I would like to thank all my friends over the years, in particular: Annelie, for always reminding me why I started this journey; Serban, for inspiring me to take leaps and helping me keep balance; the Time Agents, for listening and playing; and Soeren, for his continuous encouragement, unlimited patience and belief in me. Finally, a huge thank you to my parents and grandparents who always supported and motivated me.

# Table of Contents

<b>1</b>	<b><i>Introduction</i></b>	<b>1</b>
<b>1.1</b>	<b>The genus <i>Mycobacterium</i> and introduction to <i>Mycobacterium abscessus</i></b>	<b>2</b>
1.1.1	Non-tuberculous mycobacteria.....	3
1.1.2	Non-tuberculous mycobacteria as etiological agents .....	6
1.1.3	The <i>M. abscessus</i> complex .....	8
1.1.4	<i>M. abscessus</i> pathogenicity and prevalence .....	9
1.1.5	<i>M. abscessus</i> in cystic fibrosis patients .....	10
1.1.6	Treatment and antimicrobial resistance in <i>M. abscessus</i> .....	11
<b>1.2</b>	<b>The cell envelope of mycobacteria.....</b>	<b>15</b>
1.2.1	Mycolic acids .....	19
1.2.2	Glycopeptidolipids in the cell wall of <i>M. abscessus</i> .....	20
<b>1.3</b>	<b>Bacterial biofilms.....</b>	<b>24</b>
1.3.1	Mycobacterial biofilms.....	25
1.3.2	Biofilm formation.....	28
1.3.3	Composition of the biofilm extracellular matrix.....	28
<b>1.4</b>	<b><i>M. abscessus</i> biofilms and thesis aims.....</b>	<b>32</b>
1.4.1	Overarching aim.....	33
1.4.2	Specific aims – project 1 (Chapters 2-4).....	33
1.4.3	Specific aims – project 2 (Chapters 5-7) .....	33
<b>2</b>	<b><i>Microscopic analysis of M. abscessus biofilms</i> .....</b>	<b>34</b>
<b>2.1</b>	<b>Introduction.....</b>	<b>35</b>
2.1.1	Scanning electron microscopy in biofilm studies.....	35
2.1.2	Confocal laser scanning microscopy in biofilm studies .....	35
2.1.3	Microscopy as a tool for studying the biofilm extracellular matrix .....	36
<b>2.2</b>	<b>Results.....</b>	<b>37</b>
2.2.1	<i>M. abscessus</i> biofilms form an organized extracellular matrix .....	37
	.....	38
2.2.2	Fluorescent images reveal macromolecular content of <i>M. abscessus</i> biofilms.....	40
<b>2.3</b>	<b>Discussion .....</b>	<b>44</b>
2.3.1	Composition of the extracellular matrix .....	45
<b>3</b>	<b><i>Transcriptional profile of the M. abscessus biofilm</i> .....</b>	<b>49</b>
<b>3.1</b>	<b>Introduction.....</b>	<b>50</b>
<b>3.2</b>	<b>Results.....</b>	<b>52</b>
3.2.1	<i>M. abscessus</i> biofilms display a distinct expression profile compared to that of planktonic cultures.....	52
3.2.2	Common downregulated genes in biofilm t1 and t2 are involved in efflux regulation.....	57
3.2.3	Common upregulated genes in biofilm t1 and t2 point to changes in cell wall biosynthesis .....	57
3.2.4	Enriched metabolic pathways vary between early and late <i>M. abscessus</i> biofilms .....	60
3.2.5	Glyoxylate metabolism is upregulated in early biofilms.....	60
3.2.6	Fatty acid metabolism is upregulated in early <i>M. abscessus</i> biofilms .....	61
3.2.7	Redox metabolism and oxidoreductases are upregulated in early and late biofilms.....	61

3.2.8	Oxidative phosphorylation is downregulated in late biofilms.....	62
3.2.9	Genes related to MCE and ABC transporters are downregulated in late biofilms.....	63
<b>3.3</b>	<b>Discussion .....</b>	<b>70</b>
3.3.1	Genes involved in modulation of mycolic acid are upregulated in biofilms.....	70
3.3.2	Glyoxylate metabolism is required in non-replicative systems such as biofilms.....	71
3.3.3	Export systems are downregulated in <i>M. abscessus</i> biofilms .....	72
<b>4</b>	<b>Biochemical characterization of the <i>M. abscessus</i> biofilm extracellular matrix.....</b>	<b>74</b>
<b>4.1</b>	<b>Introduction.....</b>	<b>75</b>
<b>4.2</b>	<b>Results.....</b>	<b>76</b>
4.2.1	Comprehensive lipid profile of <i>M. abscessus</i> biofilms .....	76
4.2.2	Mycolic acid profile in <i>M. abscessus</i> biofilms .....	81
4.2.3	Analysis of carbohydrate composition of the surface exposed material of <i>M. abscessus</i> biofilms.....	85
<b>4.3</b>	<b>Discussion .....</b>	<b>87</b>
4.3.1	<i>M. abscessus</i> biofilm cells have a distinct lipid profile compared to planktonic cells.....	87
4.3.2	Glucose is the predominant monosaccharide in the <i>M. abscessus</i> surface-exposed material.....	89
<b>5</b>	<b>Biological characterization of <i>M. abscessus</i> clinical isolates .....</b>	<b>92</b>
<b>5.1</b>	<b>Introduction.....</b>	<b>93</b>
<b>5.2</b>	<b>Results.....</b>	<b>95</b>
5.2.1	Characterization of single colony and liquid broth growth of <i>M. abscessus</i> clinical isolates	95
5.2.2	Antibiotic susceptibility of <i>M. abscessus</i> clinical isolates .....	99
5.2.3	Uptake and survival of <i>M. abscessus</i> clinical isolates in murine macrophages .....	102
<b>5.3</b>	<b>Discussion .....</b>	<b>104</b>
5.3.1	<i>M. abscessus</i> clinical isolates are highly resistant to antibiotics .....	105
5.3.2	Smooth and rough <i>M. abscessus</i> strains have distinct pathways within macrophages ..	106
<b>6</b>	<b>Characterization of biofilm formation in <i>M. abscessus</i> clinical isolates .....</b>	<b>110</b>
<b>6.1</b>	<b>Introduction.....</b>	<b>111</b>
<b>6.2</b>	<b>Results.....</b>	<b>113</b>
6.2.1	<i>M. abscessus</i> clinical isolates form biofilms regardless of colony morphotype .....	113
6.2.2	Lipid profile of <i>M. abscessus</i> R biofilms differs from that of <i>M. abscessus</i> S .....	115
6.2.3	Lipid profile of <i>M. abscessus</i> clinical isolates .....	117
<b>6.3</b>	<b>Discussion .....</b>	<b>123</b>
6.3.1	All <i>M. abscessus</i> clinical isolates form biofilms.....	123
6.3.2	Lipid profiles of <i>M. abscessus</i> clinical isolates.....	124
6.3.3	Glycopeptidolipid profile in smooth and rough <i>M. abscessus</i> .....	125
<b>7</b>	<b>Genetic profile of <i>M. abscessus</i> clinical isolates .....</b>	<b>127</b>
<b>7.1</b>	<b>Introduction.....</b>	<b>128</b>
<b>7.2</b>	<b>Results.....</b>	<b>131</b>
7.2.1	Identification of subspecies of clinical isolates within the <i>M. abscessus</i> complex.....	131

7.2.2	Analysis of the GPL biosynthesis gene cluster in smooth and rough strains .....	133
7.2.3	Analysis of antibiotic resistance genes in <i>M. abscessus</i> clinical isolates.....	137
<b>7.3</b>	<b>Discussion .....</b>	<b>143</b>
7.3.1	Genetic differences between clinical isolates in the <i>gpl</i> locus .....	143
7.3.2	Genes related to antibiotic resistance.....	145
<b>8</b>	<b>General discussion.....</b>	<b>149</b>
<b>8.1</b>	<b>Conclusions.....</b>	<b>150</b>
8.1.1	Biofilm formation in <i>M. abscessus</i> .....	150
8.1.2	The key role of colony morphology in <i>M. abscessus</i> pathogenicity .....	153
<b>8.2</b>	<b>Future work.....</b>	<b>157</b>
8.2.1	Components of the biofilm extracellular matrix as biomarkers for detecting bacteria during infection .....	158
8.2.2	DNase I as a treatment for biofilms.....	159
8.2.3	Outlooks on vaccine development against biofilms .....	160
8.2.4	Biofilm infection models.....	160
8.2.5	Dual species biofilms and therapeutic approaches.....	161
<b>9</b>	<b>Materials and methods .....</b>	<b>162</b>
<b>9.1</b>	<b>Culture media.....</b>	<b>163</b>
9.1.1	Middlebrook 7H9 broth.....	163
9.1.2	Sauton's minimal media .....	163
9.1.3	Middlebrook 7H11 agar .....	163
9.1.4	cDMEM.....	163
<b>9.2</b>	<b>Bacterial culture and transformation .....</b>	<b>163</b>
9.2.1	Mycobacterial strains .....	163
9.2.2	Growth of planktonic cultures.....	164
9.2.3	Growth of biofilm cultures .....	164
9.2.4	Transformation of <i>M. abscessus</i> .....	166
<b>9.3</b>	<b>Microscopy methods.....</b>	<b>167</b>
9.3.1	Scanning electron microscopy.....	167
9.3.2	Confocal laser scanning microscopy .....	167
<b>9.4</b>	<b>Transcriptomic analysis .....</b>	<b>170</b>
9.4.1	Bacterial growth conditions for RNA extraction .....	170
9.4.2	RNA extraction.....	170
9.4.3	cDNA library preparation.....	171
9.4.4	RNA-seq analysis and differentially expressed genes .....	171
9.4.5	Metabolic pathway enrichment analysis .....	172
<b>9.5</b>	<b>Lipid analysis .....</b>	<b>173</b>
9.5.1	Radioactive labelling of <i>M. abscessus</i> cultures.....	173
9.5.2	Extraction of polar and apolar lipids .....	173
9.5.3	Extraction and analysis of fatty acid and mycolic acid methyl esters.....	174
9.5.4	Deacetylation of glycopeptidolipids.....	174
9.5.5	Quantification of radioactivity .....	174
9.5.6	Thin layer chromatography (TLC).....	175
9.5.7	Isolation of fatty acid and mycolic acid methyl esters using liquid chromatography ....	175

9.5.8	Mass spectrometry of fatty acid and mycolic acid methyl esters.....	176
<b>9.6</b>	<b>Analysis of extracellular carbohydrates in biofilms .....</b>	<b>178</b>
9.6.1	Extraction of extracellular carbohydrates.....	178
9.6.2	Synthesis of alditol acetates .....	178
9.6.3	Gas chromatography of alditol acetates .....	179
<b>9.7</b>	<b>Basic characterization of <i>M. abscessus</i> clinical isolates.....</b>	<b>180</b>
9.7.1	Growth curve.....	180
9.7.2	Determination of antibiotic minimum inhibitory concentrations .....	180
9.7.3	Whole genome sequencing.....	181
9.7.4	Crystal violet staining of biofilms .....	181
<b>9.8</b>	<b>Immune response to <i>M. abscessus</i> .....</b>	<b>183</b>
9.8.1	J774 cell line and maintenance.....	183
9.8.2	Preparation of bacterial inoculum for infection assays .....	183
9.8.3	Macrophage infections - Measuring intracellular survival using CFUs.....	184
<b>10</b>	<b>Appendices .....</b>	<b>185</b>
	Appendix 1 – Selected sections of CSLM images.....	186
	Appendix 2 – Common downregulated DEGs in <i>M. abscessus</i> biofilms t1 and t2 .....	190
	Appendix 3 – Common upregulated DEGs in <i>M. abscessus</i> biofilms t1 and t2.....	191
	Appendix 4: Chromatographs of alditol acetates of capsular monosaccharides.....	195
	Appendix 5: Permission rights.....	198
<b>11</b>	<b>References.....</b>	<b>199</b>

## LIST OF FIGURES

Figure 1.1: Mycobacterial cell envelope and <i>M. abscessus</i> mycolic acid subclasses.....	18
Figure 1.2: Generic structure of GPLs and the <i>gpl</i> locus in <i>M. abscessus</i> .....	23
Figure 1.3: Graphic representation of biofilm formation and pellicular biofilms.....	27
Figure 2.1. <i>M. abscessus</i> pellicle. Six-day old pellicle grown in Sauton's media in a 24-well plate .....	38
Figure 2.2. Scanning electron micrographs of <i>M. abscessus</i> pellicles.....	39
Figure 2.3. Confocal laser scanning microscopy pictures of mature <i>M. abscessus</i> biofilms.....	42
Figure 2.4. Correlation between ECM components and bacilli in <i>M. abscessus</i> biofilms. ....	43
Figure 3.1: Differentially expressed genes in <i>M. abscessus</i> biofilms. ....	56
Figure 3.2: Enriched metabolic pathways in <i>M. abscessus</i> biofilms .....	59
Figure 4.1: Autoradiographs of 2D TLC silica plates of outside and inside apolar lipids of <i>M. abscessus</i> planktonic and biofilm cells.....	78
Figure 4.2: Autoradiographs of 2D TLC silica plates of outside and inside apolar lipids of <i>M. abscessus</i> planktonic and biofilm cells.....	79
Figure 4.3: Autoradiographs of 2D TLC silica plates of polar lipids of <i>M. abscessus</i> planktonic and biofilm cells.....	80
Figure 4.4: Autoradiographs of 2D argentated TLC silica plates of MAMEs of <i>M. abscessus</i> planktonic and biofilm cells .....	83
Fig. 4.6: Plot of the percentage of relative abundance of different monosaccharides found in <i>M. abscessus</i> capsule .....	86
Figure 5.1: Single colony morphology of <i>M. abscessus</i> clinical isolates 1-6, with <i>M. abscessus</i> S and R strains as reference .....	97
Figure 5.2: Assessment of growth of <i>M. abscessus</i> clinical isolates in different conditions .....	98
Figure 5.3: Intracellular survival of <i>M. abscessus</i> clinical isolates in murine macrophages .....	103
Figure 6.1: Formation of biofilms in <i>M. abscessus</i> clinical isolates .....	114
Figure 6.2: Lipid profiles of <i>M. abscessus</i> S and R for planktonic and biofilm growth.....	116
Figure 6.4: Autoradiographs of 2D TLCs showing the lipid profile of <i>M. abscessus</i> clinical isolates grown in biofilms .....	120
Figure 6.5: Autoradiographs of 2D TLCs of mycolic acids of <i>M. abscessus</i> clinical isolates from biofilm and planktonic samples .....	121
Figure 6.6: Autoradiographs of 2D TLC silica plates showing deacetylated GPLs of <i>M. abscessus</i> clinical isolates .....	122
Figure 7.1: A maximum-likelihood tree from the nucleotide sequences alignment of the core genome of <i>M. abscessus</i> isolates.....	132

## LIST OF TABLES

Table 1.1: List of pathogenic NTMs grouped by growth rate and pathogenicity.....	5
Table 1.2: List of current treatment options of <i>M. abscessus</i> infections.....	13
Table 1.3: List of resistance mechanisms in <i>M. abscessus</i> .....	14
Table 2.1. Relative biovolume and correlation coefficients of ECM components as compared to bacilli in the biofilm.....	43
Table 3.1: Top 50 DEGs in 5-day old <i>M. abscessus</i> biofilms (t1).....	54
Table 3.2: Top 50 DEGs in 7-day old <i>M. abscessus</i> biofilms (t2).....	55
Table 3.3: Enriched metabolic pathways for early biofilm growth stage at day 5, t1 .....	64
Table 3.4: Enriched metabolic pathways for late biofilm growth stage at day 7, t2 .....	65
Table 4.1: Relative abundance of sugars in the <i>M. abscessus</i> ECM, showing median and standard deviation for 3 independent experiments.....	86
Table 5.1: Minimum inhibitory concentrations (MIC) of antibiotic susceptibility.....	101
Table 7.1: GPL biosynthesis related genes of <i>M. abscessus</i> type strains ( <i>M. abs</i> S, <i>M. abs</i> R) and six clinical isolates (CI-1-6).....	135
Table 7.2: Genes related to antimicrobial resistance in <i>M. abscessus</i> type strains ( <i>M. abs</i> S, <i>M. abs</i> R) and six clinical isolates (CI-1-6).....	140
Table 7.3: Genotypes in the <i>erm41</i> gene. Single nucleotide polymorphisms (SNPs) and amino acid (AA) substitutions in the <i>erm41</i> gene were identified for each strain.....	142
Table 9.1: Sauton's minimal media compositions.....	165
Table 9.2: Complete list of strains used in this study.....	165
Table 9.3: List of dyes used for biofilm matrix staining.....	169
Table 9.5: Solvent systems for separation of lipid species using thin layer chromatography.....	177
Table 9.6: Concentrations (µg/ml) and dilutants of antibiotics used for determination of minimum inhibitory concentration.....	182
Table 9.7: Breakpoints used for interpretation of antibacterial susceptibility testing.....	182

## ABBREVIATIONS

°C	Degrees centigrade
1D	One dimension
2D	Two dimensions
ABC	ATP-binding cassette
Ac <sub>2</sub> PIM <sub>2</sub> ,	Diacyl phosphatidyl- <i>myo</i> -inositol dimannoside
Ac <sub>2</sub> PIM <sub>6</sub>	Diacyl phosphatidyl- <i>myo</i> -inositol hexamannoside
AF	AlexaFluor 647
AG	Arabinogalactan
ATP	Adenosine triphosphate
BCG	Bacillus Calmette-Guérin
CF	Cystic fibrosis
CFTR	Cystic fibrosis transmembrane conductance regulator
CFU	Colony forming unit
CI	Clinical isolate
CLSM	Confocal laser scanning microscopy
DNA	Deoxyribonucleic acid
ECM	Extracellular matrix
eDNA	Extracellular DNA
FAME	Fatty acid methyl esters
FMA	Free mycolic acid
g	gram
GFP	Green fluorescent protein
GPL	Glycopeptidolipid
HIV	Human immunodeficiency virus
LAM	Lipoarabinomannan
LM	Lipomannan
M	Molar
MAC	Mycobacterium avium complex
mAGP	Mycetyl-arabinogalactan-peptidoglycan
MALDI-TOF	Matrix assisted laser desorption ionisation-time of flight
MAME	Mycolic acid methyl esters
MCE	Mammalian cell entry
MDAG	Meromycolate diacylglycerol
mg	milligram
MIC	Minimum inhibitory concentration
MIM	Mycobacterial inner membrane
ml	Millilitre
MmpL	Mycobacterial membrane protein large
MOI	Multiplicity of infection
MOM	Mycobacterial outer membrane
NADH	Reduced nicotinamide adenine dinucleotide
NR	Nile Red

NTM	Nontuberculous mycobacteria
OADC	Oleic acid, albumin, dextrose, catalase
OD	Optical density
PBS	Phosphate buffer saline
PCC	Pearson's correlation coefficient
PG	Peptidoglycan
PI	Propidium iodide
PIM	Phosphatidyl- <i>myo</i> -inositol mannosides
PVC	Polyvinyl chloride
RGM	Rapidly growing mycobacteria
RNA	Ribonucleic acid
rpm	rotations per minute
SD	Standard deviation
sDEG	Significant differentially expressed gene
SEM	Scanning electron microscopy
SGM	Slow growing mycobacteria
SNP	Single nucleotide polymorphism
SR	Sypro Ruby
SSTI	Skin and soft tissue infections
TAG	Triacylglycerol
TBAH	<i>tetra</i> -butylammonium hydroxide
TDM	Trehalose dimycolate
TFA	Trifluoroacetic acid
TLC	Thin layer chromatography
TLR	Toll-like receptor
TMM	Trehalose monomycolate
WGS	Whole genome sequencing

# **1 Introduction**

## **1.1 The genus *Mycobacterium* and introduction to *Mycobacterium abscessus***

First introduced in 1896 by Lehmann and Neumann, the genus *Mycobacterium* belongs to the phylum Actinobacteria which are characterized by their rod shape and a high GC content (Goodfellow, 2012; van Ingen, 2014). Mycobacteria are non-spore forming, non-motile, slightly curved or straight rods that are aerobic, although some species have been shown to grow under reduced oxygen conditions. The most unique and defining feature of this genus is the thick, waxy, lipid-rich cell wall which prevents successful Gram-staining. This feature resulted in mycobacteria being defined by acid-fast staining where there is a resistance to decolorization when the bacteria are stained with carbol-fuchsin and decolorized with dilute hydrochloric acid (Percival and Williams, 2013; van Ingen, 2014).

The key players of this genus responsible for disease in humans are *Mycobacterium tuberculosis*, *Mycobacterium leprae* and *Mycobacterium ulcerans*, causing tuberculosis, leprosy and Buruli ulcer disease respectively (van Ingen, 2014). Much scientific research has been focused on *M. tuberculosis* to understand its genetics, physiology, and structure to develop novel and more effective treatments. The management of tuberculosis currently relies on the Bacille Calmette-Guérin (BCG) vaccine or antibiotic therapy. The BCG vaccine, the only commercially available vaccine against tuberculosis, was discovered over 100 years ago and has variable efficacy in preventing pulmonary disease in adults, and as a result, some countries are currently not recommending vaccination (Luca and Mihaescu, 2013; Dockrell and Smith, 2017). Antibiotic therapy against tuberculosis is lengthy, requiring six months of regular access to antibiotics, which poses an issue in developing countries where distribution and healthcare access are often an issue. Additionally, the emergence of multidrug-resistant and extensively drug-resistant *M. tuberculosis* points to the alarming need to develop new, more effective treatments to combat tuberculosis (WHO, 2019).

### **1.1.1 Non-tuberculous mycobacteria**

Non-tuberculous mycobacteria (NTMs) are a group of ubiquitous, free-living, environmental mycobacteria other than *M. tuberculosis* and *M. leprae*. Over 200 species of NTMs have been identified to date, however many remain unclassified (Hoefsloot *et al.*, 2013; Ratnatunga *et al.*, 2020). The majority of NTMs do not cause disease in humans, however, in the past decades, it has become increasingly clear that some are opportunistic pathogens capable of causing a wide variety of diseases in immunocompromised humans. The prevalence of NTM disease is on the rise worldwide and yet, due to lack of information, these infections are easily missed, misdiagnosed and difficult to treat (Ratnatunga *et al.*, 2020).

Mycobacteria, and therefore NTMs, can be classified according to their growth rate (**Table 1.1**) as slowly growing mycobacteria (SGM), if it takes over 7 days for visible colonies to appear on agar plates, or rapidly growing mycobacteria (RGM) if visible colonies are formed within 7 days. There is an implied correlation between growth rate and virulence given that most of the successful human pathogens from the mycobacteria group are SGM, such as *M. tuberculosis*, *Mycobacterium avium* and *M. leprae*. Saprophytic mycobacteria, which obtain nutrients by absorbing dissolved organic material, can sometimes be detected in clinical samples but do not regularly cause disease in humans (Johansen, Herrmann and Kremer, 2020).

NTMs are found in different types of water, soils, food products, domestic and wild animals (Ratnatunga *et al.*, 2020). Their natural habitat inevitably overlaps with the human habitat as they are found in water distribution systems, pipelines, sewers, and showerheads, eventually leading to opportunistic infections. Genotypic studies in Europe and the USA have shown a high degree of overlap between clinical and environmental NTM isolates (Gebert *et al.*, 2018). NTM disease prevalence has been steadily increasing in the western world, largely in healthcare-associated infections owing to the ability of NTMs to survive in water distribution systems by forming biofilms - bacterial communities with an extracellular matrix that are resistant to disinfectants and mechanical force (El Helou *et al.*, 2013). Several hospital

outbreaks worldwide have been noted as a result of contaminated heater-cooler devices, cosmetic surgery, or catheter-associated infections (Phillips and von Reyn, 2001; Baker *et al.*, 2017; Ogunremi *et al.*, 2017).

**Table 1.1: List of pathogenic NTMs grouped by growth rate and pathogenicity**

	<b>Slow growing mycobacteria (SGM)</b>	<b>Rapidly growing mycobacteria (RGM)</b>
Opportunistic	<p><i>M. avium</i> complex (MAC):</p> <ul style="list-style-type: none"> <li>• <i>M. avium</i></li> <li>• <i>M. intraacellulare</i></li> <li>• <i>M. chimaera</i></li> </ul> <p><i>M. haemophilum</i></p> <p><i>M. xenopi</i></p> <p><i>M. kansasii</i></p> <p><i>M. simiae</i></p> <p><i>M. malmoense</i></p> <p><i>M. colombiense</i></p>	<p><i>M. abscessus</i> complex:</p> <ul style="list-style-type: none"> <li>• <i>M. abscessus</i> subsp. <i>abscessus</i></li> <li>• <i>M. abscessus</i> subsp. <i>bolletii</i></li> <li>• <i>M. abscessus</i> subsp. <i>massilinense</i></li> </ul> <p><i>M. chelonae</i></p> <p><i>M. fortuitum</i> group</p> <p><i>M. mucogenicum</i> group</p>
True pathogens	<p><i>M. marinum</i></p> <p><i>M. ulcerans</i></p>	
Saprophytes	<p><i>M. gordonaie</i></p> <p><i>M. terrae</i> complex</p>	<p><i>M. smegmatis</i></p> <p><i>M. vaccae</i></p>

### **1.1.2 Non-tuberculous mycobacteria as etiological agents**

NTMs can cause a variety of diseases in the body including skin and soft tissue infections (SSTI), lymphadenitis, aseptic meningitis, but most commonly lung infections (Faria, Joao and Jordao, 2015; Ratnatunga *et al.*, 2020). Disseminated NTM disease in patients infected with human immunodeficiency virus (HIV) was the first to raise awareness of NTMs as an etiological agent of disease in 1980s (Greene *et al.*, 1982; Sousa *et al.*, 2015). Since then, disseminated and mixed culture NTM infections have been found in other immune-compromised populations such as those with chronic pulmonary disease, renal failure, cystic fibrosis (CF), transplant recipients, and leukaemia among others. *Mycobacterium fortuitum*, *Mycobacterium chelonae* and *Mycobacterium abscessus* are amongst the RGMs found commonly in postsurgical and post-traumatic infections as well as other healthcare-associated infections (Tortoli, 2009; Faria, Joao and Jordao, 2015).

Pulmonary NTM disease has a complex pathology with many unanswered questions remaining about transmission, length of incubation and true prevalence of the disease. Incubation periods can vary from months to years because of slow growth and low virulence, making diagnosis and determination of the origin of infection difficult. The true estimate of the NTM disease burden is difficult to estimate given that the status of NTM infections as notifiable or reportable diseases varies between, and even within, countries (Prevots *et al.*, 2017). For example, in Queensland, Australia, instances of NTM infections have been notifiable since the 1960s allowing for accurate tracking of isolates and mapping of the bacterial behaviour in the population. For example, there was a significant shift in the gender of the affected patients - in 2005 mainly elderly females were affected but in 1999 it was predominantly males (Thomson, 2010). The most telling figure from this population, however, is the doubling of cases in just four years, allowing for projections that indicate that in comparison to 2012, cases in 2040 could increase by a factor of 10 - demonstrating the urgent need to study NTM pathogenesis (Thomson, Donnan and Konstantinos, 2017).

In the USA and Canada, NTMs are now more commonly isolated from pulmonary infections than *M. tuberculosis*, with an annual increase of 8.4% in documented isolates between 1997 and 2003 (Taiwo and Glassroth, 2010). Similar figures were reported in Germany, Denmark and the UK, with incidences tripling from 0.9 to 2.9 per 100 000 people in the span of 11 years (Andréjak *et al.*, 2010; Moore *et al.*, 2010; Diel *et al.*, 2017). In South Korea, a 62% increase in cases of NTM disease was seen between 2002 and 2012, and in China, the rate of infection went up from 3 to 8.5% between 2008 and 2012 (Park *et al.*, 2010; Wu *et al.*, 2014).

A detailed understanding of how NTM disease is established in humans is still lacking, and questions remain about the percentage of population exposed, the predisposing factors for successful infections, the mechanism of colonization without tissue invasion, and aspects that determine clearance in the host (Ratnatunga *et al.*, 2020). Some populations were identified that are particularly at risk of acute and chronic pulmonary NTM infections, including patients with previous mycobacterial or Aspergillus infections, Lady Windermere syndrome, bronchiectasis, and, most predominantly, CF (Medjahed, Gaillard and Reyrat, 2010; Ratnatunga *et al.*, 2020). Interestingly, reports have shown that the BCG vaccine may offer protection against *M. avium* complex (MAC) and *M. abscessus*, explaining the rise of NTM infections in countries where administration of the vaccine is reduced (Abate *et al.*, 2019).

NTM infections are difficult to detect as they are not routinely looked for in clinical laboratories, and once detected they are problematic to treat as most exhibit intrinsic or adaptive resistance to routinely used antibiotics. Standard therapy for pulmonary NTM infection caused by SGM is 12-18 months of antibiotics, with a rate of recurrence due to reinfection with MAC currently at 30-50% (Philley and Griffith, 2015; Stout, Koh and Yew, 2016). Not only are there numerous side effects of prolonged and rigorous antibiotic intake, but treatment can often be financially draining as well. In the USA, the treatment of *M. abscessus* infections can cost up to £37,500 , whereas for MAC infections the average cost of treatment per person per year is

estimated at £9,300 in Canada, £12,000 in the USA, £9,700 in the UK, £10,500 in Germany and £16,000 in France (Kasperbauer and De Groote, 2015; Goring *et al.*, 2018).

### 1.1.3 The *M. abscessus* complex

*M. abscessus* is an NTM commonly found in soil and water but it is also an emerging, opportunistic human pathogen capable of causing severe and chronic infections in immunocompromised patients (Griffith *et al.*, 2007). This bacterium was long considered to be a subspecies of *M. chelonae*, an NTM that largely causes ocular infections in immunocompromised patients. Although *M. abscessus* was initially named as a new species in 1953 after being isolated from a knee abscess, the similarity between the two bacteria continued to cause confusion until 1992 when they were officially separated by quantitative DNA hybridization (Moore and Frerichs, 1953; Kusunoki and Ezaki, 1992). Distinguishing the two species is clinically important as they cause different types of disease with distinct treatment options. Namely, *M. chelonae* is susceptible to macrolides, a group of antibiotics containing erythromycin and clarithromycin, while *M. abscessus* contains a gene that provides inducible macrolide resistance (Nessar *et al.*, 2012; Griffith *et al.*, 2015).

Today, although still debated, it is widely accepted that the *M. abscessus* complex (*M. abscessus sensu lato*) consists of *M. abscessus* subsp. *abscessus* (or *M. abscessus sensu stricto*), *M. abscessus* subsp. *massiliense* and *M. abscessus* subsp. *bolletii* – from hereinafter referred to as *M. abscessus*, *M. massiliense* and *M. bolletii* (Tortoli *et al.*, 2016). The subspecies are distinguished using sequence-based methods of housekeeping genes such as *hsp65*, *rpoB*, *secA* and 16S rRNA, based on guidelines established in 2017 (Griffith *et al.*, 2015; Tortoli *et al.*, 2016; Haworth *et al.*, 2017). In a clinical setting, the subspecies are distinguished by conventional sequencing with a particular focus on the *erm41* gene which can be used for the prediction of clarithromycin resistance (Tortoli *et al.*, 2017; Mase *et al.*, 2019). *M. bolletii* infections are rare in comparison to those with *M. abscessus* and *M. massiliense*, particularly in

Europe and the USA, which may suggest differences in pathogenicity and adaptation between the subspecies (Johansen, Herrmann and Kremer, 2020).

#### **1.1.4 *M. abscessus* pathogenicity and prevalence**

*M. abscessus* causes versatile diseases in humans – SSTI, central nervous system infections, disseminated diseases, ocular infections and, principally, infections of the respiratory tract (Medjahed, Gaillard and Reyrat, 2010; Lee *et al.*, 2015). While there have been reports of immunocompetent people suffering from *M. abscessus* infections, the vast majority of infections occur in immunocompromised patients (Piersimoni and Scarparo, 2009; Varghese *et al.*, 2012; Kadota *et al.*, 2019). Biofilms formed in water systems or on contaminated medical equipment are likely sources of *M. abscessus*, however, transmission from patient-to-patient was shown to be possible using whole genome sequence analysis of *M. abscessus* clinical isolates (Jönsson *et al.*, 2007; Bryant *et al.*, 2016; Yan *et al.*, 2020).

Determining the true disease burden of *M. abscessus* is challenging due to the difficulty in diagnosing *M. abscessus* from clinical samples in the past. However, it is believed that 2.6-17% of all NTM pulmonary infections in the USA are caused by *M. abscessus*, a prevalence that is second only to MAC (Prevots *et al.*, 2010). *M. abscessus* is highly prevalent in East Asia where *M. abscessus* complex comprised 17.2% of all clinical NTM isolates in Taiwan (2000-2008), 14.9% in Shanghai, China (2008-2012) and 26.7% in South Korea (2008-2012) (Hernández-Garduño and Elwood, 2010; Park *et al.*, 2010; Wu *et al.*, 2014). In a large study of mycobacterial isolates in Iran spanning from 2011 to 2017, about 18% of all NTM isolates contained the *M. abscessus* complex (Ayoubi *et al.*, 2020). MAC infections are more prevalent in the USA and Europe, while the *M. abscessus* complex is more common in East Asia (Simons, 2011).

SSTIs caused by *M. abscessus* are acquired through direct contact with contaminated water, such as spa or hot springs, through contaminated materials or in postsurgical patients (Lee *et al.*, 2015). *M. abscessus* has been reported to cross the blood-brain barrier and cause meningitis

and meningoencephalitis, as well as bacteraemia, which is often associated with catheter use (Talati *et al.*, 2008; El Helou *et al.*, 2013). Outbreaks mainly occur in clinical settings, following cosmetic procedures, intravenous infusion of cell therapy or mesotherapy, likely due to contaminated disinfectants or equipment (Furuya *et al.*, 2008; Koh *et al.*, 2010).

*M. abscessus* is the most commonly isolated RGM from lung infections (Medjahed, Gaillard and Reyrat, 2010; Choi *et al.*, 2018; Kwak *et al.*, 2019). The presence of a comorbid, pre-existing condition and *M. abscessus* infection leads to a rapid decline in lung function, chronic disease, mortality, and poor treatment outcome. As previously outlined, the incidence of pulmonary NTM disease is increasing worldwide – likely as a result of an aging population, instances of prior health conditions, increasing use of immunosuppressive drugs, and environmental exposure (Connell and Wilkie, 2019).

### **1.1.5 *M. abscessus* in cystic fibrosis patients**

CF is a hereditary autosomal recessive disorder causing improper functioning of the cystic fibrosis transmembrane conductance regulator (CFTR) which results in a thick and sticky mucus covering cells in the respiratory, gastrointestinal, and male reproductive tracts. Lungs are particularly sensitive to poor clearance of thick mucus allowing for repeated bacterial and fungal infections (Viviani *et al.*, 2016). An estimated 3 to 10% of CF patients in the USA and Europe are infected with *M. abscessus*, leading to either a poor clinical outcome, or life-long persistent infection without symptoms (Cystic Fibrosis Foundation, 2010). Given its high prevalence in CF patients, *M. abscessus*, along with *Staphylococcus aureus*, *Haemophilus influenzae* and *Pseudomonas aeruginosa*, is regarded as a ‘superbug’ that plagues this patient group (Haley, Colmer-Hamood and Hamood, 2012; Seddon *et al.*, 2013). A recent study demonstrated that CFTR might have a specific role in the immune response to *M. abscessus* infections, but not other mycobacteria, explaining why CF patients seem especially susceptible to these infections. CFTR appears to have a role in neutrophil chemotaxis which, along with recruitment of macrophages during *M. abscessus* infections, leads to granuloma formation and

production of radical oxygen species (ROS), and results in sequestering of *M. abscessus*. In a zebrafish model with defective *CFTR*, *M. abscessus* was able to infect more quickly, and macrophage activity and neutrophil recruitment were reduced (Bernut, Nguyen-Chi, *et al.*, 2016; Bernut *et al.*, 2019).

### **1.1.6 Treatment and antimicrobial resistance in *M. abscessus***

The current recommendation for treatment of *M. abscessus* infections, as outlined in **Table 1.2**, is combination therapy of clarithromycin and an aminoglycoside coupled with another injectable drug such as cefoxitin or imipenem (Griffith *et al.*, 2007). SSTIs are typically treated by a combination of surgical intervention and drug therapy, while lung infections are treated by combination therapy for at least two to four months with the goal of negative sputum samples after 12 months (Griffith *et al.*, 2007). None of the currently available treatments are curative or have been shown as effective in long-term sputum conversion in patients with chronic lung disease. Successful treatment of pulmonary disease is estimated at 45% but depends on the subspecies of *M. abscessus* causing the infection (56% success for *M. massiliense*, 33.0% for *M. abscessus*) (Kwak *et al.*, 2019).

The biggest impediment in the treatment of *M. abscessus* lies in the many ways it can confer resistance to antibiotics, which can be natural but also acquired or adapted (**Table 1.3**). The first obstacle for many antibiotics is the thick mycobacterial cell wall which acts as a physical barrier and has a lipid-rich content which increases hydrophobicity leading to low permeability. Inside the bacteria is the ‘intrinsic resistome’, consisting of numerous systems that confer resistance such as: (1) efflux pumps (members of the ATP-binding cassette (ABC) transporters and mycobacterial membrane protein large (MmpL) family), (2) antibiotic-modifying enzymes (phospho- and acetyltransferases effective against aminoglycosides), (3) antibiotic degrading enzymes ( $\beta$ -lactamases that degrade  $\beta$ -lactams), (4) target-modifying enzymes (such as 23S rRNA methyltransferase encoded by *erm41*) and (5) enzymes responsible for detoxification

(mercury operon regulator *MerR* providing protection against several metal compounds) (Nessar *et al.*, 2012).

Adaptive resistance occurs as a response to the external environment, following exposure to antibiotics, but without long-term genetic changes. This is particularly exemplified with macrolide resistance where prolonged exposure to clarithromycin or azithromycin induces the expression of *erm41*, encoding a ribosome methyltransferase which methylates a nucleotide in the 23S rRNA active site (Kim *et al.*, 2015; Johansen, Herrmann and Kremer, 2020). Decreased sensitivity to antibiotics happens after prolonged exposure or due to point mutations, specifically to aminoglycosides (as a result of a mutation in the *rrs* 16S rRNA gene) and clarithromycin (resistance through *rrl* and *erm41* genes) since *M. abscessus* encode a single copy of each gene, which increases the probability of phenotypic expression of mutations (Prammananan *et al.*, 1998; Brown-Elliott *et al.*, 2002; Griffith *et al.*, 2007).

In addition, there are differences in antibiotic susceptibility within the *M. abscessus* complex. *M. abscessus* and *M. bolletii* strains that contain a T28C polymorphism in the *erm41* gene exhibit inducible resistance to macrolides, while *M. massiliense* encodes for a truncated version of the *erm41* gene making this strain susceptible to macrolides (Nash *et al.*, 2009; Nessar *et al.*, 2012; Tortoli *et al.*, 2017; Mase *et al.*, 2019) The importance in identifying the subspecies prior to treatment was evidenced in a study where clarithromycin-based combination therapy effectively cleared 100% of *M. massiliense* but only 27% of *M. abscessus* (Koh *et al.*, 2011).

**Table 1.2: List of current treatment options of *M. abscessus* infections (Lee *et al.*, 2015; Novosad *et al.*, 2016)**

Type of disease	Initial treatment regimen	Treatment duration	Source
<b>Skin and soft tissue infections</b>	Macrolide in combination with amikacin, plus cefoxitin or imipenem, and surgical intervention	Minimum 4 weeks	Griffith, Aksamit, Brown-Elliott, <i>et al.</i> , 2007
<b>Pulmonary infection</b>	Macrolide in combination with intravenous antimicrobials (amikacin or cefoxitin)	Continuous until sputum samples are negative for 12 months	Griffith, Aksamit, Brown-Elliott, <i>et al.</i> , 2007
<b>Central nervous system</b>	Clarithromycin-based combination (amikacin usually used for at least the first week)	12 months	Lee <i>et al.</i> , 2012
<b>Bacteraemia</b>	Combination of two active antimicrobial agents and likely a surgical intervention for debridement of the infection site	4 weeks after last positive blood culture test	El Helou <i>et al.</i> , 2013
<b>Ocular infection</b>	Topical agents (amikacin, clarithromycin) and/or antimicrobial drugs and/or surgery	6 weeks to 6 months	Moorthy, Valluri and Rao, 2012

**Table 1.3: List of resistance mechanisms in *M. abscessus*** (Nessar *et al.*, 2012; Johansen, Herrmann and Kremer, 2020)

Drug	Target	Proteins (genes) involved	Reference
Aminoglycosides	Protein synthesis – 16S rRNA	Aminoglycoside acetyltransferase ( <i>MAB_4395</i> ) Aminoglycoside phosphotransferases ( <i>MAB_0327, MAB_0951</i> )	Rominski, Selchow, <i>et al.</i> , 2017; Dal Molin <i>et al.</i> , 2018
$\beta$ -lactams	Cell wall, penicillin-binding proteins	$\beta$ -lactamases ( <i>MAB_2875</i> )	Dubée <i>et al.</i> , 2014
Isoniazid	Mycolic acid biosynthesis - InhA	Catalase/peroxidase ( <i>katG – MAB_2470c</i> )	Rominski, Selchow, <i>et al.</i> , 2017
Rifampicin	Transcription – RNA polymerase	Rifampicin ADP-ribosyltransferase ( <i>MAB_0951</i> )	Rominski, Roditscheff, <i>et al.</i> , 2017
Macrolides	Protein synthesis – 23S rRNA	23S RNA methyltransferases ( <i>erm41</i> )	Nash <i>et al.</i> , 2009
Tetracycline	Protein synthesis	Inactivation by <i>MabTetX</i> ( <i>MAB_1496c</i> )	Rudra <i>et al.</i> , 2018
Metal compounds	-	Efflux pumps and detoxification through the mercury operon regulator <i>MerR</i> ( <i>MAB_p05c</i> ) and detoxification enzyme <i>MerA</i> ( <i>MAB_p06</i> )	Ripoll <i>et al.</i> , 2009

## 1.2 The cell envelope of mycobacteria

Mycobacterial species are notorious for their thick hydrophobic cell wall rich in complex lipids which make up approximately 60% of the cell wall weight. These lipids are structurally and chemically unique compared to other bacteria and contribute to pathogenicity, hydrophobicity, and permeability of the cell wall (Jankute *et al.*, 2015; Chiaradia *et al.*, 2017). Targeting the biosynthesis of the cell wall and its components has previously led to the successful development of anti-tuberculosis drugs such as ethionamide and isoniazid which inhibit InhA, an enoyl acyl carrier protein reductase (Jackson, 2014).

The capsule, present on the outermost layer of the cell envelope, is ~30 µm thick and, while its composition may vary between species, it predominantly consists of neutral polysaccharides, proteins and, in a minor proportion, lipids (Lemassu, Ortalo-Magné, Bardou, Silve, Lanéelle and Daffé, 1996; Sani *et al.*, 2010). The capsular layer is stripped by detergents, normally added into the media to prevent clumping of mycobacteria, when cultures are grown under laboratory conditions (Sani *et al.*, 2010). The main polysaccharides found in the capsule are α-D-glucan, D-mannan and D-arabinomannan. α-glucan in mycobacteria consists of repeating units of glucose attached by α-1,4 glycosidic linkages and α-1,6 branching and is thought mainly to contribute to the storage of carbon and evasion of the host immune system (Rashid *et al.*, 2016). The layer beneath the capsule is an outer-membrane segment that contains solvent extractable lipids that interact with mycolic acids in the core mycolyl-arabinogalactan-peptidoglycan (mAGP) complex (Jankute *et al.*, 2015). The three main components of the mAGP complex (**Fig. 1.1A**), conserved across mycobacterial species, are: 1) unique mycolic acids, 2) arabinogalactan polysaccharide (AG) and 3) network of peptidoglycan (PG) (Jankute *et al.*, 2015).

The mycobacterial outer membrane (MOM) contains lipids connected to mycolic acids in the mAGP complex. Triacylglycerol (TAG), trehalose mono- and di-mycolate (TMM and TDM,

respectively) and diacyltrehalose (DAT) are all found in this layer (Marrakchi, Lanéelle and Daffé, 2014). Mycolic acids are long-chain fatty acids (C<sub>60-90</sub>) that form an integral part of the mAGP by contributing to the fluidity and permeability of the cell wall, and they are covalently linked to AG via ester bonds (Jankute *et al.*, 2015).

The next segment of the mAGP is AG, a branched macromolecule composed of galactose (Gal) and arabinose (Ara) in the furanose (*f*) form (Besra, 1998). The subsequent layer is composed of PG which provides shape and osmotic stability to the cell and can be found in almost all bacteria in the same basic core structure of a glycan backbone with short, cross-linked peptide sidechains. PG in mycobacteria is formed of repetitive units of N-acetylglucosamine (GlcNac) and N-acetylmuramic acid (MurNac) and is unique in that a portion of MurNac residues get modified to N-glycolymuramic acid (N-MurGlyc) (Alderwick *et al.*, 2015; Jankute *et al.*, 2015).

The final layer of the mycobacterial cell wall is the plasma membrane composed of a phospholipid bilayer and referred to as the mycobacterial inner membrane (MIM) (Jankute *et al.*, 2015). MIM is rich in various phospholipids including cardiolipin (CL), phosphatidylinositol (PI), phosphatidylethanolamine (PE), phosphatidyl-*myo*-inositol mannosides (PIMs) and acetylated versions of PIMs, most commonly diacyl phosphatidyl-*myo*-inositol dimmanoside (Ac<sub>2</sub>PIM<sub>2</sub>) and di-acetylated phosphatidyl-*myo*-inositol hexamannosides (Ac<sub>2</sub>PIM<sub>6</sub>) (Bansal-Mutalik and Nikaido, 2014). Lipomannan (LM) and lipoarabinomannan (LAM) are bound to the plasma membrane through PIM anchors and have an important role in host immune response during infection, the permeability of the cell envelope, regulation of cell septation and division, and maintenance of the inner membrane integrity (Jackson, 2014).

There are differences in the cell wall structure across the genus *Mycobacterium*, particularly between NTMs and the *M. tuberculosis* complex. Phthiocerol dimycocerosate (PDIMs) and sulfoglycolipids are present in *M. tuberculosis* but not in NTMs, while glycopeptidolipids

(GPLs) are only found in NTMs (Besra, 1998). Another significant difference is the variability in mycolic acid subclasses between mycobacterial species.

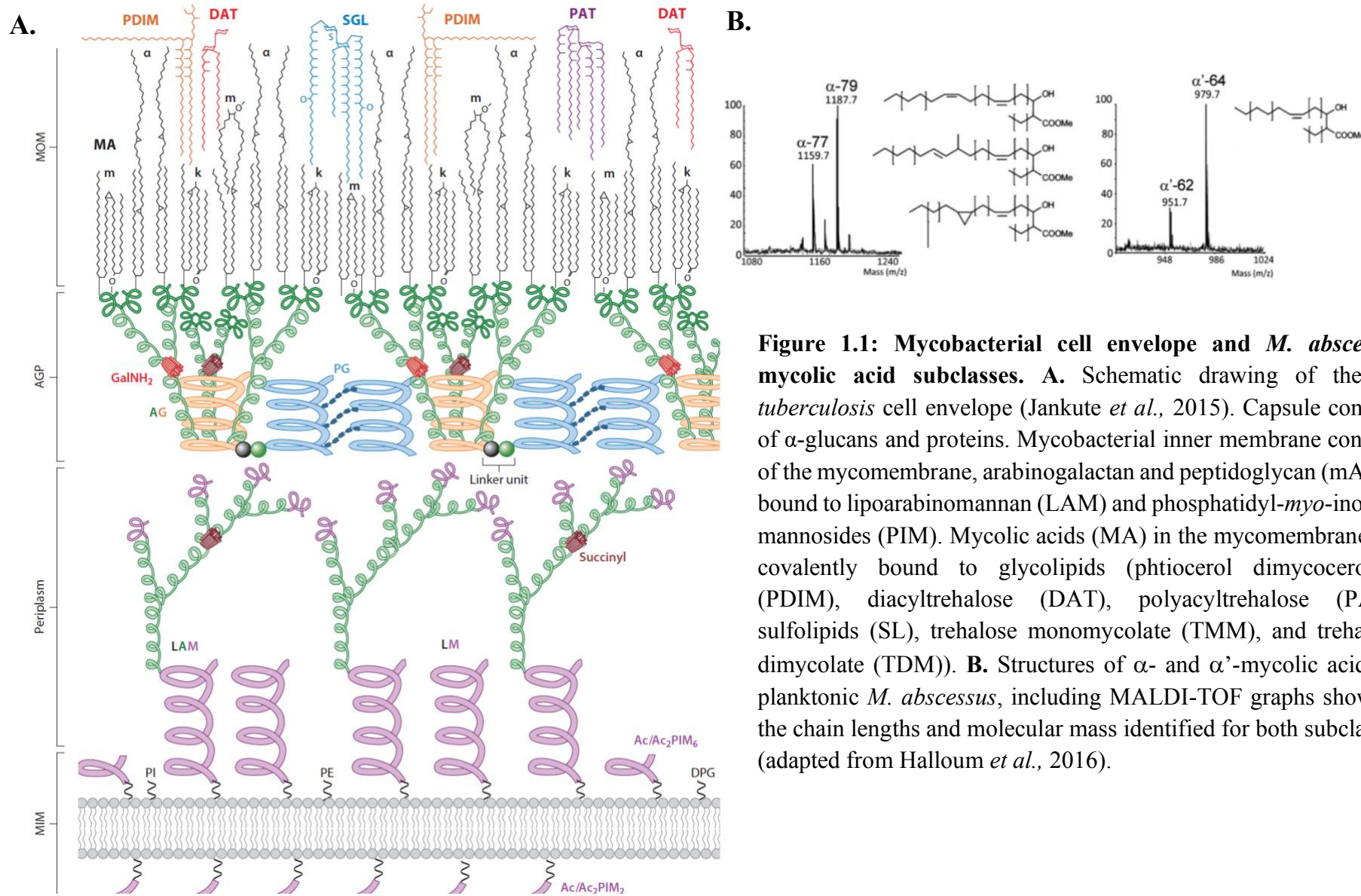


**Figure 1.1: Mycobacterial cell envelope and *M. abscessus* mycolic acid subclasses.** **A.** Schematic drawing of the *M. tuberculosis* cell envelope (Jankute *et al.*, 2015). Capsule consists of  $\alpha$ -glucans and proteins. Mycobacterial inner membrane consists of the mycomembrane, arabinogalactan and peptidoglycan (mAGP) bound to lipoarabinomannan (LAM) and phosphatidyl-*myo*-inositol mannosides (PIM). Mycolic acids (MA) in the mycomembrane are covalently bound to glycolipids (ptiocerol dimyocerosate (PDIM), diacyltrehalose (DAT), polyacyltrehalose (PAT), sulfolipids (SL), trehalose monomycolate (TMM), and trehalose dimycolate (TDM)). **B.** Structures of  $\alpha$ - and  $\alpha'$ -mycolic acids in planktonic *M. abscessus*, including MALDI-TOF graphs showing the chain lengths and molecular mass identified for both subclasses (adapted from Halloum *et al.*, 2016).

### 1.2.1 Mycolic acids

Mycolic acids are long-branched fatty acids with chain lengths of 60-90 carbons with an alkyl side chain and a hydroxyl group at the  $\alpha$  and  $\beta$  positions, respectfully (Minnikin *et al.*, 1982; Jankute *et al.*, 2015). They are covalently attached to the AGP complex and are present in the MOM in conjugation with sugars (Nataraj *et al.*, 2015). Mycolic acids are found predominantly in the genus *Mycobacterium* but are also present in *Corynebacterium*, *Nocardia* and *Rhodococcus* (Nataraj *et al.*, 2015). There are three distinct types of mycolic acids found in *M. tuberculosis*,  $\alpha$  (found in greatest abundance), keto and methoxy, however, subclasses differ in appearance and abundance within the genus *Mycobacterium* (Collins, Goodfellow and Minnikin, 1982). Epoxy mycolic acid is another subclass found in *M. smegmatis* but not in *M. tuberculosis* (Besra, 1998). In planktonic cells of *M. abscessus*,  $\alpha$ - and  $\alpha'$  are the only identified classes of mycolic acids, and their chain length and structure has been solved by MALDI-TOF and NMR (**Fig. 1.1B**).  $\alpha$ -mycolic acid is the most apolar of the mycolates and consists of a long carbon chain (C<sub>74</sub>-C<sub>80</sub>) containing two double bonds or *cis*-cyclopropyl groups in the meromycolic branch.  $\alpha'$ - mycolic acid has a shorter carbon chain (C<sub>60</sub>-C<sub>62</sub>) and contains only a single *cis*-double bond (Marrakchi, Lanéelle and Daffé, 2014).

In terms of synthesis, mycolic acids are derived from fatty acids essential for fundamental cell function, such as membrane biosynthesis, which are synthesized by a bi-modal fatty-acid synthase FAS-I (Brindley, Matsumura and Bloch, 1969). Therefore studying the mycolic acid biosynthesis pathway cannot be done through the generation of knock-outs due to the enzyme essentially (Nataraj *et al.*, 2015). The role of mycolic acids is not limited to the upkeep of the cell wall structure. Various studies of gene knock-outs of non-essential enzymes relevant to fatty acid synthesis in *M. smegmatis* revealed that mycolic acids play an extensive role in biofilm formation (Ojha *et al.*, 2005; Chen *et al.*, 2006).

## 1.2.2 Glycopeptidolipids in the cell wall of *M. abscessus*

GPLs are found in the outer layer of the MIM, and they contain a lipopeptide core with a 3-hydroxy or 3-methoxy C<sub>26</sub>-C<sub>33</sub> fatty acid chain linked to a tripeptide amino-alcohol core (Schorey and Sweet, 2008). While GPLs generally have the same lipopeptide core, they can vary in glycosylation, methylation, and acetylation patterns across mycobacterial species and serovars. They are differentiated based on the number of sugars linked to the lipopeptide core: apolar GPLs are di-glycosylated and polar GPLs are made by addition of 2,3,4-tri-hydroxylated rhamnose (**Fig. 1.2.A**). (Ripoll *et al.*, 2007). Acetylated GPLs are necessary for biofilm formation in *M. smegmatis* (Recht and Kolter, 2001).

The */gpl* locus that encodes GPL biosynthesis genes is highly conserved between *M. avium*, *M. abscessus*, and *M. smegmatis*, with minor differences (**Fig. 1.2.B**) (Gutiérrez *et al.*, 2018). *mps1* and *mps2* genes are responsible for the synthesis of the tripeptide-amino alcohol moiety. Glycosylation of the peptide is catalysed by *gft1* and *gft2*, and *gft3* is responsible for the addition of the extra rhamnose moiety to create triglycosylated GPLs. In *M. abscessus*, *atf1* and *atf2* sequentially transfer the acetyl residues (Ripoll *et al.*, 2007). Further, *rmt2*, *rmt3*, and *rmt4* genes participate in O-methylation of rhamnose, *fmt* in O-methylation of the lipid fraction and *rmlA* and *rmlB* in epimerization and activation of monosaccharides (Johansen, Herrmann and Kremer, 2020). The */gpl* locus also contains a set of genes responsible for translocation of GPLs across the plasma membrane – *mmpS4*, *mmpL4a* and *mmpL4b* – but the mechanism of translocation is still undetermined (Medjahed and Reyrat, 2009; Bernut, Viljoen, *et al.*, 2016; Johansen, Herrmann and Kremer, 2020).

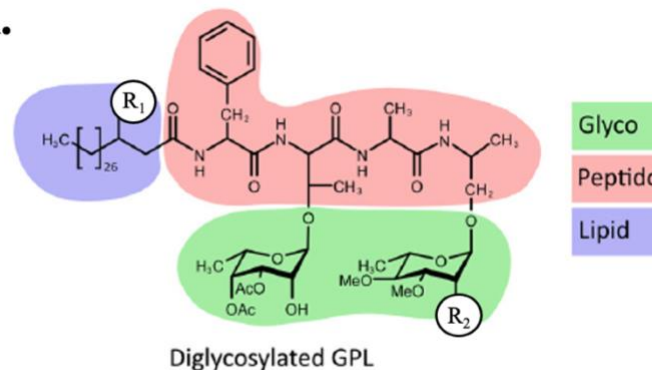
### 1.2.2.1 Morphological heterogeneity in *M. abscessus*

The presence or absence of GPLs in the cell wall of NTMs is linked to differences in colony morphology which can influence sliding motility, biofilm formation, interaction with host cells and pathogenicity. Strains with a smooth colony morphology produce and export GPLs and have a visibly glossy colony morphology on agar plates, while GPLs are absent in strains with

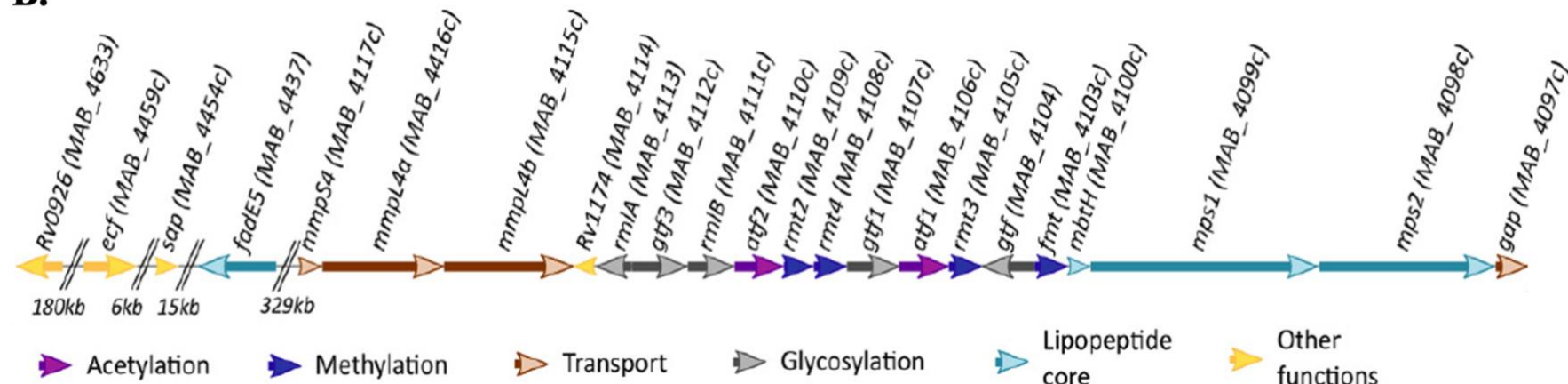
a rough morphology which have the appearance of a cording colony on agar. In *M. avium* mutants unable to produce GPLs were defective in biofilm formation and were less pathogenic than the smooth strains (Yamazaki *et al.*, 2006). However, the opposite was shown for *M. abscessus*. The GPL layer in the smooth strains masks underlying lipids, such as PIMs, that trigger the immune response through interactions with Toll-like receptor 2 (TLR2) which promotes the release of TNF- $\alpha$  and IL-8 and causes inflammation (Elizabeth R. Rhoades *et al.*, 2009; Llorens-Fons *et al.*, 2017). Therefore, the interaction of *M. abscessus* with the immune system of the host depends heavily on the colony morphology. The smooth morphotype of *M. abscessus* is engulfed as a single bacterium in a macrophage phagosome, with an electron translucent zone between the bacterial surface and the phagosomal membrane (Roux *et al.*, 2016). The smooth strain breaks down the phagosome leading to direct cytosolic contact which allows polar GPLs on the cell surface to inhibit the apoptotic response and release of cytochrome C by repressing ROS production and interacting with mitochondrial cyclophilin D, a stabilizing part of the mitochondrial transition pore (Whang *et al.*, 2017). The smooth type is able to persist in the macrophage leading to recruitment of nearby leukocytes and to granuloma formation. The rough morphotype is usually aggregated due to its hydrophobic surface and is phagocytosed in loose phagosomes containing 2-5 bacilli, or even corded clumps, with no electron translucent zone (Byrd and Lyons, 1999; Brambilla *et al.*, 2016; Roux *et al.*, 2016). The rough strain can replicate inside the phagosome leading to rupturing or phagosomal maturation which triggers autophagy and apoptosis. Once in the extracellular space, it continues to replicate and form a cord-like structure that cannot be cleared by macrophages and results in tissue damage (Byrd and Lyons, 1999; Catherinot *et al.*, 2007; Bernut *et al.*, 2014; Johansen, Herrmann and Kremer, 2020).

Much research into smooth and rough variants of *M. abscessus* has been focused on the differences in survival in macrophages and the triggering of an immune response to understand what makes *M. abscessus* a successful pathogen. Smooth variants are more commonly isolated

from the environment and patients, while the rough types are mainly associated with chronic lung infections, such as those in CF patients (Jönsson *et al.*, 2007). Based on clinical and laboratory evidence, a theory emerged on *M. abscessus* colonization of the host - smooth variants are able to colonize abnormal lung airways, perhaps in a biofilm, and the spontaneous loss of GPLs leads to a change to the invasive rough type, which causes inflammation, invasive disease and worsening clinical symptoms (Cullen *et al.*, 2000; Howard *et al.*, 2006; Elizabeth R. Rhoades *et al.*, 2009; Kreutzfeldt *et al.*, 2013). While it has been shown that *M. abscessus* can bidirectionally change its colony morphotype, the trigger behind this event is not yet understood (Howard *et al.*, 2006). One study presented that a mutation in Mmp14 led to a *M. abscessus* subsp. *bolletii* strain changing from a smooth to a rough morphotype, while another study showed a temperature dependent change in colony morphology (Elizabeth R Rhoades *et al.*, 2009; Bernut, Nguyen-Chi, *et al.*, 2016). Morphological heterogeneity is extremely clinically relevant in *M. abscessus* due to the distinct pathogenesis of smooth and rough variants, and therefore discovering the trigger for smooth-to-rough transition is a key factor to understanding the process of *M. abscessus* infection and improving current treatment.

**A.**

GPL	R <sub>1</sub>	R <sub>2</sub>
GPL-1	-OCH <sub>3</sub>	-OCH <sub>3</sub>
GPL-2	-OH	-OCH <sub>3</sub>
GPL-3	-OCH <sub>3</sub>	-OH
GPL-4	-OH	-OH
GPL-5	-OCH <sub>3</sub>	-3-ortho-methylrhamnose
GPL-6	-OH	-3-ortho-methylrhamnose

**B.**

**Figure 1.2: Generic structure of GPLs and the *gpl* locus in *M. abscessus*.** **A.** Structure of the diglycosylated GPL with sugar, peptide and lipid moiety colour coded. Table shows R<sub>1</sub> and R<sub>2</sub> functional groups which can be modified to make the molecule apolar (GPL 1-4) or polar (GPL 5-6). **B.** Organization of the *gpl* locus in *M. abscessus*. Colour code designates the function of the genes in GPL biosynthesis, and arrows indicate transcriptional orientation. Adapted from Gutiérrez *et al.*, 2018.

### 1.3 Bacterial biofilms

Biofilms are structural communities of adherent microorganisms in an extracellular matrix (ECM) that provides the cells within with a protective degree of homeostasis and stability (Hall-Stoodley and Stoodley, 2005). Even though *in vitro* studies largely focus on planktonically grown bacteria, it is estimated that in the natural environment over 99% of bacteria grow in biofilms, in sessile and sedentary populations (Costerton, Geesey and Cheng, 1978; Davey and O'toole, 2000). These communities form on various surfaces in the human environment and can be found in industry and household pipelines, biomaterials, medical devices, as well as plant, animal, and human tissue.

The first documentation of bacterial biofilms is attributed to Antoine Von Leeuwenhoek in the 17<sup>th</sup> century, who studied “little animals” from his teeth using a microscope (Jamal *et al.*, 2018). It has now been determined that he had visualized biofilms of *Selenomonas*, a crescent-shaped bacteria commonly found in the human oral cavity (Francis, 1932). Dental plaque is indeed one of the crowning examples of bacterial biofilms and researching it provided many insights into bacterial surface attachment, co-aggregation, and formation of multispecies biofilms (Costerton, Stewart and Greenberg, 1999). While oral microbiota is natural and fosters a synergistic relationship with the host, several diseases can still occur - most distinctively in the example of a pathogenic biofilm causing gingivitis and periodontitis, a chronic inflammation of the gums (Kinane, Stathopoulou and Papapanou, 2017).

Pathogenic biofilms are not unique to the oral cavity, and it is estimated that 80% of bacterial infections are associated with biofilms, particularly chronic and recurring infections (Lewis, 2001; Chen and Wen, 2011). Common examples of persistent infections where biofilms serve as a reservoir of cells used to reinfect the colonization site are *E. coli* in the urinary tract, *M. tuberculosis* in the lungs and *P. aeruginosa* in CF lung disease (Singh *et al.*, 2000; Justice *et al.*, 2004; Ojha *et al.*, 2008; Chen and Wen, 2011). In general, biofilm infections can be device or non-device associated. Device-related infections occur when biofilms form on medical

devices such as catheters, prosthetic joints, contact lenses, and the highest number, 40%, are associated with ventricular-assisted devices (Darouiche, 2004). Some examples of non-device-associated infections are aforementioned periodontitis or osteomyelitis, where bacteria from previous infections enter bones through the bloodstream (Jamal *et al.*, 2018).

Due to their structural organization and the protective ECM layer, bacterial biofilms are more resistant to mechanical stress, UV radiation, desiccation, host defence, and predators. The ECM additionally helps in the evasion of the immune system by physically “masking” the bacteria within the biofilm, inhibiting phagocytosis, chemotaxis, and activation of the complement system. This was shown to lead to a stalemate, where the pathogen physically remains within the host without complete elimination, existing in a state of decreased activity and invasiveness, leading to long-term survival and persistence (Parsek and Singh, 2003; González, Hahn and Gunn, 2018). The ECM also makes bacteria in biofilms more resistant to antibiotic treatment compared to planktonic cells (Galassi *et al.*, 2003; Greendyke and Byrd, 2008). In *M. abscessus* specifically, it was demonstrated that planktonic cells were more susceptible to several antibiotics when compared to biofilms in *in vitro* studies (Clary *et al.*, 2018; Hunt-Serracin *et al.*, 2019). Similarly, planktonic bacteria are more susceptible to treatment with antibiotics in *in vitro* studies as opposed to *in vivo*, likely due to the formation of biofilms or microcolonies that provide protection *in vivo* (Greendyke and Byrd, 2008; Clary *et al.*, 2018).

### 1.3.1 Mycobacterial biofilms

Although biofilm formation is not in itself a virulence factor, since many non-pathogenic bacterial species form biofilms, this process does facilitate survival of pathogens partially due to the accumulation and dispersal of a high enough number of bacteria to achieve an infective dose. Biofilms in mycobacteria were studied as early as 1989, and it is now known that many mycobacterial species can form biofilms including *M. tuberculosis*, *M. smegmatis*, *M. bovis* BCG, *M. avium*, *M. chelonae* and *M. abscessus* (Schulze-Robbecke and Fischeder, 1989; Chakraborty and Kumar, 2019). Pellicles, formed on the liquid-air interface (**Fig. 1.3B**), are the

most studied form of biofilms in mycobacteria, and recently studies aiming to decipher the composition of the ECM have been on the rise (Trivedi *et al.*, 2016; Vega-Dominguez *et al.*, 2020).

NTM biofilms can persist inside the human body and on medical devices, giving reason for concern since biofilms increase pathogenicity and resistance to antibiotics. *M. fortuitum* biofilm found on a prosthetic valve was identified as the etiological agent of endocarditis and *M. massilinense* was associated with biofilm persistence in a breast implant (Bosio *et al.*, 2012; Rüegg *et al.*, 2015). *M. avium* was shown to form biofilms in showerheads, releasing infectious droplets during hot showers – an infection process previously seen in *Legionella pneumophila* (Cianciotto *et al.*, 1992; Faria, Joao and Jordao, 2015). *M. chelonae* and *M. ulcerans* were both shown to form biofilm associated infection *in vivo* (Holland *et al.*, 1991; Marsollier *et al.*, 2007). Recently, two separate case studies showed formation of biofilm like microcolonies of *M. abscessus* in patient lungs (Qvist *et al.*, 2015; Fennelly *et al.*, 2016).

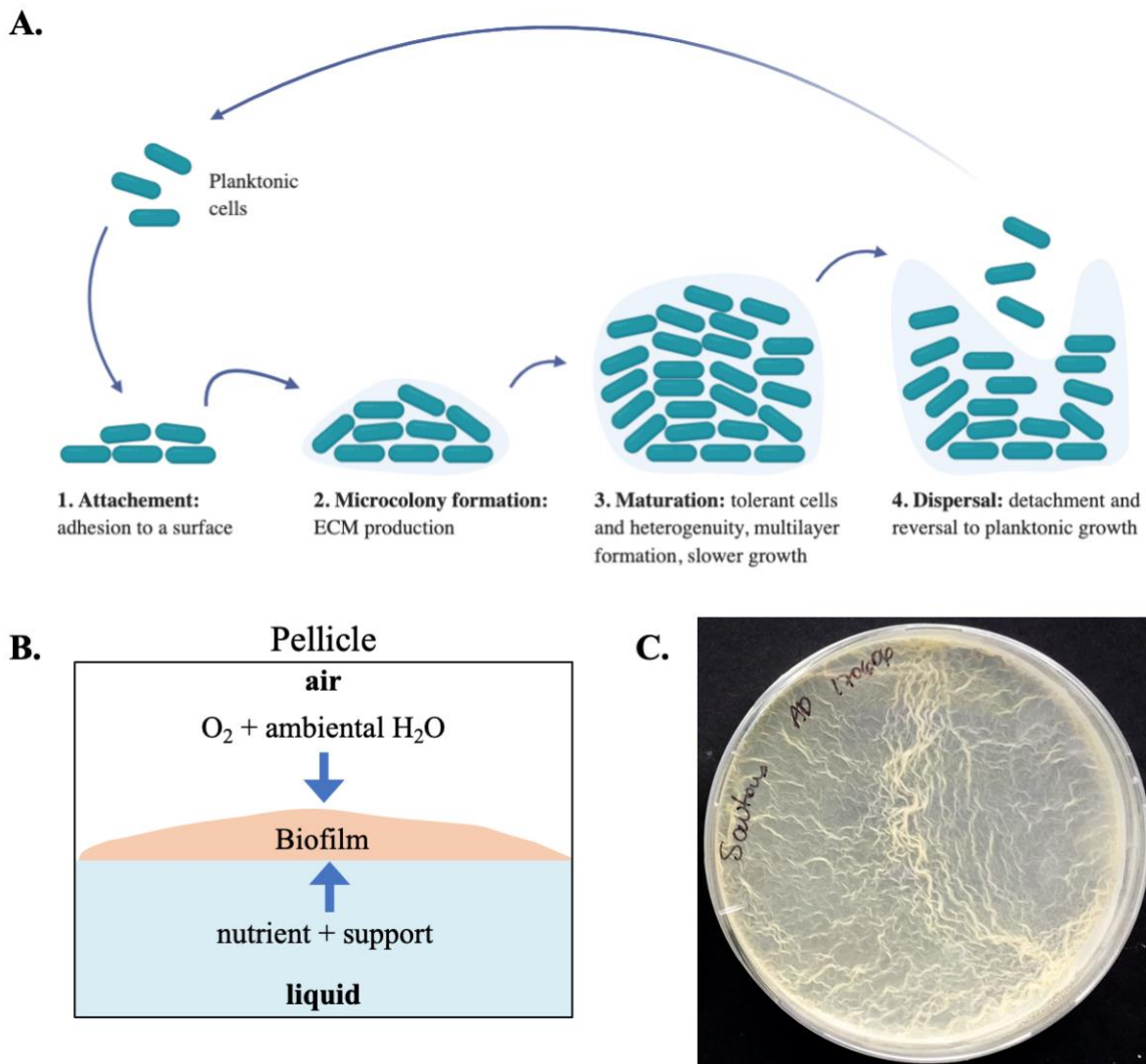


**Figure 1.3: Graphic representation of biofilm formation and pellicular biofilms.** **A.** Biofilm formation depicting all relevant stages: (1) initial formation happens by aggregation of planktonic cells, and, if applicable, adhesion to a surface, in response to environmental stress, (2) a monolayer is formed and the attachment becomes irreversible through the production of the ECM, (3) a microcolony with multiple layers is formed, there are changes in the metabolic states of the cells, (4) cells in the biofilm detach, disperse and revert to their planktonic state. **B.** Schematic representation of a pellicular biofilm formed on the liquid air interface. **C.** *M. abscessus* pellicular biofilm formed in minimal Sauton's media in a 10 cm Petri dish.

### 1.3.2 Biofilm formation

Assembly of biofilms requires several stages; including initial reversible attachment to a surface, irreversible attachment, early biofilm formation, biofilm maturation and, finally, dispersion (**Fig. 1.3A**) (Sousa *et al.*, 2015). Attachment to the surface is dependent on electrostatic interactions between the surface and bacteria, as well as availability of oxygen, nutrients and beneficial temperature (Martínez and Vadyvaloo, 2014). In some biofilms, such as the pellicular biofilm formed on the liquid air interface (**Fig 1.3B and C**) the initial step is not attachment but rather aggregation of cells. Microcolony formation and biofilm maturation are characterized by matrix formation including secretion of polysaccharides, lipids, and extracellular DNA (eDNA). Likewise during this stage, the cells undergo metabolic changes and previously it was identified that subpopulations of at least four distinct metabolic states, aerobic growth, anaerobic growth, dormant, and dead cells, exist within the biofilm (Wan *et al.*, 2018). In the step leading up to detachment, bacteria have achieved their maximum replication rate and with nutrients depleting and crowding, they disperse in search for better survival conditions. Communication between bacteria that facilitates this process is called quorum sensing and is mediated by autoinducer molecules (Koo, Falsetta and Klein, 2013).

### 1.3.3 Composition of the biofilm extracellular matrix

The ECM surrounds bacteria in the biofilm and plays a vital structural and functional role, serving as a nutrient source and offering protection to the cells from antibiotics and host-defence systems. Water makes up the largest proportion of the biofilm matrix and provides a hydrated environment for the cells embedded within, protecting them against desiccation (Potts, 1994). The ECM additionally contains eDNA and eRNA, polysaccharides, lipids, proteins and other molecules (Karygianni *et al.*, 2020). These macromolecules can be categorized as “surface associated” or “secreted extracellularly”. Surface associated are flagella, pili and other things related to adhesion to surfaces. Secreted molecules are lipids, proteins, polysaccharides and eDNA, which contribute to the scaffolding of the matrix and its function (Flemming *et al.*,

2016). The ECM promotes surface attachment, cell-cell cohesion to facilitate aggregation, offers physical stability and high viscoelasticity, and limits diffusion of antimicrobials (Karygianni *et al.*, 2020). The matrix also contains pores and channels which allow flow of water, oxygen and nutrients to all cells in the matrix (Vasudevan, 2014).

#### *1.3.3.1 Role of lipids in biofilm formation*

Lipid metabolism is highly important for biofilm formation in mycobacteria and strains defective in producing or exporting certain cell wall lipids cannot form mature pellicles (Recht and Kolter, 2001; Wang *et al.*, 2006; Ojha *et al.*, 2008; Pang *et al.*, 2012; Pacheco *et al.*, 2013; Rose and Bermudez, 2014). Heavy reliance on lipids in mycobacterial biofilm suggest that the biofilms are either held together by a waxy ECM, or that the lipids increase cell-surface hydrophobicity thereby increasing cell-to-cell interaction required for biofilm formation (Chakraborty and Kumar, 2019).

Meromycolate diacylglycerol (MDAG), mycolic acids and GPLs are all associated with biofilm formation in mycobacteria. Acetylated GPLs are important for the surface attachment stage of biofilm formation in *M. smegmatis*, but do not play as vital of a role in pellicular biofilms (Recht and Kolter, 2001; Chen *et al.*, 2006; Yang, Thomas, Li, Vilchèze, Derbyshire, Jacobs and Ojha, 2017). Accumulation of mycolic acids has been termed a hallmark of biofilm formation in mycobacteria and is observed in *M. tuberculosis*, *M. smegmatis* and *M. chelonae* (Ojha *et al.*, 2008, 2010; Totani *et al.*, 2017; Vega-Dominguez *et al.*, 2020). The increase in mycolic acids has been linked to a decrease in TDM following an enzymatic hydrolysis – however this relationship was observed in *M. smegmatis* but not in *M. avium*, where TDM is reduced but mycolic acids do not accumulate (Totani *et al.*, 2017).

Deletion of *groEL1* in *M. smegmatis* results in the inability of the biofilm to mature (Ojha *et al.*, 2005). GroEL1 is thought to interact physically with KasA, an enzyme essential to fatty acid synthesis II (FAS II), the step in mycolic acid biosynthesis where C<sub>56</sub>-C<sub>68</sub> fatty acids, short-chain mycolates or meromycolate precursors essential for biofilm maturation, are formed. The

inability to export lipids also resulted in defective biofilm formation in an *mmpL11* deletion mutant in *M. smegmatis* that was unable to translocate MDAG and a mycolate to the cell surface (Pacheco *et al.*, 2013). Furthermore, availability of mycolic acid subtypes also affects biofilm formation as defective biofilm formation was seen in an *M. tuberculosis* strain unable to produce keto-mycolates (Sambandan *et al.*, 2013).

#### *1.3.3.2 Role of polysaccharides in the extracellular matrix*

Exopolysaccharides were identified to be an essential part of the biofilm matrix in many biofilm-forming bacteria such as *P. aeruginosa*, *S. aureus* and *E. coli* (Ryder, Byrd and Wozniak, 2007; Flemming and Wingender, 2010; Koo, Falsetta and Klein, 2013; Limoli, Jones and Wozniak, 2015). In *Vibrio cholerae*, carbohydrates in the matrix were necessary for stabilization of the pillars in surface attached biofilms (Watnick and Kolter, 1999). It was, however, previously thought that mycobacterial biofilms do not contain exopolysaccharides, a premise based on the examination of the mycobacterial genome that revealed mycobacteria do not contain genes that encode exopolysaccharide production (Whiteley *et al.*, 2001). As a result, for a long time we had limited knowledge of the role of polysaccharides in the mycobacterial biofilm matrix.

Recent studies of *M. tuberculosis* pellicles have identified cellulose as a major component of the biofilm matrix, showing that cellulase was able to disrupt biofilms while  $\alpha$ -amylase was not (Trivedi *et al.*, 2016). In *M. smegmatis*, deletion of *upk*, a gene that encodes for a phosphokinase related to peptidoglycan synthesis, resulted in defective biofilm formation due to weak adherence and a missing ECM, while cell wall formation remained intact (Röse, Kaufmann and Daugelat, 2004). This indicates that export of polysaccharides is important for biofilm formation, or at least for upkeep of the structural integrity of the matrix.

#### *1.3.3.3 Role of proteins in the extracellular matrix*

Not much is known about the role of proteins in the ECM, but it was demonstrated that several structural proteins play an important role in biofilm formation. In *E. coli* and *M. tuberculosis* it

was shown that adhesins and pili are important for aggregation and adhesion (Chakraborty and Kumar, 2019). In *M. tuberculosis* thiol-induced pellicles importance of proteins was illustrated through digestion of the biofilm with Proteinase K (Trivedi *et al.*, 2016). In *M. avium* biofilms, Wag31, a cell wall biosynthesis regulator, SodA and KatG, proteins related to maintenance of REDOX homeostasis, antigen 85B and a DNA binding protein were shown to be the most abundantly present proteins in the ECM (Rose and Bermudez, 2014). However, there are still many proteins that play a key role in the biofilm structure that need to be characterized.

#### *1.3.3.4 Role of eDNA in the extracellular matrix*

eDNA is a fundamental part of the ECM in many bacterial biofilms and has been found in the ECM of *M. tuberculosis*, *M. avium*, *M. abscessus*, *M. fortuitum* and *M. chelonae* (Whitchurch *et al.*, 2002; Rose *et al.*, 2015; Rose and Bermudez, 2016; Toyofuku *et al.*, 2016; Trivedi *et al.*, 2016; Aung *et al.*, 2017; Vega-Dominguez *et al.*, 2020). While eDNA is often released by cell lysis, lytic-independent mechanisms of release also exist, and in *M. avium* FtsK/SpoIIIE-like DNA transporting pore was identified as responsible for pH-dependant export of eDNA (Rose and Bermudez, 2016). Across all biofilm forming species, the main role of eDNA is to promote attachment to surfaces and facilitate bacterial aggregation in various stages of biofilm formation (Rose *et al.*, 2015; Ibáñez de Aldecoa, Zafra and González-Pastor, 2017; Pakkulnan *et al.*, 2019). Biofilms treated with DNase become less structurally secure and are more vulnerable to antibiotics (Tetz, Artemenko and Tetz, 2009; Cavaliere *et al.*, 2014; Rose *et al.*, 2015; Trivedi *et al.*, 2016).

## **1.4 *M. abscessus* biofilms and thesis aims**

It is well established that *M. abscessus* forms biofilms in showerheads and water distribution systems, that act as a reservoir of bacteria for host infections , as well as in patient lungs drawing attention to the immediate clinical relevance of studying the composition and formation of biofilms in this species (Kuo *et al.*, 2011; Qvist *et al.*, 2015; Fennelly *et al.*, 2016). To date, studies of *M. abscessus* biofilms have been limited to testing antibiotic susceptibility and chemicals for clearance of biofilms (Clary *et al.*, 2018; Hunt-Serracin *et al.*, 2019; García-Coca *et al.*, 2020). Furthermore, many of the studies were done in different strains or clinical isolates of *M. abscessus* causing difficulty in consolidating findings. Therefore, it is imperative to expand our understanding of biofilm formation in this species as it can influence prevention and treatment of disease.

Research has shown that *M. abscessus* biofilms form in both smooth and rough morphotypes and that they can grow in various media including artificial sputum media, and even in oxygen and nutrient starved environments (Howard *et al.*, 2006; Hunt-Serracin *et al.*, 2019; Yam *et al.*, 2020). These studies gave rise to the widely accepted theory of *M. abscessus* airway colonization which describes an initial establishment with biofilms of the less virulent smooth morphotype, and then a change to the rough morphotype which causes robust infection. Biofilms harbour significantly higher resistance to many routinely used antibiotics, but can be broken down by acetic acid, *Methylobacterium* sp, disaggregation and oxygenation to a point that provides higher antibiotic susceptibility (Greendyke and Byrd, 2008; Muñoz-Egea *et al.*, 2015; Clary *et al.*, 2018; García-Coca *et al.*, 2020; Kolpen *et al.*, 2020). Presence of both eDNA and lipids in the *M. abscessus* biofilm ECM was shown, with the emphasis on the importance of GPLs given that deletion in *mmpL4b* and *mab\_3168c*, genes involved in GPL biosynthesis, resulted in impaired biofilm formation (Nessar *et al.*, 2011; Tsai *et al.*, 2013; Rose *et al.*, 2015; Rose and Bermudez, 2016; Chakraborty and Kumar, 2019).

### **1.4.1 Overarching aim**

While there are studies available on biofilm formation in different mycobacterial species, and parallels can be drawn between them, *M. abscessus* biofilms have not been studied in depth. This thesis aims to fill this knowledge gap through a novel characterization of the composition of *M. abscessus* biofilms and investigation of transcriptional changes that are caused by this type of growth. Initial studies were done in the *M. abscessus* type strain (ATCC 19977). Research was then broadened to include six pulmonary clinical isolates to provide a relevant clinical context and facilitate the study of differences between *M. abscessus* smooth and rough variants.

### **1.4.2 Specific aims – project 1 (Chapters 2-4)**

#### **Project 1 – Characterization of biofilm formation in the *M. abscessus* type strain**

Aim: Describe *M. abscessus* biofilms by investigating the changes in transcription and analysing visually and biochemically the composition of the ECM

- Visually describe the ECM of *M. abscessus* biofilms and quantify the components of the ECM
- Analyse the difference in extrapolymeric substances of *M. abscessus* biofilms as compared to planktonic cells
- Investigate the transcriptomic changes in biofilms of *M. abscessus* as compared to planktonic cells

### **1.4.3 Specific aims – project 2 (Chapters 5-7)**

#### **Project 2 – Characterization of six *M. abscessus* pulmonary isolates**

Aim: Determine phenotypic and genetic differences between *M. abscessus* clinical isolates and investigate correlation with colony morphology

- Conduct a biological characterization of six *M. abscessus* clinical isolate strains in comparison to two reference strains, *M. abscessus* smooth and rough
- Characterize biofilm formation and lipid changes in clinical isolates
- Examine the genetic differences between the clinical isolates

## 2 Microscopic analysis of *M. abscessus* biofilms

## 2.1 Introduction

### 2.1.1 Scanning electron microscopy in biofilm studies

Scanning electron microscopy (SEM) has become an important tool for structural analysis because of its large depth field used to determine topographies of surfaces at great magnifications. The technique utilizes a beam of focused, high-energy electrons to generate a variety of signals on the surface of the specimen being imaged (Alhede *et al.*, 2012; Vuotto and Donelli, 2014; Raab and Bachelet, 2017). SEM has become an essential way of determining the size and shape of bacilli as well as their localization within biofilms, and has been used in studies with several mycobacterial species to show bacterial aggregation and cording (Hall-Stoodley and Lappin-Scott, 1998; Hall-Stoodley, Keevil and Lappin-Scott, 1999; Trivedi *et al.*, 2016; Totani *et al.*, 2017; Vega-Dominguez *et al.*, 2020).

### 2.1.2 Confocal laser scanning microscopy in biofilm studies

Historically it has been difficult to obtain clear images of biofilms as they are densely packed with cells and the ECM and tend to be studied under hydrated conditions. Development of confocal laser scanning microscopy (CLSM) changed that, and first 3D images of a biofilm were published in 1991 using *Pseudomonas* as a subject (Lawrence *et al.*, 1991). CLSM combines laser excitation and subsequent emission of fluorescent molecules through a pinhole which filters out light that is not optimal for a particular focal plane, making images sharper and allowing 3D imaging of specimens that otherwise appear out of focus (Franklin *et al.*, 2015). Using CLSM, it became possible not only to describe the structure of a biofilm, but also investigate multi-culture biofilms, biofilm-substratum interaction, and observe biofilms on a single cell level in 4D, under *in situ* conditions in microfluidic chambers (Palmer and Sternberg, 1999; Franklin *et al.*, 2015). Development and refining of CLSM methods for biofilm studies is complemented by advances in image processing software used for calculating parameters

such as colocalization coefficients and biovolume, or for isolating specific components of the ECM (Schlafer and Meyer, 2017; González-Machado *et al.*, 2018).

### **2.1.3 Microscopy as a tool for studying the biofilm extracellular matrix**

Biofilm ECM is secreted by bacteria and serves a wide range of functions, from adhesion to surfaces and aggregation of bacterial cells to retention of water and serving as a nutrient source, and it is essential for biofilm formation and maturation (Flemming and Wingender, 2010; Rose *et al.*, 2015). The ECM has been deemed the “dark matter of biofilms” on account of the difficulty scientists experience in imaging it due to its density and complex composition (Flemming and Wingender, 2010; Franklin *et al.*, 2015). The ECM components, lipids, polysaccharides, proteins and eDNA, have all successfully been stained with fluorescent dyes and imaged in various bacteria (Franklin *et al.*, 2015; Trivedi *et al.*, 2016; Vega-Dominguez *et al.*, 2020). The exact composition of the *M. abscessus* biofilm matrix remains undetermined although it is assumed that the presence of these biopolymers is conserved among biofilm forming bacteria, while the exact amount of each component is expected to vary.

Much of the research on the biofilm matrix has been done in surface attached biofilms, leaving knowledge gap in pellicular biofilms (Hung *et al.*, 2013; Liu *et al.*, 2014; Trivedi *et al.*, 2016; Reichhardt and Parsek, 2019). Therefore, the overarching aim of this chapter was to describe the structure and composition of the *M. abscessus* pellicular biofilm using microscopy. Specific objectives were to visualize the ECM and describe biofilm morphology using SEM and to determine qualitatively and quantitatively the distribution of macromolecules in the ECM using fluorescent dyes and CLSM.

## 2.2 Results

### 2.2.1 *M. abscessus* biofilms form an organized extracellular matrix

Growth of a pellicular biofilm in *M. abscessus* is possible in different media and containers of varying diameters, however for the purposes of this study growth was optimized in Sauton's minimal media in a 24-well plate (Fig. 2.1). *M. abscessus* pellicles are hydrophobic and form a thick, opaque layer on top of the media and on the sides of the well, and as the biofilm matures the pellicle wrinkles until the dispersal stage, where it sinks.

SEM was used to visualize the native state of *M. abscessus* pellicles and offer insight into the detailed structure of the biofilm. Planktonic cells were grown to exponential phase prior to harvesting by centrifugation and 6-day old pellicles were gently harvested by removing media so that the pellicle rested on a coverslip, intact. Samples were fixed using glutaraldehyde and either air dried or treated with gradual alcohol dehydration. SEM was performed at the School of Metallurgy, University of Birmingham.

Micrographs of planktonic cells indicated that mycobacteria clustered when grown in a shaking culture and formed a thin envelope that surrounds that cluster; however, this envelope was unaffected by solvent treatment (Fig. 2.2.A. and B.). Upon observation of the pellicular biofilm at various magnifications (5000x, 10000x and 12000x) there was a clear difference between air-dried samples and those treated by alcohol dehydration (Fig. 2.2.C.-H.). In air-dried samples only the envelope of the ECM that surrounds and masks the cells was visible, and single cells were not (Fig. 2.2.D., F. and H.). Gradual ethanol dehydration resulted in stripping of the ECM layer, leaving the bacilli underneath exposed (Fig. 2.2.C., E. and G.). At 5000x magnification it was apparent that bacteria in a biofilm are organized in a clear and structured manner, arranged to allow for formation of pores and channels (Fig. 2.2.C.). Careful observation showed that small breaks in the ECM are visible in air-dried biofilms as well (Fig. 2.2.H.).



**Figure 2.1. *M. abscessus* pellicle.** Six-day old pellicle grown in Sauton's media in a 24-well plate. Scale bar = 8 mm.

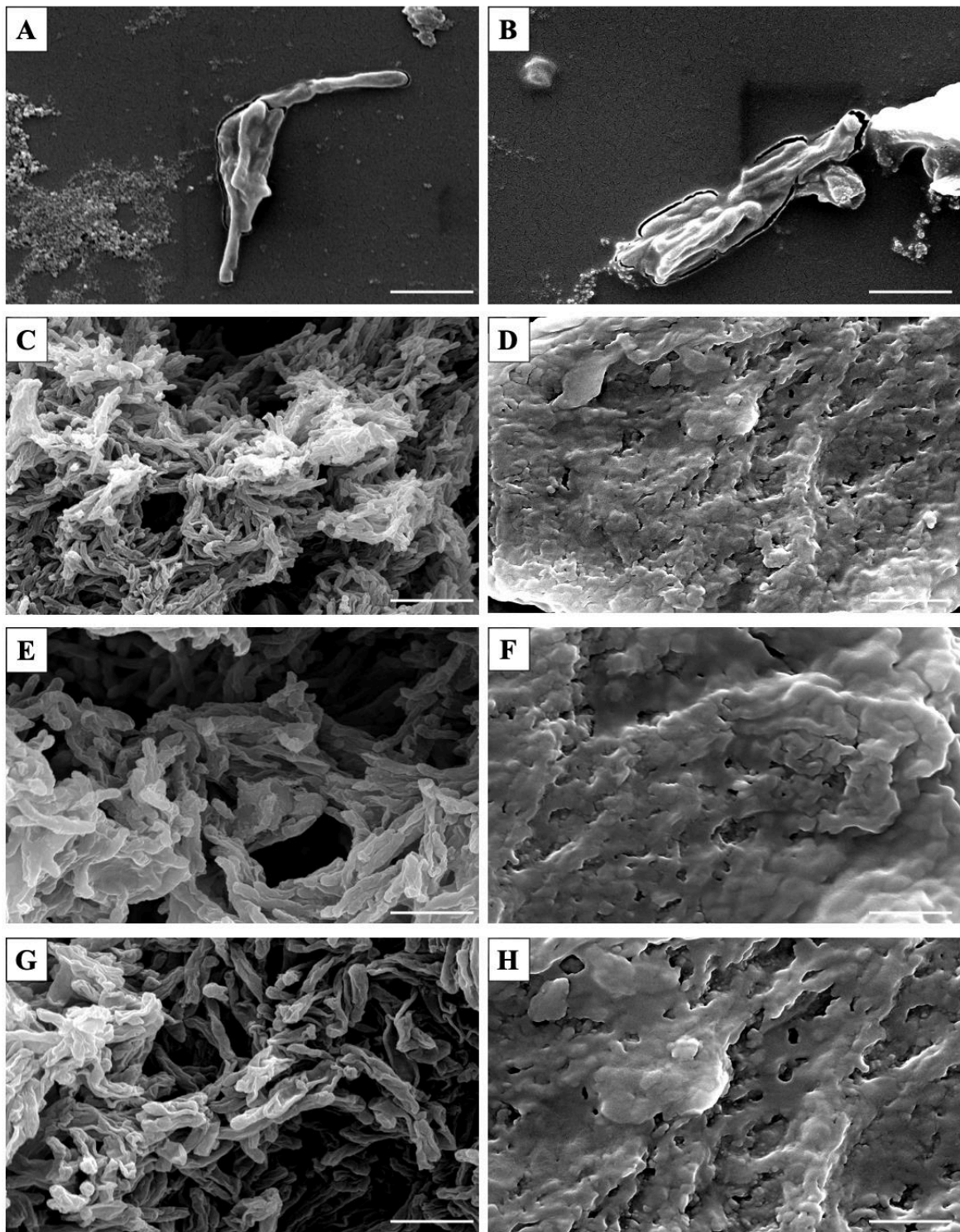


**Figure 2.2. Scanning electron micrographs of *M. abscessus* pellicles.** Samples prepared by gradual alcohol dehydration (left column) and by air-drying (right column). Side by side images in rows show the same magnification of differently treated samples. **A.** and **B.** planktonic cells, 12000x magnification, scale bar = 2 $\mu$ m; **C.** and **D.** pellicles, 5000x magnification, scale bar = 5  $\mu$ m; **E.** and **F.** pellicles, 10000x magnification, scale bar = 2  $\mu$ m; **G.** and **H.** pellicles, 12000x magnification, scale bar = 2  $\mu$ m.

## 2.2.2 Fluorescent images reveal macromolecular content of *M. abscessus* biofilms

While visualization of the *M. abscessus* pellicle with SEM revealed the existence of an ECM and illustrated in detail the architecture of the biofilm, CLSM was subsequently done to study the ECM composition. *M. abscessus* eGFP expressing strain was used for all experiments for visualization of bacteria along with four dyes that target known components of the ECM. Concanavalin A conjugated with Alexa Flour 647 (AF) stained carbohydrates, Propidium iodide (PI) nucleic acids, FilmTracer™ SYPRO® Ruby (SR) was used for proteins and Nile red (NR) for lipids. Biofilm samples were stained separately with each dye to avoid artifacts and signal crossover between channels. Microscopy revealed presence of these four components extracellularly in the biofilm matrix (**Fig. 2.3.A.-D.**). A visual assessment indicated that lipids were the most abundant biomolecule in the biofilms, while the others were present and dispersed throughout, but less abundant. Differences in congregation of *M. abscessus* eGFP cells alluded to biological variability in biofilm formation. The distribution of these biomolecules can be seen in **Appendix 1** in unedited images showing top, middle and bottom of the pellicle.

CLSM images were quantified by calculating the relative volume of each component and evaluating co-localization of the emitted signals of GFP and each dye using Pearson's coefficient and co-occurrence using the Mander's coefficient (Schlafer and Meyer, 2017), results summarised in **Table 2.1** and **Fig. 2.4**. Pearson's correlation, denoted with  $r$ , is a well-established method for presenting correlation and has been adapted to measure co-localization between fluorophores by showing the degree to which the signals linearly correlate with each other. A value of 1 (+/-) indicates a perfect positive or negative relationship, while 0 shows absence of a relationship. A high Pearson's correlation coefficient (PCC) indicates that both signals from GFP and a fluorophore increase or decrease proportionally, while a low coefficient denotes that signal intensity of one does not alter with the change in intensity of the other.

Mander's coefficients measure co-occurrence and were derived as an improvement to PCC since Pearson's is not sensitive to signal intensity between different parts of an image. M1 and M2 measure the fraction of a given signal that overlaps with another signal. M1 measures how the GFP signal overlaps with a signal emitted from a dye and M2 measures the opposite, how much of the dye signal overlaps with the GFP signal. A value of 1 indicates all the signal overlaps, while 0 means none of it does. Mander's is an excellent way to evaluate the co-occurrence of ECM components with cells in biofilms because it can quantify signal only present in the ECM, meaning the fluorophore signal that does not overlap with the GFP signal. Additionally, the biovolume of each of the ECM components relative to the biovolume of *M. abscessus* cells in the biofilm was evaluated. The results are summarized in **Table 2.1**.

Lipids were the most abundant biomolecule in *M. abscessus* biofilms (relative biovolume=1.252), with a high degree of co-localization with the cells ( $r=0.8998$ ) and a relatively high degree of co-occurrence as indicated by the M1 and M2 (**Table 2.1**). Proteins, stained with SR, had a medium degree of co-localization ( $r=0.536$ ) with cells, and a low signal overlap of SR with GFP ( $M2=0.2905$ ), indicating that the rest of the SR signal is coming from proteins present in the ECM, independent of cells. The PI signal, PI staining eDNA here, showed poor intensity correlation with GFP ( $r=0.292$ ) and GFP and PI signals overlap equally with each other at ~50% ( $M1=0.4552$ ,  $M2=0.4540$ ) indicating dispersal. Carbohydrates were by far the smallest component of the *M. abscessus* biofilm (relative biovolume=0.151) and showed a low degree of co-localization ( $r=0.151$ ). Around 70% of the AF signal overlaps with the GFP signal ( $M2=0.7351$ ) indicating a high degree of co-occurrence, but also showing that some AF signal occurs separately from the GFP signal, suggesting the remaining ~30% can be associated with carbohydrates in the ECM.

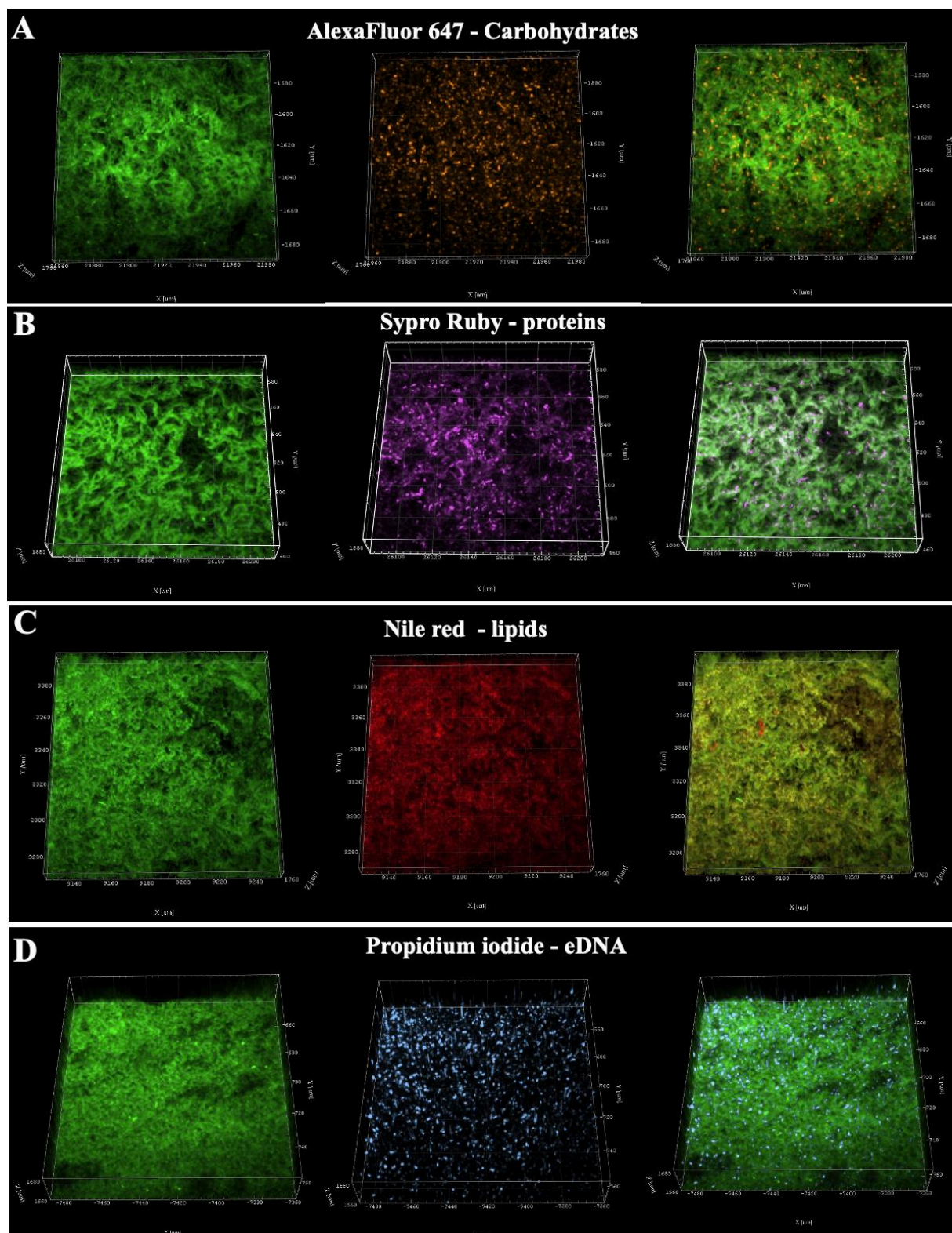


**Figure 2.3. Confocal laser scanning microscopy pictures of mature *M. abscessus* biofilms.** Images show a 3D reconstruction of a 20  $\mu\text{m}$  z-stack. Each horizontal panel shows a separate sample of *M. abscessus* GFP (first column), specific component markers (second column) and the two merged (third column). **A.** Carbohydrates stained with Concanavalin A Alexa Fluor 647; **B.** Proteins stained with Sypro Ruby; **C.** Lipids stained with Nile Red, **D.** eDNA stained with Propidium iodide.

**Table 2.1. Relative biovolume and correlation coefficients of ECM components as compared to bacilli in the biofilm** (representative of data gathered from five images of five biological replicates)

Component of ECM	Relative biovolume	Pearson's correlation coefficient	Mander's coefficient	
			M1	M2
Carbohydrates	0.166	0.151	0.473	0.7351
Lipids	1.252	0.8998	0.794	0.6872
Proteins	0.846	0.536	0.585	0.2905
eDNA	0.693	0.292	0.4552	0.4540

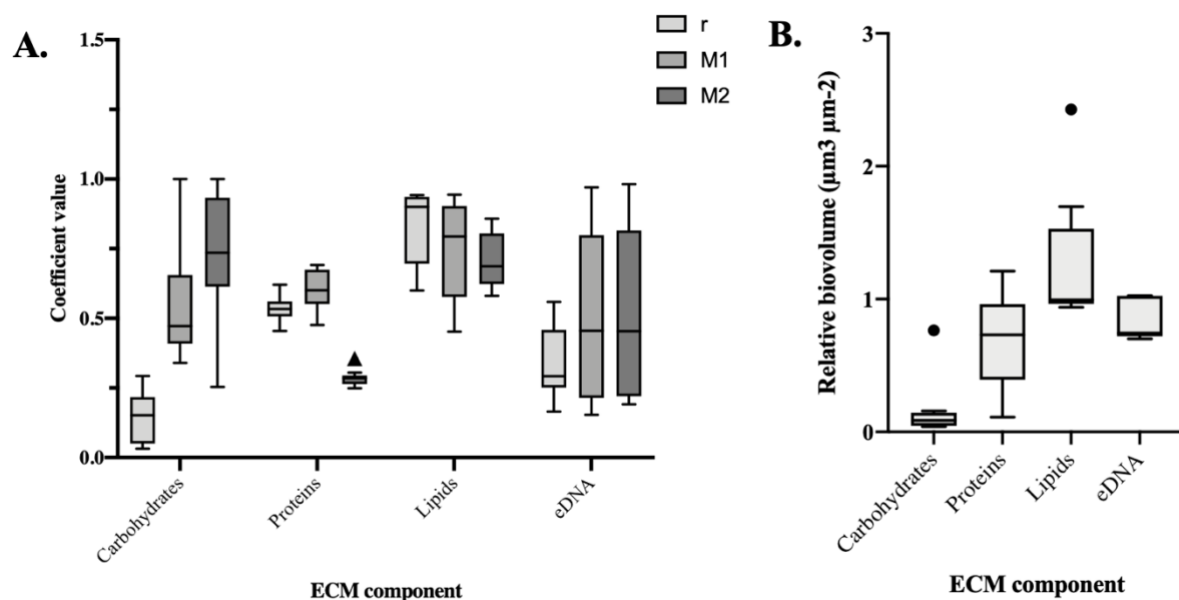


**Figure 2.4. Correlation between ECM components and bacilli in *M. abscessus* biofilms.** **A.** Correlation coefficients of ECM components with bacilli in *M. abscessus* biofilms;  $r$  = Pearson's,  $M$  = Mander's. M1 indicates the degree of overlap between the GFP signal, and the signal emitted from a dye, and M2 the opposite. **B.** Relative biovolumes of components of *M. abscessus* ECM. Lines on the bar indicate median. Coefficients are calculated based data gathered from five random images of five biological replicates.

## 2.3 Discussion

Pellicles are biofilms formed on a liquid-air interface that receive nutrients and physical support from the liquid below, and oxygen from the air exposed part of the pellicle. NTMs and bacteria in the *M. tuberculosis* complex have previously been shown to form these types of biofilms, and in this study we presented that *M. abscessus* is capable of forming them as well (**Fig. 2.1**) (Ojha *et al.*, 2008). Indeed, forming surface-attached biofilms with *M. abscessus* *in vitro* has proven a challenge as they naturally form pellicles when grown stationary. From an experimental point of view, pellicles are an excellent model for studying biofilm formation since they yield a large biomass in comparison to surface attached biofilms. Furthermore, while surface-attached biofilms are more likely to be found in pipelines and water systems, pellicles are likely to be more clinically relevant since they are not as reliant on attachment to a solid surface.

SEM of *M. abscessus* pellicles showed presence of a biofilm matrix that envelops and masks bacteria in the biofilm and that can be stripped through solvent treatment (**Fig. 2.2**). Micrographs confirm that biofilms have a specific architecture in which bacteria are organized to support the structure of the biofilms and to form pores and channels. In the earliest assessments of biofilms in the model organism *P. aeruginosa* it was shown that biofilms are arranged structures with channels and pores, and since then pores were also described in surface attached and pellicular biofilms of several mycobacterial species, indicating that pore formation is a conserved mechanism in biofilm-forming bacteria (Trivedi *et al.*, 2016; Rooney, Hoskisson and McConnell, 2019). These channels allow flow of molecules of roughly up to 5 µm in size, such as water, nutrients and oxygen, to bacteria imbedded deeper in the matrix (Stoodley, Debeer and Lewandowski, 1994; Watnick and Kolter, 1999; Sauer *et al.*, 2002).

SEM analysis of planktonic cells showed that they also aggregate while grown in shaking culture, despite the addition of detergent. From observations of SEMs of planktonic cells, we could determine that tyloxapol, the detergent, did not fully disperse all aggregates in planktonic

cultures, and an ECM-like substance covering the aggregated cells was clearly visible (**Fig. 2.2.A.** and **B.**). Planktonic ECM was not as easily stripped by ethanol dehydration as that of biofilms, most likely due to the way the samples were processed and because the targeted surface area and volume of the planktonic samples were smaller.

Microscopy images of pellicular biofilms showed formation of serpentine-like structures resembling cording, as evidenced here in CLSM images (**Fig. 2.3.A.**). Cording is aggregation of mycobacterial cells in a definitive order resembling a cord, where the orientation of the long axis of the cells is parallel to the long axis of the cord and has been identified as a virulence factor in *M. tuberculosis* (Middlebrook, Dubos and Pierce, 1947; Kalsum *et al.*, 2017). In *M. abscessus* it was previously shown that cording is only present in the rough morphotype, which is coincidentally suggested to be more virulent (Llorens-Fons *et al.*, 2017). The ATCC *M. abscessus* strain used in this study has a smooth colony morphology, and biofilms imaged with CLSM do visually resemble cords however the SEM images indicate a closer resemblance to previously published micrographs of smooth strain biofilms (Julián *et al.*, 2010).

### **2.3.1 Composition of the extracellular matrix**

Studies have been done in a range of biofilm forming bacteria to define the composition of the ECM. Lipids, proteins, eDNA and carbohydrates have all been uniformly identified as present in the ECM, and essential for biofilm formation in distinctive ways, dependent on the species and biofilm type in question. These molecules have all been shown as important for biofilm formation in mycobacteria, either by using knock-down studies of genes responsible for production of these biopolymers or by introducing enzymes used to digest them into the medium (Lemassu and Daffe, 1994; Ortalo-Magne *et al.*, 1995; Recht and Kolter, 2001; Okshevsky and Meyer, 2015; Rose *et al.*, 2015; Trivedi *et al.*, 2016). Using CLSM, we showed that the ECM of *M. abscessus* biofilms consists of lipids, polysaccharides, proteins and eDNA (**Fig. 2.3**), all previously reported to play integral roles in biofilm formation and maturation in various bacterial species (Rose *et al.*, 2015).

Little is known about the role of proteins in the ECM, but their presence is verified by protein stains and evidence that Proteinase K treatment disrupts biofilms (Trivedi *et al.*, 2016). Additionally proteins have been implicated in aggregation of mycobacteria and their attachment to other cells, especially important in biofilm formation, since mycobacteria have a tendency to aggregate and because they lack pili normally used by biofilm-forming bacteria to adhere to surfaces (Menozzi *et al.*, 1996). Using the SR protein stain, we determined that the relative biovolume of proteins in the *M. abscessus* biofilm ECM is 0.693 which is abundant, however Mander's coefficients bring that to question. Only ~30% of SR stain signal co-occurs with GFP, while vice versa is ~50%. Careful observation of the middle slice of the z-stack (**Appendix 1**) shows some background in the SR stain. The fact that the SR signal covers more area than the GFP signal could have marginally influenced the Mander's coefficients. However, this effect was minimized by using five different biological samples that were stained and visualized independently on separate days.

Studies have shown eDNA to be essential for biofilm formation and it is present in surface attached biofilms of many NTMs. Treatment of *M. avium* surface-attached biofilms with DNase I reduced the biofilm biomass, and was suggested to increase bacterial susceptibility to antibiotics (Rose *et al.*, 2015). In studies with *M. tuberculosis* pellicles, eDNA was shown to be present in the ECM but DNase I treatment did not significantly disrupt the biofilm (Trivedi *et al.*, 2016). The relative volume of eDNA in *M. abscessus* biofilms is high, indicating that eDNA likely plays an important role in biofilms, likely a structural one given that studies have shown eDNA is primarily essential in early stages of biofilm formation, for adhesion and aggregation (Das *et al.*, 2010). We found that eDNA is abundant in *M. abscessus* biofilms (relative biovolume=0.846), but that there is only ~50% co-occurrence between the fluorophore and GFP signal. This suggests that eDNA is dispersed throughout the biofilm, and likely present in areas with low cell count, which can be seen at the bottom stack of the biofilm z-stack (**Appendix 1**). All together this points to eDNA having a role in aggregation of the biofilm

formation, for adhesion and aggregation, mirroring its function in surface-attached biofilms (Das *et al.*, 2010).

Lipids are an essential part of the biofilm ECM; however, studies have indicated that they localize to the cell wall and not the extracellular space (Trivedi *et al.*, 2016). In *M. abscessus* biofilms there was a high degree of co-localization between the signal given off from lipids and the cells ( $r=0.8998$ ), however Mander's coefficients showed that the two signals do not fully co-occur. This indicates that while a significant portion of the NR signal co-occurs with GFP signal ( $M2=0.687$ ), and vice versa ( $M1=0.794$ ), there is still a portion of the signal that does not, indicating presence of lipids in the ECM separately from the cells (**Table 2.1**). Abundant lipid content in the ECM may be related to the unique mycobacterial cell wall but also to the fact that mycobacteria form pellicular biofilms which may follow a different way of assembly to surface attached biofilms, and rely more heavily on lipids for initial aggregation (Esteban and García-Coca, 2018). In general, presence of mycolic acids and surface exposed lipids has been linked with cording and with clumping in planktonic cultures of mycobacteria (Llorens-Fons *et al.*, 2017). The high degree of co-localization between lipids and cells in the *M. abscessus* biofilms is likely due to the fact that NR is a permeable dye and stains the cell wall as well as the lipids in the ECM, making our  $M2$  coefficient result important to understand because it shows that ~30% of the lipids are present in the ECM and are not co-occurring with cells.

Exopolysaccharides were identified as a major fraction of the ECM in *P. aeruginosa* biofilms as well as in *M. tuberculosis* biofilms where cellulose specifically was found to be essential (Ryder, Byrd and Wozniak, 2007; Trivedi *et al.*, 2016). Our group additionally identified polysaccharides to be an important part of *M. chelonae* biofilms and glucose to be increasingly present in early biofilm formation (Vega-Dominguez *et al.*, 2020). In *M. abscessus* biofilms, carbohydrates do not appear to play the same essential role, evidence that is supported by the trace presence of carbohydrates in the ECM (**Table 2.1**). Carbohydrates are dispersed

throughout the biofilm compared to lipids, as evidenced in CLSM images, but also in the numbers showing poor colocalization between GFP and dye signals (carbohydrate  $r = 0.151$ ). This distribution of proteins and carbohydrates in the ECM was anticipated given a previous study in RGM (*M. smegmatis*, *M. phlei*) and SGM (*M. gastri*, *M. kansasii*, *M. avium*) that showed that the extrapolymeric substance of RGMs is high in protein and low in carbohydrates (Lemassu, Ortalo-Magné, Bardou, Silve, Lanéelle, Daffé, *et al.*, 1996). In this study we showed that *M. abscessus* pellicles have an ECM that can be stripped away by alcohol dehydration and that the ECM consists of lipids, proteins, carbohydrates and eDNA in varying quantities. It was also shown that, as previously seen in literature, SEM and CLSM are efficient methods for visualization of biofilms. We hereby used CLSM images for co-localization analysis to determine the amount of signal from the dyes staining macromolecules in the matrix that overlaps with the signal emitted from GFP in the cells. Obtaining numerical data for the degree of colocalization was a valuable and necessary addition to the visual analysis. However, given that biofilms are live and dynamic structures, we observed a high degree of variability in the colocalization analysis depending on the biological replicate analysed. **Table 2.1** shows the final summary and average, while in the graphs in **Fig. 2.4** the extent of the unpredictability of the data is demonstrated through the error bars. This is as a result of variability in biological replicates, differences in the area of the biofilm being imaged and the fact that biofilms are thick specimens notorious for being difficult samples to image. This is important to understand and keep in mind when we study biofilms *in vitro* and look to apply those findings *in vivo*. Given the obvious variability we see in biofilm studies it becomes even more necessary to develop a model for studying biofilm formation in relation to human cells and for understanding what drives biofilm formation on a more regulatory level.

### **3 Transcriptional profile of the *M. abscessus* biofilm**

### 3.1 Introduction

The transcriptome of a cell is the complete set of RNA transcripts produced from a genome under specific circumstances (Blumenberg, 2019). Transcriptomic analysis has proven to be a useful tool for understanding differentially expressed genes (DEGs) during biofilm formation for many model organisms such *Candida albicans*, *E. coli* and *B. subtilis* (Lee *et al.*, 2011; Rajendran *et al.*, 2016; Pisithkul *et al.*, 2019), and especially human pathogens for whom biofilm formation is a virulence factor, such as *S. aureus*, *P. aeruginosa* and *S. Typhi* (Franklin *et al.*, 2015; Tan *et al.*, 2015; Chin *et al.*, 2017; Cornforth *et al.*, 2018). Understanding differential gene expression has made it possible to determine key molecules and pathways upregulated during biofilm formation giving insight into metabolic changes and mechanisms by which biofilms protect pathogens from antibiotics and the immune system (Franklin *et al.*, 2015).

While literature describing transcriptomes of mycobacterial biofilms has been emerging in the last few years, understanding of global transcriptome changes is still a predominantly unexplored field since many of the available studies have highly specific focus. A study of *M. tuberculosis* thiol-induced pellicle shows a downregulation in proteins related to cell division and replication and an upregulation in metabolism related to respiration, lipids and carbohydrates (Trivedi *et al.*, 2016). Another study in *M. smegmatis* shows that Lsr2, a nucleoid-associated protein, is necessary for intercellular aggregation but not for substratum attachment, and that these two stages are transcriptionally different to the biofilm maturation stage (Yang, Thomas, Li, Vilchèze, Derbyshire, Jacobs and Ojha, 2017). In *M. bovis* BCG transcription was compared between planktonic cells, intercellular aggregation and surface attachment, with the conclusion that *dosR* and *BCG0114* (*Rv0081*), encoding for transcriptional regulators related to oxygen availability, are significantly regulated throughout these stages (Flores-Valdez *et al.*, 2020). Both these studies focused on comparison of gene expression

between different developmental stages of biofilms, confirming that these are transcriptionally distinguishable.

A novel study in *M. cheloneae* identified a transcriptional difference between early and late-stage biofilms (Vega-Dominguez *et al.*, 2020). Genes related to lipids biosynthesis, glyoxylate shunt and redox metabolism are upregulated only in early stages of the biofilm, while genes related to transport and mycobactin biosynthesis are downregulated in both stages (Vega-Dominguez *et al.*, 2020). To date, the *M. abscessus* transcriptome was studied only in artificial sputum media, hypoxia, challenged with erythromycin and kanamycin or co-cultured with *Acanthamoeba castellanii* or murine macrophages (Miranda-CasoLuengo *et al.*, 2016; Dubois *et al.*, 2019).

There is a large knowledge gap in understanding transcriptional differences that occur in *M. abscessus* during biofilm formation. In this study we conducted an RNA-seq analysis of *M. abscessus* biofilms, comparing transcription at early and late biofilm stages to transcription at mid-log planktonic phase. This can lead to understanding events that trigger biofilm formation, genes that are needed for structure and maintenance, as well as events that lead to dispersal. The short-term aim of understanding these changes is investigating their correlation with the phenotypic changes outlined in Chapter 2 and identifying other significant changes in transcription that are unique to biofilms. Therefore, the specific aim of this chapter is to investigate the transcriptomic changes in biofilms of *M. abscessus* as compared to planktonic cells, and the specific objectives are to outline differentially expressed genes (DEGs) in early and late stages of the biofilm and identify metabolic pathways affected.

## 3.2 Results

### 3.2.1 *M. abscessus* biofilms display a distinct expression profile compared to that of planktonic cultures

RNA sequencing technique was used to gain insight into changes that occur on a transcriptional level in biofilm cells. RNA was extracted from early planktonic ( $OD_{600}=1$ ) and late planktonic cultures ( $OD_{600}=3$ ), and early biofilm (t1, day 5 post inoculation) and late biofilm (t2, day 7 post inoculation) cultures. The early planktonic timepoint served to provide a transcriptional profile of cells in exponential growth phase which was used as a baseline for analysis and comparison to transcriptional profile in biofilms. The late planktonic culture served as an exclusion criterion – it allowed for exclusion of DEGs that are expressed in stationary phase from the pool of DEGs identified in both biofilm timepoints, putting the focus solely on DEGs relevant to biofilms. Growth and sample collection was done by me at the University of Birmingham. The following process was done as a visiting collaboration to the Institute for Systems Biology in Seattle, with Dr Peterson and Dr Baliga.

Following RNA isolation, ribosomal RNA was depleted, and the purified sample of functionally relevant coding, messenger RNA (mRNA), and non-coding RNA transcripts was used for generation of a complementary DNA (cDNA) library. The sequenced library was analyzed by Dr Peterson and Dr Oriz at the Institute for Systems Biology. DEseq2 algorithm was used for defining the DEGs using the early planktonic time-point as a reference (Love, Huber and Anders, 2014).

Overall, 492 DEGs were identified in the late planktonic stage, 1108 DEGs in biofilm t1 and 1915 DEGs in biofilm t2. **Tables 3.1 and 3.2** show top 50 up- and downregulated genes with the highest log<sub>2</sub>fold change value in biofilm t1 and t2 respectively. After excluding overlapping DEGs from the late planktonic sample, that is genes expressed during stationary phase that may not be unique to the biofilm condition, there were 1175 significantly DEGs (sDEGs) in biofilm

t2 and 248 in biofilm t1, of which 218 were differentially expressed in both timepoints (**Fig. 3.1.A.**). A heat map (**Fig. 3.1.B.**) illustrates the directionality of the 218 DEGs in biofilms, five genes were downregulated with a high log<sub>2</sub>fold change, and the rest of the genes were upregulated at different magnitudes. The identities of these genes are listed in **Appendices 2** and **3**. Common sDEGs in both biofilm conditions suggests there is a group of core genes responsible for regulating biofilm formation, while the genes differentially expressed in each condition indicate the presence of a specific metabolic signature for each condition. DEGs were further excluded by applying an additional filter ( $p < 0.05$ , log<sub>2</sub> fold change  $<-2.0$  or  $>2.0$ ) that allowed for identification of sDEGs, which are the ones that will be referred to throughout the chapter. There were 240 sDEGs upregulated and 10 downregulated in biofilm t1, while in biofilm t2 667 were upregulated and 519 downregulated indicating a bigger change in gene expression in biofilm t2.

**Table 3.1: Top 50 DEGs in 5-day old *M. abscessus* biofilms (t1), based on log2(fold change) values**

Top 25 DEGs				Bottom 25 DEGs			
Gene_ID	Product	Log2fold	p_value	Gene_ID	Product	Log2fold	p_value
MAB_0669	Hypothetical PPE-family protein	8.225058	2.35E-43	MAB_1360c	Probable transcriptional regulator, TetR family	-3.10494	8.31E-18
MAB_4675c	Acyl-protein synthetase	7.520102	5.62E-59	MAB_1359c	Putative ABC transporter, ATP-binding protein	-2.39517	4.03E-13
MAB_4674c	Similarity with Nitrogen-fixing NifU-like proteins	7.516923	2.44E-43	MAB_4697	hypothetical protein	-2.16946	1.40E-12
	Hypothetical heavy metal transport/detoxification protein	7.447095	4.89E-29	MAB_1743	Hypothetical protein	-2.13843	0.000438
MAB_0667				MAB_1358c	Putative ABC transporter, permease protein	-2.13592	3.05E-15
MAB_1067	Hypothetical protein	7.400433	3.92E-72	MAB_2041c	Probable zinc-containing alcohol dehydrogenase	-2.05273	9.93E-16
MAB_0664	PE family protein	7.24549	6.40E-25	MAB_1742	Hypothetical protein	-2.04111	3.02E-06
MAB_0659	Putative dioxygenase	7.230631	5.46E-38	MAB_4698	hypothetical protein	-2.02801	1.06E-09
MAB_0660	hypothetical protein	7.018995	9.58E-36	MAB_2044	Probable phenylacetic acid degradation-related protein	-2.01259	1.52E-17
MAB_0662	hypothetical protein	6.855574	2.46E-20	MAB_2042c	hypothetical protein	-1.93405	7.01E-17
MAB_0661	Putative long chain fatty acid-coA ligase	6.73689	2.71E-36	MAB_4705c	Probable membrane protein, MmpS	-1.9318	5.15E-07
MAB_4673c	Putative aminotransferase/cysteine desulphydrase	6.51589	4.48E-40	MAB_4701	hypothetical protein	-1.91126	1.39E-17
MAB_1042c	Probable cytochrome c oxidase polypeptide I	6.420503	2.36E-66	MAB_0261	Probable amino acid ABC transporter, substrate binding	-1.90128	3.26E-21
MAB_2292c	hypothetical protein	6.30293	2.44E-12	MAB_3104c	hypothetical protein	-1.89139	5.97E-13
MAB_0663	Probable cyclic synthetase (peptide synthase)	6.150081	8.54E-33	MAB_0335	Probable cobalamin synthesis protein	-1.87546	0.001262
MAB_2270c	Putative peroxidase	5.95556	8.46E-46	MAB_4695c	Putative glycosyltransferase/rhamnosyltransferase	-1.85381	1.12E-11
MAB_4671c	Probable ABC transporter, ATP-binding protein	5.870151	4.37E-34	MAB_0809c	Conserved hypothetical PPE family protein	-1.84882	5.07E-05
MAB_4402	Heat shock protein Hsp20	5.730964	8.97E-14	MAB_0262	Probable amino acid ABC transporter, ATP-binding	-1.83337	2.96E-15
MAB_4672c	Probable ABC transporter, permease protein	5.584579	5.95E-31	MAB_1908c	hypothetical protein	-1.81089	2.59E-09
MAB_0665	PE family protein	5.541856	1.57E-24	MAB_0263	Possible osmoprotectant (glycine betaine/carnitine/choline/l-proline) ABC transporter ProW	-1.80181	3.43E-13
MAB_2271c	hypothetical protein	5.540703	7.44E-45	MAB_0686	Putative transcription regulator, TetR family	-1.79947	1.82E-11
MAB_4670c	Hypothetical protein	5.33765	5.13E-40	MAB_1975	hypothetical protein	-1.79848	5.34E-11
MAB_1245c	Hypothetical protein	5.094007	1.02E-15	MAB_0264	Possible osmoprotectant (glycine betaine/carnitine/choline/l-proline) ABC transporter ProZ	-1.79823	4.25E-11
MAB_0666	ESAT-6-like protein (10 kDa antigen)	5.093005	4.48E-24	MAB_1405	Hypothetical protein	-1.78386	0.000226
MAB_2275	Putative membrane protein, MmpL family	5.001934	1.66E-13	MAB_4918c	Pyruvate dehydrogenase E1 component alpha subunit	-1.7633	1.83E-09
MAB_0195c	Putative hydrolase, alpha/beta hydrolase fold	4.967002	3.32E-09				

**Table 3.2: Top 50 DEGs in 7-day old *M. abscessus* biofilms (t2) based on log2(fold change) values**

Top 25 DEGs				Bottom 25 DEGs			
Gene_ID	Product	Log2fold	p_value	Gene_ID	Product	Log2fold	p_value
MAB_0249	hypothetical protein	8.832579134	2.56E-73	MAB_0903	Putative enoyl-CoA hydratase/isomerase	-5.401884543	5.39E-21
MAB_4664	Hypothetical protein	8.608135036	8.35E-51	MAB_0894c	Putative dihydrolipoamide dehydrogenase (LpdA) Putative pyruvate dehydrogenase E1 component, beta	-5.077584167	1.64E-22
MAB_3148c	Probable polyketide synthase Pks5	8.220019369	5.11E-59	MAB_0896c	subunit	-4.756566978	4.70E-24
MAB_2027	Putative acyl carrier protein	8.193193384	1.78E-68	MAB_0904	Putative 3-hydroxyacyl-CoA dehydrogenase Putative phenylacetic acid degradation protein	-4.714758642	3.40E-19
MAB_2292c	hypothetical protein	8.189936022	1.20E-33	MAB_0906	PaaA/phenylacetate-CoA oxygenase, PaaG subunit	-4.608585563	3.95E-13
MAB_3147c	Probable conserved polyketide synthase associated protein	8.142513987	1.31E-60	MAB_0895c	Putative dihydrolipoamide s-acetyltransferase component of pyruvate dehydrogenase complex E2	-4.606815769	8.74E-31
MAB_1067	Hypothetical protein	8.039710011	4.93E-119	MAB_0897c	Probable pyruvate dehydrogenase E1 component, alpha subunit	-4.522330341	9.36E-27
MAB_0669	Hypothetical PPE-family protein	8.006780234	5.95E-70	MAB_0905	Putative enoyl-CoA hydratase/isomerase	-4.518996018	3.70E-12
	Probable 3-oxoacyl-(Acyl-carrier-protein) synthase II			MAB_0902	Probable beta-ketoacidipyl-CoA thiolase	-4.475746772	3.68E-24
MAB_2028	KasB	7.988698911	3.52E-60	MAB_4695c	Putative glycosyltransferase/rhamnosyltransferase	-4.443863176	5.75E-30
MAB_2280	hypothetical protein	7.971666544	2.78E-26	MAB_3105c	Hypothetical protease	-4.390941708	1.42E-41
MAB_0325c	Hypothetical protein	7.747274222	2.81E-44	MAB_0909	Putative phenylacetic acid degradation protein	-4.342328616	3.79E-15
MAB_2029	Putative beta-ketoacyl synthase	7.593504662	1.25E-75	MAB_0908	PaaD/phenylacetate-CoA oxygenase, PaaJ subunit	-4.273297499	1.52E-16
	Probable 3-oxoacyl-(Acyl-carrier-protein) synthase II			MAB_0900c	Putative phenylacetic acid degradation protein	-4.246028602	2.67E-17
MAB_2030	KasA	7.537451492	4.66E-60	MAB_0899c	PaaC/phenylacetate-CoA oxygenase, PaaI subunit	-4.240911517	1.56E-17
MAB_1247c	hypothetical protein	7.452450171	3.43E-49	MAB_4697	Possible ethyl tert-butyl ether degradation protein	-4.164061265	3.49E-24
	Probable malonyl CoA-acyl carrier protein			MAB_4696c	EthD	-4.129246863	3.59E-21
MAB_2034	transacylase	7.444212970	7.65E-53	MAB_4705c	Probable methyltransferase	-4.040392352	7.30E-16
MAB_2031	Putative beta-ketoacyl synthase	7.391957251	1.04E-77	MAB_0281	hypothetical protein	-4.020094240	1.89E-35
MAB_0659	Putative dioxygenase	7.262055742	1.09E-73	MAB_4701	hypothetical protein	-3.992763657	2.66E-40
MAB_2281	hypothetical protein	7.223512089	1.78E-25	MAB_0119c	Hypothetical protein	-3.975392800	4.36E-28
MAB_2278	Putative oxidoreductase	7.191863362	1.10E-20		Possible ribosomal-protein-alanine acetyltransferase	-3.936863966	4.36E-28
MAB_3900c	hypothetical protein	7.139718720	1.36E-63	MAB_1088	RimJ	-3.929988671	1.55E-17
	Hypothetical heavy metal transport/detoxification protein			MAB_2877c	Probable adenine phosphoribosyltransferase	-3.917934952	1.54E-26
MAB_0667		7.060170950	1.19E-50	MAB_0686	Putative transcription regulator, TetR family	-3.878492115	4.38E-45
MAB_2032	Probable 3-oxoacyl-[acyl-carrier protein] reductase	6.945026823	1.71E-88	MAB_4694c	Glycosyltransferase		
	Putative monooxygenase (salicylate/ hydroxybenzoate hydroxylase)						
MAB_0288	hydroxylase	6.930342213	5.75E-13				
MAB_2941	Putative oxidoreductase	6.926268040	1.02E-51				
MAB_2275	Putative membrane protein, MmpL family	6.800121856	1.92E-57				

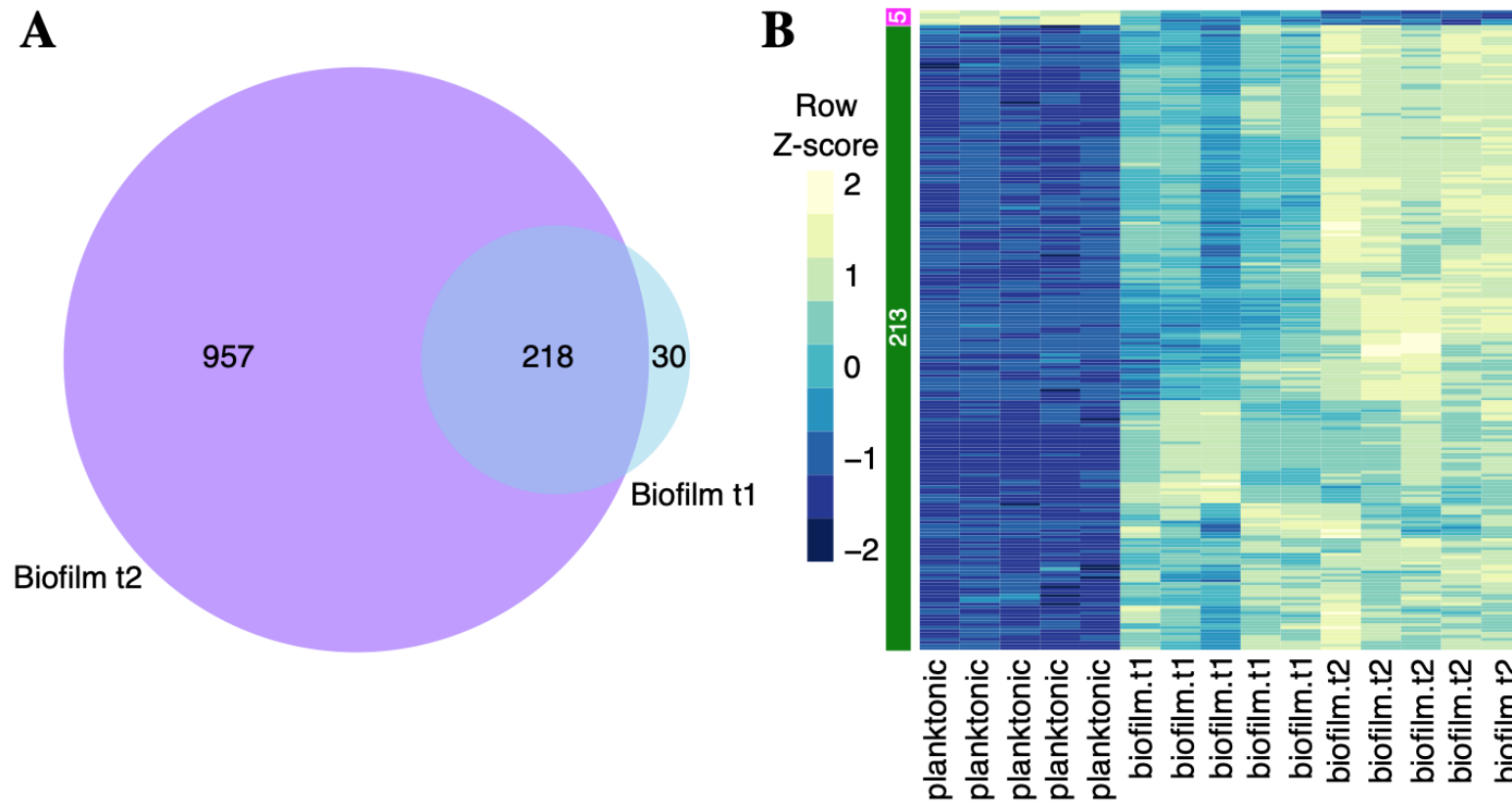


**Figure 3.1: Differentially expressed genes in *M. abscessus* biofilms.** **A.** Venn diagram illustrating common and unique DEGs expressed during biofilm t1 and t2. **B.** Heatmap of z-scores of the 218 DEGs that are significantly differentially expressed in both biofilm t1 and t2, compared to planktonic. Five repeats indicate five biological replicates used in the experiments.

### **3.2.2 Common downregulated genes in biofilm t1 and t2 are involved in efflux regulation**

Five genes are downregulated in both early, t1, and late, t2, stages of biofilm (**Appendix 2**) and they belong to two operons. *MAB\_4697* and *MAB\_4698* form one operon and although they are annotated as “hypothetical proteins” in the *M. abscessus* genome annotated database, a protein sequence BLAST search against a *M. tuberculosis* database identified them as belonging to the family of regulatory GTPase-activating proteins (GAP), at 30-40% sequence identity. Found on one operon, with two other genes, *MAB\_1358c*, *MAB\_1359c* and *MAB\_1360c* encode an ABC transporter permease protein, an ATP binding protein and a transcriptional regulator in the TetR family, respectively. A protein BLAST against an *M. tuberculosis* database, determined that *MAB\_1360c* has 54% identity sequence identity with *M. tuberculosis* RaaS (*Rv1219c*), a regulator for antimicrobial-assisted survival, while *MAB\_1359c* is homologous to the multidrug efflux system ATP-binding proteins *Rv1218c*. In *M. bovis* BCG long-term survival was increased when exposed to antibiotics as a result of the induction of transcription of RaaS (*bcg1279*) which suppresses expression of specific ATP-dependant efflux pumps (Turapov *et al.*, 2014). The study hypothesizes that during active growth, expression of RaaS is regulated, while under stressful conditions it is employed to reduce efflux, allowing the cells to slow their metabolism and focus on synthesis of storage compounds. In *M. abscessus* biofilms the opposite was shown, indicating an additional role of these proteins, or a need for expression rather than suppression of efflux systems.

### **3.2.3 Common upregulated genes in biofilm t1 and t2 point to changes in cell wall biosynthesis**

Within the 218 common upregulated sDEGs, groups of genes with similar functions could be identified (**Appendix 3**), out of which a large proportion, 77 genes, are not annotated. Thirty genes involved in lipid biosynthesis were identified and 10 membrane proteins including ABC

transporters and 2 lipid transfer proteins, Ltp1 (*MAB\_2951c* and *MAB\_0378*). This points to the importance of lipids and modulation of the cell wall in *M. abscessus* biofilms. The transporters could also be used to traffic molecules to the extracellular space, feeding into the ECM. Amongst these genes are several that encode for mycolic acid synthesis and processing, such as *KasA* and *KasB*, responsible for elongation of mycolic acids and *DesA1*, encoding a desaturase. Another gene of note amongst these is *MAB\_3148c* encoding the Pks5 protein which in *M. tuberculosis* has been linked to cell surface modifications which manifested as a change in colony morphology (Etienne *et al.*, 2009; Boritsch *et al.*, 2016).

From the eight proteins associated with PE/PPE and ESAT protein families that were identified, *MAB\_0669*, annotated as a hypothetical PPE-family protein, was the most interesting because it was highly upregulated in both conditions (log2fold: t1=8.22, t2=8.01). A protein sequence BLAST search revealed that a similar protein is present in *M. tuberculosis*, but of an unknown function. Although the function of most PE/PPE proteins is unknown, their presence in the majority of slow-growing mycobacteria and their role in host-pathogen interactions has been documented (Fishbein *et al.*, 2015; Qian *et al.*, 2020). Limited studies have shown that disruption of PE/PPE genes leads to changes in the cell surface, prevention of biofilm formation and increase in antibiotic resistance (Danilchanka, Mailaender and Niederweis, 2008; Dong *et al.*, 2012). This implies that PE/PPE have a structural role in maintenance of the cell wall integrity, explaining their upregulation in biofilms.

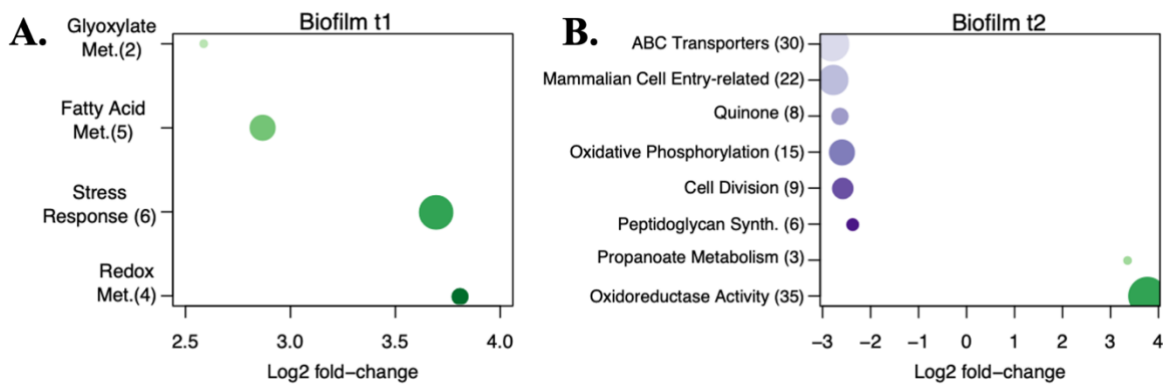


**Figure 3.2: Enriched metabolic pathways and functional groups in *M. abscessus* biofilms.** Lists of enriched metabolic pathways and functional groups showing log<sub>2</sub> fold-change for each for biofilm t1 (**A.**) and t2 (**B.**), with respect to the planktonic t1 sample. Numbers in parentheses indicate the number of DEGs associated with each functional term. This quantity is also indicated by the size of each circle (the higher the number, the bigger the node). Down- and upregulated functional terms are indicated with purple and green nodes, respectively. Darker colours indicate higher log<sub>2</sub> fold-changes.

### **3.2.4 Enriched metabolic pathways vary between early and late *M. abscessus* biofilms**

In this study we aimed to understand patterns in gene expression that lead to biofilm formation or that sustain the biofilm condition. To understand the global transcription changes, we used pathway enrichment analysis to highlight the most affected metabolic pathways. This analysis was done by Dr Peterson and Dr Oriz at Institute for Systems Biology using the Database for Annotation, Visualization, and Integrated Discovery (DAVID) (Jiao *et al.*, 2012). Enriched metabolic pathways for biofilm t1 and t2 are shown in **Figure 3.2 A.** and **B.**, respectively, and individual DEGs in each pathway are shown in **Tables 3.3** and **3.4**.

At the early biofilm stage, t1, when the biofilm is mature, four pathways were upregulated relating to stress response, fatty acid biosynthesis, glyoxylate biosynthesis and redox metabolism (**Fig. 3.2.A.**). At the late biofilm stage, t2, eight pathways were enriched: six pathways, related to ABC transporters, quinone metabolism, oxidative phosphorylation, cell division, mammalian cell entry (MCE), and peptidoglycan synthesis, were downregulated, and two pathways, related to oxidoreductase activity and propanoate metabolism, were upregulated (**Fig. 3.2.B.**).

### **3.2.5 Glyoxylate metabolism is upregulated in early biofilms**

Glyoxylate metabolism, which enables the conversion of acetyl-CoA, produced by  $\beta$ -oxidation of fatty acids, to succinate which is converted into malate during the Krebs cycle (Vallarino and Osorio, 2018), was upregulated in early biofilm stage, t1 (**Fig. 3.2.A.**). The DEGs in this pathway were L-alanine dehydrogenase, *MAB\_3100*, and isocitrate lyase, *MAB\_4095c*, which were also upregulated in biofilm t2 (**Table 3.3**). L-alanine dehydrogenase converts pyruvate to alanine, and glyoxylate to glycine causing the oxidation of NADH to NAD<sup>+</sup>. It is upregulated in a variety of conditions such as: nutrient starvation, artificial sputum media (meant to represent a CF lung environment), hypoxia, *in vitro* under persistence-inducing stresses such as

nitric oxide, *in vivo* during lung infection in mice and in persistent *M. tuberculosis* (Giffin *et al.*, 2016; Miranda-CasoLuengo *et al.*, 2016). Isocitrate lyase, *MAB\_4095c*, was also overexpressed in non-replicative persistent *M. tuberculosis* studied under hypoxic conditions. The same study suggests that as a result of upregulation of alanine dehydrogenase and isocitrate lyase, but not malate synthase, there is a shift in carbon flow through alanine dehydrogenase rather than through the glyoxylate cycle under hypoxia and non-replicative conditions in *M. tuberculosis* (Giffin *et al.*, 2016). The upregulation of these enzymes could suggest that a similar event is taking place in *M. abscessus* biofilms.

### **3.2.6 Fatty acid metabolism is upregulated in early *M. abscessus* biofilms**

Fatty acid biosynthesis pathway is upregulated by 2.8 log2 fold-change in early biofilm, t1 (**Fig. 3.2**). The five upregulated genes identified in this pathway, *MAB\_2030*, *MAB\_2028*, *MAB\_2032*, *MAB\_3354* and *MAB\_3455c*, are all involved in fatty acid chain elongation or modification. Genes encoding for KasA/B complex, *MAB\_2030* and *MAB\_2028*, involved in FAS-II cycle of fatty acid biosynthesis likely contribute to the lengthening of mycolic acids chains in biofilms. *MAB\_3354* encodes for DesA1, a desaturase protein responsible for creating double bonds in mycolic acids (Singh *et al.*, 2016). Although this pathway was not identified as upregulated in the late-stage biofilm, t2, genes encoding for KasA/B complex and DesA1 were highly upregulated (**Table 3.2**).

### **3.2.7 Redox metabolism and oxidoreductases are upregulated in early and late biofilms**

In early biofilm, t1, the highest upregulated pathway is the redox pathway with four identified DEGs, *MAB\_0660*, *MAB\_2630*, *MAB\_2631* and *MAB\_2632*, involved in this metabolism (**Table 3.3**). While *MAB\_0660* is a hypothetical protein, the rest encode for subunits of the cytochrome D ubiquinol oxidases, CydA, CydB and CydD. An *E. coli* knock-out strain of *cydAB* was unable to form a mature biofilm or an ECM, suggesting importance of these

molecules and offering a perspective for their upregulation (Beebout *et al.*, 2019). Furthermore, redox was shown to be an important metabolic state for initial formation of biofilms by several other studies. Thiol-reductive stress induces 6x quicker biofilm formation in *M. tuberculosis* and in *M. smegmatis* biofilms the NADH/NAD<sup>+</sup> ratio is 3x higher compared to planktonic cells, indicating the presence of a reductive environment (Anand *et al.*, 2015; Trivedi *et al.*, 2016). Oxidoreductase activity is strongly upregulated in biofilm t2, with 35 genes encoding for different reductases, oxidases, oxidoreductases, and desaturases upregulated (**Table 3.4**). Amongst the genes identified in this group are the same subunits of cytochrome D ubiquinol oxidases that are upregulated in early biofilms, as well as *MAB\_2467*, a ubiquinol-cytochrome C reductase, a cytochrome B subunit. Several short-chain dehydrogenase/reductases are also identified and a few hypothetical proteins. Oxidoreductases and enzymes from the similar protein family are mainly associated with energy transfer and therefore their upregulation in late stages could be associated with biofilm dispersal and reversion to planktonic growth.

### 3.2.8 Oxidative phosphorylation is downregulated in late biofilms

In the late biofilm stage, t2, the oxidative phosphorylation pathway was downregulated. Most of the genes identified in this cluster are subunits of the NADH-quinone oxidoreductase, an enzyme that plays an essential role in oxidative phosphorylation in *M. tuberculosis* and has a function of catalysing the transfer of electrons from NADH to the quinone pool (Yano *et al.*, 2014). Quinones identified as downregulated in *M. abscessus* biofilm t2 show the cluster of the same NADH-quinone oxidoreductase subunits. The same trend is seen in *M. bovis* BCG, with genes relating to oxidative phosphorylation downregulated in biofilms. In BCG this leads to a process called the Crabtree effect, where ATP is generated via glycolysis rather than oxidative phosphorylation (Zeng *et al.*, 2019).

### **3.2.9 Genes related to MCE and ABC transporters are downregulated in late biofilms**

Genes identified as related to mammalian cell entry (MCE) are downregulated in biofilm t2 in *M. abscessus* (**Fig. 3.2**). In *M. smegmatis* and *M. tuberculosis* *mce4*, an *mce* operon, is needed for cholesterol utilization and uptake (García-Fernández *et al.*, 2017). In *M. chelonae* biofilms there is also a downregulation in MCE genes in early and late biofilms, specifically when looking at operon *mce5* (Vega-Dominguez *et al.*, 2020). Deletion of all six *mce* operons leads to cell envelope changes, and results in rougher and dryer colonies in *M. smegmatis* (Klepp *et al.*, 2012). In contrast to the expression profile of MCE in *M. abscessus* biofilms, in stationary phase *M. tuberculosis* the *mce* operons are upregulated (P. Singh *et al.*, 2016).

Some of the same genes are identified as downregulated in both the MCE group and ABC transporters, such as *MAB\_1009c*, *MAB\_4567c*, *MAB\_4035*, *MAB\_4598c*, *MAB\_4031*, *MAB\_4149c*, *MAB\_4150c* and *MAB\_4148c*, all annotated as putative MCE family proteins (**Table 3.4**). *MAB\_4149c*, annotated as LprN, a lipoprotein known in *M. tuberculosis* to trigger a cell-mediated immune response, was previously identified as important for expression of ESX-4 type 7 secretion system in *M. abscessus* (Pasricha *et al.*, 2014; Laencina *et al.*, 2018). Amongst the listed ABC transporters are members of the *mce* operons, such as different genes encoding YrbE proteins, which are integral membrane protein that can function as ABC transporters.

**Table 3.3: Enriched metabolic pathways for early biofilm growth stage at day 5, t1.**

PATHWAY	LOCUS	PRODUCT	LOG2FOLD	AVG_PVALUE
Glyoxylate Metabolism	MAB_3100	L-alanine dehydrogenase (ALD)	3.140	2.20E-16
	MAB_4095c	Isocitrate lyase (AceA)	2.035	6.53E-13
Fatty acid metabolism	MAB_2030	Probable 3-oxoacyl-(Acyl-carrier-protein) synthase II KasA	2.685	3.29E-07
	MAB_2028	Probable 3-oxoacyl-(Acyl-carrier-protein) synthase II KasB	3.053	5.01E-07
Fatty acid metabolism	MAB_2032	Probable 3-oxoacyl-[acyl-carrier protein] reductase	2.113	3.23E-06
	MAB_3354	Probable acyl-[acyl-carrier protein] desaturase DesA1	3.780	2.45E-15
Stress response	MAB_3455c	Putative acyl-CoA thiolase	2.729	4.58E-10
	MAB_4265c	Chaperone ClpB	3.617	1.48E-23
Stress response	MAB_4271c	Chaperone protein DnaJ	2.937	8.70E-11
	MAB_4273c	Chaperone protein DnaK (Hsp 70)	3.941	6.27E-20
Redox metabolism	MAB_4402	Heat shock protein Hsp20	5.731	8.97E-14
	MAB_4270c	Probable heat shock protein transcriptional regulator HspR	2.304	2.45E-08
Redox metabolism	MAB_4272c	Protein GrpE (HSP-70 cofactor)	3.645	2.72E-14
	MAB_0660	Hypothetical protein	7.019	9.58E-36
Redox metabolism	MAB_2630	Probable integral membrane cytochrome D ubiquinol oxidase (Subunit I) CydA	2.636	6.45E-25
	MAB_2631	Probable cytochrome D ubiquinol oxydase CydB	3.153	5.86E-36
	MAB_2632	Probable ATP-binding protein ABC transporter CydD	2.430	4.89E-34

**Table 3.4: Enriched metabolic pathways for late biofilm growth stage at day 7, t2**

PATHWAY	LOCUS	PRODUCT	LOG2FOLD	AVG_PVALUE
Mammalian cell entry-related	MAB_1005c	Putative MCE family protein	-3.604	3.00E-35
	MAB_1006c	Putative MCE family protein	-3.244	4.15E-29
	MAB_1007c	Putative MCE family protein	-3.149	1.29E-18
	MAB_4564c	Putative Mce family protein	-3.083	2.63E-23
	MAB_1008c	Putative MCE family protein	-3.013	1.94E-25
	MAB_1009c	Putative MCE family protein	-3.009	2.18E-17
	MAB_4563c	Putative Mce family protein	-2.960	8.67E-28
	MAB_4567c	Putative Mce family protein	-2.912	8.61E-15
	MAB_4566c	Putative Mce family protein	-2.839	3.47E-21
	MAB_4594c	Putative Mce family protein	-2.831	2.02E-23
	MAB_4595c	Putative Mce family protein	-2.740	2.37E-12
	MAB_4596c	Putative Mce family protein	-2.740	8.82E-19
	MAB_4034	Putative Mce family protein	-2.718	1.60E-13
	MAB_4035	Putative Mce family protein	-2.701	4.96E-18
	MAB_4565c	Putative Mce family protein	-2.648	1.88E-19
	MAB_4598c	Putative Mce family protein	-2.627	4.41E-16
	MAB_4031	Putative Mce family protein	-2.506	1.75E-09
Quinone	MAB_4149c	Hypothetical MCE-family protein LprN	-2.463	5.70E-16
	MAB_4568c	Putative Mce family protein	-2.438	3.78E-21
	MAB_4150c	Hypothetical MCE-family protein	-2.306	2.29E-12
	MAB_4148c	Hypothetical MCE-family protein	-2.246	9.50E-17
	MAB_4030	Putative Mce family protein	-2.219	2.48E-11
	MAB_2134	NADH-quinone oxidoreductase, A subunit NuoA	-3.868	3.37E-19
	MAB_2135	NADH-quinone oxidoreductase, B subunit NuoB	-3.212	5.10E-29
	MAB_2144	NADH-quinone oxidoreductase, K subunit NuoK	-2.587	1.35E-10

<b>ABC transporters</b>	MAB_2141	NADH-quinone oxidoreductase, H subunit NuoH	-2.517	7.24E-10
	MAB_2136	NADH-quinone oxidoreductase, C subunit NuoC	-2.344	1.61E-12
	MAB_2137	NADH-quinone oxidoreductase, D subunit NuoD	-2.308	1.12E-10
	MAB_2147	NADH-quinone oxidoreductase, N subunit NuoN	-2.127	4.09E-11
	MAB_2142	NADH-quinone oxidoreductase, I subunit NuoI	-2.123	3.16E-06
	MAB_0264	Possible osmoprotectant (glycine betaine/ carnitine/choline/l-proline) ABC transporter ProZ	-3.749	3.34E-16
	MAB_1227	Putative ABC transporter, permease protein	-3.643	1.36E-15
	MAB_1012c	Putative YrbE family protein	-3.472	5.25E-34
	MAB_0263	Possible osmoprotectant (glycine betaine/ carnitine/choline/l-proline) ABC transporter ProW	-3.466	6.32E-15
	MAB_1226	Putative ABC transporter, ATP-binding protein	-3.414	1.10E-17
	MAB_1225	Putative ABC transporter, permease protein	-3.132	6.94E-19
	MAB_4601c	Putative YrbE family protein	-3.128	1.55E-32
	MAB_1228	Putative ABC transporter	-3.050	5.71E-13
	MAB_1011c	Putative YrbE family protein	-3.025	1.96E-15
	MAB_4600c	Putative YrbE family protein	-3.022	2.06E-18
	MAB_1009c	Putative MCE family protein	-3.009	2.18E-17
	MAB_3053	Putative glutamate ABC transporter, permease	-2.942	2.73E-17
	MAB_0262	Probable amino acid ABC transporter, ATP-binding	-2.936	1.21E-20
	MAB_4567c	Putative Mce family protein	-2.912	8.61E-15
	MAB_3871c	Possible ribonucleotide ABC transporter, ATP-binding	-2.900	4.70E-15
	MAB_4035	Putative Mce family protein	-2.701	4.96E-18
	MAB_4598c	Putative Mce family protein	-2.627	4.41E-16
	MAB_4031	Putative Mce family protein	-2.506	1.75E-09
	MAB_2434	Molybdenum ABC transporter ModB, permease	-2.486	1.12E-07
	MAB_0428	Probable peptide ABC transporter DppC	-2.477	3.04E-08
	MAB_4032	Putative Mce family protein	-2.465	2.93E-13

	MAB_4149c	Hypothetical MCE-family protein LprN	-2.463	5.70E-16
	MAB_4151c	Hypothetical MCE-family protein	-2.445	1.69E-12
	MAB_3052	Putative glutamate ABC transporter, permease	-2.439	8.27E-17
	MAB_4150c	Hypothetical MCE-family protein	-2.306	2.29E-12
	MAB_0277c	Probable amino acid ABC transporter, permease	-2.267	6.11E-10
	MAB_4148c	Hypothetical MCE-family protein	-2.246	9.50E-17
	MAB_2149	Hypothetical protein	-2.187	2.45E-14
	MAB_4029	Putative YrbE family protein	-2.182	1.43E-06
	MAB_3051	Putative glutamate ABC transporter, periplasmic protein	-2.071	1.41E-11
Cell division	MAB_2008	Putative cell division protein FtsQ	-3.192	1.04E-20
	MAB_0036c	Probable cell division protein RodA	-2.980	2.54E-21
	MAB_2005	Putative cell division protein FtsW	-2.734	1.05E-26
	MAB_2001	UDP-N-acetylmuramyl-tripeptide synthetase MurE	-2.690	1.93E-23
	MAB_2007	UDP-N-acetylmuramate--L-alanine ligase MurC	-2.552	9.28E-22
	MAB_2004	UDP-N-acetylmuramoylalanine--D-glutamate ligase MurD	-2.472	3.66E-19
	MAB_3074c	Probable cell division protein FtsK	-2.363	3.23E-17
	MAB_2006	UDP-N-acetylglucosamine--N-acetylmuramyl-(pentapeptide) pyrophosphoryl-undecaprenol N-acetylglucosamine transferase MurG	-2.209	9.72E-16
	MAB_2003	Phospho-N-acetylmuramoyl-pentapeptide-transferaseMurX	-2.011	7.85E-17
	MAB_2134	NADH-quinone oxidoreductase, A subunit NuoA	-3.868	3.37E-19
Oxidative phosphorylation	MAB_4422	Putative succinate dehydrogenase, flavoprotein subunit	-3.229	5.75E-18
	MAB_2135	NADH-quinone oxidoreductase, B subunit NuoB	-3.212	5.10E-29
	MAB_4423	Putative succinate dehydrogenase, iron-sulfur subunit	-2.813	8.63E-17
	MAB_2140	NADH-quinone oxidoreductase, G subunit NuoG	-2.647	4.13E-11
	MAB_2144	NADH-quinone oxidoreductase, K subunit NuoK	-2.587	1.35E-10
	MAB_2141	NADH-quinone oxidoreductase, H subunit NuoH	-2.517	7.24E-10
	MAB_2145	NADH-quinone oxidoreductase, L subunit NuoL	-2.430	2.93E-12

<b>Peptidoglycan synthesis</b>	MAB_2136	NADH-quinone oxidoreductase, C subunit NuoC	-2.344	1.61E-12
	MAB_2137	NADH-quinone oxidoreductase, D subunit NuoD	-2.308	1.12E-10
	MAB_2138	NADH-quinone oxidoreductase, E subunit NuoE	-2.260	1.13E-06
	MAB_2143	NADH-quinone oxidoreductase, J subunit NuoJ	-2.254	6.65E-11
	MAB_2139	NADH-quinone oxidoreductase, F subunit NuoF	-2.129	2.52E-09
	MAB_2147	NADH-quinone oxidoreductase, N subunit NuoN	-2.127	4.09E-11
	MAB_2142	NADH-quinone oxidoreductase, I subunit NuoI	-2.123	3.16E-06
	MAB_2001	UDP-N-acetyl muramyl-tripeptide synthetase MurE	-2.690	1.93E-23
	MAB_2007	UDP-N-acetyl muramate--L-alanine ligase MurC	-2.552	9.28E-22
	MAB_2004	UDP-N-acetyl muramoylalanine--D-glutamate ligase MurD	-2.472	3.66E-19
	MAB_1482	Probable glutamate racemase MurI	-2.276	3.05E-18
	MAB_2006	UDP-N-acetyl glucosamine--N-acetyl muramyl-(pentapeptide) pyrophosphoryl-undecaprenol N-acetyl glucosamine transferase MurG	-2.209	9.72E-16
	MAB_2003	Phospho-N-acetyl muramoyl-pentapeptide-transferase MurX	-2.011	7.85E-17
	MAB_4842	Putative arsenate reductase ArsC	6.789	9.84E-64
	MAB_2282	Putative flavin-dependent reductase	6.573	4.74E-15
	MAB_0289	hypothetical protein	5.716	9.83E-11
	MAB_2283	Putative oxidoreductase	5.465	8.68E-26
	MAB_2284	Putative halogenase	5.068	1.49E-22
	MAB_4635	Probable NADH:flavin oxidoreductase/NADH oxidase	5.058	7.26E-52
	MAB_2381	Probable oxidoreductase	5.012	1.43E-69
	MAB_2071	Probable short-chain dehydrogenase/reductase	4.921	2.90E-31
	MAB_1874	Putative oxidoreductase	4.885	7.54E-29
	MAB_2520c	hypothetical protein	4.879	2.43E-35
	MAB_0067	hypothetical protein	4.579	6.85E-27
<b>Oxidoreductase Activity</b>	MAB_0646c	Putative short-chain dehydrogenase/reductase	4.536	4.74E-33
	MAB_2631	Probable cytochrome D ubiquinol oxidase CydB	4.476	2.95E-96

	MAB_3019	Probable fatty acid hydroxylase	4.395	2.44E-26
	MAB_2630	Probable integral membrane cytochrome D ubiquinol oxidase (Subunit I) CydA	4.307	1.71E-84
	MAB_4478c	Putative short-chain dehydrogenase/reductase	3.891	7.97E-15
	MAB_2540c	Putative Short-chain dehydrogenase/reductase	3.790	1.82E-31
	MAB_3330	Putative salicylate hydroxylase	3.757	5.26E-12
	MAB_3939	hypothetical protein	3.094	3.18E-09
	MAB_0052	hypothetical protein	3.066	4.04E-11
	MAB_2678	Conserved hypothetical protein (putative oxidoreductase)	2.993	3.23E-19
	MAB_4173	Possible oxidoreductase	2.933	1.04E-21
	MAB_1588c	Putative oxidoreductase	2.927	3.10E-10
	MAB_1587c	Probable fatty acid desaturase	2.747	6.69E-09
	MAB_3377	hypothetical protein	2.747	1.61E-23
	MAB_3506c	Putative short-chain dehydrogenase/reductase	2.603	1.10E-07
	MAB_3710	Possible multi-functional enzyme with acyl-CoA-reductase activity AcrA1	2.503	2.26E-26
	MAB_0830	Probable NADH-dependent flavin oxidoreductase	2.397	5.28E-18
	MAB_4739	Probable FAD dependent oxidoreductase	2.393	1.69E-16
	MAB_2235	Possible siderophore-interacting protein	2.373	4.95E-09
	MAB_0623	Probable dehydrogenase	2.352	2.57E-11
	MAB_0380	Probable short-chain dehydrogenase/reductase	2.333	3.09E-17
	MAB_2467	Ubiquinol-cytochrome c reductase cytochrome b subunit	2.144	6.14E-29
	MAB_2966c	Possible hemoglobin-related protein HMP	2.132	2.48E-08
	MAB_1499	Putative FAD dependent oxidoreductase	2.082	6.75E-06
<b>Propanoate Metabolism</b>	MAB_4095c	Isocitrate lyase (AceA)	4.529	2.90E-42
	MAB_4617	Methylcitrate dehydratase family (MmgE/PrpD)	3.209	1.57E-12
	MAB_4619	Probable citrate synthase	2.338	7.15E-15

### **3.3 Discussion**

Transcriptomic studies of biofilm forming pathogens have shown ubiquitous differential expression of genes that act in response to stressful environments by aggregating and forming communities. There is evidence to suggest remodelling of pathways that affect central carbon metabolism and primary biosynthetic pathways, changes in genes that lead to an increase in production of the ECM and in antibiotic resistance, and a shift in cells to an energy conservation state (Chin *et al.*, 2017; Cornforth *et al.*, 2018; Pisithkul *et al.*, 2019). Transcription analysis of genes expressed in mycobacterial biofilms are limited, and to date there are none that focus on *M. abscessus* biofilms. From studies that challenged *M. abscessus* in artificial sputum media it is known that this bacteria shares similar metabolic strategies for survival as other CF pathogens and mirrors transcriptional responses that lead to persistence in mycobacteria (Miranda-CasoLuengo *et al.*, 2016). In this study, transcriptomes of early and late-stage *M. abscessus* biofilms were analysed, and overall, there is a change in gene expression that leads to modulation of the cell wall, primarily indicated by the strong upregulation of genes involved in lipid biosynthesis.

#### **3.3.1 Genes involved in modulation of mycolic acid are upregulated in biofilms**

Five genes are upregulated in the fatty acid biosynthesis pathway in early biofilms amongst which the notable ones are genes encoding for KasA/B, *MAB\_2030* and *MAB\_2028*, and a desaturase protein DesA1, *MAB\_3354*. Together this upregulation is likely to contribute to the lengthening of mycolic acid chains in biofilms and modulation of the cell wall. Previous studies showed that the fatty acid metabolism is also upregulated upon exposure of *M. abscessus* to amikacin, indicating an attempt from the bacteria to alter membrane permeability and increase chance of survival. In the oxidoreductases group that is upregulated in biofilm t2 are several short-chain dehydrogenases/reductases that play a role in lipid biosynthesis, further highlighting the importance of lipid biosynthesis throughout biofilm stages. Changes in

KasA/B have been known to alter cell wall in other mycobacteria as well. *kasA* and *kasB*, alongside *acpM* and *fas*, were upregulated during surface attachment in *M. bovis* BCG (Flores-Valdez *et al.*, 2020). In *M. tuberculosis*, downregulation of KasA/B is associated with changes in colony morphology, and in *M. smegmatis* reduction in KasA is associated with transition to biofilms (Bhatt *et al.*, 2007; Ghosh, Indi and Nagaraja, 2013).

### **3.3.2 Glyoxylate metabolism is required in non-replicative systems such as biofilms**

L-alanine dehydrogenase upregulation in biofilms suggests it has a vital role in cell regrowth particularly because modifications in the glyoxylate metabolism appear ubiquitous amongst growth environments that require arrest in growth followed by regrowth such as biofilms, nutrient starvation and persistence during infections (Giffin *et al.*, 2016). A *M. tuberculosis* L-alanine dehydrogenase deletion mutant showed a lag in resuming growth after reoxygenation, following hypoxia, and an altered NADH/NAD<sup>+</sup> ratio suggesting this enzyme's important role in preparation for regrowth (Giffin *et al.*, 2016). Deletion of isocitrate lyase in *M. tuberculosis* means that no chronic infection is established, and studies have shown that inhibition of this enzyme forces bacteria to re-enter a replicative stage (McKinney *et al.*, 2000; Van Schaik, Tom and Woods, 2009). This implies the importance of isocitrate lyase in maintenance of a non-replicative state in bacteria, which are found in biofilms as well, explaining the upregulation in expression of this gene in *M. abscessus* biofilms. In artificial sputum media *M. abscessus* genes related to the amino acid metabolism and fatty acid catabolism are upregulated, highlighting the increasing reliance on the glyoxylate shunt for growth and persistence in the CF lung, similar to results seen in chronic *P. aeruginosa* infections (Miranda-CasoLuengo *et al.*, 2016). This suggests that progression towards a biofilm, as *P. aeruginosa* does *in vivo*, would be advantageous for long term infections and in this study we identified a complimentary increase in glyoxylate metabolism (Miranda-CasoLuengo *et al.*, 2016). Together with the evidence of

downregulation of cell division and peptidoglycan biosynthesis, the upregulation in glyoxylate pathway suggests a non-replicative state for some of the cells in the biofilm. Additionally, if *M. tuberculosis* is known to use host lipid as a carbon source during infection and employ the glyoxylate pathway to preserve carbon, a similar event of energy preservation using the glyoxylate shunt might be taking place in *M. abscessus* biofilms.

### **3.3.3 Export systems are downregulated in *M. abscessus* biofilms**

MCE genes are highly conserved and ubiquitous in mycobacteria, irrespective of pathogenicity and growth phenotypes (Bachmann *et al.*, 2020). As secreted or surface exposed proteins that comprise ABC transporters and oxidoreductases, and play a role in entry to mammalian cells and intracellular survival, they are important for an array of cellular functions and biofilm formation is no exception (Forrellad *et al.*, 2013). In *M. smegmatis* the deletion of all six *mce* operons resulted in rough morphology that increased the amount of clumping in biofilms, and allowed the biofilms to persist for longer – 26 days as opposed to 8 days with wild type cells (Klepp *et al.*, 2012). In *M. tuberculosis* deletion of the *mce1* operon, which encodes an ABC lipid transporter, leads to an accumulation of free mycolic acid (FMA) in the cell wall, and a disruption of the *mce2* operon causes an accumulation in sulfolipids (Marjanovic, Iavarone and Riley, 2011; Cantrell *et al.*, 2013; Queiroz *et al.*, 2015). Perhaps the downregulation in MCE genes in *M. abscessus* late biofilms is related to changes in the cell envelope and indeed a large number of genes related to ABC transporters are downregulated in biofilm t2. *M. abscessus* could be employing a mechanism to preserve energy by limiting diffusion after the biofilm has been formed.

In conclusion, the documented transcriptional changes offer an identification of genes necessary for biofilm formation in *M. abscessus*. The upregulation of the glyoxylate metabolism and the downregulation of genes responsible for cell division and peptidoglycan biosynthesis in biofilms are indicative of an environment of energy preservation, while the

increase of redox metabolism suggests an anaerobic environment in parts of the biofilm. Genes encoding fatty acid biosynthesis are upregulated indicating cell wall alteration in biofilms or increased production of lipids – perhaps related to the lipid-rich ECM. Further analysis is required to determine how these genes fit into the bigger picture of biofilm formation *in vivo* during infections, because genetic expression is different when compared across different conditions (Miranda-CasoLuengo *et al.*, 2016; Dubois *et al.*, 2019).

## **4 Biochemical characterization of the *M. abscessus* biofilm extracellular matrix**

## 4.1 Introduction

Previously, the biofilm ECM was shown to consist of a range of secreted components (lipids, polysaccharides, proteins and eDNA), ubiquitously expressed in biofilm forming bacteria (Donlan, 2002; Flemming and Wingender, 2010; Flemming *et al.*, 2016; Karygianni *et al.*, 2020; Vega-Dominguez *et al.*, 2020). The extrapolymeric substance of some mycobacterial species has been previously characterized and carbohydrates were identified as a major component (Lemassu, Ortalo-Magné, Bardou, Silve, Lanéelle and Daffé, 1996; Trivedi *et al.*, 2016; Vega-Dominguez *et al.*, 2020). Carbohydrates were scattered in the *M. abscessus* biofilm ECM and made up a small biovolume, however lipids were demonstrated as the major component (Chapter 2). MDAG, mycolic acids and GPLs in particular have been shown as important for formation and maturation of pellicles of other mycobacterial species (Recht and Kolter, 2001; Ojha *et al.*, 2005; Pacheco *et al.*, 2013; Yang, Thomas, Li, Vilchèze, Derbyshire, Jacobs, Ojha, *et al.*, 2017; Halkerston *et al.*, 2020). An increase in FMA is universally documented in mycobacterial biofilms and seen as a hallmark of pellicle formation in this species, and it is a plausible hypothesis that these molecules make up the lipids identified in the ECM. Transcription analysis of *M. abscessus* biofilms (Chapter 3) showed an increase in the expression of mycolic acid biosynthesis genes in biofilms. This indicates that there are potential molecular changes in mycolic acids occurring during biofilm formation.

Therefore, the aim of this chapter was to study the biochemical composition of the *M. abscessus* biofilm ECM. The first objective was to conduct a comprehensive analysis of the lipid profile of planktonic and biofilm cells, with a focus on mycolic acids. The second objective was to determine the composition of surface-exposed carbohydrates in *M. abscessus* biofilms and planktonic cultures.

## 4.2 Results

### 4.2.1 Comprehensive lipid profile of *M. abscessus* biofilms

Increase in FMA is a hallmark of biofilm formation and maturation in mycobacteria and can be used as a control to affirm biofilm maturation (Ojha *et al.*, 2008; Vega-Dominguez *et al.*, 2020). This process has been observed in all studied non-tuberculous mycobacteria except in *M. avium* (Totani *et al.*, 2017). Here we analysed *M. abscessus* biofilms for lipid content at two stages of growth; T1 is defined at 5 days of growth, when the biofilm has achieved maturation, and T2 is at 7 days when biofilms are close to dispersal (pellicular biofilms sink to the bottom of the well). These were compared to samples grown in free-shaking, planktonic cultures, also collected at two timepoints: during exponential phase (T1) and stationary phase (T2). Cultures were labelled with <sup>14</sup>C-acetic acid and upon harvesting the culture, specific lipid fractions were solvent extracted and then resolved using thin layer chromatography (TLC) (described in depth in Section 9.4). Two dimensional (2D) autoradiographs of TLC plates showing the full lipid profile of *M. abscessus* are depicted in **Fig. 4.1 – 4.3**. All experiments were done in biological triplicates and were loaded with equal radioactive counts. Exported lipids are referred to from here on as ‘outside’ lipids, and lipids found in the cytosol are referred to as ‘inner/inside’ lipids. The analysis of apolar lipids revealed a slight increase in triacylglycerol (TAG) in biofilm T2 as compared to other timepoints (resolved in system A, **Fig. 4.1**). There is a prominent increase in FMA, specifically in the outside apolar lipid fraction (resolved in system B, **Fig. 4.1**). FMA refers to mycolic acids released from TDM through hydrolysis using a serine esterase. FMA accumulated slightly in planktonic T2 and biofilm T1, but the increase is most prominent in biofilm T2. Additionally, there was an increase in FMA and fatty acids in outside apolar lipids (resolved in system C, **Fig. 4.2**). There is a minor reduction in trehalose di-mycolate (TDM) in the inside apolar fraction (resolved in system D, **Fig. 4.2**) but the same is not seen in the polar fraction (system D, **Fig. 4.3**) in which an increase in GPLs in biofilm T2 is mainly observed.

There seems to be an overall increase in polar lipids resolved in system E, particularly of phosphatidyl myoinositol mannosides (PIMs) (**Fig. 4.3**).

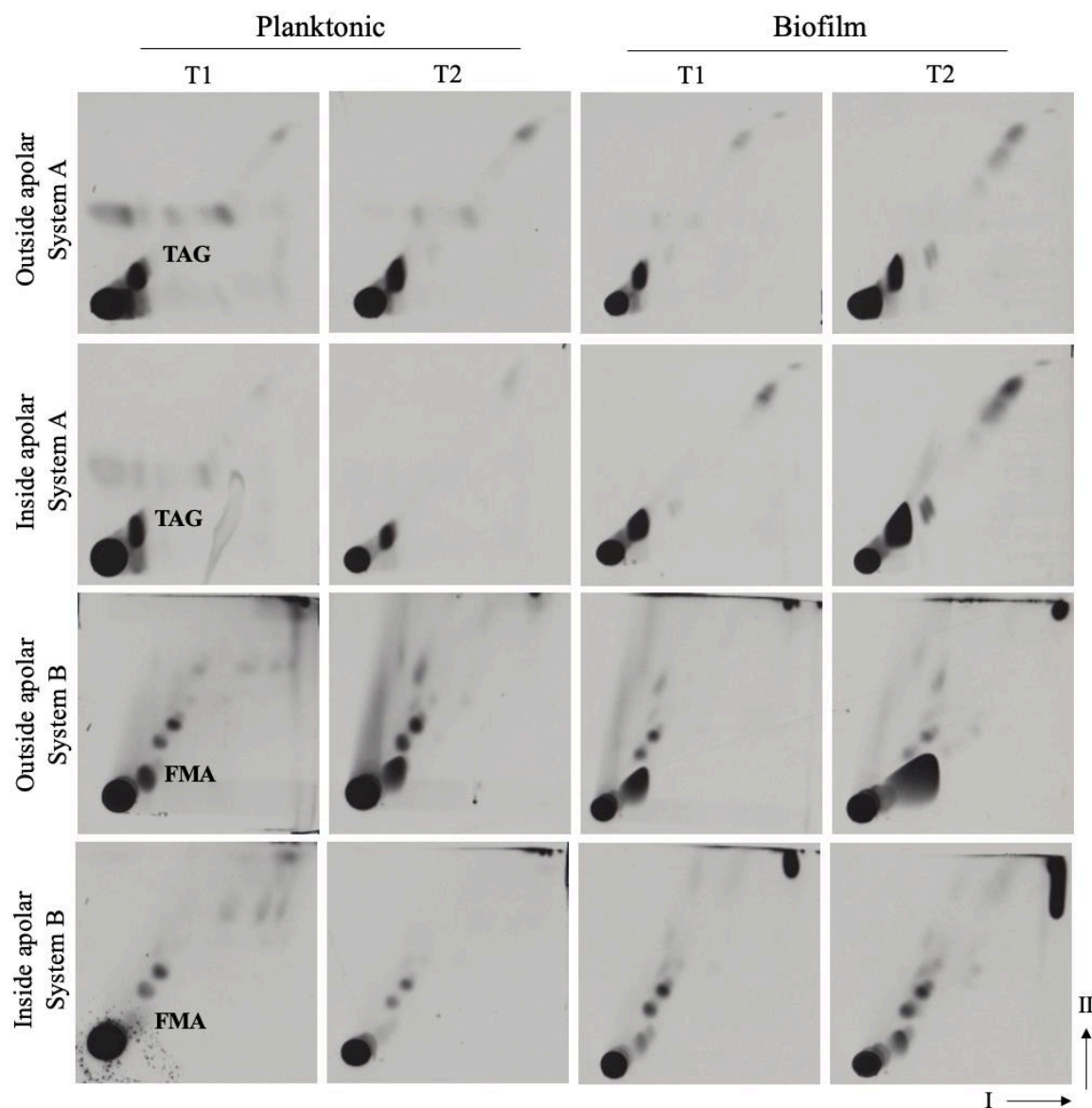


**Figure 4.1: Autoradiographs of 2D TLC silica plates of outside and inside apolar lipids of *M. abscessus* planktonic and biofilm cells.** Outside and inside apolar lipids resolved in systems A and B (see Table 9.5 for details on the composition of the solvent systems). Representative of three repeats. Planktonic cells were harvested 24h (T1) and 48h (T2) after inoculation and biofilms after 5 days (T1) and 7 days (T2). TAG, triacylglycerol; FMA, free mycolic acids.

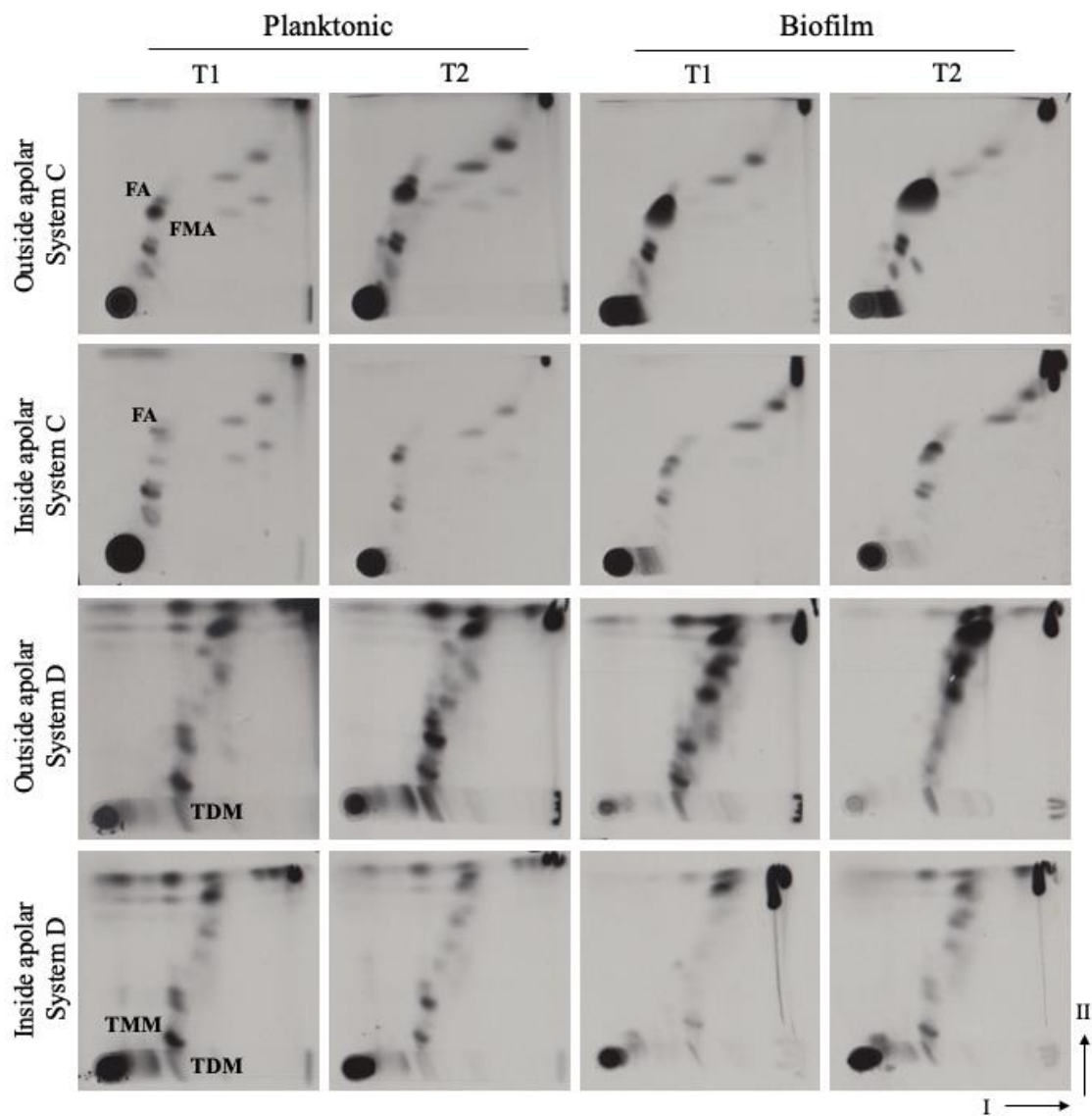


**Figure 4.2: Autoradiographs of 2D TLC silica plates of outside and inside apolar lipids of *M. abscessus* planktonic and biofilm cells.** Outside and inside apolar lipids resolved in systems C and D (see Table 9.5 for details on the solvent systems). Planktonic cells were harvested 24h (T1) and 48h (T2) after inoculation and biofilms after 5 days (T1) and 7 days (T2). Representative of three repeats. FA, fatty acid; FMA, free mycolic acids; TMM, trehalose monomycolate; TDM, trehalose dimycolate.

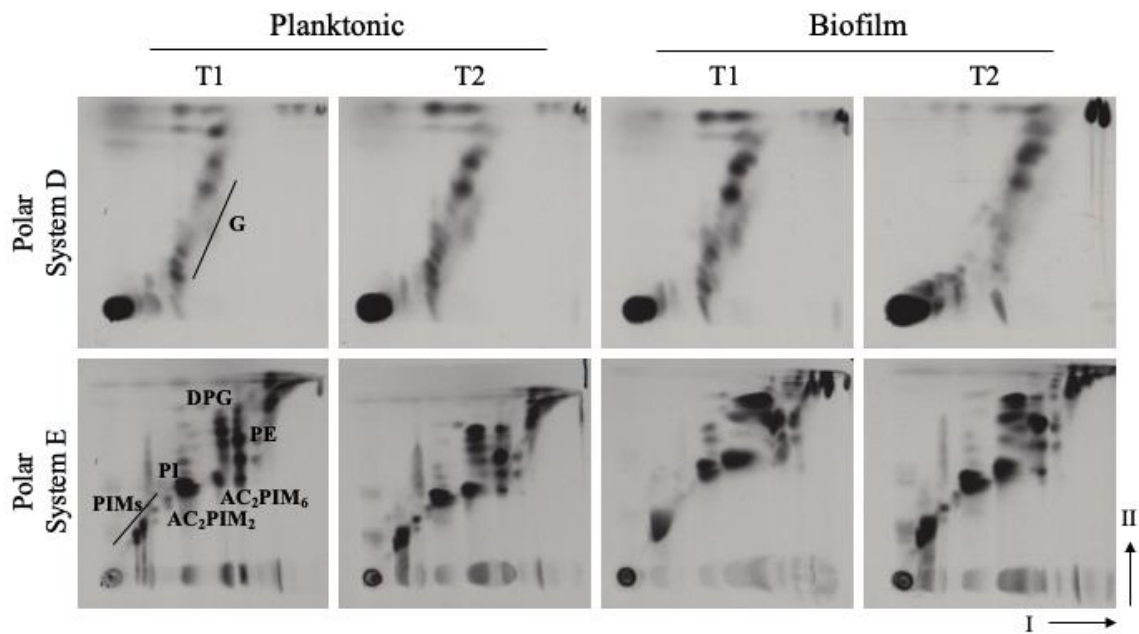


**Figure 4.3: Autoradiographs of 2D TLC silica plates of polar lipids of *M. abscessus* planktonic and biofilm cells.** Lipids are resolved in systems D and E (see Table 9.5 for details on the solvent systems). Planktonic cells were harvested 24h (T1) and 48h (T2) after inoculation and biofilms after 5 days (T1) and 7 days (T2). Representative of three repeats. TMM, trehalose, monomycolate; TDM, trehalose dimycolate; G, glycopeptidolipids; P, phospholipids; DPG, diphosphatidylglycerol; PE, phosphatidylethanolamine; PI, phosphatidylinositol; PIMs, phosphatidyl-myo-inositol mannosides; Ac<sub>2</sub>PIM<sub>2</sub>, diacyl phosphatidyl-myo-inositol dimannoside; Ac<sub>2</sub>PIM<sub>6</sub>, diacyl phosphatidyl-myo-inositol hexamannoside.

#### 4.2.2 Mycolic acid profile in *M. abscessus* biofilms

The indication of accumulation of mycolic acids in the outside and inside apolar lipid fractions of *M. abscessus* biofilms (**Fig. 4.1** and **4.2**), coupled with previous evidence of increase in gene expression of mycolic acid biosynthesis genes, prompted an investigation into molecular changes mycolic acids undergo during biofilm formation. To investigate this, mycolic acid methyl esters (MAMEs) were isolated from already existing lipid fractions as well as from wall-bound lipids that were remaining in the delipidated cell pellet. MAMEs were then separated on an argentated TLC plate in two dimensions. The silver coat ( $\text{AgNO}_3$ ) on the plates reacts with carbon double bonds in mycolates, causing molecules with a higher level of desaturation to migrate slower in the second dimension.

*M. abscessus* produces two subclasses of mycolic acids:  $\alpha$  and the shorter chained  $\alpha'$ , as shown in **Fig. 1.1.B** (Halloum *et al.*, 2016). Our studies confirm the presence of these two classes of mycolates, labelled on autoradiographs in **Fig. 4.4**. Alpha-mycolic acid consists of a long carbon chain (C<sub>74</sub>-C<sub>79</sub>) containing two *cis/trans* double bonds or *cis*-cyclopropyl groups in the meromycolate chain, while  $\alpha'$ -mycolic acid has a shorter carbon chain (C<sub>62</sub>-C<sub>64</sub>) and contains only a single *cis* double bond (Marrakchi, Lanéelle and Daffé, 2014). There was a uniform increase in MAMEs in biofilms visible in all lipid fractions (**Fig. 4.4**), with the change being most prominent in the wall-bound lipids isolated from the delipidated pellet and the inside apolar fractions. The spots representing  $\alpha$ -mycolates in the inside apolar fraction show a clear shift in the migration pattern compared to planktonic cells (**Fig. 4.4**). MAMEs isolated from biofilms migrate further on the TLC plate as compared to those isolated from planktonic cells, indicating a decrease in desaturation – since the most saturated molecules migrate furthest. This implies cyclopropanation might have occurred since this would effectively decrease the number of double bonds within the molecule.

Since the same pattern of migration was shown across all lipid fractions, but most strongly in the wall-bound fraction, this fraction was used for further analysis of molecular changes using mass spectrometry, more specifically matrix-assisted laser desorption/ionization-time of flight (MALDI-TOF). Wall bound mycolates were released from the cell wall using TBAH hydrolysis, further derived into methyl esters and  $\alpha$  and  $\alpha'$  subclasses separated using a silica column with a toluene:ethyl acetate gradient, and then ran on MALDI-TOF (**Fig. 4.5**). Only two timepoints were used, early planktonic (T1) and late biofilm (T2) to analyse the change in mature biofilms as opposed to planktonic cells in the exponential growth phase. We observed  $\alpha$ -mycolic acid classes in planktonic cells that range from C-74 to C-79, with the foremost abundant species being C-76. In biofilms we observed a range from C-74 to C-82, with C-79 being the most abundant species, indicating that longer-chain MAMEs were more abundant in biofilms (**Fig. 4.5**). From previous studies we know that in  $\alpha$  and  $\alpha'$ -mycolic acid structure the  $\alpha$ -alkyl chain consists of 21 repeating units of CH<sub>2</sub> with a methyl group at the end, so the variation we see are in elongation or cyclopropanation of the  $\beta$ -hydroxy chain (Halloum *et al.*, 2016). MALDI-TOF analysis would not reveal the suspected presence of the cyclopropane rings in  $\alpha$ -mycolates from biofilm cells, given that these modified species would simply show a mass reflecting an additional CH<sub>2</sub> unit.

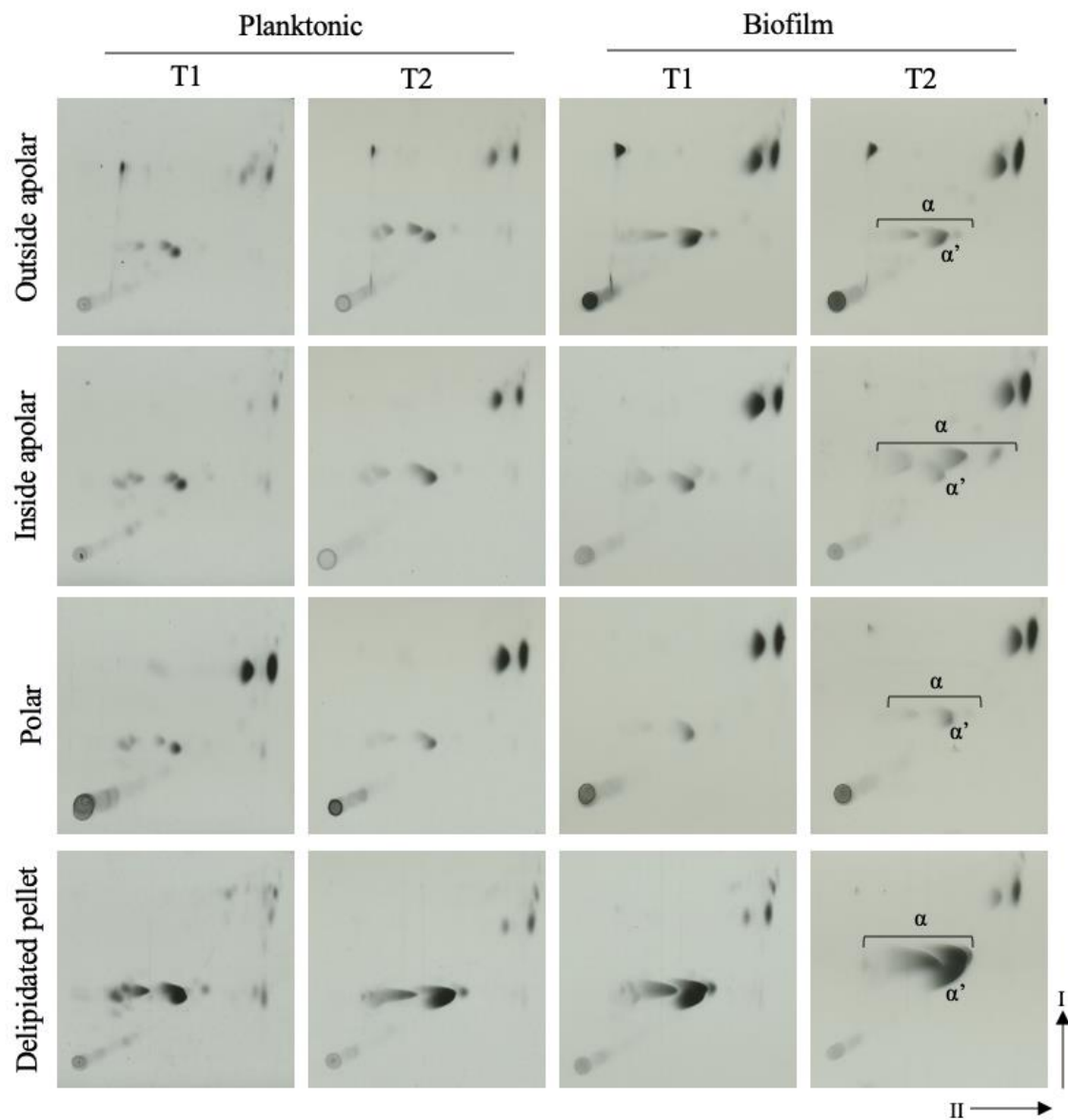


**Figure 4.4: Autoradiographs of 2D argentated TLC silica plates of MAMEs of *M. abscessus* planktonic and biofilm cells.** Lipids are resolved in system F (see Table 9.5 for details on the solvent systems). Planktonic cells were harvested 24h (T1) and 48h (T2) after inoculation and biofilms after 5 days (T1) and 7 days (T2). FAMEs and MAMEs were isolated from each lipid fraction and from the delipidated cell pellet prior to being resolved by TLC on silica plates submerged 2/3 in AgNO<sub>3</sub>. Representative of three repeats.  $\alpha$  – alpha mycolic acid,  $\alpha'$  – alpha prime mycolic acid.

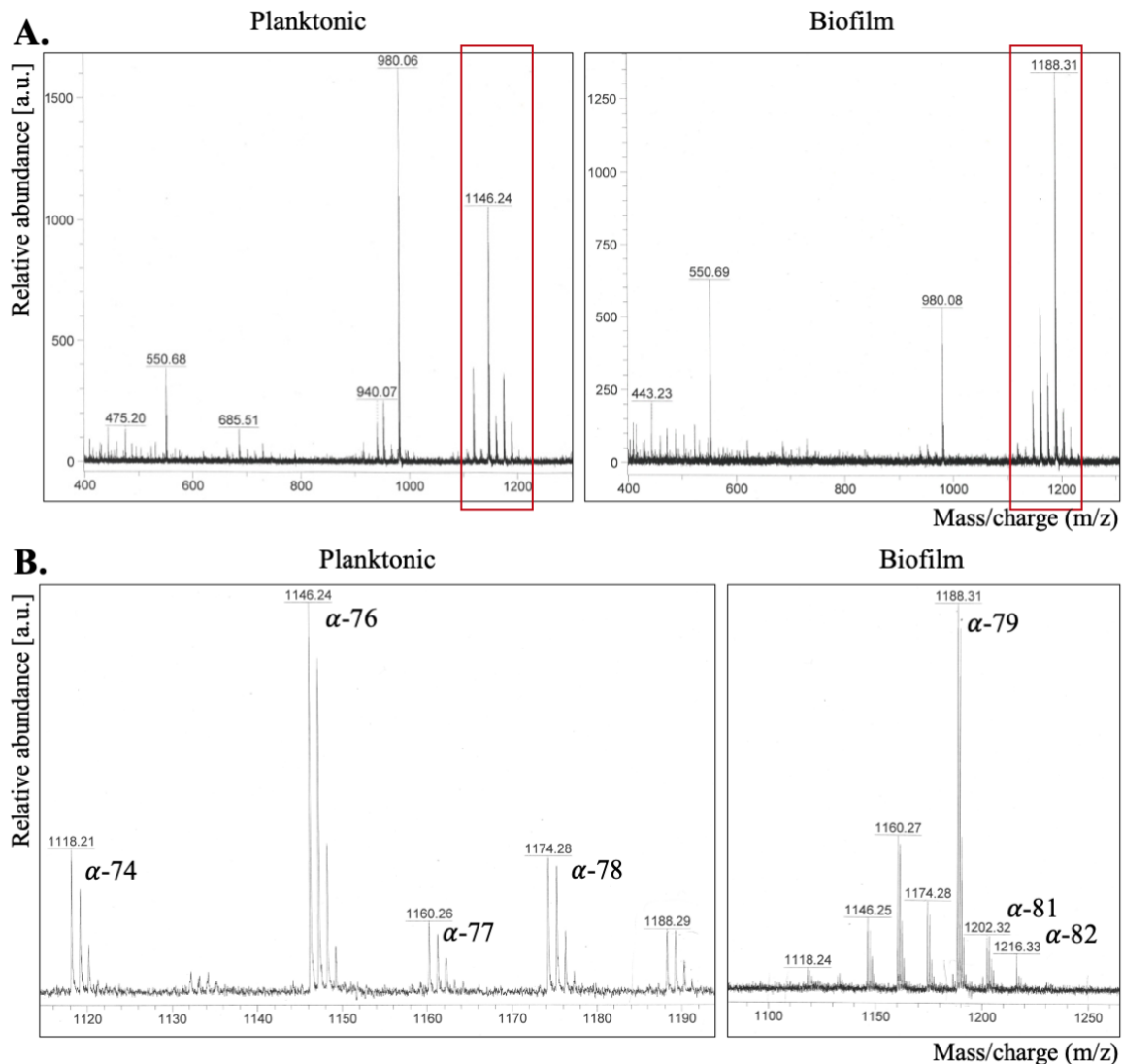


**Figure 4.5: The mass spectrometric analysis of *M. abscessus*  $\alpha$ -mycolates.** MALDI-TOF mass spectra of the solvent extraction of wall-bound  $\alpha$ -mycolates from planktonic and biofilm *M. abscessus*. Performed on a negative grid and the peaks indicate Na<sup>+</sup> adducts of  $\alpha$ -mycolic acid (MW + 23). **A.** Full mass spectra for isolated  $\alpha$ -mycolate; **B.** Zoomed in mass spectra of regions indicated by red rectangles on grids in A.

#### **4.2.3 Analysis of carbohydrate composition of the surface exposed material of *M. abscessus* biofilms**

Previous studies have shown that carbohydrates are a vital part of the mycobacterial extracellular space, meaning they were found to be a large part of the biofilm ECM but also of the capsular material of planktonic bacilli. Microscopy analysis (**Fig. 2.3**) showed that carbohydrates are indeed present in the *M. abscessus* ECM. In order to determine the carbohydrate composition of the ECM, polysaccharides were isolated and hydrolysed to monosaccharides which were derivatized to alditol acetates and resolved using gas chromatography (Grzegorzewicz and Jackson, 2013).

Isolated alditol acetates were compared to a set of standards that allowed the identification of monosaccharides by their running time. **Table 4.1** summarizes the results from three independent experiments. Glucose was identified as the predominant monosaccharide and represented over 60% of the total monosaccharide composition at each stage of growth (**Table 4.1**). Most other monosaccharides had an objectively uniform presence in planktonic and biofilm cultures, but an increase in mannose, arabinose and myo-inositol in biofilms was noted, with the increase in arabinose and myo-inositol being statistically significant.

**Table 4.1: Relative abundance of sugars in the *M. abscessus* ECM, showing median and standard deviation for 3 independent experiments.**

Monosaccharides	Planktonic		Biofilm	
	T1	T2	T1	T2
Rhamnose	1.045± 0.134	1.155± 0.007	1.130± 0.354	0.770± 0.000
Ribose	1.56± 0.141	1.945± 0.389	1.363± 0.266	1.527± 0.342
Arabinose	4.043± 0.945	3.867±0.457	5.183± 0.746	5.083± 0.545
Xylose	2.70± 2.033	1.826±0.745	1.57±0.746	0.933±0.581
Mannose	8.773±2.302	7.66±0.609	9.69±1.245	8.787±1.071
Galactose	3.523±2.407	2.323±1.378	1.68±1.097	1.957±1.489
Glucose	64.28±15.322	69.023±12.638	70.2±8.052	64.687±9.006
Myo-inositol	1.467±0.122	4.073±2.576	2.723±1.260	7.130±0.664

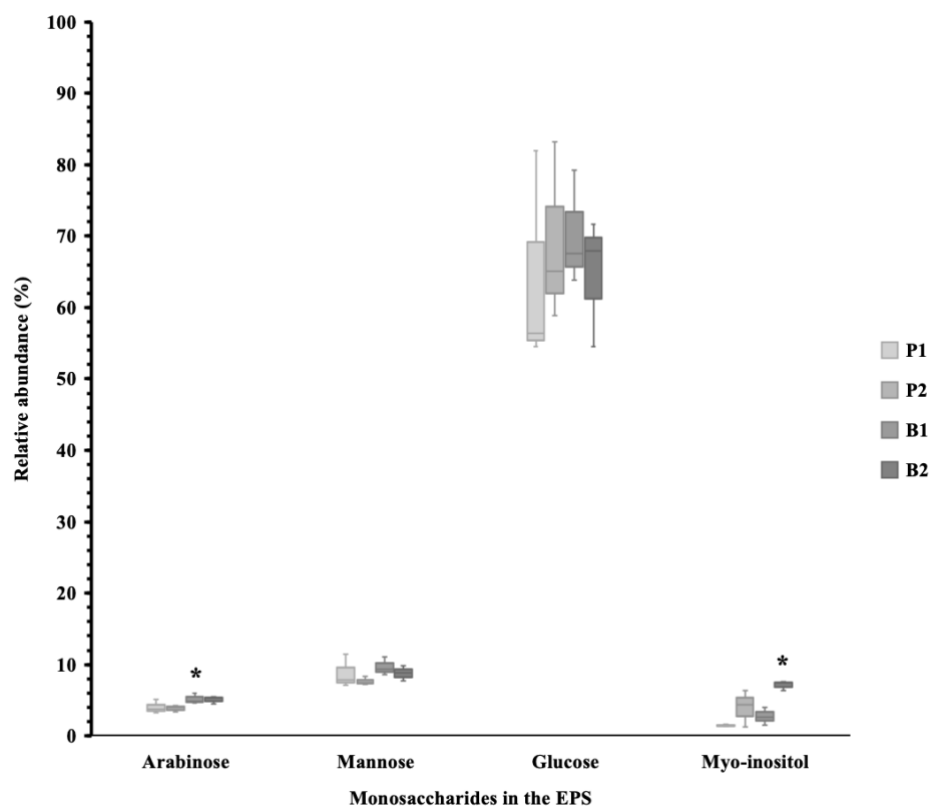


**Fig. 4.6: Plot of the percentage of relative abundance of different monosaccharides found in *M. abscessus* capsule.** Alditol acetates were derived from polysaccharides stripped from the outer layer of the cells and subjected to gas chromatography. Chromatographs of three separate experiments are shown in Appendix 4. Plot shows mean of the three experiments and lines corresponds to the median. Student's t-test was run for each timepoint in comparison to planktonic T1 (unpaired, two-tail, \* $p<0.05$ ).

## 4.3 Discussion

### 4.3.1 *M. abscessus* biofilm cells have a distinct lipid profile compared to planktonic cells

It has previously been well documented in literature that mycobacterial biofilms have distinct lipid profiles when compared to cells grown planktonically (Ojha *et al.*, 2008; Islam, Richards and Ojha, 2012). TAG was associated with biofilm growth in *M. smegmatis*, and with dormant and slow growing *M. tuberculosis* bacilli (Daniel *et al.*, 2004; Purdy *et al.*, 2013; Maurya, Bharti and Krishnan, 2019). Furthermore, TAG can store up to six time more energy than the same amount of hydrated glycogen, and is thought to serve as an energy and carbon reservoir in *Nocordia*, *Rhodococcus* and *Streptomyces* (Alvarez and Steinbüchel, 2002; Berg, Tymoczko and Stryer, 2002). This indicates a pattern of accumulation of TAG in cells that have a slower metabolic rate and need large energy storage, characteristic of cells in a biofilm, and providing a hypothesis for the increase in TAG observed in *M. abscessus* biofilms, specifically inner apolar fraction (**Fig. 4.1**).

A hallmark of biofilm formation in mycobacteria is the increase in abundance of FMA, already observed in *M. smegmatis*, *M. tuberculosis* and *M. chelonae*, was documented in *M. abscessus* (**Fig. 4.1** and **4.2**). It was shown in *M. smegmatis* biofilms that FMA are cleaved from newly synthesized TDM by a specific serine esterase, *MSMEG\_1529*, leading to the conclusion that accumulation of FMA is linked to depletion of TDM (Ojha *et al.*, 2010; Totani *et al.*, 2017). While the same process could be present in *M. abscessus*, we have not observed a definitive decrease in TDM in biofilms as compared to planktonic cells, only a slight one (**Fig. 4.2**). An increase in fatty acids (**Fig. 4.2**) is also reflective of the FMA increase given that fatty acids are precursors of mycolic acids and are made in the first stage of mycolic acid biosynthesis (Marrakchi, Lanéelle and Daffé, 2014).

Closer analysis of mycolic acid in biofilms revealed changes in length and potentially in levels of desaturation (**Fig. 4.4** and **4.5**). Shorter-chain mycolic acid (C-58 - C-68) were thought to play a role in biofilm development in *M. smegmatis* (Ojha *et al.*, 2005). However, *M. abscessus* exhibits an overall accumulation of longer chained mycolic acids and a broader range of chain lengths in biofilms as compared to planktonic cells (**Fig. 4.5**). Another notable difference is that the most abundant  $\alpha$ -mycolate in biofilms is 79 carbons long, compared to 76 in the cell wall of planktonic cells. Additionally, a shift in the migration pattern in  $\alpha$ -mycolic acid on argentated TLCs was identified, which is indicative of a decrease in desaturation, or more likely an increase in cyclopropanation (**Fig 4.4**). Cyclopropanation was shown to be important for virulence and formation of cords in *M. tuberculosis*, while *trans*-cyclopropanation of mycolic acids on TDM was shown to reduce virulence and decrease cell fluidity (Glickman, Cox and Jacobs, 2000; Rao *et al.*, 2006).

Importance of longer chain mycolic acids in biofilms was showed through studies in *M. smegmatis* and *M. bovis* BCG where the deletion of enzymes related to mycolic acid biosynthesis, specifically genes that encode KasB and GroEL1, a KasA chaperone, caused a decrease in mycolate chain length and impacted biofilm formation (Gao *et al.*, 2003; Ojha *et al.*, 2005; Wang *et al.*, 2011). In the transcriptional analysis of *M. abscessus* biofilms we reported an upregulation of the mycolic acid pathway (**Fig. 3.2**), with a specific focus on elongation and desaturation of the meromycolic chain. There is a strong upregulation of *MAB\_2030* and *MAB\_2028*, encoding for KasA/B complex which is responsible for elongation and *MAB\_3354*, encoding for DesA1, a desaturase protein responsible for addition of double bonds to the  $\beta$ -hydroxy branch (A. Singh *et al.*, 2016). The evidence from our phenotypic study, coupled with the transcriptional analysis, shows that in *M. abscessus* biofilms there is an accumulation of long chained mycolic acids, with an initial increase in desaturated molecules that likely become cyclopropanated.

An additionally consistent change observed in this lipid characterization was the increase in PIMs in biofilms. PIMs make an integral part of the cell wall and polar PIMs biosynthesis is essential for mycobacterial growth (Haites *et al.*, 2005). It has been demonstrated that PIMs of both *M. abscessus* and *M. tuberculosis* trigger the immune response by interacting with macrophage TLR2 and stimulating the release of TNF- $\alpha$ , indicating that PIMs are involved in facilitating colonization, often thought to be done through biofilm formation by the smooth colony type of *M. abscessus* (Jones *et al.*, 2001; Rhoades *et al.*, 2009). Altered acetylation of PIMs leads to defective biofilm formation suggesting PIMs could play a role in the maintenance of pellicular biofilm structure (Li *et al.*, 2020).

#### **4.3.2 Glucose is the predominant monosaccharide in the *M. abscessus* surface-exposed material**

Given that polysaccharides were established to play a structural role in biofilms, a comprehensive analysis of the composition of surface exposed polysaccharides was done, revealing glucose as the most abundant monosaccharide in *M. abscessus* biofilm ECM (Fig. 4.6). Literature showed that the most abundant carbohydrates found in the capsular material of *M. tuberculosis* are  $\alpha$ -D-glucan, D-mannan and D-arabino-D-mannan (Röse, Kaufmann and Daugelat, 2004). Other studies of mycobacterial biofilms showed that the most abundant carbohydrate present in the surface exposed material is  $\alpha$ -glucan, followed by arabinomannan and mannan, while biofilm ECM studies showed cellulose to be abundant (Ortalo-Magne *et al.*, 1995; Lemassu, Ortalo-Magné, Bardou, Silve, Lanéelle, Daffé, *et al.*, 1996; Trivedi *et al.*, 2016). Alpha-glucan is a polysaccharide composed of D-glucose and it is abundantly found in mycobacterial capsular material (Dinadayala *et al.*, 2008). Therefore, it is hypothesized that the majority of glucose found in the surface exposed material of *M. abscessus* biofilms and planktonic cells comes from  $\alpha$ -glucans that are present in the capsule. Lack of diversity amongst monosaccharides can also be explained by the fact that carbohydrates do not make up a large part of the *M. abscessus* biofilm ECM, as shown in the microscopic characterization. A study

by Lemassu *et al.*, 1996 disclosed that surface exposed material of RGM is protein rather than carbohydrate rich, and as such the carbohydrates present in the ECM are likely the same as those from the cell wall and capsule which shed into the media (Bacon and Hatch, 2008). This also explains the presence of the same molecules in planktonic and biofilm cells, even though only the biofilms have an ECM.

An interesting observation was a significant increase in arabinose in biofilm T1 and in myo-inositol in biofilm T2, as compared to planktonic T1. Increase in myo-inositol, a component of PIMs, was reflected in the lipid analysis where PIMs were shown to be slightly more abundant in biofilms when compared to planktonic cells (Fig. 4.3). The significant increase in arabinose in biofilms is also indicative of an increase in LM and LAM. There was an increase in mannose only at biofilm t1, and not t2. This is in contrast to *M. chelonae* biofilms where there was an increase in arabinose and mannose, but not myo-inositol, in biofilm t1 and t2 (Vega-Dominguez *et al.*, 2020). PIMs can be anchored to the plasma membrane, but studies have also shown that PIMs are present in the solvent extractable layer of mycobacterial cell wall. The small proportion of monosaccharides that make up PIMs, LM and LAM in the *M. abscessus* biofilm ECM shows that these glycolipids are not abundant but are nonetheless present in some form that is not anchored to the plasma membrane. Interestingly, although not significant, there is a reduction in xylose as cells enter stationary phase and mature into biofilms. The xylose likely originates from LAMs which can be capped with methylthiolxylose as a substitute for mannose (Angala *et al.*, 2017). PIMs, LM and LAM are known to modulate the immune response and to play important structural roles in the cell wall of mycobacteria, however their role in biofilms have not been explored. Observed changes in proportions of the monosaccharides point to a certain modulation of glycolipids in biofilms of *M. abscessus* which could have an influence on the structure and stability of the biofilm.

Certain changes that occur in biofilm formation in mycobacteria are conserved among species, such as the overall composition of the ECM or the increase in mycolic acids, however each

species retains a level of uniqueness that reflects their evolution and adaptation to this type of growth. *M. abscessus* biofilms show the genus-characteristic increase in FMA in biofilms, and through detailed analysis we can conclude that they also undergo a molecular change and diversification which likely plays a role in the cell wall structure and permeability and impacts the ECM composition. TAG accumulation in biofilms is likely as result of the need for energy storage in the biofilm. Glucose was identified the most abundant part of *M. abscessus* extracellular space, likely because it makes up most of the surface exposed molecules found in the capsule. However, further analysis should be done to assess the effect that these alterations have on interaction with the human immune system, on ECM permeability and drug tolerance.

## **5 Biological characterization of *M. abscessus* clinical isolates**

## 5.1 Introduction

*M. abscessus* is a complex pathogen to study due to its phenotypic heterogeneity, high antibiotic resistance, biofilm formation, and limited presence in literature so far. The first year with over 100 publications related to *M. abscessus* was 2013, and the current yearly number is approximately 250 publications. In comparison, publications on *M. avium* reached over 100 publications per year in 1986 and are now at a yearly average of approximately 400. Adding another level of intricacy, the *M. abscessus* complex is comprised of three subspecies, *M. abscessus* subsp. *abscessus*, subsp. *massiliense* and subsp. *bolletii*. Due to the lack of literature on *M. abscessus* and difficulty in isolating and characterizing this bacterium in the past, there is a lack of consensuses between techniques or strains used to study the bacterium. Therefore, the available literature is often focused on specific conditions or clinical isolates with the need to extrapolate generic conclusions from specific studies.

In an attempt to bridge this gap in literature, six pulmonary clinical isolates were obtained from a strain collection and a comparative characterization study between them and the *M. abscessus* ATCC 19977 type strain was done. No prior information was available for the strains and thus this study encompasses a “blind” biological characterization (Chapter 5), evaluation of biofilm formation and lipids (Chapter 6) and genome comparison (Chapter 7), with the aim of determining specific patterns among the strains in relation to colony morphology and subspecies within the *M. abscessus* complex. Through a thorough characterization of these isolates, we intend to broaden what is known in literature about the immunopathology of *M. abscessus* as well as evaluate the discrepancies between clinical isolates and lab strains to determine comprehensive patterns in the phenotype and genotype that can be used for developing novel treatment options.

The aim of this chapter specifically was to conduct the initial phenotypic characterization of the clinical isolates compared to a smooth and a rough variant of *M. abscessus* ATCC 19977 type strain. Firstly, the colony morphology on agar plates was described for all strains, as well

as the growth rate in different media in order to determine the optimal conditions for laboratory growth and subsequent experiments. Due to the high antibiotic resistance that *M. abscessus* exhibits, the isolates were evaluated for their susceptibility to antibiotics commonly used for treatment and the potential for the use of antibiotic cocktails consisting of  $\beta$ -lactams and  $\beta$ -lactamase inhibitors. Additionally, as a basis for further immunological studies, the ability of the strains to infect, survive and replicate in murine macrophages was assessed.

## 5.2 Results

### 5.2.1 Characterization of single colony and liquid broth growth of *M. abscessus* clinical isolates

Clinical isolates were initially streaked out on 7H11 and assessed for colony morphology. *M. abscessus* smooth (S) and rough (R) strains were used as type strains for comparison in subsequent assessments. Clinical isolates (CI) 1, 5 and 6 exhibited rough colony morphologies, were hydrophobic and “crumbly” in response to probing by sterile inoculation loops and were annotated as CI-1R, CI-5R and CI-6R (**Fig. 5.1**). CI-1R had a similar elevated and wrinkled colony formation as *M. abscessus* R while CI-5R and CI-6R were similar to each other, with flatter, thinner and less wrinkled single colonies.

Isolates numbered 2, 3 and 4 had a similar colony morphology to *M. abscessus* S, were “sticky” in response to probing by sterile inoculation loops, dissolved easily in liquid compared to the rough strains, and were thus characterized as smooth strains and annotated as CI-2S, CI-3S and CI-4S (**Fig. 5.1**). All smooth clinical isolates grew smaller colonies compared to *M. abscessus* S, 2-3 mm in diameter, as opposed to 5 mm. CI-2S initially exhibited mixed colony morphology, however throughout the study CI-2S behaved comparably to other smooth strains.

A basic characterization to assess growth of the strains in liquid culture was done keeping in mind several variables. Initially colony forming units (CFU), or viable, counts were used as an assessment of growth (**Fig. 5.2A**), given that this is an established method for determining growth in mycobacteria and traditionally the most accurate as it bypasses issues caused by clumping of cells that can render optical density (OD) measurements inaccurate. In the case of *M. abscessus* however, viable counts proved to be a poor method for determining the growth rate. It was difficult to dissociate clumps formed by rough strains, even with additional detergent and sonication, compromising accurate dilutions and enumeration of single colonies.

This was especially evident in comparison where growth conditions were the same (7H9, 37°C) but method of measuring growth was different – CFU counts in **Fig. 5.2.A** and OD in **Fig. 5.2.C**. The graph depicting viable counts is indicative of slow growth amongst rough strains, which is not the case when OD measurement was used. For this reason, OD was used for the rest of the study to measure growth, and where OD measurements were difficult to read for rough strains, it was estimated based on the OD of the smooth ones because initial characterization indicated their growth rate to be the same (**Fig. 5.2**).

Optimal temperature for growth needed to be determined, as well as any potential temperature sensitivity of the clinical isolates, and therefore growth was measured at 37°C and 30°C for a period of at least 48 h. These temperatures were chosen because some NTMs, like *M. chelonae*, grow best at 30°C and *M. abscessus* has been successfully cultured at 30°C in the past (Adekambi *et al.*, 2004; Cortes, Nessar and Singh, 2010; Preece *et al.*, 2016; Vega-Dominguez *et al.*, 2020). However, after comparison (**Fig. 5.2B** and C) it was determined that 37°C was the optimal temperature for stable growth of all strains, and in the context of this study offered better comparison to the previous study on biofilms (**Ch. 2-4**), also done by culturing at 37°C, and offered a more physiologically relevant environment given that *M. abscessus* is a human pathogen. Finally, growth in Sauton's minimal media was observed over a period of 96 h (**Fig. 5.2D**), since this media is used for biofilm studies and as expected, due to the nature of the media, growth was slower in all strains when compared to that in supplemented 7H9 media. Overall, at 37°C in 7H9 media, *M. abscessus* R and CI-1R grew faster than *M. abscessus* S, and CI-4S and CI-5R grew slower than the other strains, especially at the end of exponential phase. The main difference among the strains was the slower growth of CI-4S regardless of the condition, and the fast growth of CI-1R, however there are no significant growth defects amongst any of the strains.

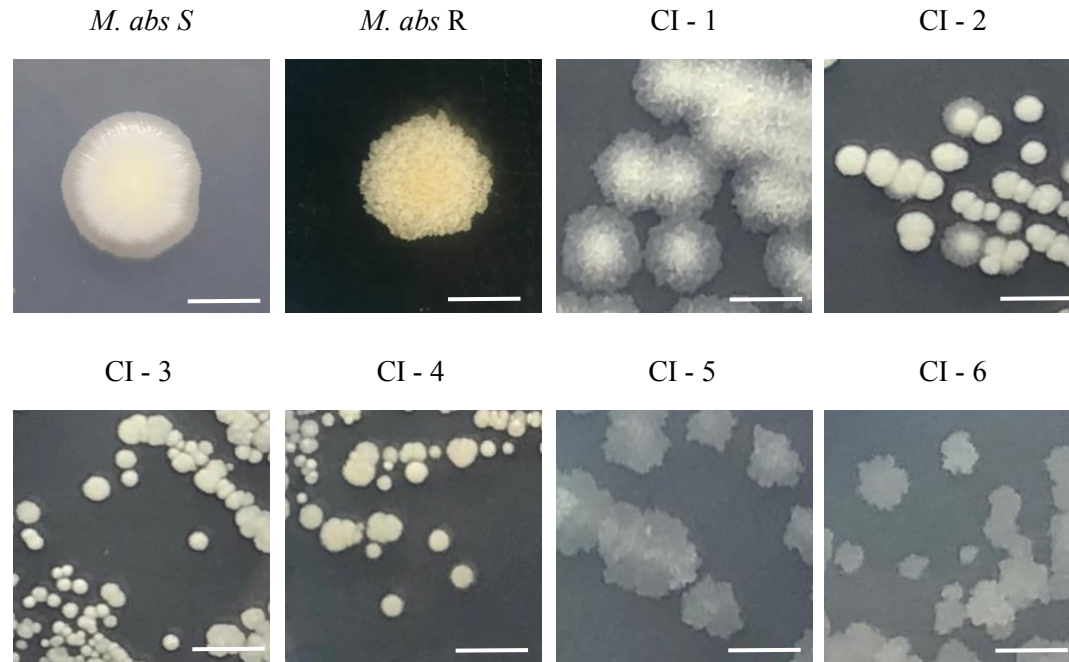


**Figure 5.1: Single colony morphology of *M. abscessus* clinical isolates 1-6, with *M. abscessus* S and R strains as reference.** Strains were grown on 7H11 agar for 3 days at 37°C and single colony formation was imaged. Scale bar = 5 mm.

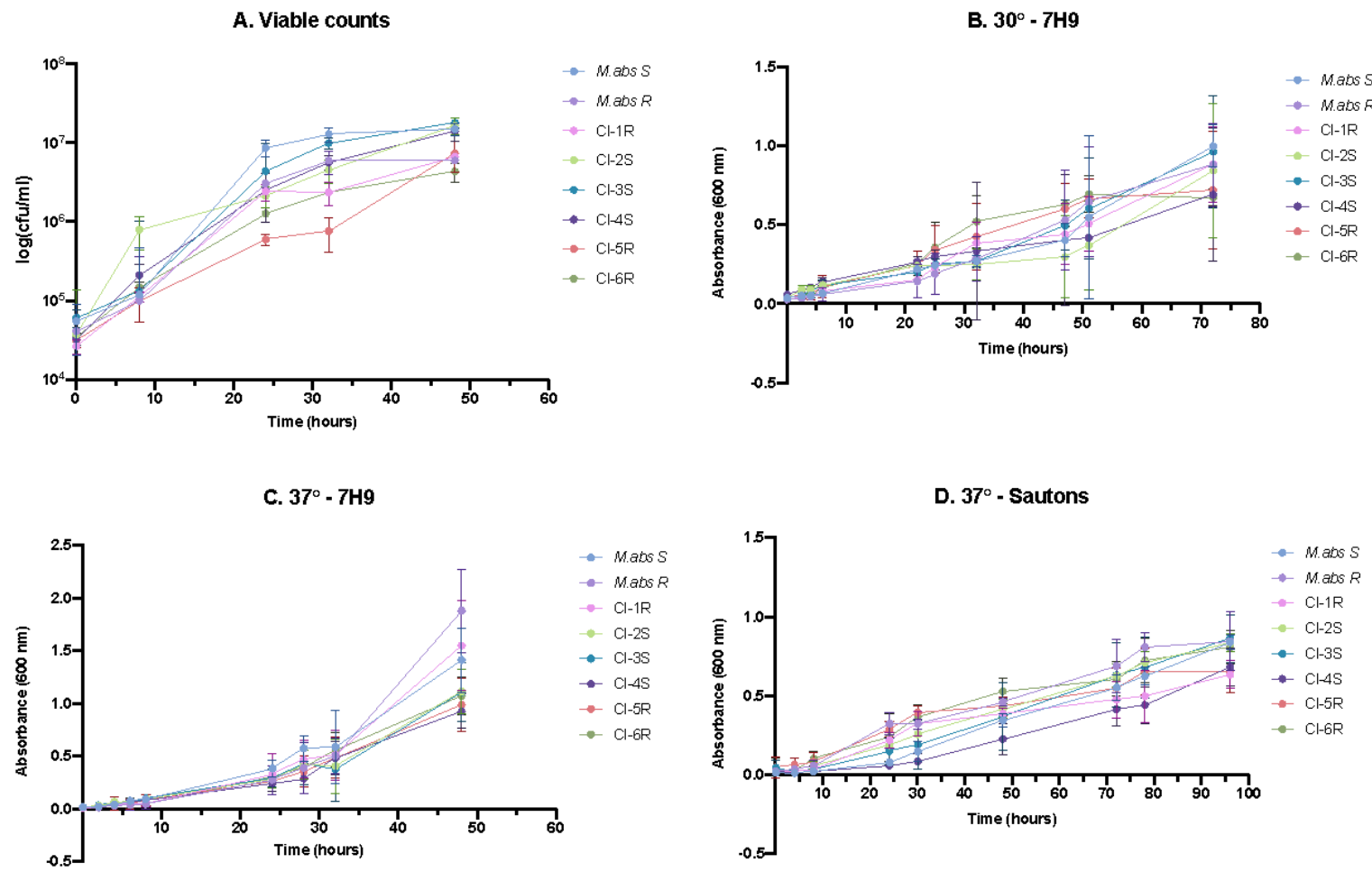


**Figure 5.2: Assessment of growth of *M. abscessus* clinical isolates in different conditions.** Growth was assessed using viable counts and OD measurement in different environments: **A.** viable cell counts shown on a logarithmic scale; Absorbance measured at OD 600 with cells grown in 7H9 at 30°C (**B.**) and 37°C (**C.**) and in Sauton's media at 37°C (**D.**). *M. abscessus* S and R were used as reference strains, each graph is representative of the mean of 5 biological replicates and error bars indicate SD.

## 5.2.2 Antibiotic susceptibility of *M. abscessus* clinical isolates

*M. abscessus* is known amongst NTMs for difficult and prolonged treatment as a result of many antibiotic resistance mechanisms (Nessar *et al.*, 2012). To evaluate antibiotic susceptibility of the clinical isolates, minimum inhibitory concentration (MIC) of three main antibiotics used for treatment (clarithromycin, amikacin and cefoxitin) was measured (Nessar *et al.*, 2012; Choi *et al.*, 2018; Chen *et al.*, 2019). Augmentin was included as a cocktail of amoxicillin and Potassium clavulanate, a  $\beta$ -lactamase inhibitor, due to evidence in literature that indicates success in bypassing intrinsic  $\beta$ -lactams resistance in mycobacteria when using similar cocktails (Kurz and Bonomo, 2012; Lopeman *et al.*, 2020). An augmentin ratio of 7:1 amoxicillin:potassium clavulanate was used in this study since it is a relevant ratio used in treatment (Huttner *et al.*, 2020). Amoxicillin alone acted as a control.

Experiments to determine the MIC of each antibiotic were performed using a standardized broth dilution method (Wiegand, Hilpert and Hancock, 2008; Jorgensen and Ferraro, 2009) and interpreted through visual reading using the official guide for testing in mycobacteria (Woods *et al.*, 2011). Susceptibility was characterized using the standardized susceptibility breakpoints for *Mycobacteria*, *Nocardia*, and other aerobic *Actinomycetes* (**Table 9.7**). As outlined in **Table 5.1**, CI-1R and CI-4S were susceptible to amikacin, CI-2S was resistant and the rest, including the reference strains, had intermediate susceptibility. All strains presented intermediate susceptibility range to cefoxitin. Due to the adaptive resistance to macrolides, growth after incubation with clarithromycin must be recorded on day 3 and day 14 (Nash *et al.*, 2009). Most strains showed resistance to clarithromycin at day 3, except CI-4S which showed intermediate susceptibility, and all strains showed resistance after day 14. CI-1R stands out as highly resistant to clarithromycin the MIC is  $\geq 64 \mu\text{g/ml}$  already at day 3. As expected, all strains were resistant to amoxicillin because *M. abscessus* encodes  $\beta$ -lactamases that make it resistant to a wide variety of antibiotics from the  $\beta$ -lactam group. Results differed with augmentin - *M.*

*abscessus* S showed intermediate susceptibility while the rest were resistant according to the breakpoints, but the MIC values were lower than for amoxicillin.

**Table 5.1: Minimum inhibitory concentrations (MIC) of antibiotic susceptibility.**  
 AMOX – Amoxicillin, AUG - Augmentin (7:1, Amoxicillin:Potassium clavulanate), AMK – Amikacin, FOX – Cefoxitin, CLR – Clarithromycin. Superscript denote R-resistant, I-intermediate susceptibility, S-susceptibility of bacteria to the given antibiotic as pre-determined based on breakpoints published by Woods *et al.*, 2011.

	MIC ( $\mu\text{g/ml}$ )					
	AMOX	AUG	AMK	FOX	CLR	
					day 3	day 14
<b><i>M. abs</i> S</b>	>128 <sup>R</sup>	16 <sup>I</sup>	32 <sup>I</sup>	64 <sup>I</sup>	32 <sup>R</sup>	>64 <sup>R</sup>
<b><i>M. abs</i> R</b>	>128 <sup>R</sup>	32 <sup>R</sup>	32 <sup>I</sup>	32 <sup>I</sup>	32 <sup>R</sup>	>64 <sup>R</sup>
<b>CI – 1R</b>	>128 <sup>R</sup>	128 <sup>R</sup>	16 <sup>S</sup>	32 <sup>I</sup>	>64 <sup>R</sup>	>64 <sup>R</sup>
<b>CI – 2S</b>	>128 <sup>R</sup>	64 <sup>R</sup>	64 <sup>R</sup>	32 <sup>I</sup>	16 <sup>R</sup>	32 <sup>R</sup>
<b>CI – 3S</b>	>128 <sup>R</sup>	64 <sup>R</sup>	32 <sup>I</sup>	32 <sup>I</sup>	16 <sup>R</sup>	>64 <sup>R</sup>
<b>CI – 4S</b>	>128 <sup>R</sup>	32 <sup>R</sup>	16 <sup>S</sup>	32 <sup>I</sup>	4 <sup>I</sup>	16 <sup>R</sup>
<b>CI – 5R</b>	>128 <sup>R</sup>	128 <sup>R</sup>	32 <sup>I</sup>	32 <sup>I</sup>	8 <sup>R</sup>	32 <sup>R</sup>
<b>CI – 6R</b>	>128 <sup>R</sup>	128 <sup>R</sup>	32 <sup>I</sup>	32 <sup>I</sup>	16 <sup>R</sup>	>64 <sup>R</sup>

### **5.2.3 Uptake and survival of *M. abscessus* clinical isolates in murine macrophages**

Infection studies were done to evaluate macrophage uptake of *M. abscessus* strains and intracellular survival of bacteria. J774 murine macrophage cell line was infected with *M. abscessus* strains at multiplicity of infection (MOI) 10 and survival was measured at 4, 24 and 72 h post infection (h.p.i.) by lysing cells, plating serial dilutions and enumerating CFUs after 3 days.

At 4 h.p.i. there was an uneven uptake of bacteria by the macrophages which could be correlated to the colony morphology of the strains (**Fig. 5.3**). Higher number of bacteria of smooth strains were taken up (on average closer to  $10^5$  log(CFU/ml) across all smooth strains) in comparison to the rough strains (on average closer to  $10^4$  log(CFU/ml)), as measured at 4 h.p.i. At 24 h.p.i. there is a decrease in the CFU count for smooth strains, compared to 4 h.p.i. but at 72 h.p.i. there is an increase compared to both previous time points. In comparison, there is no reduction in CFU counts at any time points for the rough strains, in fact they displayed an increase in survival after the initial uptake by macrophages at 4 h.p.i., with a steady rise in CFU counts. This is best illustrated with the example of CI-5R that has a statistically significant increase in bacterial count at 24 and 72 h.p.i, when compared to 4 h.p.i.

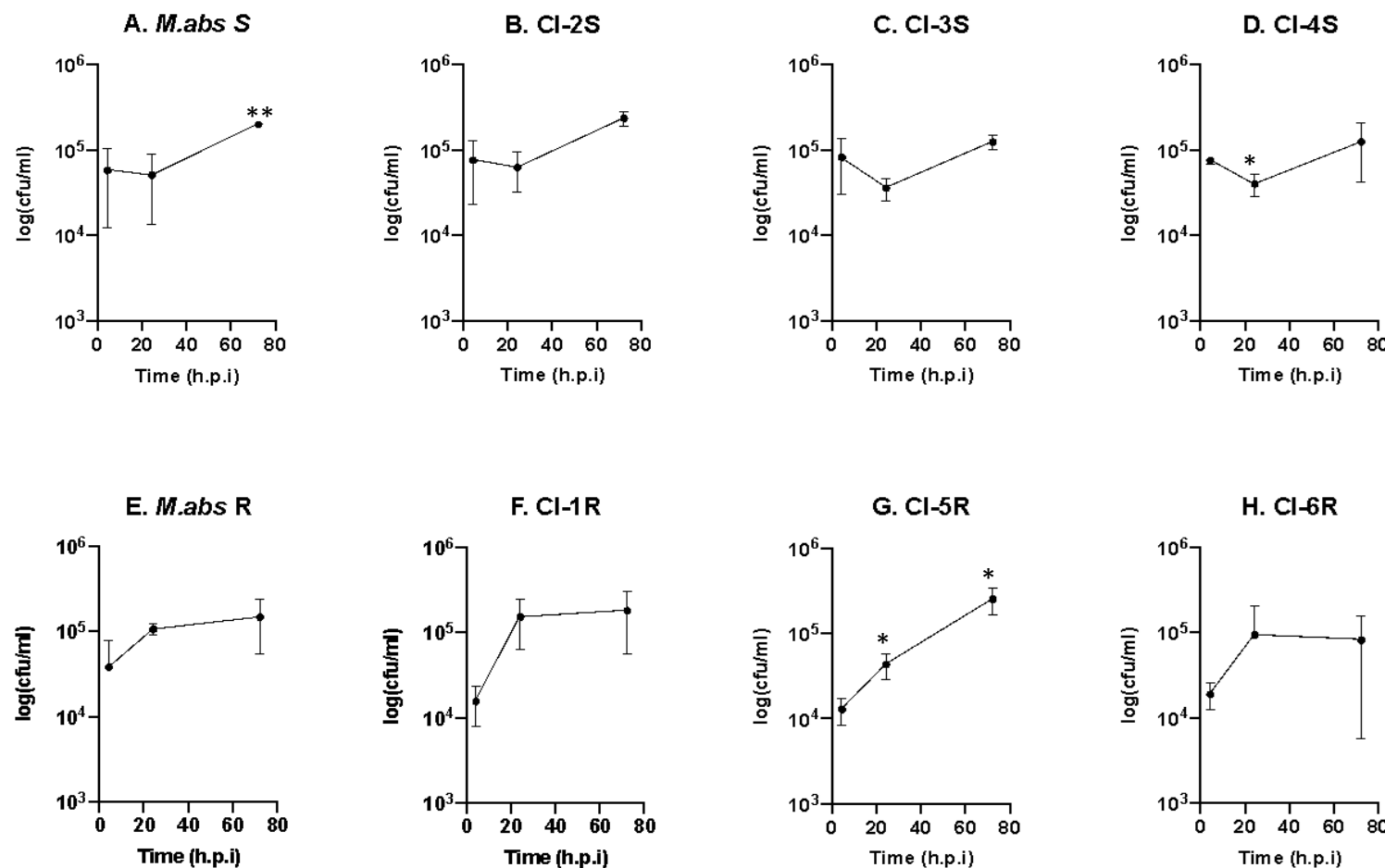


**Figure 5.3: Intracellular survival of *M. abscessus* clinical isolates in murine macrophages.** CFU/ml of 6 clinical isolates, and *M. abscessus* S and R used for reference, were measured at 4, 24 and 72 hours post infection (h.p.i.) in murine macrophage cell line J774. Data is an average of 3 independent experiments and error bars indicate  $\pm$  SD. Significance was calculated using Student's t-test (paired, one-tail; \* $p \leq 0.05$ , \*\*  $p \leq 0.01$ ).

### 5.3 Discussion

One of the most studied aspects of *M. abscessus* is this difference in virulence, colonization, and pathogenesis of smooth and rough strains, done to describe the missing links in understanding the immunopathology of *M. abscessus*. Previous literature has outlined the differences in pathogenicity between smooth and rough colony morphology in *M. abscessus*, portraying smooth colonies as initial colonizers, and rough as hyper-virulent variants that provoke an aggressive response from the immune system (Howard *et al.*, 2006; Rhoades *et al.*, 2009; Roux *et al.*, 2016). There is an ongoing debate regarding the trigger for the smooth-to-rough transition in *M. abscessus* during infection, however in the experiments exhibited here, there was no change in the colony morphotype within strains and so their behaviour was characterized based on the consistent exhibited morphology.

This study offered perspective into how variable behaviour can be amongst as little as eight strains of one bacterial species. Three smooth and three rough strains of *M. abscessus* clinical isolates were compared to laboratory reference strains of the same colony morphology, and evaluated in terms of growth, antibiotic resistance, and survival in a co-culture with macrophages. Overall, there were no notable growth defects among the clinical isolates in shaking culture regardless of the media used, and all strains grew comparatively slower at 30°C than at 37°C. Furthermore, there was no clear pattern of antibiotic resistance amongst the strains distinguishable by colony morphology, except that rough strains had a higher MIC when challenged with augmentin compared to the smooth ones (128 µg/ml for rough clinical isolates, compared to 32-64 µg/ml for smooth ones). Following the infection assay with murine macrophages, rough strains presented a consistent increase in growth up to 72 h.p.i., indicating proliferation within the phagosome, while smooth strains showed a decrease in CFU after 24 h.p.i., indicative of initial clearance by macrophages, and recovery at 72 h.p.i.

### **5.3.1 *M. abscessus* clinical isolates are highly resistant to antibiotics**

All strains were resistant to clarithromycin by day 3, apart from CI-4S which showed intermediate susceptibility. The MIC value of clarithromycin increased for all by day 14 – indicating a degree of inducible resistance. CI-1R showed the highest consistent resistance to clarithromycin with  $>64 \mu\text{g/ml}$  at day 3 and day 14. This was overall unexpected, since clarithromycin is used for *M. abscessus* treatment and strains are expected to be susceptible at least on day 3. Previous studies also demonstrated resistance in over 80% of *M. abscessus* clinical isolates, measured after day 14, while after day 3 most strains were susceptible (Nie *et al.*, 2014, 2015). Genotype and subspecies of *M. abscessus* play an important role in clarithromycin resistance and are examined further in Chapter 7.

Cefoxitin and imipenem are the only antibiotics from the  $\beta$ -lactam family used to treat *M. abscessus* infections, because they are hydrolysed by Bla\_Mab at a slow rate (Soroka *et al.*, 2014). In this study all strains showed intermediate resistance to cefoxitin with an MIC of 32  $\mu\text{g/ml}$ . Use of  $\beta$ -lactamases inhibitors was shown in several studies to increase the susceptibility of multidrug resistant (MDR) *M. tuberculosis* clinical isolates to  $\beta$ -lactams, offering a novel therapeutic approach for handling emerging antimicrobial resistance in this pathogen (Kurz and Bonomo, 2012). A cocktail of  $\beta$ -lactams and an inhibitor of  $\beta$ -lactamases was used *in vitro* to demonstrate efficacy against *M. abscessus* (Kaushik *et al.*, 2019; Story-Roller, Maggioncalda and Lamichhane, 2019; Lopeman *et al.*, 2020). Here we tested susceptibility to amoxicillin, a  $\beta$ -lactam, in combination with potassium clavulanate, a  $\beta$ -lactamase inhibitor, and showed that while all strains were resistant to amoxicillin ( $>128 \mu\text{g/ml}$ ), intermediate susceptibility was restored in one strain (*M. abscessus* S) when the cocktail was used in a 7:1 ratio (**Table 5.1**). Additionally, clinical isolates with rough colony morphology all grew at concentrations of augmentin  $>128 \mu\text{g/ml}$  while smooth strains had lower MICs but were still resistant (**Table 5.1**). This offers another affirmation that this type of treatment is a possibility in the future of *M. abscessus* disease care.

There was no clear, definitive link between colony morphology and antibiotic susceptibility among the strains evaluated in this study. All rough strains were resistant to amikacin while two of the four smooth strains, *M. abscessus* S and CI-4S, were not. Additionally, rough strains were less suspectable to augmentin than the smooth strains. This could be attributed to cell-aggregation that is more pronounced in rough strains, but the trend was not observed for all antibiotics. Absence of GPLs in the rough strains leads to cell clumping that resembles aggregation of other mycobacteria with the same morphotype such as *M. smegmatis*, *M. bovis* BCG and *M. tuberculosis*. These clumps resemble micro-colonies similar to biofilms in the sense that there is delayed penetration of antibiotics. In literature not many links have been shown between colony morphology and antibiotic tolerance. Rough strains were found to have lower susceptibility to carbonyl cyanide 3-cholorphenylhydrazone, an efflux pump inhibitor of *M. tuberculosis*, compared to the smooth morphotype (Chen *et al.*, 2021) and biofilm-like aggregates of the rough strain have been correlated with higher survival at acidic pH, tolerance to treatments with azithromycin and amikacin (Clary *et al.*, 2018). Another study found no specific correlation between the phenotypes when *M. abscessus* clinical isolates were challenged with cefoxitin, amikacin and clarithromycin, but one study found that in case of tigecycline the rough strain was more susceptible than the smooth (Rüger *et al.*, 2014).

### **5.3.2 Smooth and rough *M. abscessus* strains have distinct pathways within macrophages**

To measure survival of *M. abscessus* in macrophages we relied on CFU counts, which can be unreliable or difficult to assess with absolute certainty, especially for rough strains. Large range of error bars showing significant deviation from the mean in the survival data graph are indicative of this (**Fig. 5.3**). While certain protocols exist for determining the bacterial count prior to infections to ensure the MOI is accurately calculated, even these, to an extent, rely on estimation and there are no universally established methods. The inaccuracy in using viable counts or OD mainly consolidates in the issue of bacterial aggregation in rough strains of

mycobacteria. The clumping can to an extent be controlled using high concentration of detergent and frequent sonication, but this can impact viability of the cells and cause issues with experiment design, reproducibility of results, and artifacts. This problem is widely recognized in literature and alternative methods for evaluating growth rate have been suggested such as measurement of ATP, total protein growth, even comparison between CFU and RT-qPCR in survival (Prioli, Tanna and Brown, 1985; Meyers *et al.*, 1998; Pathak *et al.*, 2012). While there is a recognition for the need to move towards fluorescent based assays to increase accuracy and decrease time invested and human error, none have become the standardized methods so far and many researchers still rely on CFU counts or OD (Rodriguez *et al.*, 2018). Measuring the survival of strains in macrophages is the first step in unravelling the interaction between the bacteria and the immune system. This study showed that there are differences in processing of *M. abscessus* smooth and rough strains by macrophages following phagocytosis, which were previously described in literature in more detail (Byrd and Lyons, 1999; Roux *et al.*, 2016). Other studies in NTMs also showed that there is a correlation between the rough colony morphology and increased virulence in macrophages but typically saw no change in intracellular proliferation from 4 to 24 h.p.i. between smooth or rough strains, only an increase in survival after 72 h.p.i. (Julián *et al.*, 2010; Roux *et al.*, 2016).

We observed a drop in survival of the smooth strains at 24 h.p.i. followed by recovery to similar numbers as indicated by the rough strains at 72 h.p.i suggesting initial killing of the smooth strains by the macrophages and proliferation by surviving bacteria. Smooth strains are normally phagocytosed in loner phagosomes, with single bacilli, and can block phagosomal maturation and persist in the phagosomes (Johansen, Herrmann and Kremer, 2020). In this case we are likely observing clearance of a portion of phagocytosed smooth strains, while the rest persist and slowly proliferate inside the phagosome. At 4 h.p.i. a lower number of rough bacteria was phagocytosed by macrophages, compared to smooth strains, however they were able to survive and proliferate, as indicated by the rise in CFUs at 24 h.p.i. A study contributed this rapid

increase in CFUs after phagocytosis of *M. abscessus* R strains to active multiplication that leads to phagosomal rupture (Kim *et al.*, 2019). Depending on the size of the aggregates formed by the rough strain, phagocytosis is not always possible, which can leave them adhered in phagocytic cups on the periphery of macrophages. This could explain why the number of phagocytosed rough bacteria is lower than that of smooth bacterial strains. In *M. tuberculosis*, which presents with a rough colony morphotype and does not produce GPLs, there is bacterial cording, a larger number of bacilli being engulfed in macrophage phagosomes and a robust immune response including granuloma formation (Brambilla *et al.*, 2016). Literature has shown that similar is true for *M. abscessus* rough strains - they are phagocytosed in social phagosomes which they escape due to the increase in proliferation that leads to rupturing as well as due to activation of apoptosis and autophagy (Roux *et al.*, 2016; Johansen, Herrmann and Kremer, 2020). Following phagosomal escape, rough strains proliferate in the extracellular space creating cords that cannot be cleared by macrophages.

This study illustrates only the beginning of the story of the interaction between the immune system and *M. abscessus*. Further analysis is needed to determine the macrophage response and survival when challenged with *M. abscessus*. In future work this can be determined using a lactate dehydrogenase (LDH) activity assay which determines macrophage viability based on the activity of the LDH enzyme. Furthermore, a measure of the cytokine response needs to be done for a more comprehensive picture of how *M. abscessus* challenges macrophages. This can most effectively be done using multiplex Enzyme-Linked Immunosorbent Assays (ELISA) kits that test for a number of relevant cytokines at once, which gives insight into the pathways in the immune system the pathogen activates. Something to be considered in light of this study, and any subsequent cytokine studies, is the effectiveness of the cell line used. J774 is an immortalized murine macrophage cell line ubiquitously used in research labs. Studies have shown, however, that it offers a poor cytokine response to mycobacteria when compared to

other cell lines or primary cells, such as bone-marrow derived macrophages (Jordao *et al.*, 2008; Mendoza-Coronel and Castañón-Arreola, 2016).

Initial characterization of the pulmonary clinical isolates showed the presence of two distinct colony morphologies. There was minimal deviation detected in the growth rate between the strains in liquid media. Susceptibility to first line antibiotics used in pulmonary infections was evaluated and a high level of resistance was detected among all strains, however no ubiquitous pattern of resistance among smooth versus rough strains was notable. The genetic differences that contribute to the intrinsic and adaptive resistance in *M. abscessus* are further evaluated in Chapter 7, following whole genome sequencing and identification of the subspecies within the *M. abscessus* complex. Co-cultures with murine macrophages showed a difference in behaviour between smooth and rough strains after initial uptake, however further analysis is needed for more concrete conclusions and understanding the interaction between macrophages and *M. abscessus* strains.

## **6 Characterization of biofilm formation in *M. abscessus* clinical isolates**

## 6.1 Introduction

Even though in laboratory conditions scientists largely study bacteria in liquid cultures as free growing planktonic cells, in the environment 99% of bacteria grow as biofilms (Vasudevan, 2014). In fact, it is laboratory passaging of bacterial isolates that selects for planktonic and detached biofilm cells, potentially resulting in the loss of genes important for spatial and metabolic interactions within biofilms. Often lab strains of bacteria, used as a reference for studies, have impaired biofilm formation when compared to clinical isolates as a result of gene loss (Fux *et al.*, 2005). Unintentional genetic alteration as well as studies of planktonic growth increase the disparity between results collected from laboratory strains and clinical isolates.

In a study that analyzed biofilm formation among 167 strains of NTMs, it was shown that clinical isolates produced biofilms more frequently than laboratory strains (61.8% vs 55.6%) and that 87.5% of *M. abscessus* isolates formed biofilms, the highest prevalence amongst all NTM clinical strains tested (Martín-de-Hijas *et al.*, 2009). *M. abscessus* affinity for forming biofilms is additionally dangerous due to the demonstrated increased resistance to antibiotics in this growth condition - neither clarithromycin nor amikacin demonstrated significant activity against *M. abscessus* biofilms (Greendyke and Byrd, 2008). Furthermore, a direct correlation has been established between colony morphology, ability of the strain to form a biofilm and successful colonization of lung airways by *M. abscessus* (Byrd and Lyons, 1999).

Given the underlying importance biofilms play in pathogenicity of *M. abscessus*, in this chapter clinical strains introduced in Chapter 5 were evaluated for their ability to form biofilms. Additionally, following from findings outlined in Chapter 3 of alterations in the lipid profile during biofilms formation by the type strain, a complete lipid profile of clinical isolates in planktonic and biofilm growth conditions was done. A particular focus was the analysis of GPLs since their presence or absence dictates the colony morphology and ability to form biofilms. The specific objectives of this chapter were to (1) describe the ability of each strain to successfully form biofilms *in vitro*, (2) investigate the lipid profile of biofilms as compared

to the profile in planktonic cells and (3) analyse the difference in presentation of surface GPLs between clinical strains of differing colony morphology.

## 6.2 Results

### 6.2.1 *M. abscessus* clinical isolates form biofilms regardless of colony morphotype

To evaluate biofilm formation in *M. abscessus* clinical isolates, the same method was used as for the type strain and biofilms were grown for 7 days in Sauton's media, in 24-well plates (**Fig. 6.1**). There was a delay in biofilm formation by the smooth clinical isolates (CI-2S, CI-3S and CI-4S) and after 7 days the biofilm formed was patchy and thin. CI-4S formed a submerged biofilm rather than a pellicle. Strains with a rough colony morphology (CI-1R, CI-5R and CI-6R) were able to form pellicular biofilms. There was clear evidence of a pellicle floating on the liquid surface composed of bacteria aggregated into microcolonies and an ECM binding the aggregates. Crystal violet analysis was used to quantify the biofilm biomass (**Fig. 6.1B**). Crystal violet is a dye traditionally used to stain biofilms because it binds negatively charged molecules and stains both bacteria and the ECM (Ommen, Zobek and Meyer, 2017). The two reference stains, *M. abscessus* S and R, formed pellicles with the biggest biomass and amongst the clinical isolates, pellicles of rough strains had a bigger biomass than those of smooth strains.

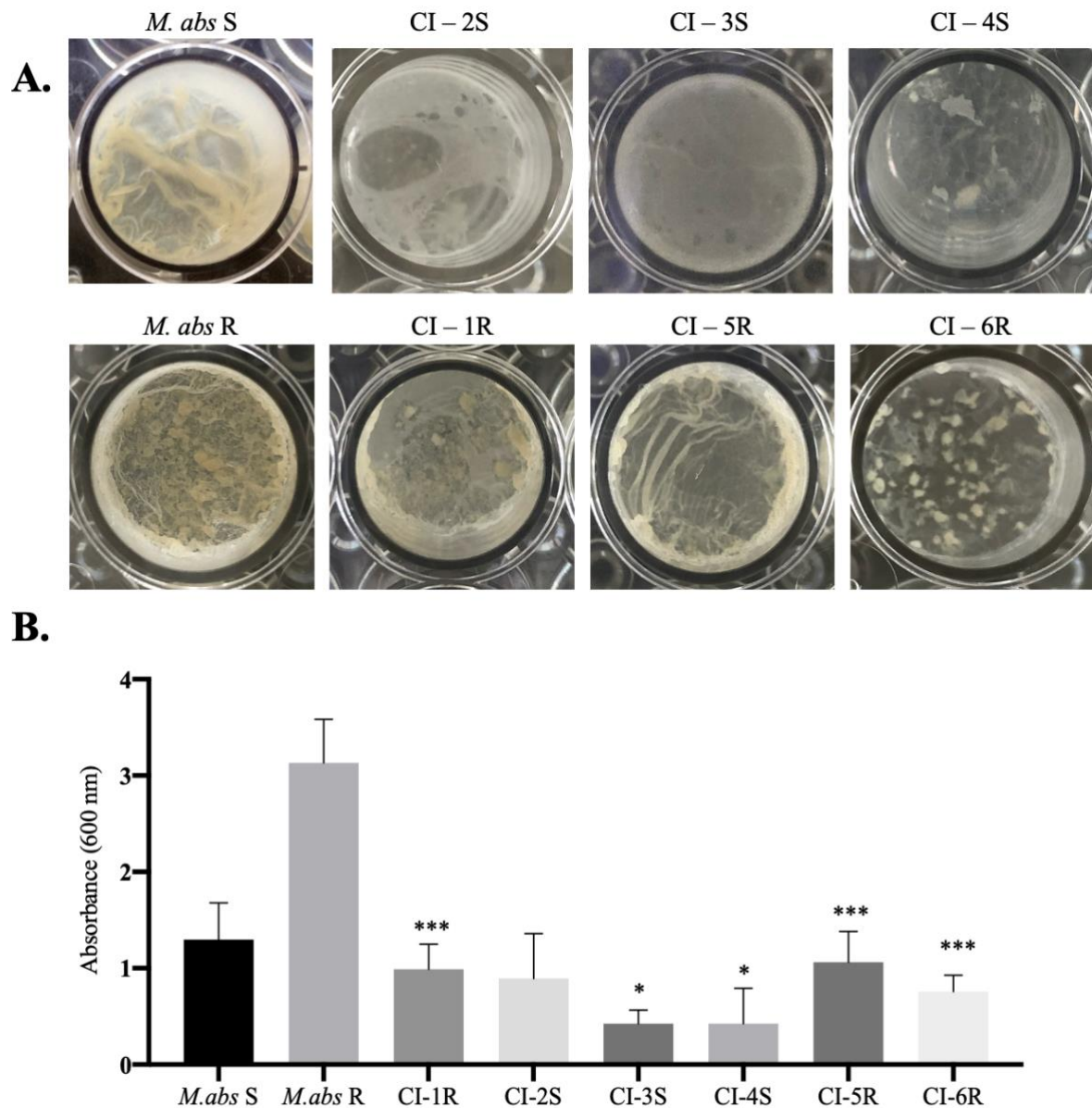


**Figure 6.1: Formation of biofilms in *M. abscessus* clinical isolates. A.** Images of biofilms formed after 6 days in Sauton's media, using either a mid-log culture or colonies from a plate as inoculum. **B.** Crystal violet quantification, using absorbance at 600 nm of biomass of biofilms inoculated from culture. Data is from quintuplicates. Student's t-test was run for each clinical isolate in comparison to its reference smooth or rough strain (unpaired, one-tail, \* $p<0.05$ ; \*\* $p<0.01$ ; \*\*\* $p<0.001$ ).

## **6.2.2 Lipid profile of *M. abscessus* R biofilms differs from that of *M. abscessus* S**

Bacteria were labelled with  $^{14}\text{C}$ , and lipids isolated for characterization as described in section 9.4. Equal radioactive counts were loaded on silica TLC plates and lipid species were separated based on polarity using different solvent systems, as outlined in 9.4.6. Lipid profiles of planktonic and pellicle cultures of *M. abscessus* S and R, as shown in **Fig. 6.2**, were analysed and used as reference profiles for clinical isolates. There were no major differences between lipid profiles of planktonic *M. abscessus* S and R, except for the polar lipid fraction (resolved in system D) in which *M. abscessus* R lacked glycopeptidolipids (GPLs) (**Fig. 6.2**). In the biofilm lipid profile, there was an increase in TAG (apolar lipids, system A) and FMA in biofilms (apolar lipids, system B) of *M. abscessus* S compared to planktonic cells of *M. abscessus* S. A similar increase was observed in *M. abscessus* R, however it is much less prominent.

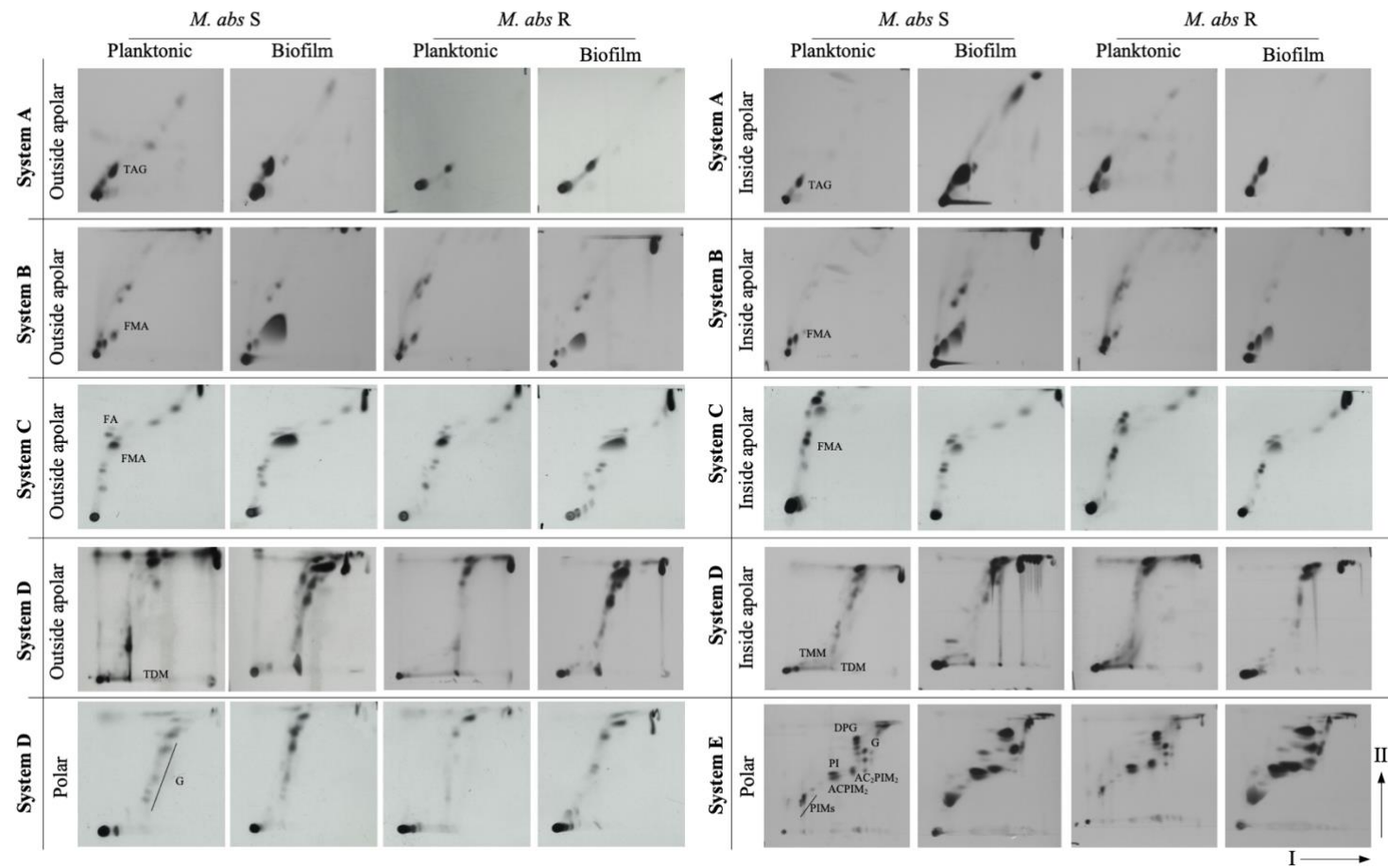


**Figure 6.2: Lipid profiles of *M. abscessus* S and R for planktonic and biofilm growth.** Autoradiographs of solvent extracted outside apolar, inside apolar and polar lipids separated by 2D TLC in solvent systems of different polarities (system description found in Table 9.5). Representative of three repeats. TAG, triacylglycerols; FA, fatty acid; FMA, free mycolic acid; TMM, trehalose, monomycolate; TDM, trehalose dimycolate; G, glycopeptidolipids; P, phospholipids; DPG, diphosphatidylglycerol; PE, phosphatidylethanolamine; PI, phosphatidylinositol; PIMs, phosphatidyl-myoinositol mannosides; Ac<sub>2</sub>PIM<sub>2</sub>, diacyl phosphatidylinositol dimannoside; Ac<sub>2</sub>PIM<sub>6</sub>, diacyl phosphatidylinositol hexamannoside.

### 6.2.3 Lipid profile of *M. abscessus* clinical isolates

TLC analysis of lipid fractions of planktonically grown clinical isolates showed no variation between the strains apart from polar lipids, resolved in system D, where GPLs were absent in rough strains (**Fig. 6.3**). Notable differences between the strains were observed in the biofilm lipid profiles (**Fig. 6.4**). There was a slight increase in TAG in all clinical isolate biofilms, but it was most prominent in the inside apolar lipid fraction of the rough strains. This was the opposite of the phenotype observed in the type strains, where the increase in TAG was documented in biofilms of *M. abscessus* S. There is a definite increase in FMA in biofilms of all strains (apolar lipid, system C), however it is smaller compared to the FMA increase in *M. abscessus* S biofilms. In the polar lipid fraction, GPLs were more prominent in the smooth strains and were either completely absent or faint in the rough ones. TDM was slightly increased in the inside apolar fraction of the rough strains, which is interesting to consider since TDM is a known cording factor in *M. tuberculosis* (Julián *et al.*, 2010).

Following from changes in the mycolic acid structure seen in *M. abscessus* S biofilms, outlined in Chapter 4, a further analysis of mycolic acids was done for all clinical isolates – first by separating MAMES isolated from the wall bound fraction in one dimension (1D) (**Fig. 6.5A**) and then in two dimensions (2D), based on desaturation of the molecules (**Fig. 6.5B**). This analysis revealed an increase in both  $\alpha$  and  $\alpha'$  mycolic acids in lipids isolated form biofilms of all strains. The mycolate profile appears uniform in all the strains, with changes in desaturation of  $\alpha$  mycolates in biofilms leading the molecules to migrate further on the TLCs when separated in 2D (**Fig. 6.5B**), as previously observed in *M. abscessus* S (**Fig. 3.4**).

Based on the observable difference in the amount of polar lipids between smooth and rough strains, and what is known from literature about the lack of GPLs in rough strains, a further analysis was done. Polar lipids were deacetylated to enable separation of each GPL subclass using TLC. The analysis revealed major differences in the GPL profile between smooth and rough strains, with rough strains lacking all or some GPLs (**Fig. 6.6**). Smooth strains exhibited

an almost identical GPL profile to *M. abscessus* S in planktonic and biofilm growth. *M. abscessus* R and CI-1R have the most similar profile in planktonic and biofilm growth, where they completely lacked GPLs, while CI-5R and CI-6R showed faint expression of GPLs. Diglycosylated GPLs run on the top of the TLC (1-4), while triglycosylated, and polar, are represented by the bottom two bands (5 and 6). In CI-5R and CI-6R there is presence of the top 4 bands and not the bottom two, indicating a potential differential acetylation pattern and absence of polar GPLs.

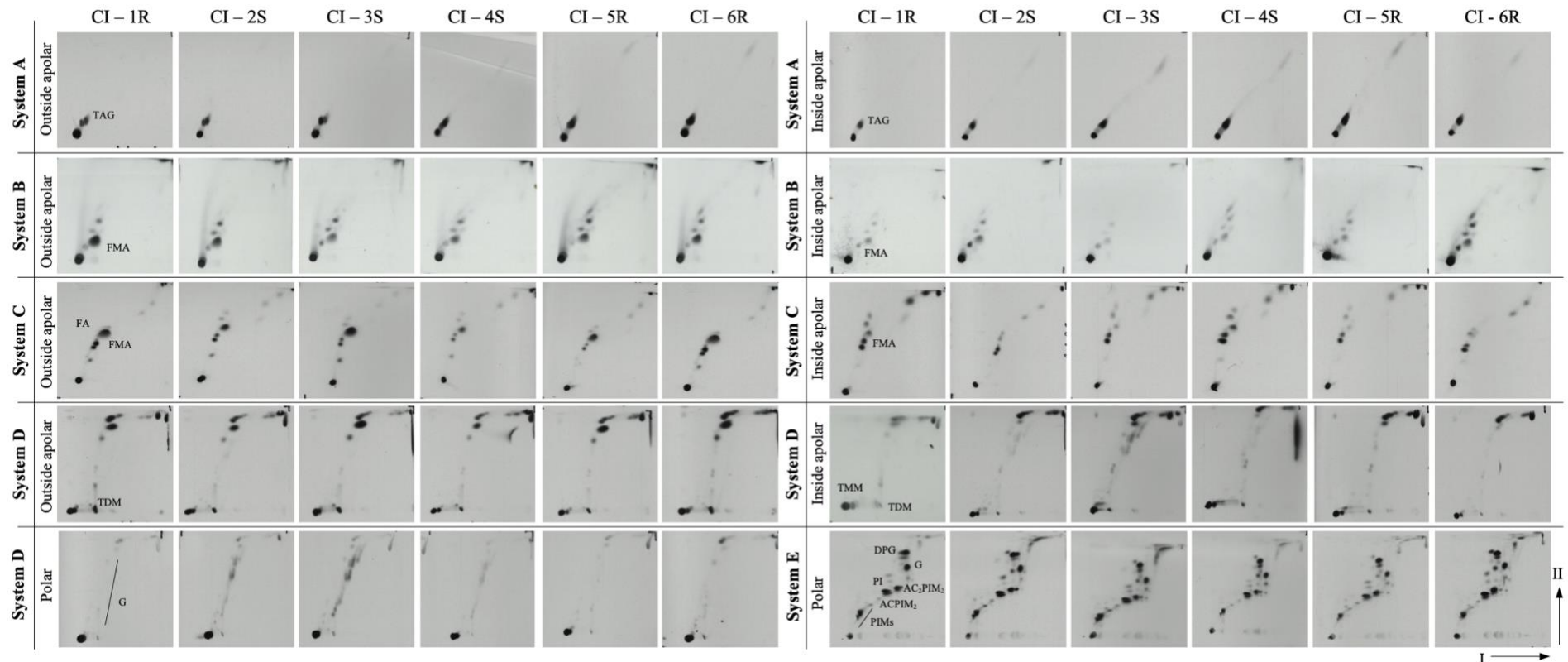


**Figure 6.3: Autoradiographs of 2D TLCs showing the lipid profile of planktonically grown *M. abscessus* clinical isolates.** Solvent extracted outside apolar, inside apolar and polar lipids separated by 2D TLC in solvent systems of different polarities (system description found in Table 9.5). **Representative of three repeats.** TAG, triacylglycerols; FA, fatty acid; FMA, free mycolic acid; TMM, trehalose, monomycolate; TDM, trehalose dimycolate; G, glycopeptidolipids; P, phospholipids; DPG, diphosphatidylglycerol; PE, phosphatidylethanolamine; PI, phosphatidylinositol; PIMs, phosphatidyl-myoinositol mannosides; Ac<sub>2</sub>PIM<sub>2</sub>, diacyl phosphatidylinositol dimannoside; Ac<sub>2</sub>PIM<sub>6</sub>, diacyl phosphatidylinositol hexamannoside.

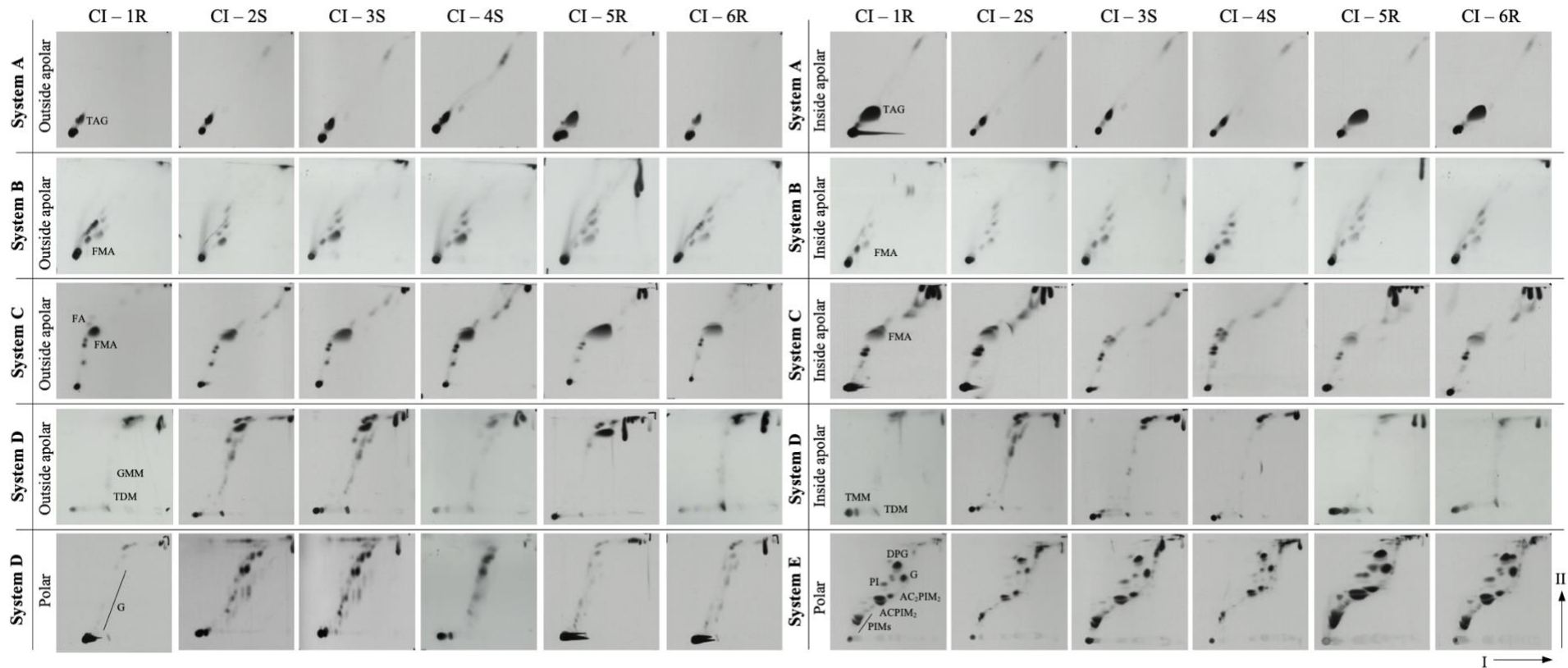


**Figure 6.4: Autoradiographs of 2D TLCs showing the lipid profile of *M. abscessus* clinical isolates grown in biofilms.** Solvent extracted outside apolar, inside apolar and polar lipids separated by 2D TLC in solvent systems of different polarities (system description found in Table 9.5). Representative of three repeats. TAG, triacylglycerols; FA, fatty acid; FMA, free mycolic acid; TMM, trehalose, monomycolate; TDM, trehalose dimycolate; G, glycopeptidolipids; P, phospholipids; DPG, diphosphatidylglycerol; PE, phosphatidylethanolamine; PI, phosphatidylinositol; PIMs, phosphatidyl-*myo*-inositol mannosides; Ac2PIM2, diacyl phosphatidylinositol dimannoside; Ac2PIM6, diacyl phosphatidylinositol hexamannoside.

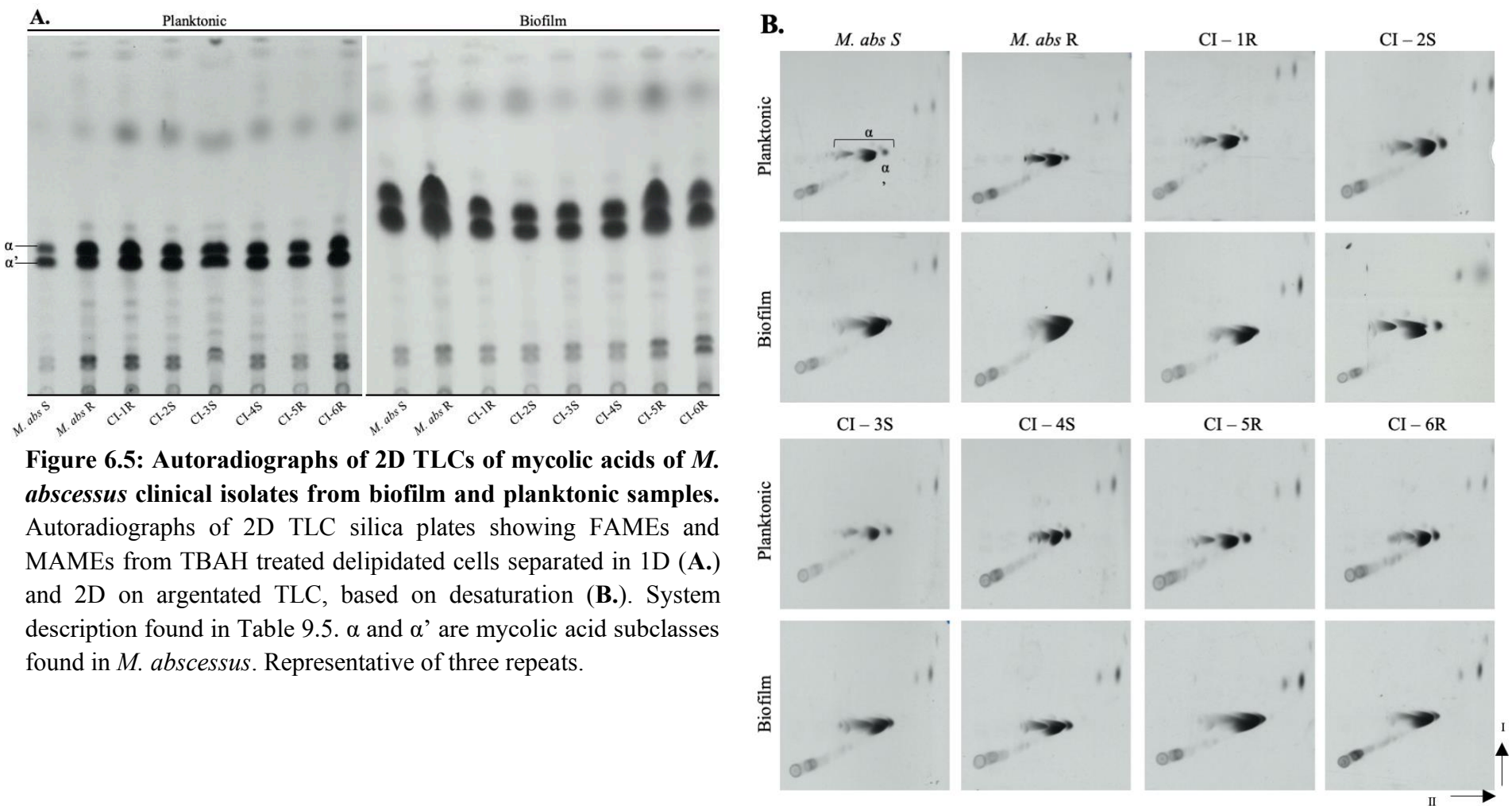


**Figure 6.5: Autoradiographs of 2D TLCs of mycolic acids of *M. abscessus* clinical isolates from biofilm and planktonic samples.**  
 Autoradiographs of 2D TLC silica plates showing FAMEs and MAMEs from TBAH treated delipidated cells separated in 1D (A) and 2D on argentated TLC, based on desaturation (B.). System description found in Table 9.5.  $\alpha$  and  $\alpha'$  are mycolic acid subclasses found in *M. abscessus*. Representative of three repeats.

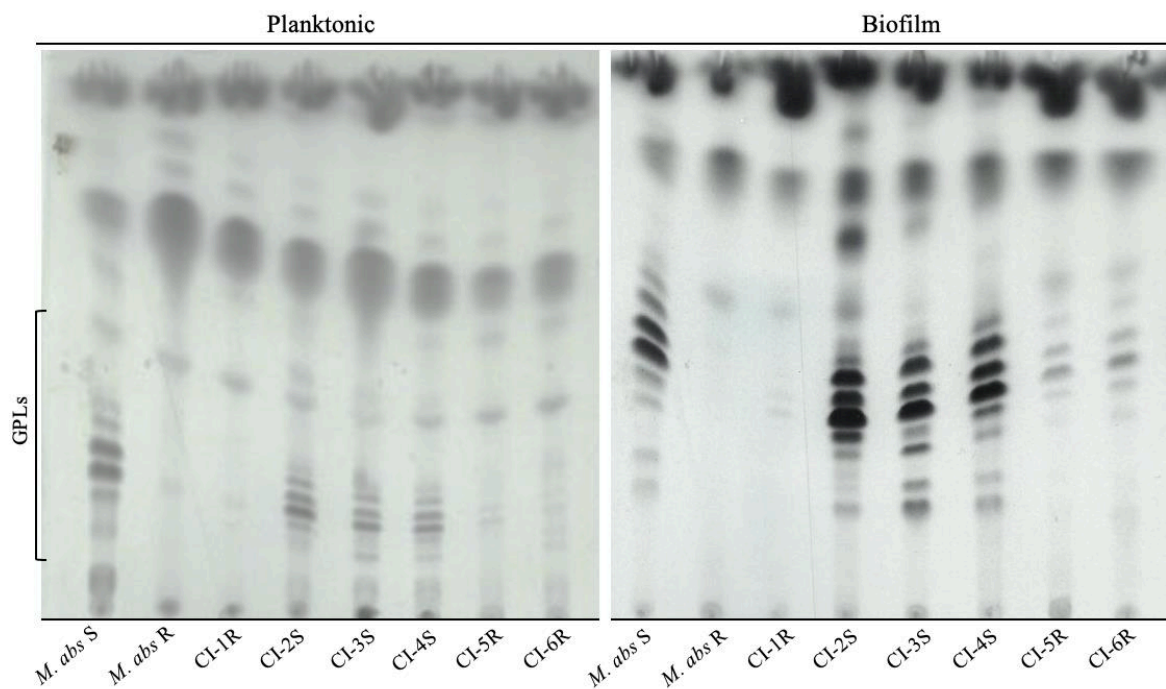


**Figure 6.6: Autoradiographs of 2D TLC silica plates showing deacetylated GPLs of *M. abscessus* clinical isolates from biofilm and planktonic samples separated in 1D.** System description found in Table 9.5. Representative of three repeats.

## 6.3 Discussion

### 6.3.1 All *M. abscessus* clinical isolates form biofilms

In this chapter the ability of *M. abscessus* clinical isolates to form biofilms was evaluated alongside their lipid profiles in both planktonic and biofilm growth stages. *M. abscessus* S and R strains maintained distinct morphologies during biofilm formation, as evidenced in **Fig. 6.1A**, and formed visually distinct biofilms. Although early reports indicated that *M. abscessus* R phenotype is defective in biofilm formation, studies have since disputed this and the ability of rough strains to form biofilms was additionally confirmed by this study (Byrd and Lyons, 1999; Clary *et al.*, 2018). Rough strains have previously been described to form large biofilm-like aggregates as opposed to surface attached or pellicular biofilms, and a similar phenotype was shown here (**Fig. 6.1A**) (Clary *et al.*, 2018). Rough biofilms were also shown to have a larger biomass, determined using crystal violet staining (**Fig. 6.1B**). This is in accordance to previous reports which showed that *M. abscessus* R biofilms had a significantly higher biomass measured on days 3, 5 and 7 as compared to *M. abscessus* S, but that the number of bacteria (CFU/cm<sup>2</sup>) was the same, indicating that the ECM was contributing to the increased biomass (Clary *et al.*, 2018).

The biofilms of rough strains contained visible cell aggregates that were connected by a thin, transparent film that allowed the pellicle to be maintained on the liquid-air interface and migrate along the sides of the well, similarly to the pellicles of *M. abscessus* S. This film also contributed to high hydrophobicity which made the pellicles difficult to resuspend in liquid. To date, limited studies show that biofilms of rough strains are stiffer and more tolerant to antibiotics compared to biofilms formed by smooth strains, but can be cleared using acetic acid just like biofilms of smooth strains (Clary *et al.*, 2018; Gloag *et al.*, 2021). Perhaps the increased hydrophobicity in rough biofilms, denser ECM and the tighter and smaller aggregates make penetration of antibiotics more difficult. Future work should focus on a microscopic

characterization of the *M. abscessus* R biofilms as was shown in Chapter 2 for *M. abscessus* S in order to determine potential differences the ECM composition between these strains. Interestingly another study reported pellicles of *M. abscessus* S and R to have different phenotypes than what we recorded, likely due to a difference in the way biofilms were grown (Clary *et al.*, 2018).

### 6.3.2 Lipid profiles of *M. abscessus* clinical isolates

Despite different phenotypes on agar and as biofilms, the lipids profiles of clinical isolates do not differ much from each other or the type strains. Increase in FMA is a hallmark of biofilm formation in NTMs, however there was only a faint increase in FMA in clinical isolate biofilms when compared to the increase in *M. abscessus* S biofilm. The highest increase in FMA is coincidentally in CI-5R, which forms a biofilm visibly most similar to that of the smooth type strain (**Fig. 6.1.A**) despite having a rough colony morphology. Little change in FMA was recorded in the lipid profile of biofilm smooth clinical isolate strains, likely due to the fact that they form weak biofilms compared to the type strain and the rough strain – also indicated by the low biomass. However, a small increase in FMA was still evident indicating true biofilm formation (**Fig. 6.4**).

An increase in TAG was evident in the inside apolar fraction of rough clinical isolates. Accumulation of TAG in *M. tuberculosis* occurs as a response to various environmental stressors *in vivo* in lungs, such as low pH or hypoxia, and is accompanied by a decrease in expression of genes related to complex lipid biosynthesis (Daniel *et al.*, 2004; Shi *et al.*, 2010). In a study of 50 *M. abscessus* clinical isolates it was shown that TAG accumulates in isolates collected at later stages of infection, which are most often rough strains, and that expression of *fadD23*, an essential enzyme in complex lipid synthesis, is reduced (Park *et al.*, 2015). This led to a hypothesis that *M. abscessus* may benefit from storing fatty acids as TAG instead of using them for the synthesis of complex lipids during infection (Park *et al.*, 2015).

### **6.3.3 Glycopeptidolipid profile in smooth and rough *M. abscessus***

The focal difference between the *M. abscessus* smooth and rough strains is the expression of GPLs, evidenced by the lack of GPLs in polar lipids after TLC analysis (Fig. 6.3, 6.4 and 6.6). In *M. abscessus* R and CI-1R there is a complete lack of GPLs, while in CI-5R and CI-6R GPL molecules are faintly visible in planktonic and in biofilm growth. There is evidence that GPLs are essential for formation of mycobacterial biofilms, specifically for initial surface attachment (Recht and Kolter, 2001; Ojha, Varma and Chatterji, 2002; Yang, Thomas, Li, Vilchèze, Derbyshire, Jacobs and Ojha, 2017). A study in *M. smegmatis* showed that rough strains lacking GPLs are defective in sliding motility and biofilm formation on polyvinyl chloride (PVC). The theory is that exposed GPLs make the cell surface hydrophobic, allowing biofilm attachment on hydrophobic PVC, while GPL-lacking strains, or rough strains, have a hydrophilic cell wall that does not favour attachment to hydrophobic surfaces (Recht and Kolter, 2001). A different study showed that a rough mutant, lacking the *mps* gene for non-ribosomal peptide synthase needed for GPL synthesis, was still able to form biofilms, but with delay (Yang, Thomas, Li, Vilchèze, Derbyshire, Jacobs and Ojha, 2017). Previous studies have shown that disruption of certain GPL biosynthesis genes leads to smooth-to-rough transition and subsequent lack of sliding motility and defective biofilm formation in the strains affected. (Ripoll *et al.*, 2007; Park *et al.*, 2015; Gutiérrez *et al.*, 2018). In the case of rough clinical isolates examined in this study, biofilm formation was possible regardless of absence of GPLs, therefore the implication that GPLs are necessary for biofilm formation is challenged. Likewise, there could be strict control of GPL biosynthesis genes which influences the final number of GPLs in the cell – which would explain the faint levels of GPLs in the CI-5R and CI-6R strains. We observed biofilm formation in rough strains with a phenotype that more resembles aggregation than biofilms of the smooth strains, bringing into question the exact role of GPLs in relation to aggregation, biofilm formation and maturation. In the next steps, it would be beneficial to look at differential gene

expression of GPL biosynthesis genes in the clinical isolates to identify which genes are commonly expressed amongst biofilm forming strains and in which stages of biofilm formation. Even though a biofilm is a universal form of growth among bacteria, differences exist between different types of biofilms. Rough strains of mycobacteria are capable of forming liquid-air interface pellicles because the formation of this type of biofilm is focused more on cell aggregation rather than surface attachment and so different molecules and events could be responsible for promoting this type of growth. Such differences are important to keep in mind when designing studies and interpreting data, because different types of biofilms can colonize medical equipment, wounds, lung airways or pipelines and understanding these subtle differences is central in determining the correct way of combating biofilms.

## **7 Genetic profile of *M. abscessus* clinical isolates**

## 7.1 Introduction

Over the years evidence has shown that bacterial laboratory strains, used routinely as reference strains in studies, in reality do not correlate with strains isolated from patients. This comes as a combined result of gene selection that prefers *in vitro* type growth and of decades of passaging that has led to the loss of genes that make the pathogen in question pathogenic (Fux *et al.*, 2005). We need look no further than the history of the BCG vaccine to see evidence of this, as it was exactly the continuous passaging of the virulent strain that made it into an attenuated live vaccine (Behr, 2002). The lab strain, *P. aeruginosa* PAO1, was shown to be missing between 0.4-19% of genes found in non-laboratory strains, and similar evidence was seen in *S. aureus* COL and *E. coli* K12, all model organisms used routinely to study pathogenesis (Head and Yu, 2004; Fux *et al.*, 2005). It is said that due to the high-flexibility of bacterial genomes and quick adaptation to *in vitro* conditions, no bacterial strain can truly contain the genome that is representative of the species as a whole (Fux *et al.*, 2005). For these reasons we set out to investigate the genetic make-up of *M. abscessus* clinical isolates in comparison to the lab strains that are routinely used for *in vitro* experiments.

*M. abscessus* complex is characterized by phenotypic heterogeneity, referring to the inducible change from smooth to rough colony morphology, as well as genotypic heterogeneity. The three subspecies within the *M. abscessus* complex, *M. abscessus*, *M. massiliense* and *M. bolletii*, are genetically close enough to be classified as one species, yet diverse enough that identification and nomenclature has caused issues in the past (Griffith *et al.*, 2015). *M. abscessus* has a typical genomic make up of an environmental bacterium that has been exposed to a diverse microbiome, with some 30% of its genome being made up of accessory genes which are shared by some but not all isolates in a population. These genes are known to include prophages, plasmids and genomic islands that *M. abscessus* acquired by horizontal gene transfer. The rest is made up of the core genome, 68% in *M. abscessus* and *M. bolletii*, and 71% in *M. massiliense*, as shown by a study that compared 40 genomes in the complex (Davidson, 2018).

It is clinically important to easily separate the subspecies of the *M. abscessus* complex because they respond differently to antimicrobial therapy (Koh *et al.*, 2011; Harada *et al.*, 2012). Additionally, acquired antimicrobial resistance in *M. abscessus* has been linked to genetic mutations. *erm41* gene has been linked to macrolide resistance in *M. abscessus* and *M. bolletii* strains, while *M. massiliense* has been shown to encode a truncated version of this rRNA methylase leaving the bacteria vulnerable to macrolides. It was also shown that polymorphisms in the 16S rRNA lead to amikacin resistance. These differences in polymorphisms in genes that contribute to antimicrobial resistance, particularly in terms of inducible resistance, as well as subspecies heterogeneity that can only be identified through genotypic analysis, highlighting the importance of analysing whole genome sequences of different *M. abscessus* strains and isolates with the goal of identifying common polymorphisms and mutations that can lead to more efficient screening, diagnostics, therapy and clinical outcomes.

Besides the high level of antimicrobial resistance in *M. abscessus* that lead to difficulties in treatment, the changes in colony morphology from smooth to rough also contributes to confusion surrounding this bacterium. Studies have shown that difference in morphology is related primarily to biofilm formation and virulence during infections, but the trigger behind the switch remains unresolved. The main difference between the two morphologies, as outlined in Chapters 5 and 6, is the lack of GPLs in rough strains. Although there is inconsistency in previously published work that suggests that this switch is genetic, the genes of the GPL locus responsible for GPL biosynthesis are important and analysing them can lead to answering at least part of the question of whether this phenotypic difference has a genetic origin.

The genomes of *M. abscessus* clinical isolates, that were so far biologically characterized in this study (Chapters 5 and 6), were sequenced alongside two laboratory type strains, *M. abscessus* S and R. The work in this chapter aimed to examine the genetic differences between clinical isolate strains in order to determine patterns among strains of the same colony morphology. To achieve this aim, the specific objectives were: (1) classify the subspecies of

each clinical isolate and construct a phylogenetic tree to determine genetic relatedness, (2) examine in depth differences in the GPL locus and (3) in genes related to antimicrobial resistance.

## 7.2 Results

### 7.2.1 Identification of subspecies of clinical isolates within the *M. abscessus* complex

Growth and sample collection of strains was done by me at the University of Birmingham. Sequencing services were performed by MicrobesNG using Illumina next-generation sequencing and data analysis was provided by Dr Vartul Sangal from Northumbria University. The pangenome of these 8 strains comprised 7,968 genes including 3,843 core genes. From the core genes, 283 were found only in 7 strains, 212 in 6, 111 in 5, 149 in 4, 396 in 3, 360 in 2, and 2,614 were unique genes (mainly annotated as hypothetical proteins or transcriptional regulators). Nearly 3.9% of the core genome is polymorphic, meaning that more than one allele of a gene occupies the gene's locus in a population. Core genome alignment was used to construct a phylogeny tree (**Fig. 7.1**). *M. abscessus* S and R, the lab strains, are closely related to each other while the clinical isolates are more distant to them and to one another. A noticeable pattern in the level of relatedness between the clinical isolates is the clustering of smooth and rough strains. However, no genes were decidedly present only in smooth or only in rough strains.

To identify subspecies of the clinical isolates the sequenced genome of each strain was compared against published reference genomes of *M. abscessus* ATCC 19977, *M. bolletii* CCUG 5018 and *M. massiliense* CCUG 48898, found on GenBank (Sekizuka *et al.*, 2014; Miranda-CasoLuengo *et al.*, 2016; Yoshida *et al.*, 2018). Pairwise average nucleotide identities (ANI), average amino-acid acid identities (AAI) and percentage of conserved proteins (POCP) were identified within the data set. CI-2S, CI-3S, CI-4S and CI-6R all belong to the subspecies *M. abscessus*, while CI-1R was identified as *M. bolletii* and CI-5R as *M. massiliense* (**Fig. 7.1**). CI-1R and CI-5R were the most distant from the smooth and rough lab strains on the phylogeny tree as well.

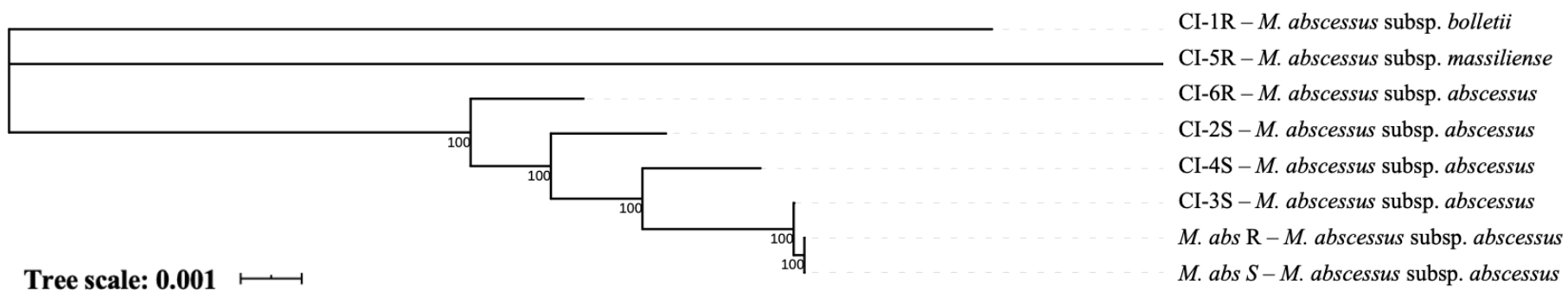


**Figure 7.1: A maximum-likelihood tree from the nucleotide sequences alignment of the core genome of *M. abscessus* isolates.** Scale bar is indicative of number of substitutions per site, and bootstrap values are mentioned at the nodes. Subspecies of each strain were identified against reference genomes for *M. abscessus* subsp. *abscessus* ATCC 19977, *M. abscessus* subsp. *bolletii* CCUG 5018 and *M. abscessus* subsp. *massiliense* CCUG 48898.

## 7.2.2 Analysis of the GPL biosynthesis gene cluster in smooth and rough strains

The principal interest in characterizing smooth and rough strains is due to the differences in disease manifestation in patients infected with one or the other. The rough variant is hypervirulent and forms cords that cause a robust immune response and tissue damage, whereas the GPLs on the surface of the smooth strain mask pathogen associated molecular patterns allowing the infection to go undetected for a period of time (Johansen, Herrmann and Kremer, 2020). Additionally, the main phenotypic differences identified in this study, outlined in Chapter 5 and 6, corresponded to differences in colony morphology of the strains. Therefore, analysing the GPL biosynthesis gene cluster was of particular interest, with the aim of identifying differences in gene representation between strains, as well as mutations, particularly in genes in rough strains, which do not express GPLs (Fig. 7.2). Genes were evaluated based on their protein sequences, since we were interested in retention of function between species. Each gene was assigned an IC score which is representative of the product of protein sequence identity and alignment (sequence coverage) between the sequence of interest and reported annotated sequence.

Analysis showed no large gene deletions in the GPL biosynthesis gene cluster in any strains, apart from *mps2* and a PE hypothetical protein *MAB\_0936c*. *mps2* encodes a non-ribosomal protein synthase involved in synthesis of the amino acid alcohol GPL core and all rough strains in this study had mutations in this gene. In the rough type strain, CI-5R and CI-6R Mps2 proteins were prematurely terminated. In the rough lab strain the protein terminated after 1875 amino acid residues (out of 2581) with 100% sequence identity, in CI-5R after 1143 and had 18 amino acid substitutions, and in CI-6R after 1122 with two amino acid substitutions, while CI-1R encoded a full-length protein but with 21 amino acid mismatches compared to the reference genome. *MAB\_0936c*, annotated as a hypothetical protein, was absent from lab strains, CI-2S and CI-3S. It has 100% sequence identity in CI-6R and CI-4S, and a single mutation, E177D, in CI-1R and CI-5R. It is found on the same operon as *MAB\_0937c*,

*MAB\_0935c*, and *MAB\_0938c*, which are present in all strains, indicating a potential specific deletion. Interestingly, *MAB\_4100c*, which encodes MbtH, a small protein of unknown function, that is an essential accessory protein in many ribosomal peptide synthetases is present in three copies in all the strains. Only one gene copy is a true ortholog found within the GPL locus, while the others were located in other places in the genome and carried a lower sequence identity.

**Table 7.1: GPL biosynthesis related genes of *M. abscessus* type strains (*M. abs* S, *M. abs* R) and six clinical isolates (CI-1-6) evaluated based on IC score (product of protein sequence identity and alignment (sequence coverage)).**

Gene	Locus_tag <sup>a</sup>	Description	IC score							
			<i>M. abs</i> S	<i>M. abs</i> R	CI-1R <sup>b</sup>	CI-2S	CI-3S	CI-4S	CI-5R <sup>c</sup>	CI-6R
<i>mmpS4</i>	MAB_4117c	Putative membrane protein, MmpS family	1	1	1	1	1	1	1	1
<i>mmpL4a</i>	MAB_4116c	Putative membrane protein, MmpL	1	1	1	1	1	0.99	1	1
<i>mmpL4b</i>	MAB_4115c	Putative membrane protein, MmpL	1	1	0.99	1	1	1	0.96	0.99
<i>Rv1174</i>	MAB_4114	Hypothetical protein	1	1	1	1	1	1	0.99	1
<i>rmlA</i>	MAB_4113	Glucose-1-phosphate thymidylyl-transferase	1	1	0.99	1	1	1	1	1
<i>gtf3</i>	MAB_4112c	Glycosyltransferase GtfA	0.95	0.95	0.94	0.94	0.95	0.95	0.94	0.95
<i>rmlB</i>	MAB_4111c	Putative epimerase/dehydratase	0.99	0.99	0.97	0.99	0.99	0.99	0.98	0.99
<i>rmt2</i>	MAB_4109c	Rhamnose 2-O-methyltransferase	1	1	0.97	1	1	1	0.98	1
<i>rmt4</i>	MAB_4108c	Rhamnose 4-O-methyltransferase	0.89	0.89	0.89	0.89	0.89	0.89	0.89	0.89
<i>gtf1</i>	MAB_4107c	Glycosyltransferase GtfA	1	1	0.99	1	1	1	0.98	1
<i>atf</i>	MAB_4106c	Integral membrane protein, acetyltransferase	1	1	0.97	0.99	1	0.99	0.97	0.99
<i>atf</i>	MAB_4110c	Integral membrane protein, acetyltransferase	1	1	0.98	0.99	1	0.99	0.97	0.99
<i>rmt3</i>	MAB_4105c	Rhamnose 3-O-methyltransferase	1	1	0.99	1	1	1	1	0.99
<i>gtf2</i>	MAB_4104	Glycosyltransferase GtfA	1	1	0.98	1	1	0.99	0.97	1
<i>fmt</i>	MAB_4103c	Fatty acid O-methyltransferase	0.97	0.97	0.95	0.97	0.97	0.96	0.96	0.96
<i>mbtH<sup>d</sup></i>	MAB_4100c	MbtH-like protein	1	1	0.98	1	1	1	1	1
<i>mps1</i>	MAB_4099c	Non-ribosomal protein synthase	1	1	0.97	1	1	0.99	0.98	0.99
<i>mps2</i>	MAB_4098c	Non-ribosomal protein synthase	1	0.81	0.99	1	1	0.99	0.77	0.68
<i>gap</i>	MAB_4097c	Conserved hypothetical protein	1	1	0.99	1	1	1	0.98	1
<i>sap</i>	MAB_4454c	Sigma-associated protein	1	1	0.99	0.99	1	0.99	0.99	0.99
<i>ecf</i>	MAB_4459c	RNA polymerase sigma-70 factor	1	1	0.98	0.99	1	0.99	0.98	0.98
<i>fadE5</i>	MAB_4437	Probable acyl-CoA dehydrogenase FadE	1	1	0.99	0.99	1	0.99	0.99	0.99

<i>Rv0926</i>	MAB_4633	Hypothetical protein	1	1	0.98	0.99	1	0.99	0.98	0.99
<i>pks</i>	MAB_0939	Probable polyketide synthase	1	1	0.98	0.99	1	0.99	0.98	0.99
<i>papA3</i>	MAB_0938c	Probable polyketide synthase associated protein PapA3	1	1	0.98	0.99	1	0.99	0.99	0.99
<i>mmpL10</i>	MAB_0937c	Putative membrane protein MmpL	1	1	0.99	1	1	1	0.99	1
PE	MAB_0936c	Hypothetical protein	-	-	0.99	-	-	1	0.98	1
<i>fadD23</i>	MAB_0935c	Putative fatty-acid-CoA ligase FadD	1	1	0.98	0.99	1	0.99	0.98	0.99
gap-like	MAB_0934	Hypothetical integral membrane protein	1	1	0.98	1	1	1	0.97	1

<sup>a</sup>Locus\_tag in reference genome *M. abscessus* subsp. *abscessus* ATCC 19977

<sup>b</sup>Identified as *M. bolletii*

<sup>c</sup>Identified as *M. massiliense*

<sup>d</sup>There are genetic sequences of 3 MbtH-like proteins in *M. abscessus*, however this is the only ortholog

### 7.2.3 Analysis of antibiotic resistance genes in *M. abscessus* clinical isolates

One of the main concerns in treating *M. abscessus* infections is the high intrinsic resistance to a range of antibiotics, including  $\beta$ -lactams, macrolides and aminoglycosides. The list of genes of interest related to antibiotic resistance in *M. abscessus* was chosen carefully through literature review (Fig. 7.2). Several genes and transcriptional regulators, previously recognised to modulate antimicrobial resistance in *M. abscessus*, were identified and their nucleotide and protein sequences checked against the reference genome *M. abscessus* ATCC 19977. Overall, genes related to antimicrobial resistance were conserved amongst the clinical isolates with the exception of *erm41*, *MAB\_4805* and mercury resistance genes.

WhiB7, encoded by *MAB\_3508c*, is a transcriptional regulator of inducible resistance to macrolides (erythromycins, clarithromycin), amikacin and tetracycline (Hurst-Hess, Rudra and Ghosh, 2017). In *M. abscessus* it regulates expression of *erm41* and *eis2* genes which modulate resistance to macrolides and aminoglycosides, respectively (Hurst-Hess, Rudra and Ghosh, 2017). It is highly conserved amongst the tested strains, with no mutations. Additionally mutations in the *rml* gene, encoding a 23S rRNA, at position 2058 and 2059, contribute to high macrolide resistance, however this gene was highly conserved amongst the strains and none carried this mutation (Bastian *et al.*, 2011).

Aminoglycoside acetyltransferase, encoded by the *MAB\_4395* gene, acetylates aminoglycosides with 2' group such as gentamicin C and kanamycin B and the deletion of this gene leads to an increase in susceptibility (Rominski, Selchow, *et al.*, 2017). All the strains carried a copy of this gene, but they are not identical in sequence as illustrated by the IC score below 1. Other aminoglycoside acetyl- and phosphotransferases, including those encoded by *eis1* and *eis2*, were also present in all the strains, with varying degrees of amino acid substitutions.

Genes related to mercury resistance (*MAB\_p05c*, *MAB\_p06*, *MAB\_p07c*, *MAB\_p22c*) were identified in *M. abscessus* S and R type strains but not in any of the clinical isolates. These

genes are found on a 23 kb resistance plasmid, pMAB23 which was also not found in the clinical isolates (Griffith *et al.*, 2015).

$\beta$ -lactams are a highly important and successful class of antibiotics that inhibit cell wall biosynthesis in bacteria (Luthra, Rominski and Sander, 2018). Mycobacteria in particular are notorious for their intrinsic resistance to  $\beta$ -lactams due to many  $\beta$ -lactamase encoding genes (Flores, Parsons and Pavelka, 2005; Griffith *et al.*, 2015; Miranda-CasoLuengo *et al.*, 2016). All the strains in this study contained common mycobacterial genes that encode for  $\beta$ -lactamases, except for *MAB\_4805*, encoding a  $\beta$ -lactamase hypothetical protein, which was absent in CI-2S, CI-5R and CI-6R. A BLAST search revealed that *MAB\_4805* is often annotated as a metallo- $\beta$ -lactamase or a hydroxyacylglyathione hydrolase, but this specific  $\beta$ -lactamase is unexplored further in *M. abscessus*. *MAB\_0591*, which encodes an ADP-Ribosyltransferase responsible for rifampicin resistance was present in all the strains.

Detection of macrolide resistance during infections is particularly important since the 23S rRNA methyltransferase in certain subspecies of *M. abscessus* offers inducible resistance to macrolides. *M. massiliense* was shown to encode a truncated version of the Erm41 protein making the bacteria susceptible to this class of antibiotics (~10% resistance, as opposed to 80% in *M. abscessus* and *M. bolletii*) (Kim *et al.*, 2010; Harada *et al.*, 2012; Nessar *et al.*, 2012). In fact, CI-5R, which belongs to the subspecies *M. massiliense*, was shown to have poor sequence identity and coverage against the reference *M. abscessus* ATCC 19977 genome. *erm41* in CI-5R has seven SNPs, two-nucleotide deletion (GC) at position 61 and a large deletion of 274 bases at position 154 and it carries three amino acid substitutions (**Table 7.3**). However, when aligned against the *M. massiliense* CCUG 48898 reference genome it had 100% sequence identity. *erm41* gene in CI-1R carries ten genetic mutations which result in three amino acid substitutions when aligned against the *M. abscessus* ATCC 19977 reference genome, however when aligned against the reference genome for *M. bolletii* strains (CCUG 5018) the sequence identity is higher with only one amino acid substitutions, L85I. This indicates subspecies

specificity when it comes to the genetic sequence of *erm41*. Within the rest of the strains, all belonging to subspecies *M. abscessus*, CI-2S and CI-4S exhibited genetic differences to the reference genome (**Table 7.3**). Interestingly, only CI-2S had the T28C mutation associated with resistance to clarithromycin.

**Table 7.2: Genes related to antimicrobial resistance in *M. abscessus* type strains (*M. abs* S, *M. abs* R) and six clinical isolates (CI-1-6) evaluated based on IC score (product of protein sequence identity and alignment (sequence coverage)). Annotation of the gene products was taken from Mycobrowser (Kapopoulou, Lew and Cole, 2011).**

Locus_tag <sup>a</sup>	Description	IC score							
		<i>M. abs</i> S	<i>M. abs</i> R	CI-1R <sup>b</sup>	CI-2S	CI-3S	CI-4S	CI-5R <sup>c</sup>	CI-6R
MAB_3508c	Putative transcriptional regulator, <i>whiB7</i>	1	1	1	1	1	1	1	1
MAB_2297	Erythromycin ribosome methyltransferase, <i>erm4I</i>	1	1	0.98	0.98	1	0.99	0.29	1
MAB_r5052	<i>rrl</i>	1	1	0.98	1	1	1	1	1
MAB_1006c	putative MCE	1	1	1	1	1	1	0.98	0.99
MAB_2302	Probable conserved membrane protein, MmpS	1	1	1	1	1	1	0.99	1
MAB_0591	Probable rifampin ADP-ribosyl transferase	1	1	0.99	1	1	1	1	0.99
MAB_4395	Aminoglycoside 2-N-acetyltransferase, [acc(2')]	0.98	0.98	0.97	0.97	0.98	0.98	0.97	0.97
MAB_4124	Conserved hypothetical protein (GNAT acetyltransferase?), <i>eis1</i>	0.94	0.94	0.92	94	94	94	0.93	94
MAB_4532c	Hypothetical protein, <i>eis2</i>	0.99	0.99	0.99	0.99	1	0.99	0.99	0.99
MAB_0327	Possible aminoglycoside phosphotransferase	1	1	1	1	1	0.99	0.97	1
MAB_0951	Putative aminoglycoside phosphotransferase	1	1	0.96	0.99	1	0.99	0.96	0.99
MAB_3637c	Putative aminoglycoside phosphotransferase	1	1	0.99	1	1	1	0.99	1
MAB_4910c	Putative aminoglycoside phosphotransferase	1	1	0.99	0.99	1	0.99	0.98	0.99
MAB_2385	Probable streptomycin phosphotransferase	1	1	0.94	0.98	1	0.90	0.96	1
MAB_p05c	Mercury resistance operon repressor MerR	1	1	-	-	-	-	-	-
MAB_p06	Mercuric reductase MerA	1	1	-	-	-	-	-	-
MAB_p22c	Mercuric transporter MerT	1	1	-	-	-	-	-	-
MAB_p07	Mercuric transporter MerH	1	1	-	-	-	-	-	-
MAB_2875	β-lactamase precursor (Penicillinase), Bla_Mab	1	1	0.95	0.99	1	0.99	0.90	0.99
MAB_0330	β-lactamase	0.96	0.96	0.95	0.95	0.96	0.95	0.94	0.95

MAB_1312	$\beta$ -lactamase-like	1	1	0.97	1	1	0.99	0.98	0.99
MAB_1870	Putative $\beta$ -lactamase	1	1	0.97	1	1	0.99	0.98	0.99
MAB_2179	$\beta$ -lactamase /esterase	1	1	0.93	1	1	1	0.90	1
MAB_2314c	$\beta$ -lactamase -like	1	1	0.98	1	1	0.99	0.95	1
MAB_2833	Probable $\beta$ -lactamase	1	1	0.97	1	1	1	0.97	0.99
MAB_4231	$\beta$ -lactamase-like protein	1	1	0.99	1	1	1	0.98	1
MAB_4800	Putative $\beta$ -lactamase	1	0.99	0.94	0.99	0.99	0.98	0.94	0.99
MAB_4947	$\beta$ -lactamase-like protein	1	1	0.99	0.99	1	0.98	0.98	0.99
MAB_1114	Putative metallo- $\beta$ -lactamase superfamily	0.99	0.99	0.96	0.99	0.99	0.99	0.96	0.99
MAB_1386	Putative esterase/lipase/ $\beta$ -lactamase	1	1	0.98	1	0.99	1	0.99	0.99
MAB_1387	Putative esterase/lipase/ $\beta$ -lactamase	0.92	0.92	0.91	0.92	0.92	0.92	0.98	0.92
MAB_0696c	Conserved hypothetical protein ( $\beta$ -lactamase?)	1	1	0.98	0.98	1	0.98	0.99	0.98
MAB_0414	Possible hydrolase ( $\beta$ -lactamase -like)	1	1	0.99	1	1	1	1	0.99
MAB_4006	Putative lipase/esterase/ $\beta$ -lactamase	1	1	0.97	1	1	1	0.97	1
MAB_4755c	Conserved hypothetical protein ( $\beta$ -lactamase?)	1	1	0.99	1	1	1	0.99	0.99
MAB_4805	$\beta$ -lactamase-like hypothetical protein	0.99	0.99	0.98	-	0.99	0.99	-	-

<sup>a</sup>Locus\_tag in reference genome *M. abscessus* subsp. *abscessus* ATCC 19977

<sup>b</sup>Identified as *M. bolletii*

<sup>c</sup>Identified as *M. massiliense*

**Table 7.3: Genotypes in the *erm41* gene.** Single nucleotide polymorphisms (SNPs) and amino acid (AA) substitutions in the *erm41* gene were identified for each strain.

Strain	SNP	AA substitutions
<i>M. abs</i> S	-	-
<i>M. abs</i> R	-	-
CI-1R*	T156G	
	T231C	
	A238G	
	C253A	
	G256T	I80V
	T336C	L85I
	A414G	Q104H
	A312C	
	A330C	
	G249A	
CI-2S	T28C	
	T159C	W10R
	A330C	I80V
	A238G	
CI-3S	-	-
CI-4S	T159C	
	G255A	
	G279T	I80V
	A330C	
	T336C	
CI-5R*	C41A	
	A46G	
	G61-	
	C62-	P14Q
	T85G	T16A
	A104G	A56T
	G123A	
	C438A	
	A466G	
CI-6R	-	-

\*aligned against the *M. abscessus* ATCC 19977 genome, not genomes of their respective subspecies

## 7.3 Discussion

Unique genes were mainly present in clinical isolates, echoing previous findings that laboratory strains lose a high percentage of their DNA once they have been passaged and used under laboratory conditions (Koskineni *et al.*, 2012). These unique genes could have been acquired by the clinical isolates through horizontal gene transfer from other bacteria they encountered prior to being isolated. Overall, the most discrepancies between sequence identity and coverage, indicated in the tables by lower IC scores (**Table 7.1** and **7.2**), were found in CI-1R and CI-5R. Given that these two strains belong to different *M. abscessus* subspecies and that they are the most genetically distant (**Fig. 7.1**) this was to be expected. In fact, the IC number seems to be directly proportional to the genetic distance on the phylogeny tree, and CI-3S, the closest related, has the least SNPs and amino acid substitutions identified. The three rough clinical isolates are the most distant from the type strains, but the closest related to each other, which may give an indication that the mutations found within them have an effect on the colony morphology. Presumably, however, genetic changes that could lead to the change in colony morphology would also be present in the type strain, *M. abscessus* R.

### 7.3.1 Genetic differences between clinical isolates in the *gpl* locus

The GPL locus is highly conserved among the strains tested in this study, as well as between different species (Gutiérrez *et al.*, 2018). There is little variability in the genetic sequences with the exception of those in *mbtH* (*MAB\_4100c*), *mps2* (*MAB\_4098c*) and *MAB\_0936c*. Three copies of the *mbtH* gene were present in all strains, however only one was a true ortholog previously reported to be related to GPL biosynthesis (Ripoll *et al.*, 2007). This is not unexpected since MbtH-like proteins are normally found in non-ribosomal protein synthesis clusters related to various functions (Quadri *et al.*, 1998). Mps1 and Mps2 are also part of a family of non-ribosomal protein synthases, and in our strains *mps1* and *mps2* are present in all the strains but with mutations that mainly affect *mps2* in all the rough strains. Previous findings identified indels and mutations in *mps1-mps2* in 77% of rough *M. abscessus* isolates compared

to smooth and mutations in *mps2* were found in rough strains isolated from patients at later disease stages (Park *et al.*, 2015). A different study showed that large deletions of *mps1-mps2* lead to colony morphology changes in a rough variant of *M. massiliense*, and CI-5R, which is missing the *mps2* gene, also belongs to the subspecies *M. massiliense* (Kim *et al.*, 2013). Transcriptional analysis showed that by repressing transcription of *mps1*, *mps2* and *gap* in the smooth strain, there is a change to the rough morphotype (Medjahed and Reyrat, 2009; Nessar *et al.*, 2011). The mutations that affected the *mps2* gene in this study mainly resulted in truncated proteins, although the mutations were not consistent among the strains. Coupled with previous evidence from literature these mutations in the *mps2* gene suggest that rough colony morphology is closely tied to expression of *mps2*.

Out of the proteins related to GPL transport and export, MmpL family proteins (*MAB\_4116c*, *MAB\_4115c*, *MAB\_0937c*), gap-like proteins (*MAB\_4097c*, *MAB\_0934*) and PE hypothetical protein (*MAB\_0936c*), the main difference is observed in the absence of *MAB\_0936c* in lab strains, CI-2S and CI-3S. Although not experimentally proven, it is thought that mutations in *mmpl4b* are responsible for loss of GPLs due to its adjacency to other GPL biosynthesis genes and likelihood of involvement in transportation of GPLs (Park *et al.*, 2015). In our strains *mmpl4b* gene had mutations in rough clinical isolates, but they were not so consistent among the strains as to lead to the conclusion that a specific SNP or amino acid substitution leads to the change in colony morphology. Previously, colonies of *mmps4* deletion mutants were shown to be exclusively rough, while producing a small amount of a “GPL-like molecule”, however all strains sequenced in this study had a full *mmps4* gene without mutations (Park *et al.*, 2015). A previous study examined a transcriptional regulator, highly conserved amongst mycobacteria, Lsr2 (*MAB\_0545*), whose expression is upregulated in rough strains, and found that while it does bind to an AT rich region upstream of *mbtH/mps1*, it alone does not have an effect on the GPL profile (Le Moigne *et al.*, 2019). *MAB\_0545* is present in all the strains and was reported to play an essential role in *M. abscessus* and *M. tuberculosis* virulence by

regulating transcription of genes related to the PE/PPE family, biosynthesis of cell wall lipids and ESX secretion system (Le Moigne *et al.*, 2019).

Previous works aimed at identifying triggers that lead to transition between the morphotypes suggested a temperature dependant change, or genetic mutations that would suggest the transition is irreversible (Elizabeth R Rhoades *et al.*, 2009; Pawlik *et al.*, 2013). Amongst the clinical isolate and lab strains of *M. abscessus* analyzed in this study, genes in the GPL locus are uniformly present, except *mps2*, suggesting that smooth to rough transition is likely regulated on a transcriptional level. SNPs that were identified in this study could have an effect on frameshift mutations, downstream truncations of genes or functional changes, however without further analysis into gene expression and proteomics it is difficult to make concrete conclusions. A previous study had identified that a SNP in the promoter region of the GPL operon (*mbtH-mps1-mps2-gap*) resulted in reduced expression of those proteins, indicating the importance of testing gene expression and downstream effects of mutations beyond the sequence analysis (Pawlik *et al.*, 2013). Additionally, while no-specific SNPs were identified in a consistent manner across the strains that could be responsible for the differences in colony morphology, on average more SNPs were identified in the rough strains as compared to the smooth ones. It is still a topic of debate in literature, with various evidence surfacing in support of both, whether the transition between morphotypes is controlled on a genetic or translational level. GPL analysis has showed that there is a slight expression of GPLs in rough strains in biofilms but not in planktonic cells (Fig. 6.6), implying that GPLs can be synthesised in rough strains but that this is regulated in some yet unexplored way that is not related to gene mutations or deletions. Equally, the GPLs that are expressed could be somewhat altered by these mutations since biofilms of rough strains visibly differ from those formed by smooth stains.

### 7.3.2 Genes related to antibiotic resistance

In the analysis of genes that contribute to antibiotic resistance in *M. abscessus*, an interesting finding was that the pMA23 plasmid was found only in the type strains. This plasmid was

previously identified in a genomic study of the *M. abscessus* ATCC 19977 strain and has 99.9% sequence identity with pMM23 plasmid found in a clinical isolate of *Mycobacterium marinum* (strain ATCC BAA-535), but has origins in *Nocardia* or *Pseudonocardia* (Stinear *et al.*, 2008; Ripoll *et al.*, 2009). The plasmid was however, only found in this strain and not in the 40 other isolates that were analyzed (Stinear *et al.*, 2008). A protein BLAST search identified these genes in 10 other NTM sequenced strains indicating that this plasmid is not widely present throughout the genus. Mercury is a highly toxic heavy metal and it was shown that the *mer* operon was initially evolved in thermophilic bacteria and has continually evolved (Boyd and Barkay, 2012). *M. abscessus* is found in soil and water, so it could have acquired the pMA23 plasmid as an adaptation mechanism to the environment. For bacteria to confer resistance to mercury and other organomercury compounds, both MerR (*MAB\_p05c*), mercury operon regulator and MerA (*MAB\_p06c*), mercury reductase and detoxification enzyme have to be functional – since these are not present in the clinical isolate strains, it would have been interesting to test them against toxic compounds and evaluate their susceptibility.

Aminoglycoside resistance in *M. abscessus* is characterized by mutations in the 16S rRNA, the main target of this class of antibiotics that prevents protein synthesis. When challenged with amikacin, which is an aminoglycoside, CI-2S was resistant and CI-4S and CI-1R were susceptible, while the rest of the strains showed intermediate resistance (**Table 5.1**). The reported intermediate susceptibility could be because of aminoglycoside phospho- and acetyltransferases which are present in every strain and can confer low level aminoglycoside resistance. Mutations directly in the ribosome, 16S rRNA, lead to high level resistance to aminoglycosides, however, CI-2S did not show any genetic difference that can be correlated with this resistance. *eis1* (*MAB\_4124*) and *eis2* (*MAB\_4532c*) have homology to *eis* (enhanced intracellular survival) genes in *M. tuberculosis* (Rv2416c) and *Anabaena variabilis* (Ava\_4977) respectively, however their intrinsic role in aminoglycoside resistance was proven only for *eis2*, while deletion of *eis1* had no effect on antibiotic susceptibility in *M. abscessus* (Rominski,

Selchow, *et al.*, 2017; Luthra, Rominski and Sander, 2018). All the strains express both *eis1* and *eis2*. Additionally, other genes annotated to encode probable aminoglycoside acetyl- and phosphotransferases are also present in the strains, and without further study it is difficult to conclude which ones, or if any, of these are responsible for intermediate and high-level resistance to amikacin shown in MIC testing in Chapter 5.

*whiB7* is one of the most conserved genes between all the tested strains in this study, having 100% sequence identity with the reference strain (**Table 7.2**). WhiB7 is induced by sub-inhibitory concentrations of clarithromycin and acts on *erm41* and *eis2*, which could explain the high level of resistance to clarithromycin observed in MIC testing with these strains (**Table 5.1**). Interestingly, *whiB7* seems to have a species-specific pattern of gene induction which could explain the differences in susceptibility between species, but also potentially between strains (Hurst-Hess, Rudra and Ghosh, 2017). Amikacin and clarithromycin are often administered together for treatment; however it was recently discovered that sub-inhibitory concentration of clarithromycin induces transcription of *whiB7* which acts on *eis2* prompting expression of an acetyltransferase that contributes to amikacin resistance (Pryjma *et al.*, 2017). This phenomenon, at least partially, explained restricted clinical efficacy of *M. abscessus* combination therapy and illustrated another important reason for genotyping of *M. abscessus*, and in general NTM, clinical isolates during infection.

*erm41* gene is extremely important in *M. abscessus* treatment because it encodes a functional protein in two out of the three subspecies. *M. massiliense* has deletions in the gene which result in translation of a truncated version of the protein (Kim *et al.*, 2010). CI-5R is a *M. massiliense* strain with a truncated protein and high sequence identity to that in the reference genome of *M. massiliense* CCUG 48898. It is expected that this strain would be susceptible to clarithromycin, however it showed resistance. Amongst the rest of the strains tested, CI-1R, *M. bolletii*, had the most SNPs and amino acid substitutions, which could perhaps be correlated to the high level of resistance to clarithromycin this strain exhibited when compared to the other strains (**Table**

**5.1).** The protein sequence of 23S rRNA methyltransferase in other strains had high homology to the *M. abscessus* ATCC 19977 strain, which was expected given they belong to the *M. abscessus* subspecies. MIC testing for clarithromycin is read after day 3, to identify highly resistant strains, and day 14, to identify strains with inducible resistance. Strains that have inducible resistance measurable on day 14 were reported to carry the T28C *erm41* sequevar, while the highly resistant ones may have additional mutations, such as those in *rrl*, and show measurable resistance at day 3 as well (Nash *et al.*, 2009). None of the strains in this study carried mutations in the *rrl* described to lead to macrolide resistance, and only CI-2S carried the T28C mutation associated with acquired resistance to clarithromycin despite most of the strains showing resistance (**Table 5.1**).

*M. abscessus* is resistant to the majority of antibiotics from the β-lactam class except cefoxitin and imipenem (Luthra, Rominski and Sander, 2018). Cefoxitin was shown to have only moderate activity *in vitro*, and all the strains showed intermediate susceptibility to cefoxitin at 32 µg/ml and 64 µg/ml. Cefoxitin is a substrate of Bla\_Mab (*MAB\_2875*) which is found in all the strains, however this antibiotic is hydrolysed at a slow rate which is likely why the strains show a degree of susceptibility (Luthra, Rominski and Sander, 2018). The use of β-lactamase inhibitors has been shown as successful in partially restoring susceptibility to β-lactams *in vitro* and in this study using amoxicillin and clavulanate (Luthra, Rominski and Sander, 2018).

In conclusion there were no surprise findings during genomic analysis of antimicrobial resistance genes in clinical isolate strains. Similarly, to what was seen for GPL genes, the most mutations are present in CI-1R and CI-5R, which is logical given that they belong to different subspecies. MIC for all tested antibiotics were relatively high, most measuring intermediate susceptibility (**Table 5.1**). Cross-referencing this phenotype with the large number of genes that *M. abscessus* carries responsible for resistance to a variety of antimicrobials, it is evident why infections with these bacteria are difficult to treat. Additionally, while there may be genetic variations between strains, antibiotic resistance genes seem to be highly conserved.

## **8 General discussion**

## 8.1 Conclusions

*M. abscessus* is an emerging opportunistic pathogen and across the globe, it is the most commonly isolated RGM from pulmonary infections caused by NTMs (To *et al.*, 2020). Treatment options are lengthy, limited and successful in less than 50% of the cases (Kwak *et al.*, 2019). *M. abscessus* employs a variety of mechanisms which make it a successful and difficult to clear pathogen. Namely, *M. abscessus* displays phenotypic heterogeneity which plays a key role in infection and virulence. The *M. abscessus* complex comprises three subspecies with unique characteristics which demonstrate variability in antibiotic resistance that is already high due to intrinsic and adaptive mechanisms. Additionally, *M. abscessus* has been shown to form biofilms in patient lungs which is associated with an increase in antibiotic tolerance, persistence and immune evasion (Qvist *et al.*, 2015; Fennelly *et al.*, 2016). Therefore, this thesis set out to explore biofilm formation in *M. abscessus* with the aim of understanding how the biofilm is formed, its composition and the molecular changes that occur in this type of growth, and with the long-term goal of contributing to development of novel therapeutics. For a better understanding of *M. abscessus* strains that cause infections, we used pulmonary clinical isolates from a strain collection which broadened our understanding of the behaviours and genotypes of the rough and smooth colony morphotypes. The morphological heterogeneity plays an essential role in pathogenesis, biofilm formation and antibiotic tolerance and is imperative to understanding the process of infection by *M. abscessus*.

### 8.1.1 Biofilm formation in *M. abscessus*

In general, biofilms offer a protective environment to bacteria and the ECM obscures pathogen recognition by the immune system that is tuned to recognizing specific patterns on bacterial surfaces (Vasudevan, 2014). This is important for virulence and mode of infection of *M. abscessus* which presents as two distinct phenotypic morphotypes that are based on surface expression of GPLs. Biofilms formed by smooth strains *in vivo* are presumed to act as reservoirs

and to persist, before the bacterium undergoes the morphological change to the rough strain which leads to an inflammatory infection. Therefore, the initial, in depth characterization of biofilms in this study was done with the *M. abscessus* smooth type strain.

In short, the appearance and contents of the biofilm ECM were described revealing that the *M. abscessus* biofilm is a structure of organized bacilli enveloped in an ECM composed of predominantly lipids, as well as proteins, carbohydrates and eDNA, and that this is comparable to ECMs of biofilms formed by other NTMs. A recent study examined the ECMs of *M. bolletii*, *M. avium* and *M. fortuitum* surface attached biofilms formed under thiol-reductive stress (Chakraborty *et al.*, 2021). They showed that, similarly to *M. tuberculosis* biofilms, the ECM of NTM biofilms formed under these conditions are rich in carbohydrates, drug tolerant and can be disrupted using proteinase K and cellulase, but not lipase or  $\alpha$ -Amylase (Trivedi *et al.*, 2016; Chakraborty *et al.*, 2021). Although the lipid content of the *M. bolletii* biofilm was not assessed in the study, the implication of the lipase treatment is that lipids do not play an important role on the ECM. This poses interesting questions on potential differences in biofilm formation between *M. abscessus* subspecies, as well as how the environment that the biofilms are formed, and the type of biofilm formed potentially influence the composition of the ECM. In this study the unique transcriptional profile of *M. abscessus* biofilms was described as one that promotes survival, protection, and modulation of the cell envelope. Of note is the increase in expression profiles of genes related to the fatty acid biosynthesis, which specifically affects molecular changes in mycolic acids in terms of elongation of the meromycolyl chain and desaturation, that likely leads to cyclopropanation. In general, bacteria in biofilms demonstrate an increase in saturated fatty acids, and it is believed that this alteration of the membrane fluidity is a purposeful response that leads to limitation of exchanges, conservation of energy and survival – consistent with what we established through transcriptional analysis (Dubois-Brissonnet, Trotier and Briandet, 2016).

An environment of energy preservation in *M. abscessus* pellicular biofilms was illustrated through the upregulation of glyoxylate metabolism and isocitrate lyase and the downregulation of cell division and peptidoglycan biosynthesis. The increase in redox metabolism and oxidoreductases suggests an anaerobic environment in parts of the biofilm. In fact, the CF lung environment is known to have hypoxic conditions and it was shown that *in vitro* bacterial aggregation leads to a decrease in oxygen consumption leading to slower growth, low aerobic respiration and an increase in resistance to aminoglycosides (Kolpen et al., 2020). Increase in the glyoxylate metabolism was also seen in *M. abscessus* grown in artificial sputum media, meant to mimic the CF lung environment, which further underlined shared metabolic strategies among CF pathogens and among persistent mycobacteria (Miranda-CasoLuengo et al., 2016). Biofilm composition and structure are often limiting factors in research because biofilm formation varies based on environmental factors and media composition, and so global, conserved transcriptional changes should be critically reviewed if analysing large-scale data (Tolker-Nielsen, 2015).

In the transcriptomic analysis of *M. abscessus* we identified specific signatures related to biofilm formation ubiquitous amongst mycobacterial biofilms, as well as contradictory ones – that is those that differ between species. For example, genes related to oxidative phosphorylation are downregulated in *M. bovis* BCG and *M. abscessus* biofilms, but upregulated in *M. chelonae* (Zeng et al., 2019; Vega-Dominguez et al., 2020). This points to another limitation of studying transcriptomics in biofilms which was previously highlighted by several microarray studies in *P. aeruginosa* where scientists failed to detect consistent specific biofilm signatures amongst different species (Whiteley et al., 2001; Waite et al., 2005; Folsom et al., 2010). Meanwhile studies have shown that certain events are necessary for the initial formation of biofilms and therefore conserved, such as expression of adhesins or c-di-GMP, or export of eDNA and polysaccharides (Hengge, 2009). Overall, this suggests that the initial biofilm aggregation or attachment is governed by specific pathways, but subsequent steps are

largely dependent on the environmental factors and adaptive response, which points to the issue of close comparison between types of biofilms or biofilms of different species. It also implicates the necessity to study the same sample in diverse conditions in order to understand which signatures are specific to biofilm formation and which are specific to a particular condition. In light of these limitations, and in an attempt to bridge the gap between lab studies and clinical applications, we extended our study of the *M. abscessus* biofilm, initially focused on the type strain (ATCC 19977), to include six pulmonary clinical isolates.

### **8.1.2 The key role of colony morphology in *M. abscessus* pathogenicity**

An initial biological characterization of clinical isolates of *M. abscessus* was done evaluating colony morphology, growth rate, biofilm formation, intracellular survival in macrophages, lipid profile and antibiotic susceptibility. The measured parameters are relevant to generating a holistic view of the phenotype of each strain, discerning patterns between strains isolated from different infections as well as patterns between strains of different morphologies. The phenotypic changes were then evaluated with genotypic studies. The main findings indicated that heterogeneity in morphology of *M. abscessus* variants is a key driver of phenotype and virulence.

As expected, smooth clinical isolates expressed surface GPLs and presented a lipid profile that reflected that of the smooth type strain. However, they formed biofilms that were submerged and disrupted. In contrast, rough clinical isolates, despite absence of GPLs, formed pellicular biofilms with aggregated microcolonies. A portion of phagocytosed smooth bacteria was killed by macrophages at 24 h.p.i, but numbers increased by 72 h.p.i, which indicated partial clearance by macrophages, but also potential for long-term blocking of phagosomal maturation and persistence, previously shown in literature. Rough strains proliferated following phagocytosis by macrophages, consistent with previous reports of active proliferation after phagocytosis that leads to phagosomal rupture. Genetic differences between the clinical strains laid in disparities

among the subspecies - the largest deviation from the lab strains was observed in CI-1R and CI-5R, which were identified as *M. massiliense* and *M. bolletii* subspecies, respectively.

Despite previous claims that GPLs are completely absent in *M. abscessus* rough morphotype, our findings suggest that GPLs can in fact be expressed by the rough strains (Roux *et al.*, 2016; Whang *et al.*, 2017). GPLs play a central role in the ability of NTMs to form biofilms, however the GPL-expressing clinical isolates in this study showed defective or submerged pellicle formation despite GPL expression, while rough strains formed pellicles and CI-5R and CI-6R showed presence of some subclasses of GPLs - especially visible in biofilm growth (Gutiérrez *et al.*, 2018). “GPL-like molecules” have been reported in a *M. smegmatis* strain with *mmps4* deletion mutations and it is not without foundation that we could be seeing the same here (Deshayes *et al.*, 2010; Park *et al.*, 2015). A recent study investigating human co-infections with strains of two colony morphologies in *M. abscessus* also reported a GPL expressing rough strain (Gutiérrez *et al.*, 2021). This prompts further molecular studies into GPLs synthesized by each strain.

The novel comparison of biofilms formed by *M. abscessus* clinical isolates of different morphologies contributes to the knowledge of biofilms formed by rough strains, and a new school of thought that indicates that these biofilms are in fact more robust and hyper-aggregative in comparison to those made by smooth strains. While it was the prevailing view that *M. abscessus* chronic infections are caused by the smooth, biofilm forming morphotype, recent studies, including this one, have disputed that (Clary *et al.*, 2018; Gloag *et al.*, 2021). There has been a recent shift in defining biofilms as not only a surface attached structure, but as free-floating aggregates, which allows for biofilm associated infections to be included in the definition. This is additionally supported by evidence that in cystic fibrosis lung infections, *P. aeruginosa* bacterial aggregates are found dispersed within the mucus rather than adhered to the epithelium (Bjarnsholt *et al.*, 2009). It is likely that in the case of *M. abscessus*, both smooth and rough strains form biofilm-like aggregates in the lungs that contribute to chronic infection.

A study showed that regardless of morphotype the *M. abscessus* biofilms had a lower mucociliary and cough clearance index compared to the model organism for studying biofilms and infections in cystic fibrosis patients, *P. aeruginosa* (Gloag *et al.*, 2021). This indicates a probable high level of bacterial aggregation of *M. abscessus* in patients which results in poor clearance and leads to chronic infection, regardless of morphology. Indeed both phenotypes have been associated with chronic infections (Park *et al.*, 2015; Qvist *et al.*, 2015). Studies showed that on average rough strains are more commonly isolated from CF infection, in varying proportions (Jönsson *et al.*, 2007; Kim *et al.*, 2008; Rüger *et al.*, 2014).

Cell wall lipids are amongst the most extensively studied molecules in mycobacteria because they play an all-round important role in survival, adaptation, permeability, pathogenicity, immune evasion and much more, and they are significant in planktonic and biofilm cells alike. In this study we showed an accumulation of FMA in biofilms of the type strain, and a change in desaturation and an increase in length of mycolic acids. This is the hallmark demonstrated in all biofilm-forming mycobacteria. Indeed, in-depth lipid analysis of the rough type strain and clinal isolates revealed a slight increase in FMA but a definitive ubiquitous shift in desaturation of mycolic acids in biofilms, as reported in the smooth type strain, indicating a consistent phenotype in *M. abscessus*. The biofilm lifestyle has been shown to propagate an increase in membrane fatty acids in other bacteria as well, such as *P. aeruginosa*, *S. aureus*, *L. monocytogenes* and *S. Typhimurium* (Dubois-Brissonnet, Trotier and Briandet, 2016). Biofilms harbour higher proportions of saturated fatty acids compared to planktonic cells which has been linked to higher phase transition temperature, stability and density of packing and could increase membrane rigidity (Denich *et al.*, 2003). These findings point to a universal adaptation system amongst bacteria in which the concentration of lipids is increased during biofilm formation and lipid molecules undergo molecular changes that support the biofilm lifestyle.

In conclusion it is important to include various samples in a study to more accurately identify specific patterns in behaviour, phenotype, or genotype. For example, in *P. aeruginosa*, quorum

sensing genes are less expressed and antimicrobial resistance genes are more expressed in human infections than in *in vitro* studies, indicating the importance of considering clinical settings (Cornforth *et al.*, 2018). Our biological and genomic analysis of clinical isolates as compared to lab strains additionally highlighted these types of differences, further prompting questions of gene expression and behaviour in more infection-relevant settings. Therefore, it is important to expand research to different subspecies and conditions because these are living, ever changing and adapting organisms, which makes combating them in hospital and clinical environments challenging.

## 8.2 Future work

Characterization of *M. abscessus* biofilms done in this study has set the foundations for future work on understanding molecular events that lead to cellular aggregation, biofilm maturation and subsequent dissemination, as well as into novel ways of dispelling biofilm formation in the environment and in a clinical setting. In a natural progression of this work, the fluorescence microscopy and transcriptomic methods used to study biofilm formation should be adapted to further the same study in clinical isolates and understand characteristics common to biofilm formation, or more precisely cell aggregation, regardless of the type of biofilm formed. There is evidence that different species of *Pseudomonas* form distinctive types of biofilms, even when co-cultured together, and based on the evidence we saw of visual differences between biofilms formed by clinical isolates, this study could reveal important complementary differences on a transcriptomic level (Tolker-Nielsen, 2015).

Although useful for providing an overview, populations level gene expression studies are insufficient for dissecting gene expression events that lead to specific states and could lead to missing gene expression in a small number of cells, such as different subpopulations in the biofilm. A more detailed study would focus on transcriptomic studies of subpopulations within the biofilm and on metabolomic studies. The first could be achieved by using a novel method called microSPLiT, a version of single-cell RNA-seq modified for use in bacteria. In this method cellular origin of RNA is labelled through combinatorial barcoding, and it can detect subpopulations of cells as rare as 0.142% of >25,000 in *B. subtilis* (Kuchina *et al.*, 2021). However, the technique requires a permeabilization step that may be an issue due to the mycobacterial cell wall composition. Regardless, the development of this new and exciting method should be monitored because of its high sensitivity and potential for application in biofilm subpopulation studies. Additionally, by studying metabolites and alterations in metabolic pathways in biofilm populations we could create a more comprehensive insight into biofilm formation and dissociation. As an add-on, studying microRNAs from transcriptomic

analysis alongside metabolites might give insight into quorum sensing and signalling that leads to biofilm formation. In *V. cholerae* quorum sensing molecules were discovered at an intra-species, intra-genus and inter-species levels, and regulatory small RNAs were found to be instrumental in the control of biofilm formation and dispersal (Papenfort *et al.*, 2015). Quorum sensing is still largely unexplored in mycobacteria, although the role of c-di-GMP has been documented as important for regulation and further studies have been done in *M. tuberculosis* (Sharma, Petchiappan and Chatterji, 2014; Hegde, 2020).

Using random insertion transposon mutagenesis, we could identify mutants defective in biofilm formation at different stages and therefore identify genes essential to this process. Likewise, we could knock-out genes of interest previously identified through our transcriptomics screening as important and upregulated during biofilm formation and evaluate if their products would make adequate drug targets for future studies.

### **8.2.1 Components of the biofilm extracellular matrix as biomarkers for detecting bacteria during infection**

In the previously mentioned examples of biofilm-like bacterial aggregates of *M. abscessus* in patient lungs, the bacteria were stained by a peptide nucleic acid (PNA) fluorescent *in situ* hybridisation (FISH) probe for fluorescence microscopy or using acid-fast staining in histopathology samples (Qvist *et al.*, 2015; Fennelly *et al.*, 2016). In the future, the protocol for staining ECM components used in our study could potentially be applied to staining clinical samples to identify whether the infection is manifested as a biofilm. A novel study of *M. tuberculosis* pellicles identified cellulose as a major component of the ECM, and in continuation of that study cellulose was used a biomarker to detect *M. tuberculosis* in mice, non-human primates and lung tissue obtained from patients (Chakraborty *et al.*, 2021). In the same study they demonstrated *in vivo* that biofilms harbour drug tolerant bacteria and that cellulase treatment increases sensitivity to antibiotics. This has major implications on future

treatment options for diseases caused by mycobacteria, especially given the growing evidence of biofilm formations during infections.

### **8.2.2 DNase I as a treatment for biofilms**

In real world application, understanding the composition and formation of biofilms in different species is key to developing therapeutic treatments for patients with biofilm infections as well as for developing successful disinfectants and cleaning products. One of the main therapeutic approaches is targeting the ECM. A therapeutic idea shown as effective in *in vitro* experiments with *P. aeruginosa*, *V. cholerae*, *E. coli*, *Listeria monocytogenes*, among others, is to target eDNA in biofilms using DNase (Harmsen *et al.*, 2010; Tetz and Tetz, 2010; Seper *et al.*, 2011; Lauková *et al.*, 2020). Recombinant human DNase has been successfully used in CF patients to reduce mucus viscosity in lungs for the last 20 years, and additional DNase treatment could provide further benefits by acting on bacterial biofilms of pathogens that often plague CF patients (Lauková *et al.*, 2020). However, a study of 20 *P. aeruginosa* strains showed that eDNA was a major component of 18 biofilms, and DNase was able to disrupt only early biofilms in some studies and mature biofilms in others (Murakawa, 1973; Nemoto *et al.*, 2003). This indicates that DNase treatment may not always be suitable or have the same efficacy. Additionally, while eDNA is a component of all biofilms, it is not always the major one and therefore the treatment could be adapted using different enzymes. Previous *in vitro* studies showed that cellulase and protease treatment were able to inhibit biofilm formation in *M. tuberculosis*, while DNase treatment in *M. avium* biofilms lead to a reduction in biomass and co-culture of DNase with antibiotics significantly increased susceptibility to antibiotics (Rose *et al.*, 2015; Trivedi *et al.*, 2016). Combined DNase and proteinase treatment was used successfully in compromising the composition and structural integrity of multispecies fungal and bacterial oral biofilms, and trypsin, β-glucosidase and DNase I have been used *in vitro* to degrade dual-species biofilms of *P. aeruginosa* and *S. aureus*, which commonly co-infect wounds (Karygianni, Attin and Thurnheer, 2020; Pirlar *et al.*, 2020). Enzymatic treatment has

been shown as successful in dispelling single and multispecies biofilms, enhancing antibiotic susceptibility as well as enhancing efficiency of cleaners in removing biofilms, however despite being well researched it is not yet used widely for patient treatment.

### **8.2.3 Outlooks on vaccine development against biofilms**

Another interesting treatment approach is vaccine development that specifically targets and prevents biofilm formation. At present this is a relatively unexplored area, particularly in mycobacteria, however there are two notable examples. Vimco© is a vaccine developed and marketed by HIPRA which contains a biofilm-forming inactivated strain of *S. aureus* used for active immunization to reduce and prevent mastitis development in sheep and goats (Sanz, Calvo and Medrano, 2017; Rodríguez Fernández *et al.*, 2018). A vaccine that produces DNABII targeting antibodies is effective *in vitro* in sequestering biofilms formation and was shown to have 85% efficacy in chinchillas in delaying onset of otitis media (D'Andrea and Lau, 2020). This vaccine is based on targeting the DNABII, a DNA binding protein that interacts with eDNA and plays a role in maintenance of the ECM structure (D'Andrea and Lau, 2020).

### **8.2.4 Biofilm infection models**

In future developments of novel approaches, the most important factor to consider is finding successful models for testing. Throughout this study we showed discrepancies between clinical and lab strains, as well as among the *M. abscessus* complex. Ensuing steps should be focused on further immunological characterization of clinical isolates and lab strains using infection studies with primary cells, and monitoring host cell survival and response. Transcriptomic analysis of both bacteria and the host cells would offer broad insight into the host-pathogen interaction, immune activation and response as well as expression of bacterial virulence genes. Long term, a biofilm infection model should be established. This model would allow for a more clinically relevant study of biofilms and provide insight into interaction between biofilms and mammalian cells in terms of phagocytosis, bacterial and macrophage survival. Co-culturing of mammalian cells and bacteria would provide a simple and effective model to trial success and

safety of enzyme and antibiotics treatment. An initial model could use biofilm-like cell aggregates, rather than full surface attached or pellicular biofilms, since evidence has shown that this may be the most clinically relevant model. A similar model has already been devised using 3D lung epithelial cells (A549 cell line), *P. aeruginosa* and *M. abscessus*. The study showed that antibiotics were more effective in inhibition of single- and dual-species biofilms in the cell model compared to plastic, and that *M. abscessus* biofilm formation was not induced by antibiotics in the 3D cell model (Rodríguez-Sevilla *et al.*, 2018).

### **8.2.5 Dual species biofilms and therapeutic approaches**

Recent evidence emerged that showed that *M. abscessus* had competitive advantage in dual species biofilms, indicating that antibiotic therapy targeting *P. aeruginosa* at early stages of biofilm formation may favour *M. abscessus* colonization (Rodríguez-Sevilla *et al.*, 2018, 2019).

*M. abscessus* also degrades quinolone signals of *P. aeruginosa* thus gaining competitive advantage (Birmes *et al.*, 2017). Other studies of dual-species biofilms have emerged which aim to dissect the intricate interactions between different biofilm forming bacterial and fungal species. Single-species biofilms are already complicated communities that vary from species to species and integration of other bacteria or fungi as well as host cells into consideration makes the issue extremely complex and multifaceted. However, it is important to consider and to further develop multi-species biofilm models, so that treatment options can evolve with the newfound knowledge of the interaction between different species and situations where treatment of one bacterium offers competitive advantage to another, worsening clinical outcome for the patient, can be avoided.

## **9 Materials and methods**

## **9.1 Culture media**

### **9.1.1 Middlebrook 7H9 broth**

2.35 g of powder was dissolved in 450 ml miliQ water. Solution was autoclaved at 121°C for 25 min and then supplemented with 10% OADC (Oleic acid, Albumin, Dextrose and Catalase) and 0.2% sterile glycerol.

### **9.1.2 Sauton's minimal media**

Sauton's minimal media was prepared from the chemicals listed in **Table 9.1** and adjusted to pH 7.2 using HCl or KOH prior to autoclaving at 121°C for 25 min.

### **9.1.3 Middlebrook 7H11 agar**

7H11 (Middlebrook) agar was made by dissolving 10.25 g of powder in 450 ml miliQ water. Solution was sterilized by autoclaving at 121°C for 25 min. After autoclaving, 20% OADC enrichment and 0.5% glycerol was added. The agar was then distributed aseptically at 20 ml per 10 cm Petri dish.

### **9.1.4 cDMEM**

Gibco Dulbecco's Modified Eagle Media GlutaMAX<sup>TM</sup>-I (ThermoFisher Scientific), containing 1% Hepes (1M), 1% L-glutamine (200 mM) and 1% Sodium Pyruvate (100 mM), was supplemented with 10% fetal bovine serum (FBS, heat inactivated at 56°C for 30 min, from Sigma-Aldrich)) and 1% Penicillin/Streptomycin (Sigma-Aldrich). Media was stored at 4°C and heated to 37°C prior to use.

## **9.2 Bacterial culture and transformation**

### **9.2.1 Mycobacterial strains**

The list of all mycobacterial strains, their origins and nomenclature used for experiments in this dissertation can be found in **Table 9.2**.

## **9.2.2 Growth of planktonic cultures**

Planktonic cultures were grown shaking at 180 rpm, at 37°C for 24 h, unless stated otherwise.

Where necessary, planktonic cultures were supplemented with Tyloxapol (Sigma Aldrich) to a final concentration of 0.05%.

## **9.2.3 Growth of biofilm cultures**

Bacterial cultures grown on 7H11 agar plates were resuspended in sterile PBS and diluted to OD<sub>600</sub> 0.05 in Sauton's media. This inoculum was aliquoted in a 24-well plate at 1.5 ml/well and grown stationary at 37°C for six days, until pellicles have formed but before maturation and sinking.

**Table 9.1: Sauton's minimal media compositions** (Cortes, Nessar and Singh, 2010)

<b>Chemical</b>	<b>Amount per 1L of ddH<sub>2</sub>O</b>
L-Asparagine	4 g
Potassium citrate	3.18 g
1% ZnSO <sub>4</sub> in miliQ water	100 µl
K <sub>2</sub> HPO <sub>4</sub>	0.5 g
MgSO <sub>4</sub>	0.5 g
Ammonium ferric citrate	0.05 g
Glycerol	60 ml
50% glucose*	10 ml

\*added after autoclaving

**Table 9.2: Complete list of strains used in this study**

<b>Dissertation nomenclature</b>	<b>Strain name</b>	<b>Source</b>
<i>M. abscessus</i> or <i>M. abscessus</i> S when compared to other strains	<i>Mycobacterium abscessus</i> ATCC 19977	ATCC
<i>M. abscessus</i> eGFP	<i>Mycobacterium abscessus</i> pMV306_eGFP_zeo	ATCC 19977 strain transformed with pMV306_eGFP_zeo plasmid strain exhibiting rough colony morphology, a gift from Prof Barer, University of Leicester
<i>M. abscessus</i> R	<i>Mycobacterium abscessus</i>	Scottish Mycobacteria Reference
CI-1R	MR396779D	Laboratory at the Royal Infirmary of Edinburgh
CI-2S	MM010643H	Scottish Mycobacteria Reference
CI-3S	MR412105D	Laboratory at the Royal Infirmary of Edinburgh
CI-4S	MR362894N	Scottish Mycobacteria Reference
CI-5R	MR146069R	Laboratory at the Royal Infirmary of Edinburgh
CI-6R	MM010767G	Scottish Mycobacteria Reference

## **9.2.4 Transformation of *M. abscessus***

### *9.2.4.1 Preparation of electrocompetent cells*

To make electrocompetent cells *M. abscessus* was grown in cultures of 100 ml in 7H9. Once the cells reached mid-log to stationary phase ( $OD_{600}$  0.8), they were chilled on ice and spun down at 3900 rpm, 10 min at 4°C. The pellet was kept on ice and washed 3x with chilled 10% glycerol. Cells were resuspended in a final volume of 10 ml 10% glycerol and 200  $\mu$ l was aliquoted in 1.5 ml Eppendorf tubes. If cells were not used for electroporation 1h after making, they were stored at -80°C.

### *9.2.4.2 Electroporation*

Electrocompetent cells were transformed with pMV306\_eGFP plasmid containing a zeocin resistance cassette. 5  $\mu$ l (0.5-1 $\mu$ g) of pMV306\_eGFP was added to 200  $\mu$ l of electrocompetent *M. abscessus* and left on ice for 5 min. The suspension was added to a chilled cuvette with a 1 mm gap and transformed (2.5 kV, 25 mF, 1000 ohms). Samples were recovered in 1 ml of 7H9 for 4 h at 37°C and shaking at 180 rpm. They were then centrifuged and 700  $\mu$ l of the supernatant was discarded. The remaining 500  $\mu$ l of the supernatant was used to resuspend the pellet and 50  $\mu$ l, 100  $\mu$ l and 250  $\mu$ l were plated on 7H11 agar supplemented with 50  $\mu$ g/ml zeocin (Invitrogen) for selection. After 5 days, 3 visible colonies from each plate were grown in 7H9 broth with 50  $\mu$ g/ml zeocin. Once they reached an  $OD_{600}$  0.8, they were mixed 1:1 with 50% glycerol to a total volume of 1 ml and frozen at -80°C in a cryovial.

## 9.3 Microscopy methods

### 9.3.1 Scanning electron microscopy

*M. abscessus* pellicles were grown in Sauton's media to maturation as described in 9.2.3. Using 70% ethanol sterilized microscopy cover slips and tweezers, the biofilms were collected from the wells and transferred to a new 24-well plate. Samples were fixed overnight at 4°C with 2% glutaraldehyde freshly prepared in phosphate buffer.

The following steps were then performed by Paul Stanley at the School of Metallurgy of the University of Birmingham. Samples were prepared using two methods: airdrying or gradient alcohol dehydration. Airdrying: samples were left to air dry on an absorbent tissue. Gradient dehydration: samples were dehydrated through a gradient of ethanol solutions (25%, 50%, 75% and 100%) for 15 mins at room temperature and then air dried. All samples were mounted on SEM stubs, gold coated and examined in Philips XL-30 (LaB6) with Link Isis EDS.

### 9.3.2 Confocal laser scanning microscopy

#### 9.3.2.1 Sample preparation

*M. abscessus* S or *M. abscessus* eGFP were used for all microscopy experiments and biofilms were grown as described in 9.2.3. The biofilm was scooped onto a microscopy glass cover slip ( $\varnothing=16$  mm) and placed in an empty 24-well plate, washed 2x with PBS and fixed with 4% paraformaldehyde for 30 min. After a wash with PBS, samples were stained with dyes listed in

**Table 9.3.** All dyes were freshly prepared from the original stock on the day of staining. After staining, samples were once again rinsed twice with PBS and left to air dry. Dry cover slips were mounted on glass slides using ProLong<sup>TM</sup> Diamond Antifade Mountant for 30 min. Coverslips were secured with neutral nail polish and imaged within 24h of staining.

#### 9.3.2.2 CLSM image acquisition

Samples were visualized at the Birmingham Advanced Light Microscopy Facility on TIRF Nikon A1R Confocal Microscope. All samples were imaged at 100x oil magnification with

pinhole size of 1 Airy units. Scan size was 1024 and scanning speed 1/8 with an average of 4.

Laser settings used for each fluorophore are outline in **Table 9.4**.

### 9.3.2.3 *Analysis of image data*

For co-localization analysis and calculation of biovolume, five images selected at random were taken from five distinct biological samples. The data was then analyzed using software Icy, which was programmed using the Protocols plug-in to create automated pipelines for each of the analysis (De Chaumont *et al.*, 2012). Images were first denoised using a Gaussian filter and then the threshold was calculated using the Li method through the Thresholder plug-in. Images were binarized to create a region of interest (ROI) from which a signal was extracted for colocalization analysis using the Co-localization Studio plug-in. The outputs were Pearson's and Mander's coefficient. The ROI Statistics plug-in was additionally used to determine the biovolume.

**Table 9.3: List of dyes used for biofilm matrix staining**

Dye	Target	[Stock solution]	[Working solution] (dilutant)	Incubation time
Propidium iodide	Nucleic acids (extracellular)	1 mM	15 µM (water)	30 min
Nile Red	Lipids	30 mM	1 µM (water)	30 min
Concanavalin A	α-mannose and α-glucose in the pyranose configuration.	100 mg/mL	100 µg/mL (0.1 M NaHCO <sub>3</sub> )	45 min
AlexaFlour647				
FilmTracer™				
SYPRO™ Ruby				
Biofilm Matrix Stain (ThermoFisher)	Proteins	-	As is	45 min

**Table 9.4: Parameters for image acquisition**

Fluorophore	Laser wavelength (nm)	Emission (nm)
eGFP	488	494-524
Nile Red	514.5	602-644
Propidium iodide	561.4	570-620
SyproRuby	457.9	608-638
Alexa	639	663-738

## **9.4 Transcriptomic analysis**

### **9.4.1 Bacterial growth conditions for RNA extraction**

Planktonic and pellicle cultures of *M. abscessus* were set up in Sauton's media at a starting OD<sub>600</sub> 0.05. Samples were harvested at an early and late time point. Planktonic cultures were harvested at exponential phase, OD<sub>600</sub> 1 (planktonic t1), and early stationary phase OD<sub>600</sub> 3 (planktonic t2). Early pellicles were harvested after 5 days (biofilm t1) and late after 7 days when the pellicle was fully mature (biofilm t2). Five biological replicates were used.

### **9.4.2 RNA extraction**

During harvesting, cells were kept on ice and spun at 4000 rpm at 4°C. Pellets were washed 1x with cold PBS and frozen directly at -80°C. 600 µl of freshly prepared lysozyme (5 mg/mL in TE pH8.0) was added to ~200 µl of pellet to digest the bacterial cell wall. Mixture was transferred to a bead beating tube and incubated at 37°C for 30 min. Subsequently 1/10<sup>th</sup> of 10% SDS, 3M NaCO<sub>3</sub> (pH 5.2) and 720 µl Acid Phenol (pH 4.2) were sequentially added with 2 min bead beating steps in-between. The samples were inverted for 1 min at the end of the process. Samples were incubated at 65°C for 5 min and mixed by inverting every 30 sec. Following a 5 min centrifugation at 14000 rpm, aqueous phase was removed to a fresh tube, topped with 600 µl of acid Phenol (pH 4.2) and mixed by inverting. The centrifugation step was repeated, and the aqueous phase topped with 500 µl of chloroform:isoamyl alcohol. The same centrifugation step was repeated and 1/10th volume of NaCO<sub>3</sub>, 3 volumes of 100% ethanol and 1 µl of glycogen was added, mixed well and left to precipitate overnight at -20°C. The precipitate was washed once with 70% ethanol, air dried and resuspended in 30 µl of RNase-free H<sub>2</sub>O. Concentration of RNA was checked on Thermo Scientific *NanoDrop* and the quality with Agilent 2100 BioAnalyzer System using the appropriate cassette (Agilent RNA 6000 Nano Kit).

### **9.4.3 cDNA library preparation**

10 µg of isolated RNA was treated with DNase for 30 min at 37°C and ethanol precipitated overnight at -20°C. Precipitate was resuspended in 30 µl of water, and the concentrate and quality checked as before. For removal of ribosomal RNA the Ribo-Zero rRNA removal kit (Illumina) was used without deviations from the manufacturer's instructions. The quality of RNA was checked on a BioAnalyzer Nano chip (Agilent). TruSeq Stranded mRNA kit (Illumina) was used for subsequent steps of cDNA strand synthesis, adenylation of 3' ends, ligation and PCR amplification. Final dsDNA product was measured on Qubit and based on this concentration samples are prepared for sequencing.

### **9.4.4 RNA-seq analysis and differentially expressed genes**

RNA sequencing was performed in the Institute for Systems Biology (ISB) in Seattle, USA. The following is a summary of the work they did. Samples were pooled and sequenced using an Illumina NextSeq Instrument. Paired-end 75 bp reads were checked for technical artifacts using Illumina default quality filtering steps. Raw FASTQ read data were processed using the R package DuffyNGS as described previously (Vignali et al., 2011). Briefly, raw reads were passed through an alignment pipeline that first filtered out unwanted rRNA transcripts and then the main genomic alignment stage against the genome. Reads were aligned to *M. abscessus* (ASM6918) with Bowtie2 (Langmead and Salzberg, 2012), using the command line option “very-sensitive.” BAM files from the genomic alignment were combined into read depth wiggle tracks that recorded both uniquely mapped and multiply mapped reads to each of the forward and reverse strands of the genome(s) at single-nucleotide resolution. Gene transcript abundance was then measured by summing total reads landing inside annotated gene boundaries, expressed as both RPKM and raw read counts. RNA-seq data (raw fastq files and read counts) have been deposited in the GEO repository under accession number GSE165352.

A panel of 5 DE tools was used to identify gene expression changes between 5-day old biofilms (biofilm t1) samples and planktonic samples (24 h, t1) or 7-day old biofilms (biofilm t2)

samples and planktonic samples (24 h, t1). The tools included (i) RoundRobin (in-house); (ii) RankProduct (Breitling et al., 2004); (iii) significance analysis of microarrays (SAM) (Tusher et al., 2001); (iv) EdgeR (Robinson and Smyth, 2008); and (v) DESeq2 (Love et al., 2014). Each DE tool was called with appropriate default parameters and operated on the same set of transcription results, using RPKM abundance units for RoundRobin, RankProduct, and SAM and raw read count abundance units for DESeq2 and EdgeR. All 5 DE results were then synthesized, by combining gene DE rank positions across all 5 DE tools. Specifically, a gene's rank position in all 5 results was averaged, using a generalized mean to the 1/2 power, to yield the gene's final net rank position. Each DE tool's explicit measurements of differential expression (fold change) and significance (P-value) were similarly combined via appropriate averaging (arithmetic and geometric mean, respectively). Genes with averaged absolute log2 fold change bigger than two and multiple hypothesis adjusted P-value < 0.01 were considered differentially expressed.

#### **9.4.5 Metabolic pathway enrichment analysis**

We mapped the significantly differentially expressed genes at biofilm t1 and t2 against the most recent genome-scale metabolic network construction of *M. tuberculosis* H37Rv iEK1011 (Kavvas et al., 2018) by identifying orthologs using OrthoVenn2 (Ling Xu et al., 2019 NAR). We used the subsystem definitions outlined in iEK1011 to explore pathway usage at the network level. We identified metabolic pathways that were significantly enriched in the *M. abscessus* biofilm stages (Benjamini Hochberg corrected hypergeometric P-value <= 0.05). For these pathways, we calculated the average fold-change of all genes. Additionally, we performed functional enrichment analysis of *M. abscessus* DEG sets with DAVID (Huang et al., 2008 Nat. Protoc.). Only functional terms with adjusted P-value < 0.05 were considered as overrepresented.

## **9.5 Lipid analysis**

### **9.5.1 Radioactive labelling of *M. abscessus* cultures**

Planktonic cultures and biofilm cultures were grown, from the same inoculum, as described in 9.2.2 and 9.2.3. Planktonic cultures were labelled with  $^{14}\text{C}$  acetic acid (1  $\mu\text{Ci}/\mu\text{l}$  PekinElmer) after 24 h and collected after another 24 h of growth. Biofilms were labelled after 5 days and harvested after another 2 days of growth. Cultures were harvested by centrifugation (4000 rpm, 10 min) in 10 ml glass tubes sealed with polytetrafluoroethane (Teflon®)-lined screw cap. They were then washed with PBS and dried at 55°C under air flow.

### **9.5.2 Extraction of polar and apolar lipids**

The outside apolar lipid fraction was extracted by resuspending the dried cell pellet in 2 ml of petroleum ether 60–80°C (PE) and mixing it on a tube rotor for 1 h. Tubes were then centrifuged (4000 rpm, 10 min) and the supernatant saved. This was repeated once more and the tube containing the PE extract was dried on the heating block at 55°C under air flow.

The cell pellet was further treated with 2 ml 0.3% NaCl:methanol (10:1) and 2 ml PE, then mixed on the tube rotor for 15 min and centrifuged. The upper phase was transferred to a new tube, and 2 ml of PE added to the pellet containing tube, and the same extraction was repeated. The resulting fraction was the inside apolar lipid fraction.

To extract polar lipids, 2.3 ml chloroform:methanol:0.3% NaCl (9:10:3) was added to the dry pellet, mixed for 1 h and centrifuged for 15 min. The supernatant was saved in a new tube and 750  $\mu\text{l}$  chloroform:methanol:0.3% NaCl (5:10:4) was added to the pellet, mixed for 30 min and centrifuged for 5 min. Supernatants were pooled in the new tube and the same extraction repeated. Subsequently, 1.3 ml chloroform and 0.3% NaCl each was added to the pooled extract, mixed for 5 min and then centrifuged for 5 min. The lower phase was transferred to a new tube and dried at 55°C under air flow.

### **9.5.3 Extraction and analysis of fatty acid and mycolic acid methyl esters**

Dry pellets of extracted lipids as well as the delipidated cell pellet were incubated in 2 ml of 5% tetrabutylammonium hydroxide (TBAH) overnight at 95°C. Then 4 ml dichloromethane, 500 µl iodomethane, and 2 ml H<sub>2</sub>O were added, and the solution was mixed for 30 mins and centrifuged (4000 rpm, 5 min). Lower phase was transferred to a new tube and washed 3x with water, while the upper aqueous phase was discarded each time. Finally, the lower phase was dried and resuspended in 3 ml diethyl ether. Tubes were sonicated for 5 min and centrifuged. The supernatant containing fatty acid and mycolic acid methyl esters was transferred to a new tube and dried.

### **9.5.4 Deacetylation of glycopeptidolipids**

Fraction of polar lipids was evaporated from a glass tube and the sample was sonicated for 30 min in 0.2N NaOH/CH<sub>3</sub>OH and 500 µl chloroform:methanol (2:1). Sample was then incubated at 37°C for 3 h and neutralized with 83 µl 6N HCl. Sample was centrifuged (10 min, 3900 rpm) following the addition of 6 ml chloroform and 1 ml H<sub>2</sub>O. Organic phase was collected in a new tube and evaporated. The dry pellet was resuspended in 3 ml acetone and sonicated for 30 min. Supernatant was collected in a new tube after centrifugation for 15 min at 3900 rpm. Thin layer chromatography was used to resolve deacetylated GPLs on a silica plate in chloroform:methanol (9:1) in one dimension (1D).

### **9.5.5 Quantification of radioactivity**

To determine radioactive counts the sample was resuspended in 200 µl of 2:1 chloroform:methanol. 5 µl of each sample was taken into a scintillation vial, dried and then resuspended in 10 ml of scintillation liquid (Ecoscint A, National Diagnosis). A pre-set protocol for <sup>14</sup>C-labelled samples in the TRI-CARB 2700TR Liquid Scintillation Analyzer was used to measure counts per minute (CPM) for each sample. Drops per minute (DPM) were calculated

using the following equation, where 0.95 represents the decimal efficiency of the Analyzer for  $^{14}\text{C}$  samples: DPM = CPM/0.95.

### **9.5.6 Thin layer chromatography (TLC)**

Radioactive counts of  $^{14}\text{C}$  labelled samples were adjusted so that 25,000 counts are loaded on each silica TLC plate F254 (Merck). In case of two-dimensional (2D) TLC, square plates were used in dimensions of 6.7x6.7 cm. Samples were run in solvent systems outlined in **Table 9.5**. After running, the plates were allowed to air dry and were exposed to Carestream BIOMAX MR film for 72 h.

Subclasses of FAMEs and MAMEs were separated using 2D argentation TLC as described by Singh et al. 2016. 75% of the plate was dipped in 10% aqueous solution of  $\text{AgNO}_3$  and plates were dried at 90°C for 15 mins prior to loading with the sample.

In case of non-radioactively labelled lipids, dry weight of cell pellets was used as measure to equalize loading 100  $\mu\text{g}$  of lipid on each TLC plate. After being run in the desired solvent system, the plates were air dried. Lipids and carbohydrates were visualized by dipping in 5% ethanolic molybdophosphoric acid (MPA) and 1% ethanolic 1-Naphthol, respectively, and then dried at 100°C using a heat gun.

### **9.5.7 Isolation of fatty acid and mycolic acid methyl esters using liquid chromatography**

Liquid chromatography was used to separate and isolate each lipid molecule from the lipid fraction that contained fatty acid and mycolic acid methyl esters. For this experiment cultures were scaled up to 3 l for planktonic and 500 ml for biofilms, and  $^{14}\text{C}$  labeling was not used. After lipid isolation an initial TLC that was run for confirmation and a silica column was used to separate the lipids into fractions that could be used for mass spectrometry.

A silica column was packed and soaked in toluene. The sample was resuspended in a minimal amount of toluene and loaded on the column. A solvent gradient of neat toluene and then toluene:ethyl acetate (99:1, 98:2, 97:3, 96:4) was then sequentially applied to the column and fractions collected in glass tubes. To visualize which lipid species were isolated in which collected fraction, 1D TLC plates of the fractions were run in toluene:ethyl acetate (15:1) and stained with 5% molybdophosphoric acid (MPA). Based on these TLCs, fractions that contained only lipids of interest were dried, pooled and sent for analysis with mass spectrometry.

### **9.5.8 Mass spectrometry of fatty acid and mycolic acid methyl esters**

The chosen MAMEs samples were analysed by Chi Tsang in the Centre for Chemical and Materials Analysis in the School of Chemistry, University of Birmingham using Voyager DE-STR MALDI-TOF instrument.

**Table 9.5: Solvent systems for separation of lipid species using thin layer chromatography**

System	Direction	Solvents	Proportions
<b>A</b>	1 (x3)	Petroleum ether 60-80/ethyl acetate	98:2
	2	Petroleum ether (60-80)/acetone	98:2
<b>B</b>	1 (x3)	Petroleum ether (60-80)/acetone	92:8
	2	Toulene/acetone	95:4
<b>C</b>	1	Chloroform/methanol	96:4
	2	Toulene/acetone	80:20
<b>D</b>	1	Chloroform/ methanol/water	100:14:0.8
	2	Chloroform/acetone/methanol/water	50:60:2.5:3
<b>E*</b>	1	Chloroform/methanol/water	60:30:6
	2	Chloroform/acetic acid (glacial)/methanol/water	40:25:3:6
<b>F</b>	1	Hexane/ethyl acetate	19:1
	2	Petroleum ether 60-80/diethyl ether	17:3
<b>G</b>	1	Chloroform/methanol	90:10

\*a day was left in between running directions 1 and 2 for the water to completely evaporate

## **9.6 Analysis of extracellular carbohydrates in biofilms**

### **9.6.1 Extraction of extracellular carbohydrates**

Planktonic and biofilm bacterial pellets, from three different experiments, were disrupted mechanically using 4 mm glass beads (10 g for 2 g pellet) by gentle shaking for 2 min. Samples were then resuspended in 50 ml miliQ water and centrifuged at 3000 rpm for 15 min at 4°C. The supernatant was recovered and passed through a 0.2 µm pore filter. The sample was then concentrated to a 1/10<sup>th</sup> of its volume using lyophilization or a rota-evaporator, depending on availability.

Chloroform and methanol were added to the concentrated sample to obtain a final ratio of 1:2:0.8 chloroform:methanol:water. The solution was mixed on a rotor for 1h and centrifuged (3000 rpm, 10 min). The aqueous phase was collected, and the interface transferred to a separate tube where it was re-extracted three times. Extracts from the interface were pooled with the aqueous phase and dried. Sample was resuspended in 2 ml water and digested with Proteinase K (Promega) for 12 h at 50°C. Following this, the sample was dialyzed through a 3kDa membrane for 48 h, against miliQ water and 100 µl of the dialyzed sample was used for derivatization to alditol acetates.

### **9.6.2 Synthesis of alditol acetates**

Several standards were prepared at the beginning of the protocol and treated the same as the sample of interest throughout the derivatization. Standards of the following molecules were prepared at a concentration of 10 mg/ml: arabinose, fucose, galactose, mannose, myo-inositol, rhamnose, ribose and xylose. A standards solution was prepared in a glass tube using 10 µl of each standard, and 100 µl of dialyzed materials (**section 9.5.1**) were used as samples of interest. 10 µl (1 µg) of the internal standard was added to all the samples (including the standards) and the samples were then dried under air flow. After the addition of 250 µl of 2M trifluoracetic

acid (TFA), samples were incubated at 120°C for 2 h and then dried. Then the samples were resuspended in 100 µl methanol and dried, twice.

Meanwhile, a reducing agent was prepared by mixing sodiumborodeuteride (1mg/ml) in a solution of 1M aqueous ammonium hydroxide:95% ethanol (1:1). 200 µl of the reducing agent was added to the dried samples and the reaction was left to run overnight at room temperature. The reaction was stopped with the addition of 50 µl of glacial acetic acid, and the sample was then dried. Next, 100 µl of 10% glacial acetic acid in methanol was added to the sample and evaporated under a stream of air. This was repeated 3 more times and finally, 100 µl of methanol was added to each tube and evaporated.

For the acetylation, 100 µl of acetic anhydride was added to each tube and incubated at 120°C for 2 h. After cooling down the samples were dried and 2 ml of chloroform and 1 ml of miliQ water was added to each tube. The solution was vortexed thoroughly and mixed on a rotor for 15 min, and then centrifuged at 3000 rpm for 5 min. The upper aqueous phase was discarded and 1 ml of miliQ water was again added. The samples were mixed and centrifuged as before and the resulting organic phase was collected and dried. These samples were used for gas chromatography.

### **9.6.3 Gas chromatography of alditol acetates**

The synthesized alditol acetate samples were analysed in the Centre for Chemical and Materials Analysis in the School of Chemistry, University of Birmingham by gas chromatography.

## **9.7 Basic characterization of *M. abscessus* clinical isolates**

### **9.7.1 Growth curve**

Planktonic cultures were inoculated from glycerol stocks of each strain and grown for 24 h. When in exponential phase, they were diluted to OD<sub>600</sub> 0.05 in appropriate media to start the growth curve measurements. For the growth curve measured using CFU counts - at 8, 24, 32 and 48 h 100 µl of each culture was taken, serially diluted in PBS and 10 µl of each dilution was plated on 7H11 to be enumerated after 3 days of incubation at 37°C. For the growth curves measured using OD readings, cultures were diluted into 96 well plates which were incubated at 30°C or 37°C degrees, and OD was measured every 4 h (when possible) using a Promega Microplate Reader.

### **9.7.2 Determination of antibiotic minimum inhibitory concentrations**

Liquid minimum inhibitory concentrations (MIC) assays were carried out according to the Broth microdilution protocol (Wiegand, Hilpert and Hancock, 2008; Jorgensen *et al.*, 2009). Amikacin, cefoxitin, clarithromycin, amoxicillin and augmentin (amoxicillin:potassium clavulanate 7:1 mix) were serially diluted in 7H9 (**Table 9.6**). Mid-log shaking cultures were adjusted to a final concentration of OD<sub>600</sub> 0.05. Cells and media incubated without antibiotic were used as a positive control, and cells incubated with high concentration of amikacin (1 mg/ml) were used as a negative control. Care was taken that the concentration of DMSO in a well did not exceed 2%, and DMSO was additionally added to controls where necessary. The assay was incubated statically for 3 days at 37 °C, and 14 days for clarithromycin. The MIC was determined as the lowest antibiotic concentration where visible bacterial growth could not be detected according to the published guidelines (Woods *et al.*, 2011). Assays were done in triplicate.

### **9.7.3 Whole genome sequencing**

All strains were streaked out on 7H11 plates and incubated until a lawn formed. The lawn was scraped into tubes provided and genome sequencing was performed by MicrobesNG using Illumina Sequencing, which is supported by the BBSRC (grant number BB/L024209/1).

#### *9.7.3.1 Genome annotation*

Genome assemblies were annotated using prokka and were compared using roary. The default criteria included a minimum of 95% sequence identity to define genes to the core genome.

#### *9.7.3.2 Identifying strain subspecies and relatedness*

The core genome alignment was used for construction of the phylogenetic tree (Maximum-Likelihood) using IQ-Tree (10000 ultrafast bootstrap and 1000 SH-LRT branch tests), after stripping the sites with gaps. Subspecies of all strains were identified using pairwise average nucleotide identities (ANI), average amino acid identities (AAI) and percentage of conserved proteins (POCP) within the dataset against *M. abscessus* subsp. *abscessus* ATCC 19977 (GenBank ID: CU458896.1), *M. abscessus* subsp. *bolletii* CCUG 5018 (GenBank ID: AP018436.1) and *M. abscessus* subsp. *massiliense* CCUG 48898 (GenBank ID: AP014547.1) and the plasmid in *M. abscessus* subsp. *abscessus* pMAB23 (GenBank ID: CU458745.1).

### **9.7.4 Crystal violet staining of biofilms**

Biofilms from all strains were grown in 7H9 and Sauton's media for 6 days, as described in Section 9.2.3. Residual media was removed by pipetting from under the biofilm prior to air drying. 100 µl of 0.5% of crystal violet was then added to each well and incubated at room temperature for 10 min. The dye was washed using PBS until all residual stain was gone, and samples were again air dried. 200 µl of 95% ethanol was added to each well to extract the stain and incubated at room temperature for 10 min, after which it was transferred to a clear 96 well plate and absorbance was measured at 600 nm ( $A_{600}$ ) using a spectrophotometer.

**Table 9.6: Concentrations (µg/ml) and dilutants of antibiotics used for determination of minimum inhibitory concentration**

	Antibiotic	Dilutant	Highest concentration	Lowest concentration	
AMK	Amikacin	Water	256	1	
FOX	Cefoxitin	DMSO	512	2	
CLR	Clarithromycin	DMSO	64	0.5	
AMOX	Amoxicillin	Water	128	0.5	
AUG	Augmentin (7:1)	AMOX Potassium clavulanate	Water	128 18	0.5 0.07

**Table 9.7: Breakpoints used for interpretation of antibacterial susceptibility testing based on (Woods *et al.*, 2011)**

Antibacterial agent	MIC breakpoints		
	Susceptible	Intermediate susceptibility	Resistance
AMOX	-	-	$\geq 128$
AUG*	$\leq 8/4$	16/8	$\geq 32/64$
AMK	$\leq 16$	32	$\geq 64$
FOX	$\leq 16$	32-64	$\geq 128$
CLR	$\leq 2$	4	$\geq 8$

\*determined for *Nocardia* and other Actinomycetes but not for Mycobacteria (Woods *et al.*, 2011)

## **9.8 Immune response to *M. abscessus***

### **9.8.1 J774 cell line and maintenance**

J774 murine macrophage cell line was maintained at 37°C, 5% CO<sub>2</sub> in cDMEM consisting of Gibco Dulbecco's Modified Eagle Media GlutaMAX™-I (ThermoFisher Scientific) supplemented with 10% fetal bovine serum (Sigma-Aldrich) and 1% Penicillin/Streptomycin (Sigma-Aldrich).

#### *9.8.1.1 Defrosting*

Cells frozen in liquid N<sub>2</sub> were gently defrosted in a 37°C water bath. Defrosted cells were transferred to a 15 ml flacon tube, topped with 9 ml of DMEM and centrifuged at 1000 rpm for 10 min to remove DMSO. Supernatant was discarded, and the cell pellet gently resuspended in DMEM and the cells were then incubated at 37°C, 5% CO<sub>2</sub>.

#### *9.8.1.2 Passaging*

The cells take ~17h to double and were normally grown to 80% confluency in a flask before being passaged. To passage the cells old media was discarded and new media added to the same flask. A cell scraper was used to dislodge the cells attached to the flask into the new media, which was then aliquoted according to the desired split. Cells were sub-cultured to a maximum of 18 passages.

#### *9.8.1.3 Freezing*

1x10<sup>6</sup> cells were pelleted down and re-suspended in 1 ml freezing media (50% FBS, 40% cDMEM, 10% DMSO) and frozen in 1.2 ml external thread Corning cryovials. Frozen cells were initially kept at -20°C for 2h, then -80°C for 24h and finally moved to liquid N<sub>2</sub> for long-term storage.

### **9.8.2 Preparation of bacterial inoculum for infection assays**

7H9 broth was inoculated with bacterial strains straight from glycerol stocks. The cultures were grown to mid-log phase (~OD<sub>600</sub> 0.8). Prior to dilution to OD<sub>600</sub> 0.05 cells were passed through

a 0.27 G needle to disrupt any clumps. Diluted culture was grown shaking until it reached end of log/beginning of stationary phase. Then, 1 ml of the cultures was aliquoted to cryovials and frozen at -80°C. After 3 days, 3 aliquots of each strain were taken and serially diluted 1:10 in PBS. 100 µl of selected dilutions ( $10^{-3}$ - $10^{-6}$ ) were plated on 7H11 agar for enumeration 3-4 days later. This provided an enumerated inoculum that could be defrosted and used directly on the day of infection.

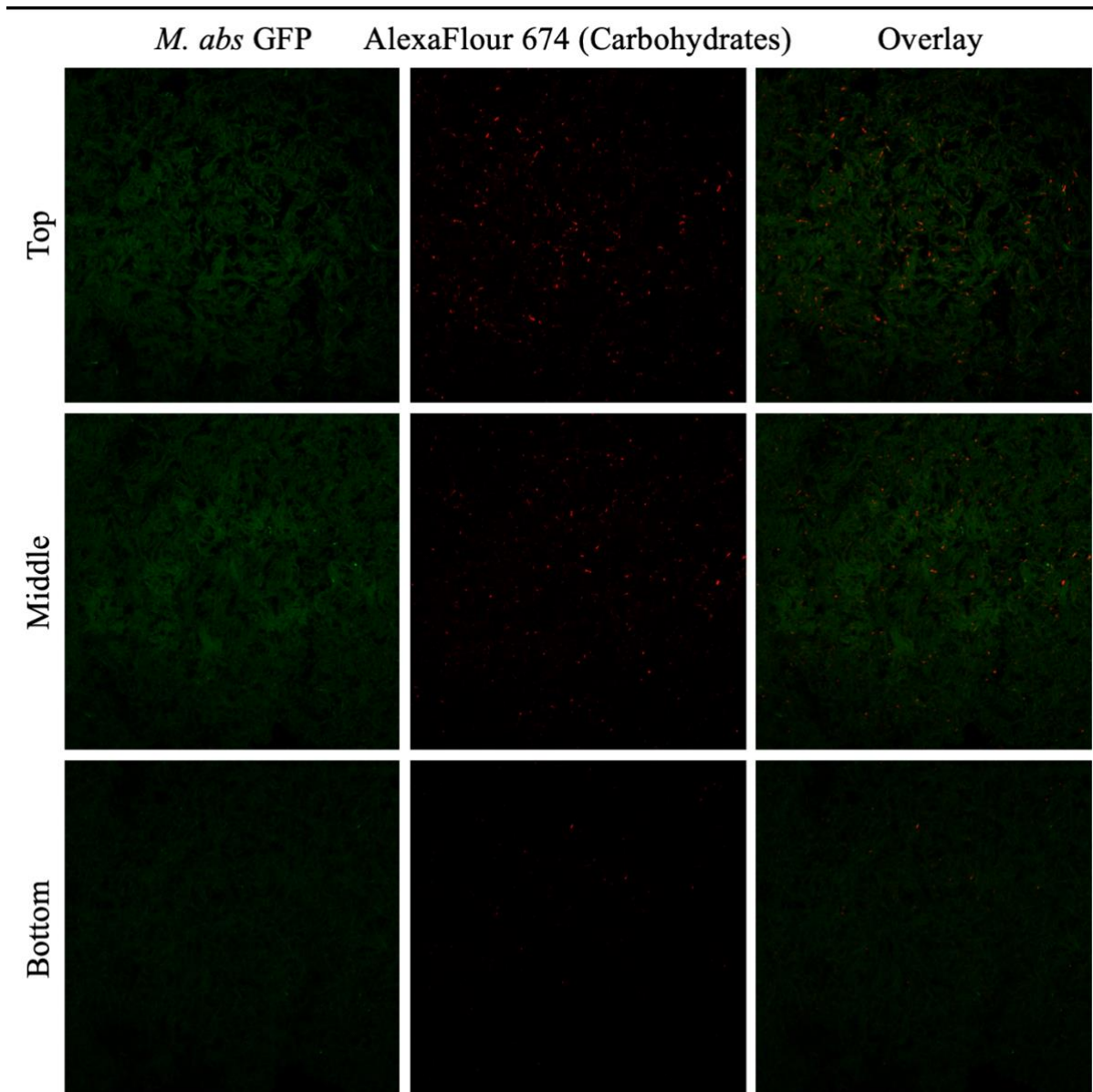
### **9.8.3 Macrophage infections - Measuring intracellular survival using CFUs**

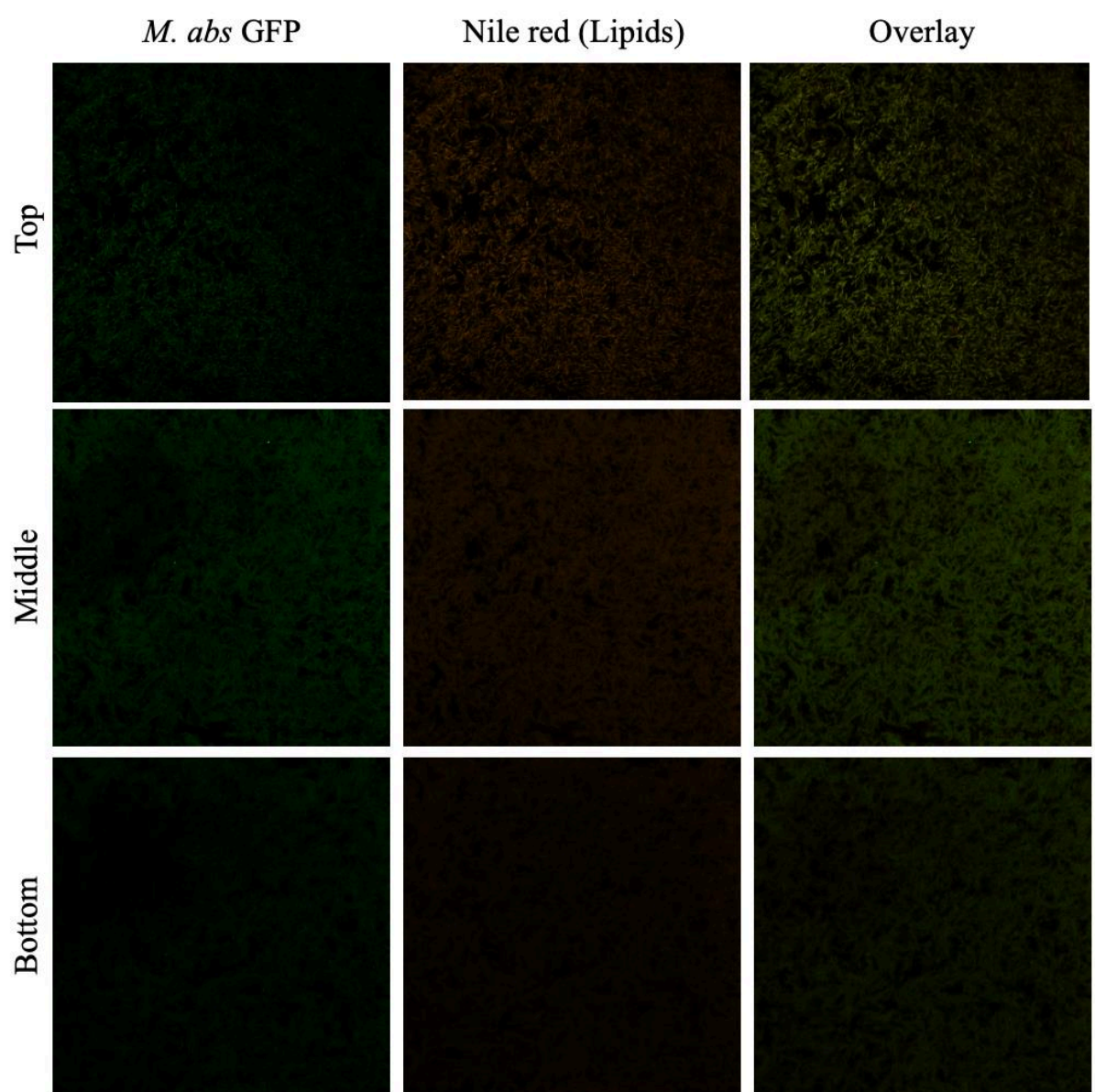
J774 cells were seeded at a density of  $0.01 \times 10^6$  cells/well in 200 µl of infection media (IM: DMEM + 50% FBS, no P/S) in a 96-well plate, 24 h prior to infection and incubated at 37°C, 5% CO<sub>2</sub>. Three separate plates were used for three timepoints: 4, 24 and 72 h.p.i. On the day of infection, cryovials containing enumerated bacterial inoculum were defrosted and appropriately diluted in IM to infect at multiplicity of infection (MOI) 10 (10 bacteria/macrophage). IM was removed from cells, and the bacterial inoculum in IM added to begin infection. 200 µl of IM was added to uninfected wells. After 3 h, media was removed from the cells, and cells were incubated for 1 h with IM supplemented with 250 µg/ml AMK to kill extracellular bacteria. Cells were then washed with PBS, and plates designated for collection at 24 and 72 h.p.i. were incubated with IM+75 µg/ml amikacin. Plates designated for collection at 4 h timepoint were washed with PBS and incubated for 10 min at room temperature with 100 µl of 0.5% Triton-X in PBS to burst open the macrophages. This suspension was then serially diluted in PBS and 5µl of each dilution was plated on 7H11, incubated for 3 days and then enumerated. Same collection process was repeated at 24 h and 72 h.

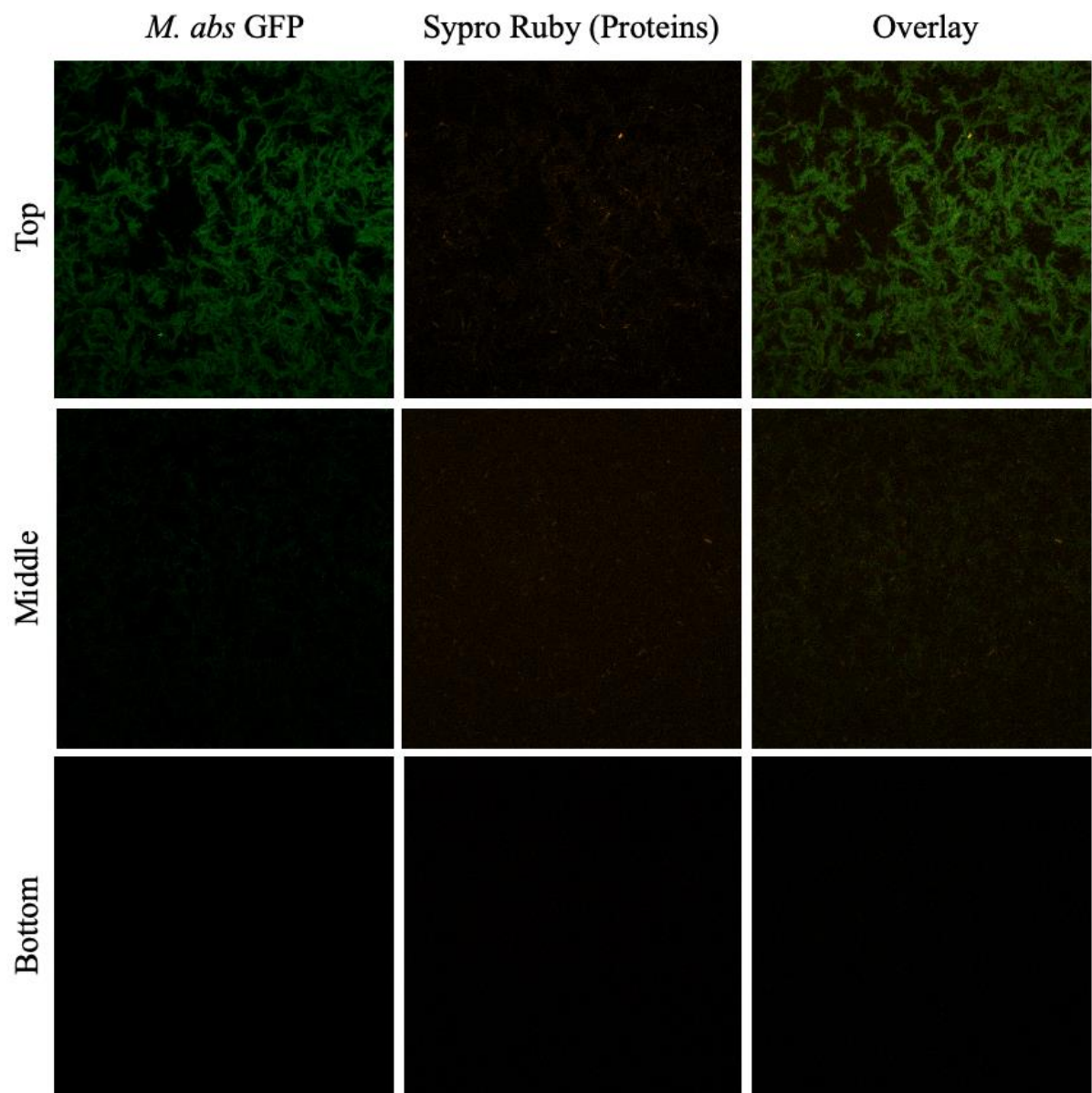
# **10 Appendices**

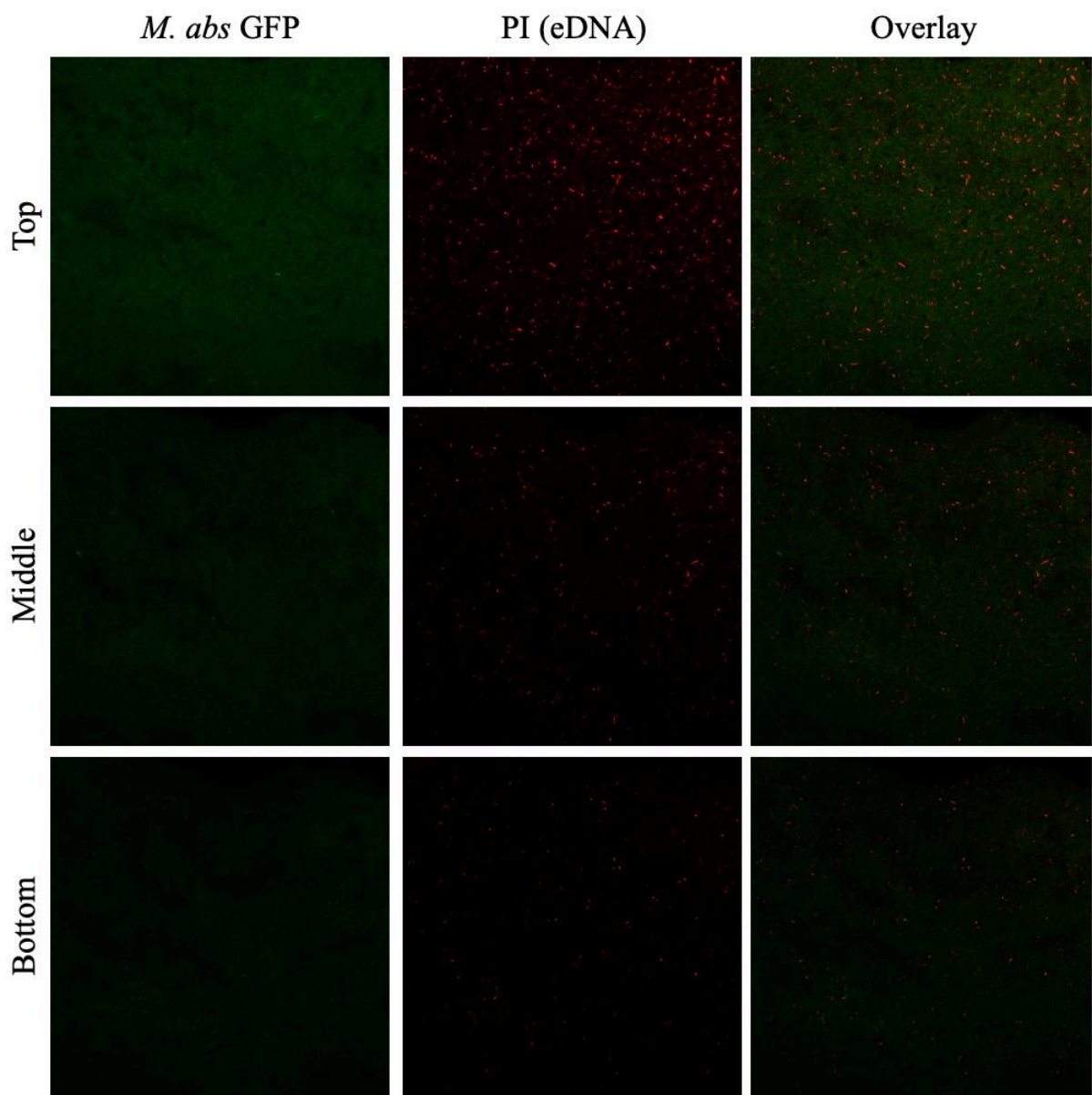
## Appendix 1 – Selected sections of CSLM images

Top, middle, and bottom sections of z-stacks of *M. abscessus* GFP biofilms stained with various dyes that target biofilm ECM components, before processing and analysis. Complementary to Fig. 2.3.









## **Appendix 2 – Common downregulated DEGs in *M. abscessus* biofilms t1 and t2**

<b>Gene_ID</b>	<b>Product name</b>
MAB_4697	hypothetical protein
MAB_1359c	Putative ABC transporter, ATP-binding protein
MAB_1360c	Probable transcriptional regulator, TetR family
MAB_4698	hypothetical protein
MAB1358c	Putative ABC transporter, permease protein

### Appendix 3 – Common upregulated DEGs in *M. abscessus* biofilms t1 and t2

Gene_ID	Product name	Gene_ID	Product name
MAB_0249	hypothetical protein	MAB_1084c	hypothetical protein
MAB_4664	Hypothetical protein	MAB_2444c	Conserved hypothetical protein (metal-dependent phosphohydrolase?)
MAB_3148c	Probable polyketide synthase Pks5	MAB_3427	hypothetical protein
MAB_2027	Putative acyl carrier protein	MAB_2020c	Possible bifunctional enzyme HhdD isomerase cyclase/dehydrase
MAB_2292c	hypothetical protein	MAB_3019	Probable fatty acid hydroxylase
MAB_1067	Hypothetical protein	MAB_1241c	hypothetical protein
MAB_0669	Hypothetical PPE-family protein	MAB_0857	Putative monooxygenase
MAB_2028	Probable 3-oxoacyl-(Acyl-carrier-protein) synthase II KasB	MAB_1083c	hypothetical protein
MAB_2280	hypothetical protein	MAB_4233c	Putative monooxygenase (luciferase-like)
MAB_0325c	Hypothetical protein	MAB_2630	Probable integral membrane cytochrome D ubiquinol oxidase (Subunit I) CydA
MAB_2029	Putative beta-ketoacyl synthase	MAB_4714c	Probable fatty-acid-coa ligase FadD
MAB_2030	Probable 3-oxoacyl-(Acyl-carrier-protein) synthase II KasA	MAB_2382	Conserved hypothetical protein (pyridoxamine 5'-phosphate oxidase-related)
MAB_1247c	hypothetical protein	MAB_4882c	Putative phosphatase
MAB_2034	Probable malonyl CoA-acyl carrier protein transacylase	MAB_3957	Superoxide dismutase SodM
MAB_2031	Putative beta-ketoacyl synthase	MAB_4715c	hypothetical protein
MAB_0659	Putative dioxygenase	MAB_0049	ESAT-6-like protein
MAB_2281	hypothetical protein	MAB_3904	hypothetical protein
MAB_2278	Putative oxidoreductase	MAB_0383c	Putative transcriptional regulator, PadR-like
MAB_3900c	hypothetical protein	MAB_4671c	Probable ABC transporter, ATP-binding protein
MAB_0667	Hypothetical heavy metal transport/detoxification protein	MAB_4418	Succinate-semialdehyde dehydrogenase
MAB_2032	Probable 3-oxoacyl-[acyl-carrier protein] reductase	MAB_0302	Putative monooxygenase
MAB_0288	Putative monooxygenase (salicylate/ hydroxybenzoate hydroxylase)	MAB_2394	hypothetical protein
MAB_2275	Putative membrane protein, MmpL family	MAB_3429	Putative integral membrane protein
MAB_4675c	Acyl-protein synthetase	MAB_4623c	5-methyltetrahydropteroyltriglutamate-homocysteine S-methyltransferase
MAB_4842	Putative arsenate reductase ArsC	MAB_3466c	Hypothetical protein
MAB_0287	Probable fatty-acid-CoA ligase FadD	MAB_2274c	hypothetical protein
MAB_2907	hypothetical protein	MAB_4234c	Putative FMNH2-utilizing oxygenase
MAB_0664	PE family protein	MAB_4232c	Putative oxygenase

MAB_2279	Probable ornithine aminotransferase	MAB_1916c	3-methyl-2-oxobutanoate hydroxymethyltransferase
MAB_1042c	Probable cytochrome c oxidase polypeptide I	MAB_2738c	Hypothetical protein
MAB_0717	Probable dehydrogenase/reductase	MAB_2950c	hypothetical protein
MAB_4884c	Hypothetical protein	MAB_0668c	Probable O-methyltransferase OmT
MAB_0660	hypothetical protein	MAB_0924c	Putative organic hydroperoxide resistance protein/OsmC-like protein
MAB_4139	Putative transcription regulator, ArsR family	MAB_4478c	Putative short-chain dehydrogenase/reductase
MAB_2282	Putative flavin-dependent reductase	MAB_3028	RNA polymerase sigma factor
MAB_4140	hypothetical protein	MAB_1528c	Probable oxidoreductase
MAB_1245c	Hypothetical protein	MAB_1381	Putative oxidoreductase EphD
MAB_1923c	hypothetical protein	MAB_4309c	Putative serine protease
MAB_1246c	Hypothetical protein	MAB_3925	hypothetical protein
MAB_4402	Heat shock protein Hsp20	MAB_0378	Probable lipid-transfer protein Ltp1/thiolase
MAB_3438	Putative short-chain dehydrogenase/reductase	MAB_4272c	Protein GrpE (HSP-70 cofactor)
MAB_0295	Putative phenazine biosynthesis protein PhzC	MAB_2540c	Putative Short-chain dehydrogenase/reductase
MAB_2277	Probable aldehyde dehydrogenase	MAB_2916	hypothetical protein
MAB_2847c	hypothetical protein	MAB_1891	hypothetical protein
MAB_4428	Putative short chain dehydrogenase/reductase	MAB_3016c	hypothetical protein
MAB_4843	Hypothetical protein	MAB_4672c	Probable ABC transporter, permease protein
MAB_1244c	Hypothetical protein	MAB_2951c	Probable lipid-transfer protein Ltp1
MAB_0661	Putative long chain fatty acid-coA ligase	MAB_4670c	Hypothetical protein
MAB_1243c	Hypothetical protein	MAB_2489	hypothetical protein
MAB_3874c	Putative dioxygenase	MAB_1117c	Hypothetical protein
MAB_0662	hypothetical protein	MAB_4355	Hypothetical fumarylacetoacetate (FAA) hydrolase family
MAB_2886c	Hypothetical protein	MAB_0182c	Hypothetical protein
MAB_4857	hypothetical protein	MAB_2917	Putative hydrolase
MAB_4408c	Putative alkylhydroperoxidase C	MAB_0215	Possible transcriptional regulator
MAB_4674c	Similarity with Nitrogen-fixing NifU-like proteins	MAB_4624	Putative phenylacetic acid degradation protein
MAB_0195c	Putative hydrolase, alpha/beta hydrolase fold	MAB_0048	Probable PE family protein
MAB_2270c	Putative peroxidase	MAB_4683c	Hypothetical protein
MAB_3902c	hypothetical protein	MAB_4852c	Phosphate ABC transporter, periplasmic protein
MAB_2021c	Putative carboxymuconolactone decarboxylase	MAB_3587c	hypothetical protein
MAB_1242c	Hypothetical protein	MAB_4362	Putative long-chain-fatty-acid--CoA ligase

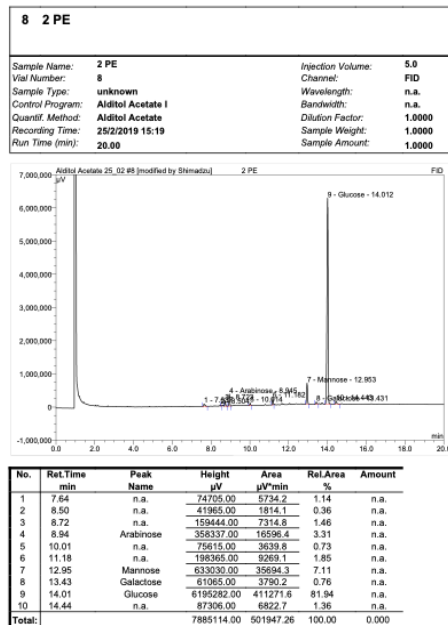
MAB_3455c	Putative acyl-CoA thiolase	MAB_2490	hypothetical protein
MAB_2271c	hypothetical protein	MAB_4682c	Hypothetical protein
MAB_4407c	Putative alkylhydroperoxidase AhpD	MAB_0929	hypothetical protein
MAB_2283	Putative oxidoreductase	MAB_4944c	Putative cytochrome P450
MAB_4181	Sulfate adenylate transferase, subunit 2 (CysD)	MAB_2903	Hypothetical protein
MAB_0301	Putative carboxylesterase	MAB_2234c	Conserved hypothetical protein (AAA ATPase?)
MAB_1380	hypothetical protein	MAB_2228c	ESAT-6-like protein esxH
MAB_2286	hypothetical protein	MAB_2608	Putative hydrolase, alpha/beta fold
MAB_4883c	Exopolyphosphatase, putative	MAB_4271c	Chaperone protein DnaJ
MAB_0665	PE family protein	MAB_0765	Hypothetical conserved integral membrane protein
MAB_0663	Probable cyclic synthetase (peptide synthase)	MAB_2632	Probable ATP-binding protein ABC transporter CydD
MAB_2276c	Putative regulatory protein	MAB_3354	Probable acyl-[acyl-carrier protein] desaturase DesA1
MAB_0469c	Hypothetical protein	MAB_4850c	Phosphate ABC transporter, permease protein PstA-1
MAB_1231	hypothetical protein	MAB_0453c	hypothetical protein
MAB_3358c	Putative acyltransferase	MAB_4851c	Phosphate ABC transporter, permease protein PstC-2
MAB_4636	hypothetical protein	MAB_3763	Probable cutinase cut2 precursor
MAB_4855c	Hypothetical protein	MAB_3937	Hypothetical protein
MAB_1170	hypothetical protein	MAB_0379	Conserved hypothetical protein (MaoC-like dehydratase?)
MAB_1169	Putative hydrolase, alpha/beta fold	MAB_4495	Hypothetical protein
MAB_2541c	Probable transcriptional regulatory protein TetR	MAB_3586c	Putative transcriptional regulator, TetR family
MAB_2284	Putative halogenase	MAB_1588c	Putative oxidoreductase
MAB_4635	Probable NADH:flavin oxidoreductase/NADH oxidase	MAB_0216	hypothetical protein
MAB_0666	ESAT-6-like protein (10 kDa antigen)	MAB_2949c	Conserved hypothetical protein (possible dehydratase)
MAB_2381	Probable oxidoreductase	MAB_4419	Tartrate dehydrogenase
MAB_4265c	Chaperone ClpB	MAB_2204	Conserved hypothetical protein (FxsA cytoplasmic membrane protein?)
MAB_4273c	Chaperone protein DnaK (Hsp 70)	MAB_2233c	hypothetical protein
MAB_4945c	Hypothetical protein	MAB_2229c	Hypothetical PE family protein
MAB_3018	Putative transcriptional regulator, GntR family	MAB_3210c	hypothetical protein
MAB_2071	Probable short-chain dehydrogenase/reductase	MAB_1587c	Probable fatty acid desaturase
MAB_1874	Putative oxidoreductase	MAB_4788c	hypothetical protein
MAB_1394c	hypothetical protein	MAB_0046	Probable PE family protein
MAB_4789c	Hypothetical protein	MAB_4668c	AMP-dependent synthetase and ligase
MAB_3467c	18 kDa antigen (HSP 16.7)	MAB_0103	Probable monooxygenase EthA

MAB_0827	Hypothetical short-chain dehydrogenase/reductase	MAB_4646	hypothetical protein
MAB_3068c	Possible transcriptional regulatory protein	MAB_0454c	Putative metal-binding protein
MAB_4673c	Putative aminotransferase/cysteine desulfhydrase	MAB_2269c	Putative transcriptional regulator, MerR family
MAB_4354	Putative NADH dehydrogenase/NAD(P)H nitroreductase	MAB_2395	Probable acyl-CoA dehydrogenase FadE
MAB_2240	Putative ferredoxin	MAB_1399	Probable peptidase
MAB_0925c	Putative transcriptional regulator, MarR family	MAB_0183c	Putative cation transporter
MAB_1030	hypothetical protein	MAB_0930	Putative ferredoxin/ferredoxin--NADP reductase
MAB_2607	Putative flavin-containing monooxygenase	MAB_3787	hypothetical protein
MAB_3903	hypothetical protein	MAB_4877c	hypothetical protein
MAB_4748c	Conserved hypothetical protein (pyridoxamine 5'-phosphate oxidase?)	MAB_2948c	Probable short-chain dehydrogenase/reductase
MAB_4095c	Isocitrate lyase (AceA)	MAB_3938	Putative Clp protease subunit
MAB_2592c	hypothetical protein	MAB_4270c	Probable heat shock protein transcriptional regulator HspR
MAB_2606c	Putative transcriptional regulator, TetR family	MAB_1224	hypothetical protein
MAB_2631	Probable cytochrome D ubiquinol oxydase CydB	MAB_1031c	Probable manganese transport protein MntH
MAB_4845	Low-affinity inorganic phosphate transporter PitA	MAB_0357c	hypothetical protein
MAB_3905	Hypothetical protein	MAB_4666c	hypothetical protein
MAB_4361	Hypothetical fumarylacetoacetate hydrolase family	MAB_2480	hypothetical protein
MAB_2232c	Putative FtsK/SpoIIIE family protein		

## Appendix 4: Chromatographs of alditol acetates of capsular monosaccharides

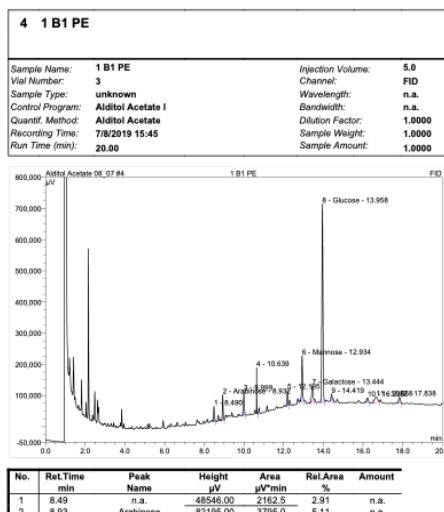
### Chromatographs - Planktonic T1

Operator:Shimadzu Timebase:GC2010\_SYSTEM1 Sequence:Alditol Acetate 25\_02 Page 1-1  
26/2/2019 10:07 AM



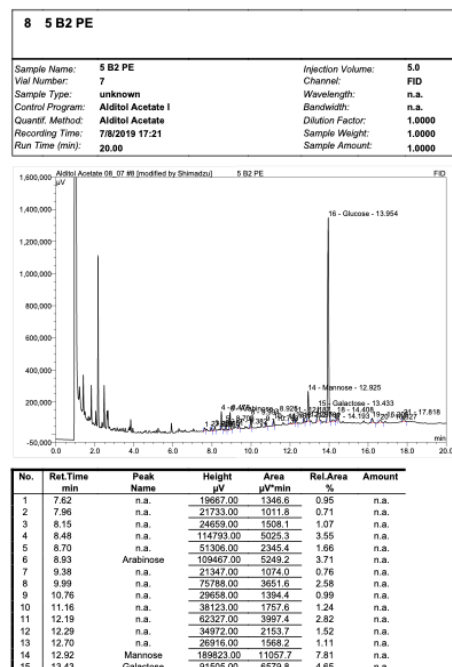
Chromleon (c) Dionex 1996-2006  
Default Test/Integration Version 6.80 SR8 Build 2623 (156243)

Operator:Shimadzu Timebase:GC2010\_SYSTEM1 Sequence:Alditol Acetate 08\_07 Page 1-1  
8/8/2019 12:35 PM



Chromleon (c) Dionex 1996-2006  
Default Test/Integration Version 6.80 SR8 Build 2623 (156243)

Operator:Shimadzu Timebase:GC2010\_SYSTEM1 Sequence:Alditol Acetate 08\_07 Page 1-2  
8/8/2019 12:40 PM



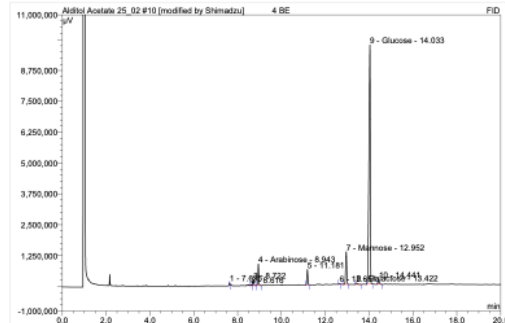
Chromleon (c) Dionex 1996-2006  
Default Test/Integration Version 6.80 SR8 Build 2623 (156243)

## Chromatographs - Planktonic T2

Operator:Shimadzu Timebase:GC2010\_SYSTEM1 Sequence:Alditol Acetate 25\_02 Page 1-1  
26/2/2019 10:08 AM

### 10 4 BE

Sample Name:	4 BE	Injection Volume:	5.0
Vial Number:	10	Channel:	FID
Sample Type:	unknown	Wavelength:	n.a.
Control Program:	Alditol Acetate I	Bandwidth:	n.a.
Quantif. Method:	Alditol Acetate	Dilution Factor:	1.0000
Recording Time:	25/2/2019 16:06	Sample Weight:	1.0000
Run Time (min):	20.00	Sample Amount:	1.0000



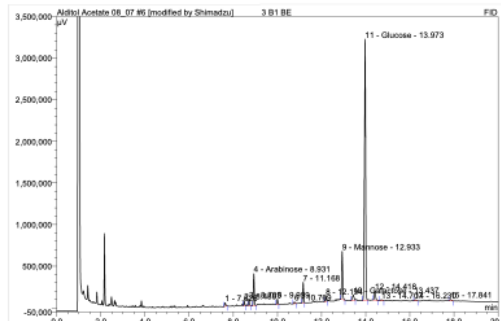
No.	Ret.Time min	Peak Name	Height μV	Area μV·min	Rel.Area %	Amount
1	7.63	n.a.	105525.00	3939.5	0.45	n.a.
2	8.62	n.a.	48515.00	1994.5	0.23	n.a.
3	8.72	n.a.	228759.00	10384.5	1.19	n.a.
4	8.94	Arabinose	874267.00	40704.4	4.68	n.a.
5	11.18	n.a.	622155.00	29207.0	3.36	n.a.
6	12.65	n.a.	36328.00	1703.5	0.20	n.a.
7	12.95	Mannose	1320838.00	75253.0	8.65	n.a.
8	13.42	Galactose	61488.00	4330.0	0.50	n.a.
9	14.03	Glucose	9696955.00	689115.8	79.25	n.a.
10	14.44	n.a.	193309.00	12869.1	1.48	n.a.
Total:			13188139.00	8689501.25	100.00	0.000

Chromelcon (c) Dionex 1996-2006  
Version 6.80 SR8 Build 2623 (156243)

Operator:Shimadzu Timebase:GC2010\_SYSTEM1 Sequence:Alditol Acetate 08\_07 Page 1-2  
8/8/2019 12:39 PM

### 6 3 B1 BE

Sample Name:	3 B1 BE	Injection Volume:	5.0
Vial Number:	5	Channel:	FID
Sample Type:	unknown	Wavelength:	n.a.
Control Program:	Alditol Acetate I	Bandwidth:	n.a.
Quantif. Method:	Alditol Acetate	Dilution Factor:	1.0000
Recording Time:	7/8/2019 16:33	Sample Weight:	1.0000
Run Time (min):	20.00	Sample Amount:	1.0000



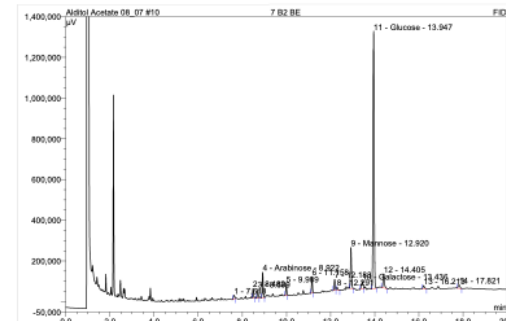
No.	RetTime min	Peak Name	Height μV	Area μV·min	RelArea %	Amount
1	7.63	n.a.	42509.00	2593.3	0.90	n.a.
2	8.49	n.a.	62180.00	2605.0	0.91	n.a.
3	8.71	n.a.	79388.00	3538.8	1.23	n.a.
4	8.93	Arabinose	383061.00	17394.6	6.04	n.a.
5	10.00	n.a.	65031.00	2960.4	1.03	n.a.
6	10.77	n.a.	21141.00	1113.1	0.39	n.a.
7	11.17	n.a.	246963.00	11501.3	4.00	n.a.
8	12.19	n.a.	61120.00	2941.4	1.02	n.a.
9	12.93	Mannose	580474.00	31851.6	11.07	n.a.
10	13.44	Galactose	64554.00	5395.3	1.87	n.a.
11	13.97	Glucose	313957.00	194347.7	67.52	n.a.
12	14.42	n.a.	11455.00	7750.9	2.69	n.a.
13	14.71	n.a.	12482.00	1132.3	0.39	n.a.
14	16.23	n.a.	14479.00	1219.8	0.42	n.a.
15	17.84	n.a.	16693.00	1477.9	0.51	n.a.

Chromelcon (c) Dionex 1996-2006  
Version 6.80 SR8 Build 2623 (156243)

Operator:Shimadzu Timebase:GC2010\_SYSTEM1 Sequence:Alditol Acetate 08\_07 Page 1-1  
8/8/2019 12:41 PM

### 10 7 B2 BE

Sample Name:	7 B2 BE	Injection Volume:	5.0
Vial Number:	9	Channel:	FID
Sample Type:	unknown	Wavelength:	n.a.
Control Program:	Alditol Acetate I	Bandwidth:	n.a.
Quantif. Method:	Alditol Acetate	Dilution Factor:	1.0000
Recording Time:	7/8/2019 18:09	Sample Weight:	1.0000
Run Time (min):	20.00	Sample Amount:	1.0000



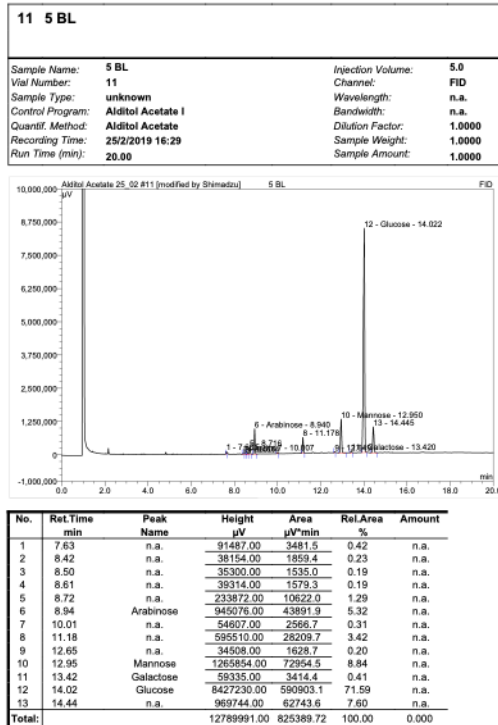
No.	RetTime min	Peak Name	Height μV	Area μV·min	RelArea %	Amount
1	7.62	n.a.	19208.00	1361.1	1.13	n.a.
2	8.48	n.a.	46185.00	1997.4	1.65	n.a.
3	8.70	n.a.	44417.00	2021.3	1.67	n.a.
4	8.92	Arabinose	124365.00	5842.4	4.83	n.a.
5	9.99	n.a.	57267.00	2556.6	2.11	n.a.
6	11.16	n.a.	80552.00	3702.3	3.06	n.a.
7	12.18	n.a.	54795.00	2761.4	2.28	n.a.
8	12.29	n.a.	16850.00	1236.1	1.02	n.a.
9	12.92	Mannose	200171.00	11310.7	9.35	n.a.
10	13.44	Galactose	38214.00	3234.4	2.67	n.a.
11	13.95	Glucose	1263900.00	77210.3	63.83	n.a.
12	14.40	n.a.	68508.00	4833.2	4.00	n.a.
13	16.21	n.a.	15980.00	1316.5	1.09	n.a.
14	17.62	n.a.	16844.00	1577.8	1.30	n.a.
Total:			2047256.00	120961.72	100.00	0.000

Chromelcon (c) Dionex 1996-2006  
Version 6.80 SR8 Build 2623 (156243)

## Chromatographs - Biofilm T1

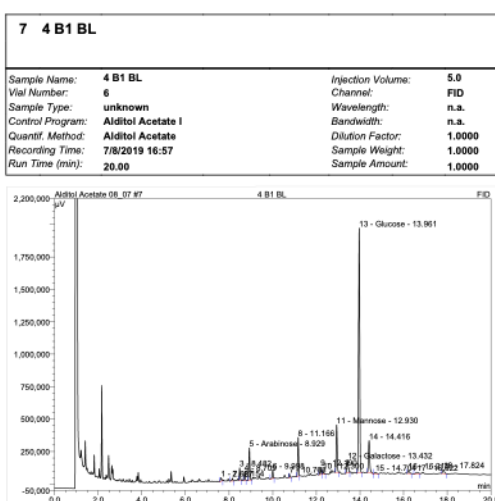
## Chromatographs - Biofilm T2

Operator:Shimadzu Timebase:GC2010\_SYSTEM1 Sequence:Alditol Acetate 25\_02  
Page 1-1  
26/2/2019 10:09 AM



Chromeleon (c) Dionex 1996-2006  
Version 6.80 SR8 Build 2623 (156243)

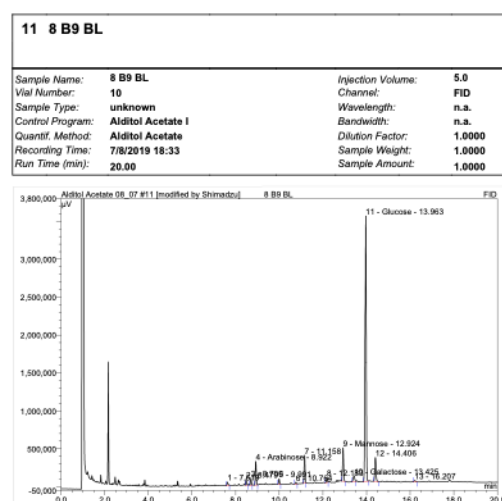
Operator:Shimadzu Timebase:GC2010\_SYSTEM1 Sequence:Alditol Acetate 08\_07  
Page 1-2  
8/8/2019 12:39 PM



Default Test/Integration

Chromeleon (c) Dionex 1996-2006  
Version 6.80 SR8 Build 2623 (156243)

Operator:Shimadzu Timebase:GC2010\_SYSTEM1 Sequence:Alditol Acetate 08\_07  
Page 1-1  
8/8/2019 12:41 PM



Default Test/Integration

Chromeleon (c) Dionex 1996-2006  
Version 6.80 SR8 Build 2623 (156243)

## Appendix 5: Permission rights

1. Permission rights under the order licence ID 1128016-1 from Annual Review to use Figure 1 as Figure 1.1A in this thesis from publication: Halloum, I., Carrère-Kremer, S., Blaise, M., Viljoen, A., Bernut, A., Le Moigne, V., Vilchèze, C., Guérardel, Y., Lutfalla, G., Herrmann, J.-L.L., Jacobs, W.R., Kremer, L., Kremer, L., 2016. Deletion of a dehydratase important for intracellular growth and cording renders rough *Mycobacterium abscessus* avirulent. Proc. Natl. Acad. Sci. U. S. A. 113, E4228–E4237. <https://doi.org/10.1073/pnas.1605477113>
2. Permission rights to use Figure S4 in Figure 1.1B of this thesis from publication: Halloum, I., Carrère-Kremer, S., Blaise, M., Viljoen, A., Bernut, A., Le Moigne, V., Vilchèze, C., Guérardel, Y., Lutfalla, G., Herrmann, J.-L.L., Jacobs, W.R., Kremer, L., Kremer, L., 2016. Deletion of a dehydratase important for intracellular growth and cording renders rough *Mycobacterium abscessus* avirulent. Proc. Natl. Acad. Sci. U. S. A. 113, E4228–E4237. <https://doi.org/10.1073/pnas.1605477113>

Permission not required according to: “Permission is not required to use original figures or tables for noncommercial and educational use (i.e., in a review article, in a book that is not for sale) if the article published under the exclusive PNAS License to Publish”. <https://www.pnas.org/page/about/rights-permissions>

3. Figure 1.2 is taken from publication: Gutiérrez, A.V., Viljoen, A., Ghigo, E., Herrmann, J.L., Kremer, L., 2018. Glycopeptidolipids, a double-edged sword of the *Mycobacterium abscessus* complex. Front. Microbiol. <https://doi.org/10.3389/fmicb.2018.01145>

Permission rights to use and reproduce this figure are as follows: Copyright © 2018 Gutiérrez, Viljoen, Ghigo, Herrmann and Kremer. This is an open-access article distributed under the terms of the **Creative Commons Attribution License (CC BY)**. The use, distribution or reproduction in other forums is permitted, provided the original author(s) and the copyright owner are credited and that the original publication in this journal is cited, in accordance with accepted academic practice. No use, distribution or reproduction is permitted which does not comply with these terms.

## **11 References**

Abate, G. et al. (2019) 'BCG vaccination induces *M. avium* and *M. abscessus* cross-protective immunity', *Frontiers in Immunology*. Front Immunol, 10(FEB), p. 234. doi: 10.3389/fimmu.2019.00234.

Adekambi, T. et al. (2004) 'Amoebal Coculture of *Mycobacterium massiliense* sp. nov. from the Sputum of a Patient with Hemoptoic Pneumonia', *Journal of Clinical Microbiology*, 42(12), pp. 5493–5501. doi: 10.1128/JCM.42.12.5493-5501.2004.

Alderwick, L. J. et al. (2015) 'The mycobacterial cell wall—peptidoglycan and arabinogalactan', *Cold Spring Harbor Perspectives in Medicine*. Cold Spring Harbor Laboratory Press, 5(8), pp. 1–16. doi: 10.1101/cshperspect.a021113.

Alhede, M. et al. (2012) 'Combination of microscopic techniques reveals a comprehensive visual impression of biofilm structure and composition', *FEMS Immunology and Medical Microbiology*. doi: 10.1111/j.1574-695X.2012.00956.x.

Alvarez, H. M. and Steinbüchel, A. (2002) 'Triacylglycerols in prokaryotic microorganisms', *Applied Microbiology and Biotechnology*. doi: 10.1007/s00253-002-1135-0.

Anand, A. et al. (2015) 'Polyketide Quinones Are Alternate Intermediate Electron Carriers during Mycobacterial Respiration in Oxygen-Deficient Niches', *Molecular Cell*. Cell Press, 60(4), pp. 637–650. doi: 10.1016/j.molcel.2015.10.016.

Andréjak, C. et al. (2010) 'Nontuberculous pulmonary mycobacteriosis in Denmark: Incidence and prognostic factors', *American Journal of Respiratory and Critical Care Medicine*. doi: 10.1164/rccm.200905-0778OC.

Angala, S. kumar et al. (2017) 'Biosynthesis of the methylthioxylose capping motif of lipoarabinomannan in Mycobacterium tuberculosis', *ACS chemical biology*. NIH Public Access, 12(3), p. 682. doi: 10.1021/ACSCHEMBIO.6B01071.

Aung, T. T. et al. (2017) 'Discovery of novel antimycobacterial drug therapy in biofilm of pathogenic nontuberculous mycobacterial keratitis', *Ocular Surface*. doi: 10.1016/j.jtos.2017.06.002.

Ayoubi, S. et al. (2020) 'Prevalence of *Mycobacterium abscessus* among the patients with nontuberculous mycobacteria', *Archives of Iranian Medicine*. Academy of Medical Sciences of I.R. Iran, pp. 163–168.

Bachmann, N. L. et al. (2020) 'Key Transitions in the Evolution of Rapid and Slow Growing Mycobacteria Identified by Comparative Genomics', *Frontiers in Microbiology*. doi: 10.3389/fmicb.2019.03019.

Baker, A. W. et al. (2017) 'Two-phase hospital-associated outbreak of *Mycobacterium abscessus*: Investigation and mitigation', *Clinical Infectious Diseases*. doi: 10.1093/cid/ciw877.

Bansal-Mutalik, R. and Nikaido, H. (2014) 'Mycobacterial outer membrane is a lipid bilayer and the inner membrane is unusually rich in diacyl phosphatidylinositol dimannosides', *Proceedings of the National Academy of Sciences*. National Academy of Sciences, 111(13), pp. 4958–4963. doi: 10.1073/pnas.1403078111.

Bastian, S. et al. (2011) 'Assessment of Clarithromycin Susceptibility in Strains Belonging to the *Mycobacterium abscessus* Group by erm(41) and rrl Sequencing', *Antimicrobial Agents and Chemotherapy*, 55(2), pp. 775–781. doi: 10.1128/AAC.00861-10.

Beebout, C. J. et al. (2019) 'Respiratory heterogeneity shapes biofilm formation and host colonization in uropathogenic *Escherichia coli*', *mBio*. doi: 10.1128/mBio.02400-18.

Behr, M. A. (2002) 'BCG - Different strains, different vaccines?', *Lancet Infectious Diseases*. doi: 10.1016/S1473-3099(02)00182-2.

Berg, J. M., Tymoczko, J. L. and Stryer, L. (2002) *Triacylglycerols Are Highly Concentrated Energy Stores*, *Biochemistry*.

Bernut, A. et al. (2014) '*Mycobacterium abscessus* cording prevents phagocytosis and promotes abscess formation.', *Proceedings of the National Academy of Sciences of the United States of America*. National Academy of Sciences, 111(10), pp. E943-52. doi: 10.1073/pnas.1321390111.

- Bernut, A., Viljoen, A., et al. (2016) 'Insights into the smooth-to-rough transitioning in *Mycobacterium bolletii* unravels a functional Tyr residue conserved in all mycobacterial MmpL family members', *Molecular Microbiology*, 99(5), pp. 866–883. doi: 10.1111/mmi.13283.
- Bernut, A., Nguyen-Chi, M., et al. (2016) 'Mycobacterium abscessus-Induced Granuloma Formation Is Strictly Dependent on TNF Signaling and Neutrophil Trafficking.', *PLoS pathogens*. Edited by M. A. Behr. Public Library of Science, 12(11), p. e1005986. doi: 10.1371/journal.ppat.1005986.
- Bernut, A. et al. (2019) 'CFTR Protects against *Mycobacterium abscessus* Infection by Fine-Tuning Host Oxidative Defenses', *Cell Reports*. Elsevier B.V., 26(7), pp. 1828–1840.e4. doi: 10.1016/j.celrep.2019.01.071.
- Besra, G. S. (1998) 'Preparation of Cell-Wall Fractions from Mycobacteria', in *Mycobacteria Protocols*. New Jersey: Humana Press, pp. 91–104. doi: 10.1385/0-89603-471-2:91.
- Bhatt, A. et al. (2007) 'The *Mycobacterium tuberculosis* FAS-II condensing enzymes: Their role in mycolic acid biosynthesis, acid-fastness, pathogenesis and in future drug development', *Molecular Microbiology*. doi: 10.1111/j.1365-2958.2007.05761.x.
- Birmes, F. S. et al. (2017) 'Mycobacterium abscessus subsp . abscessus Is Capable of Degrading Pseudomonas aeruginosa Quinolone Signals', *Frontiers in Microbiology*, 8(March), pp. 1–10. doi: 10.3389/fmicb.2017.00339.
- Bjarnsholt, T. et al. (2009) 'Pseudomonas aeruginosa biofilms in the respiratory tract of cystic fibrosis patients', *Pediatric Pulmonology*. Pediatr Pulmonol, 44(6), pp. 547–558. doi: 10.1002/ppul.21011.
- Blumenberg, M. (2019) 'Introductory Chapter: Transcriptome Analysis', in *Transcriptome Analysis*. IntechOpen. doi: 10.5772/intechopen.85980.
- Boritsch, E. C. et al. (2016) 'Pks5-recombination-mediated surface remodelling in *Mycobacterium tuberculosis* emergence', *Nature Microbiology*. Nature Publishing Group, 1(2), pp. 1–11. doi: 10.1038/nmicrobiol.2015.19.
- Bosio, S. et al. (2012) 'Mycobacterium fortuitum prosthetic valve endocarditis: a case for the pathogenetic role of biofilms', *Cardiovascular Pathology*, 21(4), pp. 361–364. doi: 10.1016/j.carpath.2011.11.001.
- Boyd, E. S. and Barkay, T. (2012) 'The mercury resistance operon: From an origin in a geothermal environment to an efficient detoxification machine', *Frontiers in Microbiology*. Frontiers Research Foundation, 3(OCT), p. 349. doi: 10.3389/fmicb.2012.00349.
- Brambilla, C. et al. (2016) 'Mycobacteria clumping increase their capacity to damage macrophages', *Frontiers in Microbiology*. Frontiers Media SA, 7(OCT), p. 1562. doi: 10.3389/fmicb.2016.01562.
- Brindley, D. N., Matsumura, S. and Bloch, K. (1969) 'Mycobacterium phlei fatty acid synthetase - A bacterial multienzyme complex', *Nature*. Nature Publishing Group, 224(5220), pp. 666–669. doi: 10.1038/224666a0.
- Brown-Elliott, B. A. et al. (2002) 'Clarithromycin Resistance in *Mycobacterium abscessus*', *Journal of Clinical Microbiology*. American Society for Microbiology, 39(7), pp. 2745–2746. doi: 10.1128/jcm.39.7.2745-2746.2001.
- Bryant, J. M. et al. (2016) 'Emergence and spread of a humantransmissible multidrug-resistant nontuberculous mycobacterium', *Science*. American Association for the Advancement of Science, 354(6313), pp. 751–757. doi: 10.1126/science.aaf8156.
- Byrd, T. F. and Lyons, C. R. (1999) 'Preliminary characterization of a *Mycobacterium abscessus* mutant in human and murine models of infection.', *Infection and immunity*. American Society for Microbiology (ASM), 67(9), pp. 4700–7.
- Cantrell, S. A. et al. (2013) 'Free mycolic acid accumulation in the cell wall of the mce1 operon mutant strain of *Mycobacterium tuberculosis*', *Journal of Microbiology*. doi: 10.1007/s12275-013-3092-y.
- Catherinot, E. et al. (2007) 'Hypervirulence of a rough variant of the *Mycobacterium abscessus* type strain', *Infection and Immunity*. doi: 10.1128/IAI.00835-06.
- Cavaliere, R. et al. (2014) 'The biofilm matrix destabilizers, EDTA and DNaseI, enhance the susceptibility of nontypeable *Hemophilus influenzae* biofilms to treatment with ampicillin and ciprofloxacin', *MicrobiologyOpen*.

Blackwell Publishing Ltd, 3(4), pp. 557–567. doi: 10.1002/mbo3.187.

Chakraborty, P. et al. (2021) ‘Biofilm formation in the lung contributes to virulence and drug tolerance of *Mycobacterium tuberculosis*’, *Nature Communications*. Nature Research, 12(1), pp. 1–17. doi: 10.1038/s41467-021-21748-6.

Chakraborty, P. and Kumar, A. (2019) ‘The extracellular matrix of mycobacterial biofilms: Could we shorten the treatment of mycobacterial infections?’, *Microbial Cell*. doi: 10.15698/mic2019.02.667.

De Chaumont, F. et al. (2012) ‘Icy: an open bioimage informatics platform for extended reproducible research’, *Nature Methods*, 9, pp. 690–6.

Chen, J. et al. (2019) ‘Clinical efficacy and adverse effects of antibiotics used to treat *Mycobacterium abscessus* pulmonary disease’, *Frontiers in Microbiology*. Frontiers Media S.A., 10(AUG). doi: 10.3389/fmicb.2019.01977.

Chen, J. M. et al. (2006) ‘Roles of Lsr2 in colony morphology and biofilm formation of *Mycobacterium smegmatis*’, *Journal of Bacteriology*. doi: 10.1128/JB.188.2.633-641.2006.

Chen, L. and Wen, Y. M. (2011) ‘The role of bacterial biofilm in persistent infections and control strategies’, in *International Journal of Oral Science*. doi: 10.4248/IJOS11022.

Chen, S. et al. (2021) ‘Carbonyl cyanide 3-chlorophenylhydrazone (CCCP) exhibits direct antibacterial activity against *Mycobacterium abscessus*’, *Infection and Drug Resistance*. Dove Medical Press Ltd, 14, pp. 1199–1208. doi: 10.2147/IDR.S303113.

Chiaradia, L. et al. (2017) ‘Dissecting the mycobacterial cell envelope and defining the composition of the native mycomembrane’, *Scientific Reports*. Nature Publishing Group, 7(1), pp. 1–12. doi: 10.1038/s41598-017-12718-4.

Chin, K. C. J. et al. (2017) ‘Transcriptomic study of *Salmonella enterica* subspecies *enterica* serovar Typhi biofilm’, *BMC Genomics*. BioMed Central Ltd., 18(1), p. 836. doi: 10.1186/s12864-017-4212-6.

Choi, H. et al. (2018) ‘Treatment outcomes of macrolide-susceptible *Mycobacterium abscessus* lung disease’, *Diagnostic Microbiology and Infectious Disease*. doi: 10.1016/j.diagmicrobio.2017.12.008.

Cianciotto, N. P. et al. (1992) ‘*Legionella pneumophila* mip gene potentiates intracellular infection of protozoa and human macrophages.’, *Proceedings of the National Academy of Sciences of the United States of America*. National Academy of Sciences, 89(11), pp. 5188–91. doi: 10.1073/pnas.89.11.5188.

Clary, G. et al. (2018) ‘*Mycobacterium abscessus* smooth and rough morphotypes form antimicrobial-tolerant biofilm phenotypes but are killed by acetic acid’, *Antimicrobial Agents and Chemotherapy*, 62(3). doi: 10.1128/AAC.01782-17.

Collins, M. D., Goodfellow, M. and Minnikin, D. E. (1982) ‘A survey of the structures of mycolic acids in *Corynebacterium* and related taxa’, *Journal of General Microbiology*. Microbiology Society, 128(1), pp. 129–149. doi: 10.1099/00221287-128-1-129.

Connell, D. W. and Wilkie, M. (2019) ‘Pulmonary *Mycobacterium abscessus*: Can we identify the road to improved outcomes?’, *European Respiratory Journal*. European Respiratory Society. doi: 10.1183/13993003.01121-2019.

Cornforth, D. M. et al. (2018) ‘*Pseudomonas aeruginosa* transcriptome during human infection’, *Proceedings of the National Academy of Sciences of the United States of America*. National Academy of Sciences, 115(22), pp. E5125–E5134. doi: 10.1073/pnas.1717525115.

Cortes, M. A. M., Nessar, R. and Singh, A. K. (2010) ‘Laboratory maintenance of *Mycobacterium abscessus*’, *Current Protocols in Microbiology*, (SUPP.18). doi: 10.1002/9780471729259.mc10d01s18.

Costerton, J. W., Geesey, G. G. and Cheng, K. J. (1978) ‘How bacteria stick.’, *Scientific American*. doi: 10.1038/scientificamerican0178-86.

Costerton, J. W., Stewart, P. S. and Greenberg, E. P. (1999) ‘Bacterial biofilms: A common cause of persistent infections’, *Science*. doi: 10.1126/science.284.5418.1318.

Cullen, A. R. et al. (2000) ‘*Mycobacterium abscessus* infection in cystic fibrosis. Colonization or infection?’, *American journal of respiratory and critical care medicine*. American Thoracic Society New York, NY, 161(2 Pt 1), pp. 641–5. doi: 10.1164/ajrccm.161.2.9903062.

Cystic Fibrosis Foundation (2010) ‘Cystic Fibrosis Foundation Patient Registry, 2010 Annual Data Report’, *Cystic Fibrosis Foundation Publications*.

D’Andrea, M. M. and Lau, G. W. (2020) ‘DNABII targeting antibodies as vaccines against biofilm diseases’, *EBioMedicine*. Elsevier B.V., p. 102921. doi: 10.1016/j.ebiom.2020.102921.

Dal Molin, M. et al. (2018) ‘Molecular mechanisms of intrinsic streptomycin resistance in *Mycobacterium abscessus*’, *Antimicrobial Agents and Chemotherapy*. American Society for Microbiology, 62(1). doi: 10.1128/AAC.01427-17.

Daniel, J. et al. (2004) ‘Induction of a novel class of diacylglycerol acyltransferases and triacylglycerol accumulation in *Mycobacterium tuberculosis* as it goes into a dormancy-like state in culture’, *Journal of Bacteriology*. J Bacteriol, 186(15), pp. 5017–5030. doi: 10.1128/JB.186.15.5017-5030.2004.

Danilchanka, O., Mailaender, C. and Niederweis, M. (2008) ‘Identification of a novel multidrug efflux pump of *Mycobacterium tuberculosis*’, *Antimicrobial Agents and Chemotherapy*. Antimicrob Agents Chemother, 52(7), pp. 2503–2511. doi: 10.1128/AAC.00298-08.

Darouiche, R. O. (2004) ‘Treatment of Infections Associated with Surgical Implants’, *New England Journal of Medicine*. doi: 10.1056/nejmra035415.

Das, T. et al. (2010) ‘Role of extracellular DNA in initial bacterial adhesion and surface aggregation.’, *Applied and environmental microbiology*. American Society for Microbiology (ASM), 76(10), pp. 3405–8. doi: 10.1128/AEM.03119-09.

Davey, M. E. and O’tolle, G. A. (2000) ‘Microbial Biofilms: from Ecology to Molecular Genetics’, *Microbiology and Molecular Biology Reviews*. doi: 10.1128/mmbr.64.4.847-867.2000.

Davidson, R. M. (2018) ‘A closer look at the genomic variation of geographically diverse mycobacterium abscessus clones that cause human infection and disease’, *Frontiers in Microbiology*. doi: 10.3389/fmicb.2018.02988.

Denich, T. J. et al. (2003) ‘Effect of selected environmental and physico-chemical factors on bacterial cytoplasmic membranes’, *Journal of Microbiological Methods*. Elsevier, pp. 149–182. doi: 10.1016/S0167-7012(02)00155-0.

Deshayes, C. et al. (2010) ‘MmpS4 promotes glycopeptidolipids biosynthesis and export in *Mycobacterium smegmatis*’, *Molecular Microbiology*. Blackwell Publishing Ltd, 78(4), pp. 989–1003. doi: 10.1111/j.1365-2958.2010.07385.x.

Diel, R. et al. (2017) ‘Burden of non-tuberculous mycobacterial pulmonary disease in Germany’, *European Respiratory Journal*. doi: 10.1183/13993003.02109-2016.

Dinadayala, P. et al. (2008) ‘Comparative structural analyses of the α-glucan and glycogen from *Mycobacterium bovis*’, *Glycobiology*. doi: 10.1093/glycob/cwn031.

Dockrell, H. M. and Smith, S. G. (2017) ‘What have we learnt about BCG vaccination in the last 20 years?’, *Frontiers in Immunology*. Frontiers Media S.A. doi: 10.3389/fimmu.2017.01134.

Dong, D. et al. (2012) ‘PPE38 modulates the innate immune response and is required for *Mycobacterium marinum* virulence’, *Infection and Immunity*. Infect Immun, 80(1), pp. 43–54. doi: 10.1128/IAI.05249-11.

Donlan, R. M. (2002) *Biofilms: Microbial life on surfaces, Emerging Infectious Diseases*. Centers for Disease Control and Prevention. doi: 10.3201/eid0809.020063.

Dubée, V. et al. (2014) ‘β-Lactamase inhibition by avibactam in *Mycobacterium abscessus*’, *Journal of Antimicrobial Chemotherapy*. Oxford University Press, 70(4), pp. 1051–1058. doi: 10.1093/jac/dku510.

Dubois-Brissonnet, F., Trotier, E. and Briandet, R. (2016) ‘The biofilm lifestyle involves an increase in bacterial membrane saturated fatty acids’, *Frontiers in Microbiology*. Frontiers Media S.A., 7(OCT), p. 1673. doi: 10.3389/fmicb.2016.01673.

Dubois, V. et al. (2019) ‘*Mycobacterium abscessus* virulence traits unraveled by transcriptomic profiling in amoeba and macrophages’, *PLoS Pathogens*. doi: 10.1371/journal.ppat.1008069.

Esteban, J. and García-Coca, M. (2018) ‘Mycobacterium biofilms’, *Frontiers in Microbiology*. Frontiers, p. 2651. doi: 10.3389/fmicb.2017.02651.

Etienne, G. et al. (2009) ‘Identification of the polyketide synthase involved in the biosynthesis of the surface-exposed lipooligosaccharides in mycobacteria’, *Journal of Bacteriology*. doi: 10.1128/JB.01235-08.

Faria, S., Joao, I. and Jordao, L. (2015) ‘General Overview on Nontuberculous Mycobacteria, Biofilms, and Human Infection’, *Journal of Pathogens*. Hindawi, 2015, pp. 1–10. doi: 10.1155/2015/809014.

Fennelly, K. P. et al. (2016a) ‘Biofilm formation by *Mycobacterium abscessus* in a lung cavity’, *American Journal of Respiratory and Critical Care Medicine*. doi: 10.1164/rccm.201508-1586IM.

Fennelly, K. P. et al. (2016b) ‘Biofilm Formation by *Mycobacterium abscessus* in a Lung Cavity’, *American Journal of Respiratory and Critical Care Medicine*. American Thoracic Society, 193(6), pp. 692–693. doi: 10.1164/rccm.201508-1586IM.

Fishbein, S. et al. (2015) ‘Phylogeny to function: PE/PPE protein evolution and impact on *Mycobacterium tuberculosis* pathogenicity’, *Molecular Microbiology*. Blackwell Publishing Ltd, 96(5), pp. 901–916. doi: 10.1111/mmi.12981.

Flemming, H.-C. and Wingender, J. (2010) ‘The biofilm matrix’, *Nature Publishing Group*, 8. doi: 10.1038/nrmicro2415.

Flemming, H. C. et al. (2016) ‘Biofilms: An emergent form of bacterial life’, *Nature Reviews Microbiology*. doi: 10.1038/nrmicro.2016.94.

Flores-Valdez, M. A. et al. (2020) ‘Transcriptional portrait of *M. bovis* BCG during biofilm production shows genes differentially expressed during intercellular aggregation and substrate attachment’, *Scientific Reports*. doi: 10.1038/s41598-020-69152-2.

Flores, A. R., Parsons, L. M. and Pavelka, M. S. (2005) ‘Genetic analysis of the β-lactamases of *Mycobacterium tuberculosis* and *Mycobacterium smegmatis* and susceptibility to β-lactam antibiotics’, *Microbiology*. doi: 10.1099/mic.0.27629-0.

Folsom, J. P. et al. (2010) ‘Physiology of *Pseudomonas aeruginosa* in biofilms as revealed by transcriptome analysis’, *BMC Microbiology*. BioMed Central, 10, p. 294. doi: 10.1186/1471-2180-10-294.

Forrellad, M. A. et al. (2013) ‘Virulence factors of the mycobacterium tuberculosis complex’, *Virulence*. doi: 10.4161/viru.22329.

Francis, E. (1932) ‘Antony van Leeuwenhoek and his “Little Animals”’, *Science*. doi: 10.1126/science.76.1982.597.

Franklin, M. J. et al. (2015) ‘New Technologies for Studying Biofilms’, *Microbiology Spectrum*. American Society for Microbiology, 3(4). doi: 10.1128/microbiolspec.mb-0016-2014.

Furuya, E. Y. et al. (2008) ‘Outbreak of *Mycobacterium abscessus* Wound Infections among “Lipotourists” from the United States Who Underwent Abdominoplasty in the Dominican Republic’, *Clinical Infectious Diseases*, 46(8), pp. 1181–1188. doi: 10.1086/529191.

Fux, C. A. et al. (2005) ‘Can laboratory reference strains mirror “real-world” pathogenesis?’, *Trends in Microbiology*. doi: 10.1016/j.tim.2004.11.001.

Galassi, L. et al. (2003) ‘Nontuberculous mycobacteria in hospital water systems: Application of HPLC for identification of environmental mycobacteria’, *Journal of Water and Health*, 1(3), pp. 133–139.

Gao, L. Y. *et al.* (2003) ‘Requirement for kasB in mycobacterium mycolic acid biosynthesis, cell wall impermeability and intracellular survival: Implications for therapy’, *Molecular Microbiology*. doi: 10.1046/j.1365-2958.2003.03667.x.

García-Coca, M. *et al.* (2020) ‘Inhibition of *Mycobacterium abscessus*, *M. chelonae*, and *M. fortuitum* biofilms by Methylobacterium sp’, *Journal of Antibiotics*. doi: 10.1038/s41429-019-0232-6.

García-Fernández, J. *et al.* (2017) ‘Molecular and functional analysis of the mce4 operon in *Mycobacterium smegmatis*’, *Environmental Microbiology*. doi: 10.1111/1462-2920.13869.

Gebert, M. J. *et al.* (2018) ‘Ecological Analyses of Mycobacteria in Showerhead Biofilms and Their Relevance to Human Health’, *mBio*. doi: 10.1128/mBio.01614-18.

Ghosh, S., Indi, S. S. and Nagaraja, V. (2013) ‘Regulation of lipid biosynthesis, sliding motility, and biofilm formation by a membrane-anchored nucleoid-associated protein of *Mycobacterium tuberculosis*’, *Journal of Bacteriology*. doi: 10.1128/JB.02081-12.

Giffin, M. M. *et al.* (2016) ‘Role of Alanine Dehydrogenase of *Mycobacterium tuberculosis* during Recovery from Hypoxic Nonreplicating Persistence’, *PLoS ONE*. doi: 10.1371/journal.pone.0155522.

Glickman, M. S., Cox, J. S. and Jacobs, W. R. (2000) ‘A Novel Mycolic Acid Cyclopropane Synthetase Is Required for Cording, Persistence, and Virulence of *Mycobacterium tuberculosis*’, *Molecular Cell*, 5(4), pp. 717–727. doi: 10.1016/S1097-2765(00)80250-6.

Gloag, E. S. *et al.* (2021) ‘*Mycobacterium abscessus* biofilms have viscoelastic properties which may contribute to their recalcitrance in chronic pulmonary infections’, *Scientific Reports*. doi: 10.1038/s41598-021-84525-x.

González-Machado, C. *et al.* (2018) ‘Visualization and quantification of the cellular and extracellular components of salmonella agona biofilms at different stages of development’, *PLoS ONE*. doi: 10.1371/journal.pone.0200011.

González, J. F., Hahn, M. M. and Gunn, J. S. (2018) ‘Chronic biofilm-based infections: Skewing of the immune response’, *Pathogens and Disease*. Oxford University Press, p. 23. doi: 10.1093/femspd/fty023.

Goodfellow, M. (2012) ‘Phylum XXVI. Actinobacteria phyl. nov.’, in *Bergey’s Manual® of Systematic Bacteriology*. doi: 10.1007/978-0-387-68233-4\_3.

Goring, S. M. *et al.* (2018) ‘The cost of *Mycobacterium avium* complex lung disease in Canada, France, Germany, and the United Kingdom: a nationally representative observational study’, *BMC health services research*. doi: 10.1186/s12913-018-3489-8.

Greendyke, R. and Byrd, T. F. (2008) ‘Differential antibiotic susceptibility of *Mycobacterium abscessus* variants in biofilms and macrophages compared to that of planktonic bacteria’, *Antimicrobial Agents and Chemotherapy*. American Society for Microbiology (ASM), 52(6), pp. 2019–2026. doi: 10.1128/AAC.00986-07.

Greene, J. B. *et al.* (1982) ‘*Mycobacterium avium*-intracellulare: a cause of disseminated life-threatening infection in homosexuals and drug abusers.’, *Annals of internal medicine*, 97(4), pp. 539–46.

Griffith, D. E. *et al.* (2007) ‘An official ATS/IDSA statement: Diagnosis, treatment, and prevention of non tuberculous mycobacterial diseases’, *American Journal of Respiratory and Critical Care Medicine*. American Thoracic Society, pp. 367–416. doi: 10.1164/rccm.200604-571ST.

Griffith, D. E. *et al.* (2015) ‘*Mycobacterium abscessus*: “Pleased to meet you, hope you guess my name???”’, *Annals of the American Thoracic Society*. American Thoracic Society, pp. 436–439. doi: 10.1513/AnnalsATS.201501-015OI.

Gutiérrez, A. V. *et al.* (2018) ‘Glycopeptidolipids, a double-edged sword of the *Mycobacterium abscessus* complex’, *Frontiers in Microbiology*. Frontiers Media S.A. doi: 10.3389/fmicb.2018.01145.

Gutiérrez, A. V. *et al.* (2021) ‘Beyond phenotype: The genomic heterogeneity of co-infecting *Mycobacterium abscessus* smooth and rough colony variants in cystic fibrosis patients’, *Journal of Cystic Fibrosis*. Elsevier B.V., 20(3), pp. 421–423. doi: 10.1016/j.jcf.2021.02.002.

Haites, R. E. *et al.* (2005) ‘Function of phosphatidylinositol in mycobacteria’, *Journal of Biological Chemistry*. doi: 10.1074/jbc.M413443200.

Haley, C. L., Colmer-Hamood, J. A. and Hamood, A. N. (2012) ‘Characterization of biofilm-like structures formed by *Pseudomonas aeruginosa* in a synthetic mucus medium’, *BMC Microbiology*, 12(1), p. 181. doi: 10.1186/1471-2180-12-181.

Halkerston, R. *et al.* (2020) ‘The role of mature mycolic acids in mycobacterial biofilm formation and interactions with the human complement system’, *Access Microbiology*. Microbiology Society, 2(1), p. 38. doi: 10.1099/acmi.mim2019.po0006.

Hall-Stoodley, L., Keevil, C. W. and Lappin-Scott, H. M. (1999) ‘*Mycobacterium fortuitum* and *Mycobacterium chelonae* biofilm formation under high and low nutrient conditions.’, *Journal of applied microbiology*, 85 Suppl 1, pp. 60S-69S. doi: 10.1111/j.1365-2672.1998.tb05284.x.

Hall-Stoodley, L. and Lappin-Scott, H. (1998) ‘Biofilm formation by the rapidly growing mycobacterial species *Mycobacterium fortuitum*’, *FEMS Microbiology Letters*. doi: 10.1016/S0378-1097(98)00422-4.

Hall-Stoodley, L. and Stoodley, P. (2005) ‘Biofilm formation and dispersal and the transmission of human pathogens’, *Trends in Microbiology*, 13(1), pp. 7–10. doi: 10.1016/j.tim.2004.11.004.

Halloum, I. *et al.* (2016) ‘Deletion of a dehydratase important for intracellular growth and cording renders rough *Mycobacterium abscessus* avirulent.’, *Proceedings of the National Academy of Sciences of the United States of America*. National Academy of Sciences, 113(29), pp. E4228–E4237. doi: 10.1073/pnas.1605477113.

Harada, T. *et al.* (2012) ‘Clinical and microbiological differences between *Mycobacterium abscessus* and *Mycobacterium massiliense* lung diseases’, *Journal of Clinical Microbiology*. doi: 10.1128/JCM.01175-12.

Harmsen, M. *et al.* (2010) ‘Role of extracellular DNA during biofilm formation by *Listeria monocytogenes*’, *Applied and Environmental Microbiology*, 76(7), pp. 2271–2279. doi: 10.1128/AEM.02361-09.

Haworth, C. S. *et al.* (2017) ‘British Thoracic Society guidelines for the management of non-tuberculous mycobacterial pulmonary disease (NTM-PD)’, *Thorax*. BMJ Publishing Group, pp. ii1–ii64. doi: 10.1136/thoraxjnl-2017-210927.

Head, N. E. and Yu, H. (2004) ‘Cross-Sectional Analysis of Clinical and Environmental Isolates of *Pseudomonas aeruginosa*: Biofilm Formation, Virulence, and Genome Diversity’, *Infection and Immunity*. doi: 10.1128/IAI.72.1.133-144.2004.

Hegde, S. R. (2020) ‘Computational Identification of the Proteins Associated With Quorum Sensing and Biofilm Formation in *Mycobacterium tuberculosis*’, *Frontiers in Microbiology*. Frontiers Media S.A., 10, p. 3011. doi: 10.3389/fmicb.2019.03011.

El Helou, G. *et al.* (2013) ‘Rapidly growing mycobacterial bloodstream infections’, *The Lancet Infectious Diseases*. Lancet Infect Dis, 13(2), pp. 166–174. doi: 10.1016/S1473-3099(12)70316-X.

Hengge, R. (2009) ‘Principles of c-di-GMP signalling in bacteria’, *Nature Reviews Microbiology*. Nature Publishing Group, pp. 263–273. doi: 10.1038/nrmicro2109.

Hernández-Garduño, E. and Elwood, R. K. (2010) ‘Increasing incidence of nontuberculous mycobacteria, Taiwan, 2000–2008’, *Emerging Infectious Diseases*. Centers for Disease Control and Prevention, p. 1047. doi: 10.3201/eid1606.100228.

Hoefsloot, W. *et al.* (2013) ‘The geographic diversity of nontuberculous mycobacteria isolated from pulmonary samples: An NTM-NET collaborative study’, *European Respiratory Journal*, 42(6), pp. 1604–1613. doi: 10.1183/09031936.00149212.

Holland, S. P. *et al.* (1991) ‘Biofilm and Scleral Buckle-associated Infections: A Mechanism for Persistence’, *Ophthalmology*. doi: 10.1016/S0161-6420(91)32199-7.

Howard, S. T. *et al.* (2006) ‘Spontaneous reversion of *Mycobacterium abscessus* from a smooth to a rough

morphotype is associated with reduced expression of glycopeptidolipid and reacquisition of an invasive phenotype', *Microbiology*. Microbiology Society, 152(6), pp. 1581–1590. doi: 10.1099/mic.0.28625-0.

Hung, C. et al. (2013) 'Escherichia coli biofilms have an organized and complex extracellular matrix structure', *mBio*. doi: 10.1128/mBio.00645-13.

Hunt-Serracin, A. C. et al. (2019) 'Mycobacterium abscessus cells have altered antibiotic tolerance and surface glycolipids in artificial cystic fibrosis sputum medium', *Antimicrobial Agents and Chemotherapy*. doi: 10.1128/AAC.02488-18.

Hurst-Hess, K., Rudra, P. and Ghosh, P. (2017) 'Mycobacterium abscessus WhiB7 regulates a species-specific repertoire of genes to confer extreme antibiotic resistance', *Antimicrobial Agents and Chemotherapy*, 61(11). doi: 10.1128/AAC.01353-17.

Huttner, A. et al. (2020) 'Oral amoxicillin and amoxicillin-clavulanic acid: properties, indications and usage', *Clinical Microbiology and Infection*. Elsevier B.V., pp. 871–879. doi: 10.1016/j.cmi.2019.11.028.

Ibáñez de Aldecoa, A. L., Zafra, O. and González-Pastor, J. E. (2017) 'Mechanisms and regulation of extracellular DNA release and its biological roles in microbial communities', *Frontiers in Microbiology*. doi: 10.3389/fmicb.2017.01390.

van Ingen, J. (2014) 'Section 8: Clinical Microbiology: Bacteria', *Clinical Microbiology: Bacteria*, pp. 1565–1578. doi: 10.1016/B978-0-7020-6285-8.00180-5.

Islam, M. S., Richards, J. P. and Ojha, A. K. (2012) 'Targeting drug tolerance in mycobacteria: a perspective from mycobacterial biofilms', *Expert Rev Anti Infect Ther*, 10(9), pp. 1055–1066. doi: 10.1586/eri.12.88.

Jackson, M. (2014) 'The mycobacterial cell envelope-lipids', *Cold Spring Harbor Perspectives in Medicine*. Cold Spring Harbor Laboratory Press, 4(10). doi: 10.1101/cshperspect.a021105.

Jamal, M. et al. (2018) 'Bacterial biofilm and associated infections', *Journal of the Chinese Medical Association*. doi: 10.1016/j.jcma.2017.07.012.

Jankute, M. et al. (2015) 'Assembly of the Mycobacterial Cell Wall.', *Annual review of microbiology*. Annual Reviews, 69(1), pp. 405–23. doi: 10.1146/annurev-micro-091014-104121.

Jiao, X. et al. (2012) 'DAVID-WS: a stateful web service to facilitate gene/protein list analysis', *Bioinformatics*. Oxford Academic, 28(13), pp. 1805–1806. doi: 10.1093/bioinformatics/bts251.

Johansen, M. D., Herrmann, J. L. and Kremer, L. (2020) 'Non-tuberculous mycobacteria and the rise of *Mycobacterium abscessus*', *Nature Reviews Microbiology*. Nature Research, pp. 392–407. doi: 10.1038/s41579-020-0331-1.

Jönsson, B. E. et al. (2007) 'Molecular epidemiology of *Mycobacterium abscessus*, with focus on cystic fibrosis', *Journal of Clinical Microbiology*, 45(5), pp. 1497–1504. doi: 10.1128/JCM.02592-06.

Jorgensen, J. H. H. et al. (2009) 'Antimicrobial susceptibility testing: A review of general principles and contemporary practices', *Clinical Infectious Diseases*, 49(11), pp. 1749–1755. doi: 10.1086/647952.

Julian, E. et al. (2010) 'Microscopic Cords, a Virulence-Related Characteristic of *Mycobacterium tuberculosis*, Are Also Present in Nonpathogenic Mycobacteria', *JOURNAL OF BACTERIOLOGY*, 192(7), pp. 1751–1760. doi: 10.1128/JB.01485-09.

Justice, S. S. et al. (2004) 'Differentiation and developmental pathways of uropathogenic *Escherichia coli* in urinary tract pathogenesis', *Proceedings of the National Academy of Sciences of the United States of America*. doi: 10.1073/pnas.0308125100.

Kadota, N. et al. (2019) 'Mycobacterium abscessus ssp. abscessus infection progressing to empyema from vertebral osteomyelitis in an immunocompetent patient without pulmonary disease: A case report', *BMC Pulmonary Medicine*. BioMed Central Ltd., 19(1), pp. 1–5. doi: 10.1186/s12890-019-0860-4.

Kalsum, S. et al. (2017) 'The cording phenotype of *Mycobacterium tuberculosis* induces the formation of

extracellular traps in human macrophages', *Frontiers in Cellular and Infection Microbiology*. doi: 10.3389/fcimb.2017.00278.

Kapopoulou, A., Lew, J. M. and Cole, S. T. (2011) 'The MycoBrowser portal: A comprehensive and manually annotated resource for mycobacterial genomes', *Tuberculosis*. doi: 10.1016/j.tube.2010.09.006.

Karygianni, L. et al. (2020) 'Biofilm Matrixome: Extracellular Components in Structured Microbial Communities', *Trends in Microbiology*. doi: 10.1016/j.tim.2020.03.016.

Karygianni, L., Attin, T. and Thurnheer, T. (2020) 'Combined DNase and Proteinase Treatment Interferes with Composition and Structural Integrity of Multispecies Oral Biofilms', *Journal of Clinical Medicine*. MDPI AG, 9(4), p. 983. doi: 10.3390/jcm9040983.

Kasperbauer, S. H. and De Groote, M. A. (2015) 'The treatment of rapidly growing mycobacterial infections', *Clinics in Chest Medicine*. doi: 10.1016/j.ccm.2014.10.004.

Kim, B.-R. et al. (2019) 'Phagosome Escape of Rough *Mycobacterium abscessus* Strains in Murine Macrophage via Phagosomal Rupture Can Lead to Type I Interferon Production and Their Cell-To-Cell Spread', *Frontiers in Immunology*, 10, p. 125. doi: 10.3389/fimmu.2019.00125.

Kim, Byoung Jun et al. (2013) 'Rough colony morphology of *Mycobacterium massiliense* Type II genotype is due to the deletion of glycopeptidolipid locus within its genome', *BMC Genomics*, 14(1). doi: 10.1186/1471-2164-14-890.

Kim, H. Y. et al. (2008) 'Proportions of *Mycobacterium massiliense* and *Mycobacterium bolletii* strains among Korean *Mycobacterium chelonae*-*Mycobacterium abscessus* group isolates', *Journal of Clinical Microbiology*, 46(10), pp. 3384–3390. doi: 10.1128/JCM.00319-08.

Kim, H. Y. et al. (2010) '*Mycobacterium massiliense* is differentiated from *mycobacterium abscessus* and *mycobacterium bolletii* by erythromycin ribosome methyltransferase gene (*erm*) and clarithromycin susceptibility patterns', *Microbiology and Immunology*, 54(6), pp. 347–353. doi: 10.1111/j.1348-0421.2010.00221.x.

Kim, S. Y. et al. (2015) 'The drug susceptibility profile and inducible resistance to macrolides of *Mycobacterium abscessus* and *Mycobacterium massiliense* in Korea', *Diagnostic Microbiology and Infectious Disease*. BioMed Central, 81(2), pp. 107–111. doi: 10.1016/j.diagmicrobio.2014.10.007.

Kinane, D. F., Stathopoulou, P. G. and Papapanou, P. N. (2017) 'Periodontal diseases', *Nature Reviews Disease Primers*. doi: 10.1038/nrdp.2017.38.

Klepp, L. I. et al. (2012) 'Impact of the deletion of the six mce operons in *Mycobacterium smegmatis*', *Microbes and Infection*. doi: 10.1016/j.micinf.2012.01.007.

Koh, S. J. et al. (2010) 'An outbreak of skin and soft tissue infection caused by *Mycobacterium abscessus* following acupuncture', *Clinical Microbiology and Infection*. doi: 10.1111/j.1469-0912.2009.03026.x.

Koh, W.-J. et al. (2011) 'Clinical Significance of Differentiation of *Mycobacterium massiliense* from *Mycobacterium abscessus*', *American Journal of Respiratory and Critical Care Medicine*, 183(3), pp. 405–410. doi: 10.1164/rccm.201003-0395OC.

Kolpen, M. et al. (2020) 'Biofilms of *Mycobacterium abscessus* complex can be sensitized to antibiotics by disaggregation and oxygenation', *Antimicrobial Agents and Chemotherapy*. doi: 10.1128/AAC.01212-19.

Koo, H., Falsetta, M. L. and Klein, M. I. (2013) 'The Exopolysaccharide Matrix: A Virulence Determinant of Cariogenic Biofilm', *Journal of Dental Research*. International Association for Dental Research, 92(12), pp. 1065–1073. doi: 10.1177/0022034513504218.

Koskineni, S. et al. (2012) 'Selection-driven gene loss in bacteria', *PLoS Genetics*. doi: 10.1371/journal.pgen.1002787.

Kreutzfeldt, K. M. et al. (2013) 'Molecular Longitudinal Tracking of *Mycobacterium abscessus* spp. during Chronic Infection of the Human Lung', *PLoS ONE*. Public Library of Science, 8(5), p. e63237. doi: 10.1371/journal.pone.0063237.

Kuchina, A. et al. (2021) 'Microbial single-cell RNA sequencing by split-pool barcoding', *Science*. American Association for the Advancement of Science, 371(6531). doi: 10.1126/science.aba5257.

Kuo, Y. M. et al. (2011) 'Disseminated *Mycobacterium abscessus* infection and showerheads, Taiwan', *Emerging Infectious Diseases*. Centers for Disease Control and Prevention (CDC), pp. 2077–2078. doi: 10.3201/eid1711.110050.

Kusunoki, S. and Ezaki, T. (1992) 'Proposal of *Mycobacterium peregrinum* sp. nov., nom. rev., and Elevation of *Mycobacterium chelonae* subsp. *abscessus* (Kubica et al.) to Species Status: *Mycobacterium abscessus* comb. nov.', *International Journal of Systematic Bacteriology*, 42(2), pp. 240–245. doi: 10.1099/00207713-42-2-240.

Kwak, N. et al. (2019) 'Mycobacterium abscessus' pulmonary disease: Individual patient data meta-analysis', *European Respiratory Journal*. doi: 10.1183/13993003.01991-2018.

Laencina, L. et al. (2018) 'Identification of genes required for *Mycobacterium abscessus* growth in vivo with a prominent role of the ESX-4 locus', *Proceedings of the National Academy of Sciences of the United States of America*. doi: 10.1073/pnas.1713195115.

Lauková, L. et al. (2020) 'Deoxyribonucleases and their applications in biomedicine', *Biomolecules*. MDPI AG, pp. 1–20. doi: 10.3390/biom10071036.

Lawrence, J. R. et al. (1991) 'Optical sectioning of microbial biofilms', *Journal of Bacteriology*. doi: 10.1128/jb.173.20.6558-6567.1991.

Lee, J. H. et al. (2011) 'Transcriptomic analysis for genetic mechanisms of the factors related to biofilm formation in *Escherichia coli* O157:H7', *Current Microbiology*. doi: 10.1007/s00284-010-9862-4.

Lee, M. R. et al. (2012) 'CNS infections caused by *Mycobacterium abscessus* complex: clinical features and antimicrobial susceptibilities of isolates', *Journal of Antimicrobial Chemotherapy*. doi: 10.1093/jac/dkr420.

Lee, M. R. et al. (2015) 'Mycobacterium abscessus complex infections in humans', *Emerging Infectious Diseases*. Centers for Disease Control and Prevention, 21(9), pp. 1638–1646. doi: 10.3201/eid2109.141634.

Lemassu, A., Ortalo-Magné, A., Bardou, F., Silve, G., Lanéelle, M. A. and Daffé, M. (1996) 'Extracellular and surface-exposed polysaccharides of non-tuberculous mycobacteria', *Microbiology*. doi: 10.1099/13500872-142-6-1513.

Lemassu, A., Ortalo-Magné, A., Bardou, F., Silve, G., Lanéelle, M. A., Daffé, M., et al. (1996) 'Extracellular and surface-exposed polysaccharides of non-tuberculous mycobacteria', *Microbiology*. Microbiology Society, 142(6), pp. 1513–1520. doi: 10.1099/13500872-142-6-1513.

Lemassu, A. and Daffé, M. (1994) 'Structural features of the exocellular polysaccharides of *Mycobacterium tuberculosis*', *Biochemical Journal*, 297(2), pp. 351–357. doi: 10.1042/bj2970351.

Lewis, K. (2001) 'Riddle of biofilm resistance', *Antimicrobial Agents and Chemotherapy*. doi: 10.1128/AAC.45.4.999-1007.2001.

Li, M. et al. (2020) 'The Two-Component Locus MSMEG\_0244/0246 Together With MSMEG\_0243 Affects Biofilm Assembly in *M. smegmatis* Correlating With Changes in Phosphatidylinositol Mannosides Acylation', *Frontiers in Microbiology*. Frontiers Media S.A., 11. doi: 10.3389/fmicb.2020.570606.

Limoli, D. H., Jones, C. J. and Wozniak, D. J. (2015) 'Bacterial Extracellular Polysaccharides in Biofilm Formation and Function.', *Microbiology spectrum*. NIH Public Access, 3(3). doi: 10.1128/microbiolspec.MB-0011-2014.

Liu, Z. et al. (2014) 'Study on the promotion of bacterial biofilm formation by a salmonella conjugative plasmid and the underlying mechanism', *PLoS ONE*. doi: 10.1371/journal.pone.0109808.

Llorens-Fons, M. et al. (2017) 'Trehalose polyphleates, external cell wall lipids in *Mycobacterium abscessus*, are associated with the formation of clumps with cording morphology, which have been associated with virulence', *Frontiers in Microbiology*. doi: 10.3389/fmicb.2017.01402.

- Love, M. I., Huber, W. and Anders, S. (2014) ‘Moderated estimation of fold change and dispersion for RNA-seq data with DESeq2’, *Genome Biology*. BioMed Central Ltd., 15(12), p. 550. doi: 10.1186/s13059-014-0550-8.
- Luca, S. and Mihaescu, T. (2013) ‘History of BCG Vaccine.’, *Maedica*. Amaltea Medical, Editura Magister, 8(1), pp. 53–8.
- Luthra, S., Rominski, A. and Sander, P. (2018) ‘The role of antibiotic-target-modifying and antibiotic-modifying enzymes in *Mycobacterium abscessus* drug resistance’, *Frontiers in Microbiology*. Frontiers Media S.A., p. 2179. doi: 10.3389/fmicb.2018.02179.
- Marjanovic, O., Iavarone, A. T. and Riley, L. W. (2011) ‘Sulfolipid accumulation in *Mycobacterium tuberculosis* disrupted in the mce2 operon’, *Journal of Microbiology*. doi: 10.1007/s12275-011-0435-4.
- Marrakchi, H., Lanéelle, M. A. and Daffé, M. (2014) ‘Mycolic acids: Structures, biosynthesis, and beyond’, *Chemistry and Biology*, pp. 67–85. doi: 10.1016/j.chembiol.2013.11.011.
- Marsollier, L. et al. (2007) ‘Impact of *Mycobacterium ulcerans* biofilm on transmissibility to ecological niches and Buruli ulcer pathogenesis’, *PLoS Pathogens*. doi: 10.1371/journal.ppat.0030062.
- Martín-de-Hijas, N. Z. et al. (2009) ‘Biofilm development by clinical strains of non-pigmented rapidly growing mycobacteria.’, *Clinical microbiology and infection : the official publication of the European Society of Clinical Microbiology and Infectious Diseases*, 15(10), pp. 931–936. doi: 10.1111/j.1469-0691.2009.02882.x.
- Martínez, L. C. and Vadyvaloo, V. (2014) ‘Mechanisms of post-transcriptional gene regulation in bacterial biofilms.’, *Frontiers in cellular and infection microbiology*. Frontiers Media SA, 4, p. 38. doi: 10.3389/fcimb.2014.00038.
- Mase, A. et al. (2019) ‘PCR amplification of the erm(41) gene can be used to predict the sensitivity of *Mycobacterium abscessus* complex strains to clarithromycin’, *Experimental and Therapeutic Medicine*. doi: 10.3892/etm.2019.8289.
- Maurya, R. K., Bharti, S. and Krishnan, M. Y. (2019) ‘Triacylglycerols: Fuelling the hibernating *Mycobacterium tuberculosis*’, *Frontiers in Cellular and Infection Microbiology*. doi: 10.3389/fcimb.2018.00450.
- McKinney, J. D. et al. (2000) ‘Persistence of *Mycobacterium tuberculosis* in macrophages and mice requires the glyoxylate shunt enzyme isocitrate lyase’, *Nature*. doi: 10.1038/35021074.
- Medjahed, H., Gaillard, J. L. and Reyrat, J. M. (2010) ‘*Mycobacterium abscessus*: a new player in the mycobacterial field’, *Trends in Microbiology*, pp. 117–123. doi: 10.1016/j.tim.2009.12.007.
- Medjahed, H. and Reyrat, J. M. (2009) ‘Construction of *Mycobacterium abscessus* defined glycopeptidolipid mutants: Comparison of genetic tools’, *Applied and Environmental Microbiology*. American Society for Microbiology (ASM), 75(5), pp. 1331–1338. doi: 10.1128/AEM.01914-08.
- Menozzi, F. D. et al. (1996) ‘Identification of a heparin-binding hemagglutinin present in mycobacteria’, *Journal of Experimental Medicine*. doi: 10.1084/jem.184.3.993.
- Middlebrook, G., Dubos, R. J. and Pierce, C. (1947) ‘VIRULENCE AND MORPHOLOGICAL CHARACTERISTICS OF MAMMALIAN TUBERCLE BACILLI.’, *The Journal of experimental medicine*. doi: 10.1084/jem.86.2.175.
- Minnikin, D. E. et al. (1982) ‘The Mycolic Acids of *Mycobacterium chelonei*’, *Microbiology*. Microbiology Society, 128(4), pp. 817–822. doi: 10.1099/00221287-128-4-817.
- Miranda-CasoLuengo, A. A. et al. (2016) ‘Functional characterization of the *Mycobacterium abscessus* genome coupled with condition specific transcriptomics reveals conserved molecular strategies for host adaptation and persistence’, *BMC Genomics*, 17(1), p. 553. doi: 10.1186/s12864-016-2868-y.
- Le Moigne, V. et al. (2019) ‘Lsr2 is an important determinant of intracellular growth and virulence in *Mycobacterium abscessus*’, *Frontiers in Microbiology*. Frontiers Media S.A., 10(APR), p. 905. doi: 10.3389/fmicb.2019.00905.

Moore, J. E. et al. (2010) 'Increasing reports of non-tuberculous mycobacteria in England, Wales and Northern Ireland, 1995–2006', *BMC Public Health*. doi: 10.1186/1471-2458-10-612.

Moore, M. and Frerichs, J. B. (1953) 'An unusual acid-fast infection of the knee with subcutaneous, abscess-like lesions of the gluteal region; report of a case with a study of the organism, *Mycobacterium abscessus*, n. sp', *The Journal of investigative dermatology*, 20(2), pp. 133–169. doi: 10.1038/jid.1953.18.

Moorthy, R. S., Valluri, S. and Rao, N. A. (2012) 'Nontuberculous Mycobacterial Ocular and Adnexal Infections', *Survey of Ophthalmology*. doi: 10.1016/j.survophthal.2011.10.006.

Muñoz-Egea, M. C. et al. (2015) 'Effect of ciprofloxacin in the ultrastructure and development of biofilms formed by rapidly growing mycobacteria', *BMC Microbiology*. doi: 10.1186/s12866-015-0359-y.

Murakawa, T. (1973) 'Slime Production by *Pseudomonas aeruginosa* IV. Chemical Analysis of Two Varieties of Slime Produced by *Pseudomonas aeruginosa*', *Japanese Journal of Microbiology*. Jpn J Microbiol, 17(6), pp. 513–520. doi: 10.1111/j.1348-0421.1973.tb00937.x.

Nash, K. A. et al. (2009) 'A Novel gene, erm(41), confers inducible macrolide resistance to clinical isolates of *Mycobacterium abscessus* but is absent from *Mycobacterium chelonae*', *Antimicrobial Agents and Chemotherapy*, 53(4), pp. 1367–1376. doi: 10.1128/AAC.01275-08.

Nataraj, V. et al. (2015) 'Mycolic acids: Deciphering and targeting the Achilles' heel of the tubercle bacillus', *Molecular Microbiology*, 98(1), pp. 7–16. doi: 10.1111/mmi.13101.

Nemoto, K. et al. (2003) 'Effect of Varidase (streptodornase) on biofilm formed by *Pseudomonas aeruginosa*', *Chemotherapy*. Chemotherapy, 49(3), pp. 121–125. doi: 10.1159/000070617.

Nessar, R. et al. (2011) 'Deletion of the mmpL4b gene in the *Mycobacterium abscessus* glycopeptidolipid biosynthetic pathway results in loss of surface colonization capability, but enhanced ability to replicate in human macrophages and stimulate their innate immune response', *Microbiology*. doi: 10.1099/mic.0.046557-0.

Nessar, R. et al. (2012) '*Mycobacterium abscessus*: A new antibiotic nightmare', *Journal of Antimicrobial Chemotherapy*, 67(4), pp. 810–818. doi: 10.1093/jac/dkr578.

Nie, W. et al. (2014) 'Species identification of *Mycobacterium abscessus* subsp. *abscessus* and *Mycobacterium abscessus* subsp. *bolletii* using rpoB and hsp65, and susceptibility testing to eight antibiotics', *International Journal of Infectious Diseases*, 25, pp. 170–174. doi: 10.1016/j.ijid.2014.02.014.

Nie, W. et al. (2015) 'Species Identification and Clarithromycin Susceptibility Testing of 278 Clinical Nontuberculosis Mycobacteria Isolates', *BioMed Research International*. Hindawi Limited, 2015. doi: 10.1155/2015/506598.

Novosad, S. A. et al. (2016) 'Treatment of *Mycobacterium abscessus* infection', *Emerging Infectious Diseases*. doi: 10.3201/eid2203.150828.

Ogunremi, T. et al. (2017) 'Mycobacterium chimaera infections in post-operative patients exposed to heater-cooler devices: An overview', *Canada Communicable Disease Report*. doi: 10.14745/ccdr.v43i05a05.

Ojha, A. et al. (2005) 'GroEL1: A dedicated chaperone involved in mycolic acid biosynthesis during biofilm formation in mycobacteria', *Cell*, 123(5), pp. 861–873. doi: 10.1016/j.cell.2005.09.012.

Ojha, A. K. et al. (2008) 'Growth of *Mycobacterium tuberculosis* biofilms containing free mycolic acids and harbouring drug-tolerant bacteria', *Molecular Microbiology*. Wiley-Blackwell, 69(1), pp. 164–174. doi: 10.1111/j.1365-2958.2008.06274.x.

Ojha, A. K. et al. (2010) 'Enzymatic hydrolysis of trehalose dimycolate releases free mycolic acids during mycobacterial growth in biofilms', *Journal of Biological Chemistry*, 285(23), pp. 17380–17389. doi: 10.1074/jbc.M110.112813.

Ojha, A. K., Varma, S. and Chatterji, D. (2002) 'Synthesis of an unusual polar glyopeptidolipid in glucose-limited culture of *Mycobacterium smegmatis*', *Microbiology*. doi: 10.1099/00221287-148-10-3039.

Okshevsky, M. and Meyer, R. L. (2015) 'The role of extracellular DNA in the establishment, maintenance and perpetuation of bacterial biofilms', *Critical Reviews in Microbiology*. doi: 10.3109/1040841X.2013.841639.

Ommen, P., Zobek, N. and Meyer, R. L. (2017) 'Quantification of biofilm biomass by staining: Non-toxic safranin can replace the popular crystal violet', *Journal of Microbiological Methods*. Elsevier B.V., 141, pp. 87–89. doi: 10.1016/j.mimet.2017.08.003.

Ortalo-Magne, A. et al. (1995) 'Molecular composition of the outermost capsular material of the tubercle bacillus', *Microbiology*. Microbiology Society, 141(7), pp. 1609–1620. doi: 10.1099/13500872-141-7-1609.

Pacheco, S. A. et al. (2013) 'MmpL11 protein transports mycolic acid-containing lipids to the mycobacterial cell wall and contributes to biofilm formation in *Mycobacterium smegmatis*', *Journal of Biological Chemistry*. American Society for Biochemistry and Molecular Biology, 288(33), pp. 24213–24222. doi: 10.1074/jbc.M113.473371.

Pakkulnan, R. et al. (2019) 'Extracellular DNA facilitates bacterial adhesion during *Burkholderia pseudomallei* biofilm formation', *PLoS ONE*. doi: 10.1371/journal.pone.0213288.

Palmer, R. J. and Sternberg, C. (1999) 'Modern microscopy in biofilm research: Confocal microscopy and other approaches', *Current Opinion in Biotechnology*. doi: 10.1016/S0958-1669(99)80046-9.

Pang, J. M. et al. (2012) 'The polyketide pks1 contributes to biofilm formation in *Mycobacterium tuberculosis*', *Journal of Bacteriology*. doi: 10.1128/JB.06304-11.

Papenfort, K. et al. (2015) 'Differential RNA-seq of *Vibrio cholerae* identifies the VqmR small RNA as a regulator of biofilm formation', *Proceedings of the National Academy of Sciences of the United States of America*. National Academy of Sciences, 112(7), pp. E766–E775. doi: 10.1073/pnas.1500203112.

Park, I. K. et al. (2015) 'Clonal Diversification and Changes in Lipid Traits and Colony Morphology in *Mycobacterium abscessus* Clinical Isolates.', *Journal of clinical microbiology*. American Society for Microbiology, 53(11), pp. 3438–47. doi: 10.1128/JCM.02015-15.

Park, Y. S. et al. (2010) 'Rapid increase of non-tuberculous mycobacterial lung diseases at a tertiary referral hospital in South Korea', *International Journal of Tuberculosis and Lung Disease*.

Parsek, M. R. and Singh, P. K. (2003) 'Bacterial Biofilms: An Emerging Link to Disease Pathogenesis', *Annual Review of Microbiology*. Annu Rev Microbiol, pp. 677–701. doi: 10.1146/annurev.micro.57.030502.090720.

Pasricha, R. et al. (2014) 'The *Mycobacterium tuberculosis* recombinant LprN protein of mce4 operon induces Th-1 type response deleterious to protection in mice', *Pathogens and Disease*. doi: 10.1111/2049-632X.12200.

Pawlak, A. et al. (2013) 'Identification and characterization of the genetic changes responsible for the characteristic smooth-to-rough morphotype alterations of clinically persistent *Mycobacterium abscessus*', *Molecular Microbiology*. John Wiley & Sons, Ltd, 90(3), pp. 612–629. doi: 10.1111/mmi.12387.

Percival, S. L. and Williams, D. W. (2013) *Mycobacterium*. Second Edi, *Microbiology of Waterborne Diseases: Microbiological Aspects and Risks: Second Edition*. Second Edi. Elsevier. doi: 10.1016/B978-0-12-415846-7.00009-3.

Philley, J. V. and Griffith, D. E. (2015) 'Treatment of slowly growing mycobacteria', *Clinics in Chest Medicine*. doi: 10.1016/j.ccm.2014.10.005.

Phillips, M. S. and von Reyn, C. F. (2001) 'Nosocomial Infections Due to Nontuberculous Mycobacteria', *Clinical Infectious Diseases*. doi: 10.1086/323126.

Piersimoni, C. and Scarparo, C. (2009) 'Extrapulmonary infections associated with nontuberculous mycobacteria in immunocompetent persons', *Emerging Infectious Diseases*, pp. 1351–1358. doi: 10.3201/eid1509.081259.

Pirlar, R. F. et al. (2020) 'Combinatorial effects of antibiotics and enzymes against dual-species *Staphylococcus aureus* and *Pseudomonas aeruginosa* biofilms in the wound-like medium', *PLoS ONE*. Public Library of Science, 15(6), p. e0235093. doi: 10.1371/journal.pone.0235093.

Pisithkul, T. et al. (2019) 'Metabolic remodeling during biofilm development of *bacillus subtilis*', *mBio*. doi: 10.1128/mBio.00623-19.

Potts, M. (1994) 'Desiccation tolerance of prokaryotes', *Microbiological Reviews*. doi: 10.1128/mmbr.58.4.755-805.1994.

Poyntz, H. C. et al. (2014) 'Non-tuberculous mycobacteria have diverse effects on BCG efficacy against *Mycobacterium tuberculosis*', *Tuberculosis*. doi: 10.1016/j.tube.2013.12.006.

Prammananan, T. et al. (1998) 'A Single 16S Ribosomal RNA Substitution Is Responsible for Resistance to Amikacin and Other 2-Deoxystreptamine Aminoglycosides in *Mycobacterium abscessus* and *Mycobacterium chelonae*', *The Journal of Infectious Diseases*, 177(6), pp. 1573–1581. doi: 10.1086/515328.

Preece, C. L. et al. (2016) 'A novel culture medium for isolation of rapidly-growing mycobacteria from the sputum of patients with cystic fibrosis', *Journal of Cystic Fibrosis*. Elsevier B.V., 15(2), pp. 186–191. doi: 10.1016/j.jcf.2015.05.002.

Prevots, D. R. et al. (2010) 'Nontuberculous mycobacterial lung disease prevalence at four integrated health care delivery systems', *American Journal of Respiratory and Critical Care Medicine*, 182(7), pp. 970–976. doi: 10.1164/rccm.201002-0310OC.

Prevots, D. R. et al. (2017) 'Nontuberculous mycobacterial pulmonary disease: An increasing burden with substantial costs', *European Respiratory Journal*. European Respiratory Society. doi: 10.1183/13993003.00374-2017.

Pryjma, M. et al. (2017) 'Antagonism between front-line antibiotics clarithromycin and amikacin in the treatment of *Mycobacterium abscessus* infections is mediated by the whiB7 gene', *Antimicrobial Agents and Chemotherapy*. American Society for Microbiology, 61(11). doi: 10.1128/AAC.01347-17.

Purdy, G. E. et al. (2013) 'Characterization of mycobacterial triacylglycerols and monomeromycolyl diacylglycerols from *Mycobacterium smegmatis* biofilm by electrospray ionization multiple-stage and high-resolution mass spectrometry', *Analytical and Bioanalytical Chemistry*. doi: 10.1007/s00216-013-7179-4.

Qian, J. et al. (2020) 'Role of the PE/PPE Family in Host–Pathogen Interactions and Prospects for Anti-Tuberculosis Vaccine and Diagnostic Tool Design', *Frontiers in Cellular and Infection Microbiology*. Frontiers Media S.A., p. 743. doi: 10.3389/fcimb.2020.594288.

Quadri, L. E. N. et al. (1998) 'Identification of a *Mycobacterium tuberculosis* gene cluster encoding the biosynthetic enzymes for assembly of the virulence-conferring siderophore mycobactin', *Chemistry and Biology*. Elsevier Ltd, 5(11), pp. 631–645. doi: 10.1016/S1074-5521(98)90291-5.

Queiroz, A. et al. (2015) 'Comparative metabolic profiling of mce1 operon mutant vs wild-type *Mycobacterium tuberculosis* strains', *Pathogens and disease*. doi: 10.1093/femspd/ftv066.

Qvist, T. et al. (2015) 'Chronic pulmonary disease with *Mycobacterium abscessus* complex is a biofilm infection', *European Respiratory Journal*, 46(6), pp. 1823–1826. doi: 10.1183/13993003.01102-2015.

Raab, N. and Bachelet, I. (2017) 'Resolving biofilm topography by native scanning electron microscopy', *Journal of Biological Methods*. doi: 10.14440/jbm.2017.173.

Rajendran, R. et al. (2016) 'Integrating *Candida albicans* metabolism with biofilm heterogeneity by transcriptome mapping', *Scientific Reports*. doi: 10.1038/srep35436.

Rao, V. et al. (2006) 'Trans-cyclopropanation of mycolic acids on trehalose dimycolate suppresses *Mycobacterium tuberculosis*-induced inflammation and virulence', *Journal of Clinical Investigation*. J Clin Invest, 116(6), pp. 1660–1667. doi: 10.1172/JCI27335.

Rashid, A. M. et al. (2016) 'Assembly of  $\alpha$ -Glucan by GlgE and GlgB in Mycobacteria and Streptomycetes', *Biochemistry*. American Chemical Society, 55(23), pp. 3270–3284. doi: 10.1021/acs.biochem.6b00209.

Ratnatunga, C. N. et al. (2020) 'The Rise of Non-Tuberculosis Mycobacterial Lung Disease', *Frontiers in Immunology*. doi: 10.3389/fimmu.2020.00303.

Recht, J. and Kolter, R. (2001) ‘Glycopeptidolipid acetylation affects sliding motility and biofilm formation in *Mycobacterium smegmatis*.’, *Journal of bacteriology*. American Society for Microbiology, 183(19), pp. 5718–24. doi: 10.1128/JB.183.19.5718-5724.2001.

Reichhardt, C. and Parsek, M. R. (2019) ‘Confocal laser scanning microscopy for analysis of *Pseudomonas aeruginosa* biofilm architecture and matrix localization’, *Frontiers in Microbiology*. doi: 10.3389/fmicb.2019.00677.

Rhoades, Elizabeth R. et al. (2009) ‘Mycobacterium abscessus Glycopeptidolipids Mask Underlying Cell Wall Phosphatidyl- myo -Inositol Mannosides Blocking Induction of Human Macrophage TNF- $\alpha$  by Preventing Interaction with TLR2’, *The Journal of Immunology*. doi: 10.4049/jimmunol.0802181.

Ripoll, F. et al. (2007) ‘Genomics of glycopeptidolipid biosynthesis in *Mycobacterium abscessus* and *Mycobacterium chelonae*’, *BMC Genomics*. BioMed Central, 8(8), p. 114. doi: 10.1186/1471-2164-8-114.

Ripoll, F. et al. (2009) ‘Non mycobacterial virulence genes in the genome of the emerging pathogen *Mycobacterium abscessus*’, *PLoS ONE*. Edited by N. Ahmed. Public Library of Science, 4(6), p. e5660. doi: 10.1371/journal.pone.0005660.

Rodríguez-Sevilla, G. et al. (2018) ‘Influence of three-dimensional lung epithelial cells and interspecies interactions on antibiotic efficacy against *Mycobacterium abscessus* and *Pseudomonas aeruginosa*’, *Pathogens and Disease*. Oxford University Press, 76(4). doi: 10.1093/femspd/fty034.

Rodríguez-Sevilla, G. et al. (2019) ‘Antimicrobial treatment provides a competitive advantage to *Mycobacterium abscessus* in a dual-species biofilm with *pseudomonas aeruginosa*’, *Antimicrobial Agents and Chemotherapy*. American Society for Microbiology, 63(11). doi: 10.1128/AAC.01547-19.

Rodríguez Fernández, J. A. et al. (2018) *Efficacy of vaccination against biofilm-producing staphylococci as a preventive measure against subclinical mastitis in lacaune and manchega sheep in Spain*.

Rominski, A., Selchow, P., et al. (2017) ‘Elucidation of *Mycobacterium abscessus* aminoglycoside and capreomycin resistance by targeted deletion of three putative resistance genes’, *Journal of Antimicrobial Chemotherapy*. Oxford University Press, 72(8), pp. 2191–2200. doi: 10.1093/jac/dkx125.

Rominski, A., Roditscheff, A., et al. (2017) ‘Intrinsic rifamycin resistance of *Mycobacterium abscessus* is mediated by ADP-ribosyltransferase MAB\_0591’, *Journal of Antimicrobial Chemotherapy*. Oxford University Press, 72(2), pp. 376–384. doi: 10.1093/jac/dkw466.

Rooney, L. M., Hoskisson, P. A. and McConnell, G. (2019) ‘Of microscopes and microbes: characterising a novel nutrient uptake system in *Escherichia coli* biofilms’.

Röse, L., Kaufmann, S. H. E. and Daugelat, S. (2004) ‘Involvement of *Mycobacterium smegmatis* undecaprenyl phosphokinase in biofilm and smegma formation’, *Microbes and Infection*, 6(11), pp. 965–971. doi: 10.1016/j.micinf.2004.05.011.

Rose, S. J. et al. (2015) ‘*Mycobacterium avium* Possesses Extracellular DNA that Contributes to Biofilm Formation, Structural Integrity, and Tolerance to Antibiotics’, *PLOS ONE*. Edited by T. Coenye. Public Library of Science, 10(5), p. e0128772. doi: 10.1371/journal.pone.0128772.

Rose, S. J. and Bermudez, L. E. (2014) ‘*Mycobacterium avium* biofilm attenuates mononuclear phagocyte function by triggering hyperstimulation and apoptosis during early infection’, *Infection and Immunity*. American Society for Microbiology, 82(1), pp. 405–412. doi: 10.1128/IAI.00820-13.

Rose, S. J. and Bermudez, L. E. (2016) ‘Identification of Bicarbonate as a Trigger and Genes Involved with Extracellular DNA Export in Mycobacterial Biofilms.’, *mBio*. American Society for Microbiology, 7(6), pp. e01597-16. doi: 10.1128/mBio.01597-16.

Roux, A.-L. et al. (2016) ‘The distinct fate of smooth and rough *Mycobacterium abscessus* variants inside macrophages’, *Open Biology*. The Royal Society, 6(11), p. 160185. doi: 10.1098/rsob.160185.

Rudra, P. et al. (2018) ‘High levels of intrinsic tetracycline resistance in *Mycobacterium abscessus* are conferred

by a tetracycline-modifying monooxygenase', *Antimicrobial Agents and Chemotherapy*. American Society for Microbiology, 62(6). doi: 10.1128/AAC.00119-18.

Rüegg, E. et al. (2015) 'Multisite Infection with *Mycobacterium abscessus* after Replacement of Breast Implants and Gluteal Lipofilling', *Case Reports in Infectious Diseases*. Hindawi, 2015, pp. 1–6. doi: 10.1155/2015/361340.

Rüger, K. et al. (2014) 'Characterization of rough and smooth morphotypes of *Mycobacterium abscessus* isolates from clinical specimens', *Journal of Clinical Microbiology*. American Society for Microbiology (ASM), 52(1), pp. 244–250. doi: 10.1128/JCM.01249-13.

Ryder, C., Byrd, M. and Wozniak, D. J. (2007) 'Role of polysaccharides in *Pseudomonas aeruginosa* biofilm development', *Current Opinion in Microbiology*. NIH Public Access, pp. 644–648. doi: 10.1016/j.mib.2007.09.010.

Sambandan, D. et al. (2013) 'Keto-mycolic acid-dependent pellicle formation confers tolerance to drug-sensitive *Mycobacterium tuberculosis*', *mBio*. American Society for Microbiology (ASM), 4(3), pp. e00222-13. doi: 10.1128/mBio.00222-13.

Sani, M. et al. (2010) 'Direct Visualization by Cryo-EM of the Mycobacterial Capsular Layer: A Labile Structure Containing ESX-1-Secreted Proteins'. Edited by L. Ramakrishnan. Public Library of Science, 6(3), p. e1000794.

Sanz, M. A., Calvo, ; and Medrano, ; (2017) *Case Study: Vaccination against Staphylococci biofilms in prevention of subclinical mastitis in manchengo sheep*.

Sauer, K. et al. (2002) 'Pseudomonas aeruginosa Displays Multiple Phenotypes during Development as a Biofilm', *JOURNAL OF BACTERIOLOGY*, 184(4), pp. 1140–1154. doi: 10.1128/JB.184.4.1140-1154.2002.

Van Schaik, E. J., Tom, M. and Woods, D. E. (2009) 'Burkholderia pseudomallei isocitrate lyase is a persistence factor in pulmonary melioidosis: Implications for the development of isocitrate lyase inhibitors as novel antimicrobials', *Infection and Immunity*. doi: 10.1128/IAI.00609-09.

Schlafer, S. and Meyer, R. L. (2017) 'Confocal microscopy imaging of the biofilm matrix', *Journal of Microbiological Methods*. Elsevier B.V., pp. 50–59. doi: 10.1016/j.mimet.2016.03.002.

Schorey, J. S. and Sweet, L. (2008) 'The mycobacterial glycopeptidolipids: Structure, function, and their role in pathogenesis', *Glycobiology*. Oxford University Press, pp. 832–841. doi: 10.1093/glycob/cwn076.

Schulze-Robbecke, R. and Fischeder, R. (1989) 'Mycobacteria in biofilms', *Zentralblatt fur Hygiene und Umweltmedizin*.

Seddon, P. et al. (2013) 'Prevalence of nontuberculous mycobacteria in cystic fibrosis clinics, United Kingdom, 2009', *Emerging Infectious Diseases*, 19(7), pp. 1128–1130. doi: 10.3201/eid1907.120615.

Sekizuka, T. et al. (2014) 'Complete genome sequence and comparative genomic analysis of *Mycobacterium massiliense* JCM 15300 in the *Mycobacterium abscessus* group reveal a conserved genomic island MmGI-1 related to putative lipid metabolism', *PLoS ONE*. doi: 10.1371/journal.pone.0114848.

Seper, A. et al. (2011) 'Extracellular nucleases and extracellular DNA play important roles in *Vibrio cholerae* biofilm formation', *Molecular Microbiology*. Wiley-Blackwell, 82(4), pp. 1015–1037. doi: 10.1111/j.1365-2958.2011.07867.x.

Sharma, I. M., Petchiappan, A. and Chatterji, D. (2014) 'Quorum sensing and biofilm formation in mycobacteria: Role of c-di-GMP and methods to study this second messenger', *IUBMB Life*. Blackwell Publishing Ltd, pp. 823–834. doi: 10.1002/iub.1339.

Shi, L. et al. (2010) 'Carbon flux rerouting during *Mycobacterium tuberculosis* growth arrest', *Molecular Microbiology*. Mol Microbiol, 78(5), pp. 1199–1215. doi: 10.1111/j.1365-2958.2010.07399.x.

Simons, S. (2011) 'Nontuberculous Mycobacteria in Respiratory Tract Infections, Eastern Asia', *Emerging Infectious Diseases*. doi: 10.3201/eid1703100604.

Singh, A. et al. (2016) 'Identification of a Desaturase Involved in Mycolic Acid Biosynthesis in *Mycobacterium*

*smegmatis.*', *PLoS ONE*. Public Library of Science, 11(10), p. e0164253. doi: 10.1371/journal.pone.0164253.

Singh, P. et al. (2016) 'Analysis of expression profile of mce operon genes (mce1, mce2, mce3 operon) in different *Mycobacterium tuberculosis* isolates at different growth phases', *Indian Journal of Medical Research*. doi: 10.4103/0971-5916.184305.

Singh, P. K. et al. (2000) 'Quorum-sensing signals indicate that cystic fibrosis lungs are infected with bacterial biofilms', *Nature*. doi: 10.1038/35037627.

Soroka, D. et al. (2014) 'Characterization of broad-spectrum mycobacterium abscessus class A β-lactamase', *Journal of Antimicrobial Chemotherapy*. J Antimicrob Chemother, 69(3), pp. 691–696. doi: 10.1093/jac/dkt410.

Sousa, S. et al. (2015) 'Nontuberculous mycobacteria pathogenesis and biofilm assembly', *International Journal of Mycobacteriology*. No longer published by Elsevier, 4(1), pp. 36–43.

Stinear, T. P. et al. (2008) 'Insights from the complete genome sequence of *Mycobacterium marinum* on the evolution of *Mycobacterium tuberculosis*', *Genome Research*. Cold Spring Harbor Laboratory Press, 18(5), pp. 729–741. doi: 10.1101/gr.075069.107.

Stoodley, P., Debeer, D. and Lewandowski, Z. (1994) 'Liquid flow in biofilm systems.', *Applied and environmental microbiology*. American Society for Microbiology (ASM), 60(8), pp. 2711–6.

Stout, J. E., Koh, W. J. and Yew, W. W. (2016) 'Update on pulmonary disease due to non-tuberculous mycobacteria', *International Journal of Infectious Diseases*, pp. 123–134. doi: 10.1016/j.ijid.2016.03.006.

Taiwo, B. and Glassroth, J. (2010) 'Nontuberculous mycobacterial lung diseases', *Infectious Disease Clinics of North America*. doi: 10.1016/j.idc.2010.04.008.

Talati, N. J. et al. (2008) 'Spectrum of CNS disease caused by rapidly growing mycobacteria', *The Lancet Infectious Diseases*, 8(6), pp. 390–398. doi: 10.1016/S1473-3099(08)70127-0.

Tan, X. et al. (2015) 'Transcriptome analysis of the biofilm formed by methicillin-susceptible *Staphylococcus aureus*', *Scientific Reports*. Nature Publishing Group, 5(1), p. 11997. doi: 10.1038/srep11997.

Tetz, G. V., Artymenko, N. K. and Tetz, V. V. (2009) 'Effect of DNase and antibiotics on biofilm characteristics', *Antimicrobial Agents and Chemotherapy*. doi: 10.1128/AAC.00471-08.

Tetz, V. V. and Tetz, G. V. (2010) 'Effect of extracellular DNA destruction by DNase I on characteristics of forming biofilms', *DNA and Cell Biology*. DNA Cell Biol, 29(8), pp. 399–405. doi: 10.1089/dna.2009.1011.

Thomson, R., Donnan, E. and Konstantinos, A. (2017) 'Notification of nontuberculous mycobacteria: An Australian perspective', *Annals of the American Thoracic Society*. doi: 10.1513/AnnalsATS.201612-994OI.

Thomson, R. M. (2010) 'Changing epidemiology of pulmonary nontuberculous mycobacteria infections', *Emerging Infectious Diseases*. doi: 10.3201/eid1610.091201.

To, K. et al. (2020) 'General Overview of Nontuberculous Mycobacteria Opportunistic Pathogens: *Mycobacterium avium* and *Mycobacterium abscessus*', *Journal of Clinical Medicine*. MDPI AG, 9(8), p. 2541. doi: 10.3390/jcm9082541.

Tolker-Nielsen, T. (2015) 'Biofilm development', in *Microbial biofilms*. 2nd edn, pp. 54–66. doi: 10.1016/B978-0-12-801238-3.99205-5.

Tortoli, E. (2009) 'Clinical manifestations of nontuberculous mycobacteria infections', *Clinical Microbiology and Infection*, 15(10), pp. 906–910. doi: 10.1111/j.1469-0691.2009.03014.x.

Tortoli, E. et al. (2016) 'Emended description of *Mycobacterium abscessus*, *Mycobacterium abscessus* subsp. *abscessus* and *Mycobacterium abscessus* subsp. *bolletii* and designation of *Mycobacterium abscessus* subsp. *massiliense* comb. nov.', *International Journal of Systematic and Evolutionary Microbiology*, 66(11), pp. 4471–4479. doi: 10.1099/ijsem.0.001376.

Tortoli, E. et al. (2017) 'The new phylogeny of the genus *Mycobacterium*: The old and the news', *Infection*,

*Genetics and Evolution*, 56. doi: 10.1016/j.meegid.2017.10.013.

Totani, T. et al. (2017) ‘Effects of nutritional and ambient oxygen condition on biofilm formation in *Mycobacterium avium* subsp. *hominissuis* via altered glycolipid expression’, *Scientific Reports*. Nature Publishing Group, 7, p. 41775. doi: 10.1038/srep41775.

Toyofuku, M. et al. (2016) ‘Environmental factors that shape biofilm formation’, *Bioscience, Biotechnology, and Biochemistry*, 80(1), pp. 7–12. doi: 10.1080/09168451.2015.1058701.

Trivedi, A. et al. (2016) ‘Thiol reductive stress induces cellulose-anchored biofilm formation in *Mycobacterium tuberculosis*’, *Nature Communications*. Nature Publishing Group, 7, p. 11392. doi: 10.1038/ncomms11392.

Tsai, S. H. et al. (2013) ‘Mab\_3168c, a Putative Acetyltransferase, Enhances Adherence, Intracellular Survival and Antimicrobial Resistance of *Mycobacterium abscessus*’, *PLoS ONE*. Public Library of Science, 8(6), p. e67563. doi: 10.1371/journal.pone.0067563.

Turapov, O. et al. (2014) ‘Antimicrobial treatment improves mycobacterial survival in nonpermissive growth conditions’, *Antimicrobial Agents and Chemotherapy*. doi: 10.1128/AAC.02774-13.

Vallarino, J. G. and Osorio, S. (2018) ‘Organic acids’, in *Postharvest Physiology and Biochemistry of Fruits and Vegetables*. doi: 10.1016/B978-0-12-813278-4.00010-5.

Varghese, B. et al. (2012) ‘First case report of chronic pulmonary lung disease caused by *Mycobacterium abscessus* in two immunocompetent patients in Saudi Arabia’, *Annals of Saudi Medicine*, 32(3), pp. 312–314. doi: 10.5144/0256-4947.2012.312.

Vasudevan, R. (2014) ‘Biofilms: Microbial Cities of Scientific Significance’, *Journal of Microbiology & Experimentation*. MedCrave Online, 1(3), pp. 1–0.

Vega-Dominguez, P. et al. (2020) ‘Biofilms of the non-tuberculous *Mycobacterium chelonae* form an extracellular matrix and display distinct expression patterns’, *Cell Surface*. doi: 10.1016/j.tcs.2020.100043.

Viviani, L. et al. (2016) ‘Epidemiology of nontuberculous mycobacteria (NTM) amongst individuals with cystic fibrosis (CF)’, *Journal of Cystic Fibrosis*. Elsevier B.V., 15(5), pp. 619–623. doi: 10.1016/j.jcf.2016.03.002.

Vuotto, C. and Donelli, G. (2014) ‘Field emission scanning electron microscopy of biofilm-growing bacteria involved in nosocomial infections’, *Methods in Molecular Biology*. doi: 10.1007/978-1-4939-0467-9\_6.

Waite, R. D. et al. (2005) ‘Transcriptome analysis of *Pseudomonas aeruginosa* growth: Comparison of gene expression in planktonic cultures and developing and mature biofilms’, *Journal of Bacteriology*. American Society for Microbiology (ASM), 187(18), pp. 6571–6576. doi: 10.1128/JB.187.18.6571-6576.2005.

Wan, N. et al. (2018) ‘Bacterial metabolism during biofilm growth investigated by <sup>13</sup>C tracing’, *Frontiers in Microbiology*. Frontiers Media S.A., 9(NOV). doi: 10.3389/fmicb.2018.02657.

Wang, G. et al. (2006) ‘Increased vancomycin MICs for *Staphylococcus aureus* clinical isolates from a university hospital during a 5-year period’, *Journal of Clinical Microbiology*. American Society for Microbiology, 44(11), pp. 3883–3886. doi: 10.1128/JCM.01388-06.

Wang, X. M. et al. (2011) ‘Biochemical and immunological characterization of a cpn60.1 knockout mutant of *Mycobacterium bovis* BCG’, *Microbiology*. doi: 10.1099/mic.0.045120-0.

Watnick, P. I. and Kolter, R. (1999) ‘Steps in the development of a *Vibrio cholerae* El Tor biofilm.’, *Molecular microbiology*, 34(3), pp. 586–95.

Whang, J. et al. (2017) ‘*Mycobacterium abscessus* glycopeptidolipids inhibit macrophage apoptosis and bacterial spreading by targeting mitochondrial cyclophilin D’, *Cell Death and Disease*. Nature Publishing Group, 8(8), p. e3012. doi: 10.1038/cddis.2017.420.

Whitchurch, C. B. et al. (2002) ‘Extracellular DNA required for bacterial biofilm formation’, *Science*. doi: 10.1126/science.295.5559.1487.

Whiteley, M. et al. (2001) ‘Gene expression in *Pseudomonas aeruginosa* biofilms.’, *Nature*. Nature Publishing Group, 413(6858), pp. 860–864. doi: 10.1038/35101627.

WHO (2019) *Global Tuberculosis Report 2019*.

Wiegand, I., Hilpert, K. and Hancock, R. E. W. W. (2008) ‘Agar and broth dilution methods to determine the minimal inhibitory concentration (MIC) of antimicrobial substances’, *Nature Protocols*. Nature Publishing Group, 3(2), pp. 163–175. doi: 10.1038/nprot.2007.521.

Woods, G. L. et al. (2011) *M24 Susceptibility Testing of Mycobacteria, Nocardiae, and Other Aerobic Actinomycetes, Approved Standard (Clinical and Laboratory Standards Institute;)*.

Wu, J. et al. (2014) ‘Increase in nontuberculous mycobacteria isolated in Shanghai, China: Results from a population-based study’, *PLoS ONE*. doi: 10.1371/journal.pone.0109736.

Yam, Y. K. et al. (2020) ‘Extreme Drug Tolerance of *Mycobacterium abscessus* “Persisters”’, *Frontiers in Microbiology*. doi: 10.3389/fmicb.2020.00359.

Yamazaki, Y. et al. (2006) ‘The ability to form biofilm influences *Mycobacterium avium* invasion and translocation of bronchial epithelial cells’, *Cellular Microbiology*, 8(5), pp. 806–814. doi: 10.1111/j.1462-5822.2005.00667.x.

Yan, J. et al. (2020) ‘Investigating transmission of *Mycobacterium abscessus* amongst children in an Australian cystic fibrosis centre’, *Journal of Cystic Fibrosis*. Elsevier B.V., 19(2), pp. 219–224. doi: 10.1016/j.jcf.2019.02.011.

Yang, Y., Thomas, J., Li, Y., Vilchèze, C., Derbyshire, K. M., Jacobs, W. R. and Ojha, A. K. (2017) ‘Defining a temporal order of genetic requirements for development of mycobacterial biofilms’, *Molecular Microbiology*. doi: 10.1111/mmi.13734.

Yang, Y., Thomas, J., Li, Y., Vilchèze, C., Derbyshire, K. M., Jacobs, W. R., Ojha, A. K., et al. (2017) ‘Defining a temporal order of genetic requirements for development of mycobacterial biofilms’, *Molecular Microbiology*, 105(5), pp. 794–809. doi: 10.1111/mmi.13734.

Yano, T. et al. (2014) ‘Mycobacterium tuberculosis type II NADH-menaquinone oxidoreductase catalyzes electron transfer through a two-site ping-pong mechanism and has two quinone-binding sites’, *Biochemistry. Biochemistry*, 53(7), pp. 1179–1190. doi: 10.1021/bi4013897.

Yoshida, M. et al. (2018) ‘Complete genome sequence of a type strain of *Mycobacterium abscessus* subsp. *bolletii*, a member of the *Mycobacterium abscessus* complex’, *Genome Announcements*. doi: 10.1128/genomeA.01530-17.

Zeng, S. et al. (2019) ‘Cpn60.1 (GroEL1) contributes to mycobacterial crabtree effect: Implications for biofilm formation’, *Frontiers in Microbiology*. doi: 10.3389/fmicb.2019.01149.